

4.1 Coordination and redox state-dependent structural changes of the heme-based oxygen sensor AfGcHK associated with intraprotein signal transduction

Stranava, M.; Man, P.; Skálová, T.; Kolenko, P.; Blaha, J.; Fojtikova, V.; Martínek, V.; Dohnálek, J.; Lengalova, A.; Rosůlek, M.; Shimizu, T.; Martínková, M.: *J. Biol. Chem.* (2017) 292, 20921–20935 (IF₂₀₁₉ 4,1).

Podíl předkladatelky na této práci: 20 % (*exprese a purifikace proteinu AfGcHK, technická asistence, příprava obrázků*)

potvrzeno korespondujícím autorem, doc. RNDr. Markétou Martínkovou, Ph.D.

Coordination and redox state–dependent structural changes of the heme-based oxygen sensor AfGcHK associated with intraprotein signal transduction

Received for publication, September 12, 2017, and in revised form, October 18, 2017. Published, Papers in Press, November 1, 2017, DOI 10.1074/jbc.M117.817023

Martin Stranava[‡], Petr Man^{‡§1}, Tereza Skálová[¶], Petr Kolenko^{¶||}, Jan Blaha[‡], Veronika Fojtiková[‡], Václav Martínek[‡], Jan Dohnálek[¶], Alžbeta Lengalová[‡], Michal Rosůlek^{‡§1}, Toru Shimizu[‡], and Markéta Martínková^{‡2}

From the [‡]Department of Biochemistry, Faculty of Science, Charles University, Hlavova (Albertov) 2030/8, Prague 2, 128 43 Czech Republic, the [§]Institute of Microbiology of the Czech Academy of Sciences, v.v.i., Biocev, 252 50 Vestec, Czech Republic, the [¶]Institute of Biotechnology of the Czech Academy of Sciences, v.v.i., Biocev, 252 50 Vestec, Czech Republic, and the ^{||}Department of Solid State Engineering, Faculty of Nuclear Sciences and Physical Engineering, Czech Technical University in Prague, Brehova 7, 115 19 Praha 1, Czech Republic

Edited by F. Peter Guengerich

The heme-based oxygen sensor histidine kinase AfGcHK is part of a two-component signal transduction system in bacteria. O₂ binding to the Fe(II) heme complex of its N-terminal globin domain strongly stimulates autophosphorylation at His¹⁸³ in its C-terminal kinase domain. The 6-coordinate heme Fe(III)-OH[−] and -CN[−] complexes of AfGcHK are also active, but the 5-coordinate heme Fe(II) complex and the heme-free apo-form are inactive. Here, we determined the crystal structures of the isolated dimeric globin domains of the active Fe(III)-CN[−] and inactive 5-coordinate Fe(II) forms, revealing striking structural differences on the heme-proximal side of the globin domain. Using hydrogen/deuterium exchange coupled with mass spectrometry to characterize the conformations of the active and inactive forms of full-length AfGcHK in solution, we investigated the intramolecular signal transduction mechanisms. Major differences between the active and inactive forms were observed on the heme-proximal side (helix H5), at the dimerization interface (helices H6 and H7 and loop L7) of the globin domain and in the ATP-binding site (helices H9 and H11) of the kinase domain. Moreover, separation of the sensor and kinase domains, which deactivates catalysis, increased the solvent exposure of the globin domain-dimerization interface (helix H6) as well as the flex-

ibility and solvent exposure of helix H11. Together, these results suggest that structural changes at the heme-proximal side, the globin domain-dimerization interface, and the ATP-binding site are important in the signal transduction mechanism of AfGcHK. We conclude that AfGcHK functions as an ensemble of molecules sampling at least two conformational states.

The heme-based oxygen sensor kinase from the soil bacterium *Anaeromyxobacter* sp. Fw109-5, AfGcHK is a globin-coupled oxygen sensor (GCS)³ consisting of an N-terminal heme-binding globin domain and a C-terminal histidine kinase domain (1, 2). AfGcHK is an element of a two-component signal transduction system (3–6) in which the binding of O₂ to the heme Fe(II) complex of its oxygen-sensing globin domain significantly enhances the autophosphorylation activity of its kinase domain via intramolecular signal transduction (Fig. 1). The phosphate group is subsequently transferred from His¹⁸³ of the AfGcHK to the Asp⁵² and Asp¹⁶⁹ residues of its cognate response regulator protein (1, 2, 7) (supplemental Fig. S1). Like the 6-coordinate heme Fe(II)-O₂ complex, the 6-coordinate heme Fe(III)-OH[−] and CN[−] complexes are also active, despite having a different redox state at the iron center (8). However, AfGcHK containing a globin domain with a 5-coordinate Fe(II) heme complex or a heme-free apo-globin domain exhibits low kinase activity (8). This strongly suggests

This work was supported in part by Charles University Grant UNCE 204025/2012; Grant Agency of the Czech Republic Grant 15-19883S; Grant Agency of Charles University Grants 362115 and 704217; Ministry of Education, Youth, and Sports of the Czech Republic Grant LM2015043 CIISB, Biocev - Crystallization, Diffraction and LTC17065 in frame of COST Action CA15126 MOBIEU; ERDF fund Grants CZ.02.1.01/0.0/0.0/16_013/0001776 and CZ.1.05/1.1.00/02.0109; and Grant Agency of the Czech Technical University in Prague Grant SGS16/246/OHK4/3T/14. This work was also partly funded by Instruct, part of the European Strategy Forum on Research Infrastructures (ESFRI) and supported by national member subscriptions. The authors declare that they have no conflicts of interest with the contents of this article.

This article contains supplemental information on the crystal structure of AfGcHK globin domain, a structural comparison of the isolated globin domains of AfGcHK and other GCSs, supplemental Table S1, and supplemental Figs. S1–S8.

The atomic coordinates and structure factors (codes 5OHE and 5OHF) have been deposited in the Protein Data Bank (<http://www.pdb.org/>).

¹ Recipient of financial support from NPU II (LQ1604).

² To whom correspondence should be addressed. Tel.: 420-22-195-1242; Fax: 420-22-195-1283; E-mail: marketa.martinkova@natur.cuni.cz.

³ The abbreviations used are: GCS, globin-coupled oxygen sensor; AfGcHK, a globin-coupled histidine kinase from *Anaeromyxobacter* sp. Fw109-5; EcDOS, *E. coli* direct oxygen sensor or heme-regulated phosphodiesterase from *E. coli* or EcDosP; Fe(III), Fe(III)-protoporphyrin IX complex, or hemin; Fe(II), Fe(II)-protoporphyrin IX complex; FixL, an oxygen-sensor histidine kinase with the heme-bound PAS domain that regulates nitrogen fixation in *Rhizobium meliloti* or *Bradyrhizobium japonicum*; GAF, domain conserved in cyclic GMP-specific and stimulated phosphodiesterases, adenylate cyclases, and *E. coli* formate hydrogenlyase transcriptional activator; GsGCS, globin-coupled sensor from *G. sulfurreducens*; HDX-MS, hydrogen/deuterium exchange coupled with mass spectrometry; HK853, the sensor histidine kinase from *T. maritima*; PAS, Per (*Drosophila* period clock protein)-Arnt (vertebrate aryl hydrocarbon receptor nuclear translocator)-Sim (*Drosophila* single-minded protein); YddV, heme-bound diguanylate cyclase from *E. coli* or EcDosC; PDB, Protein Data Bank; RMSD, root mean square deviation.

Protein structures of a heme-based oxygen sensor kinase AfGcHK

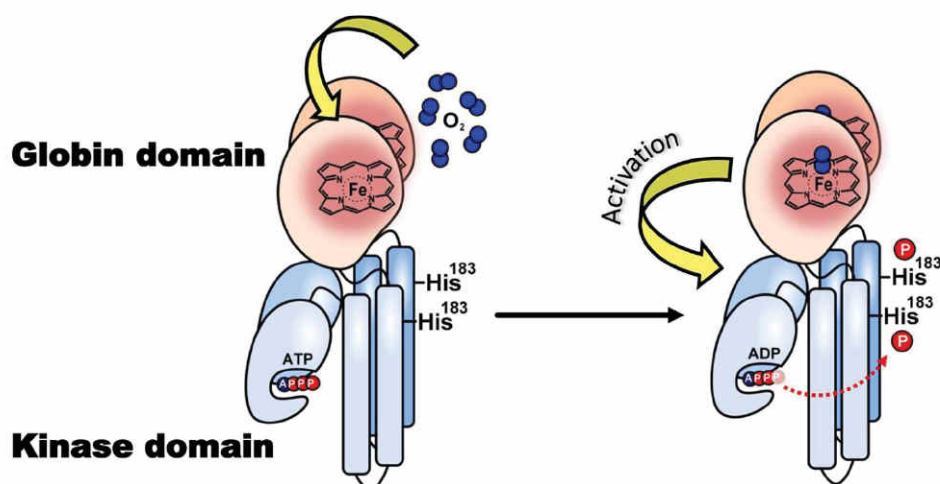


Figure 1. Intramolecular signal transduction of homodimeric AfGcHK. O₂ binds to the heme Fe(II) complex in the globin domain at the N terminus, changing the structure of the protein surrounding the heme. These structural changes function as a signal that is transduced to the kinase domain (at the C terminus), activating the kinase reaction and inducing autophosphorylation at His¹⁸³.

that structural changes near the heme-binding site in the globin domain are tightly linked to the catalytic regulation of the kinase domain via intraprotein signal transduction.

To understand the molecular mechanism of this intramolecular signal transduction, it is important to know 1) how the structure of the globin domain differs between the Fe(III) (active) and Fe(II) (inactive) heme complex-bound forms and between forms with and without axial ligands; 2) how structural changes in the globin domain propagate to the kinase domain; and 3) how the transition from the inactive to the active state in response to the transduction of the globin domain signal affects the kinase domain.

The structure–function relationships of oxygen sensors containing a heme-bound globin, PAS, and GAF folds have been investigated in various proteins (2). Both heme iron reduction and the binding of external axial ligands such as O₂ can induce global structural changes (affecting both the heme surroundings and more distant regions) in the isolated heme-bound PAS domains of oxygen sensors, such as FixL (9, 10) and EcDOS (11, 12). However, these effects were found to be less pronounced in the isolated heme-bound GAF domains of oxygen sensors, such as DosS/DosT, than those observed for the PAS domain (13–15). Additionally, changes in heme redox state or external ligand binding had no significant impact on the structure of the isolated heme-bound globin domain of GCS (16–18). In this work, we present the first X-ray crystal structures of heme Fe(III) and Fe(II) complexes of the isolated dimeric globin domain of AfGcHK, revealing large structural differences between the active and inactive forms in the vicinity of the heme and at the globin dimerization interface.

Importantly, no X-ray crystal structure of any full-length heme-based oxygen sensor has yet been reported. We previously studied the full-length AfGcHK protein in solution by combining hydrogen/deuterium exchange coupled with mass spectrometry (HDX–MS) with homology modeling (7). However, the structural changes in this protein caused by heme redox state changes and the binding of different axial ligands (both of which are closely linked to catalytic regulation) have not been characterized.

This work uses HDX–MS to describe the structural differences between the active and inactive forms of full-length AfGcHK and its isolated globin and kinase domains in solution and analyzes structural differences between the active and inactive forms of the AfGcHK globin domain revealed by X-ray crystallography. It was found that changes in the heme redox state and axial ligand binding to the heme iron complex lead to structural alterations in the heme-proximal side of the globin domain and affect domain–domain interactions within the dimeric globin domains. Differences were also observed around the two helices forming the ATP-binding site necessary for autophosphorylation in the kinase domain. These structural changes associated with catalytic regulation revealed by HDX–MS corroborated the conclusions drawn by analyzing the X-ray crystal structures of the isolated globin domain in two redox states.

Results

We first determined the X-ray crystal structures of isolated AfGcHK globin domains bearing heme in the Fe(III)-CN[−] form (active state) and containing heme Fe(II) (inactive state) complexes and then compared them with HDX–MS data for the full-length AfGcHK protein.

Crystal structure of the isolated heme Fe(III)-CN[−] globin domain (PDB code 5OHE)

The crystal structure of the isolated globin domain in the presence of KCN was solved at a resolution of 1.85 Å. Relevant data processing parameters and structure characteristics are presented in Table 1.

Overall structure—The asymmetric unit of the crystal consists of four dimers (Fig. 2A) formed by eight protein chains (AB, CD, EF, and GH) positioned in a disphenoidal arrangement. The crystal structure confirms that the domain adopts the characteristic globin fold of GCSs (Fig. 2B). Each monomer consists of seven helices, H1–H7 (also known as helices A–G (2)), and seven loops, L1–L7. RMSD values of coordinates of C^α atoms of the aligned protein chains (monomers) are in the range of 0.2–0.5 Å with no significant difference between the

Table 1
Data processing statistics and structure refinement parameters

Values in parentheses refer to the highest-resolution shell.

	Globin domain of AfGcHK with heme Fe(III)-CN ⁻	Globin domain of AfGcHK with cyanide, partially reduced (the dithionite-soaked crystal)
PDB code	5OHE	5OHF
Data processing statistics		
Space group	P4 ₁ 2 ₁ 2	P4 ₁ 2 ₁ 2
Unit-cell parameters		
<i>a</i> , <i>b</i> , <i>c</i> (Å)	78.1, 78.1, 441.8	77.7, 77.7, 441.2
<i>α</i> , <i>β</i> , <i>γ</i> (degrees)	90.0, 90.0, 90.0	90.0, 90.0, 90.0
Resolution range (Å)	46.82–1.85 (1.88–1.85)	49.17–1.8 (1.83–1.80)
No. of observations	1,413,447 (62,729)	931,937 (47,063)
No. of unique reflections	118,539 (5739)	127,077 (6192)
Data completeness (%)	100 (100)	100 (100)
Average redundancy	11.9 (10.9)	7.3 (7.6)
Mosaicity (degrees)	0.118	0.07
Average <i>I</i> /σ(<i>I</i>)	11.1 (1.9)	16.7 (2.7)
Solvent content (%)	46	46
Matthews coefficient (Å ³ /Da)	2.27	2.27
<i>R</i> _{merge} ^a	0.139 (1.157)	0.059 (0.761)
<i>R</i> _{p.i.m.}	0.059 (0.517)	0.034 (0.442)
<i>CC</i> _{1/2}	0.998 (0.804)	0.993 (0.844)
Structure refinement parameters		
<i>R</i> _{work} ^a	0.192	0.190
<i>R</i> _{free}	0.241	0.239
<i>R</i> _{all}	0.194	0.192
Average <i>B</i> -factor (Å ²)	24	28
RMSD bond lengths from ideal (Å)	0.015	0.009
RMSD bond angles from ideal (degrees)	1.653	1.267
Number of non-hydrogen atoms	11,456	12,325
Dimers per asymmetric unit (chains)	AB, CD, EF, GH	AB, CD, EF, GH
No. of water molecules	1117	1017
Ramachandran statistics		
Residues in favored regions (%)	100	99.9
No. of outliers	0	0

^a $R_{\text{merge}} = \sum_h \sum_i |I_{hi} - \langle I_h \rangle| / \sum_h \sum_i I_{hi}$, $R_{\text{p.i.m.}} = \sum_h \sum_i (n_h - 1)^{-1/2} |I_{hi} - \langle I_h \rangle| / \sum_h \sum_i I_{hi}$, and $R = \sum_h \|F_{h,\text{obs}} - |F_{h,\text{calc}}|\| / \sum_h |F_{h,\text{obs}}|$, where I_{hi} is the observed intensity, $\langle I_h \rangle$ is the mean intensity of multiple observations of symmetry-related reflections, and $F_{h,\text{obs}}$ and $F_{h,\text{calc}}$ are the observed and calculated structure factor amplitudes. R_{work} is the *R* factor calculated on 95% of reflections excluding a random subset of 5% of reflections marked as “free.” The final structure refinement was performed on all observed structure factors.

structures of the monomers. The fold of the dimer is most similar to that of the globin domain of *Geobacter sulfurreducens* GCS (PDB code 2W31 (17), 34% sequence identity); the RMSD between the C^α atom coordinates of the aligned dimers is 1.4 Å (PDBFold (19)).

Crystal contacts, electron density, and B-factors; differences among the chains—All four dimers in the asymmetric unit have approximately the same contact surface area at the dimer interface (as determined by a PISA assembly analysis (20)) except in the region of residues Arg⁵⁵–Val⁶⁵. This region is very well localized in the electron density map in chains A and D due to stabilizing interchain contacts within the asymmetric unit. The remaining chains form weaker water-mediated contacts with symmetry-related chains. In chains C and G, this region exhibits higher disorder and weaker electron density. This is also reflected in *B*-factors of the protein chains; the C and G chains of the dimer had higher chain-averaged *B*-factors than the other chains (28 and 31 Å², respectively, compared with 21–23 Å² for the others). The higher average *B*-factors of both chains are primarily due to *B*-factor “hot spots” around residues 55–65, which are close to the heme-binding pocket. These observations are in agreement with the greater susceptibility of chains C and G to structural changes and in part explain why the effects of the dithionite soaking were observed only in chain G (see below).

Dimer interface—Interestingly, the dimer interface largely consists of water-mediated hydrogen bonds. The interface

between protein chains A and B features 28 water molecules involved in water-mediated hydrogen bonds, of which 12 participate in residue-water-residue and four participate in residue-water-water-residue bonds (Fig. 2C). Another eight water molecules together with a chloride ion fill a large cavity in the upper part of the dimerization interface (the area labeled *part I* of the dimerization interface in Fig. 2C), which is located opposite the kinase domain in the full-length protein. The total interface area varies between 1722 and 1800 Å², depending on the pair of chains analyzed, and accounts for around 21% of the total monomer surface area of 8500 Å². The interface can be divided into two regions (Fig. 2C): *part I* and *part II*. *Part I* features mainly van der Waals interactions and water-mediated hydrogen bonds and has no direct protein–protein hydrogen bonds. *Part II* is close to the C-terminus (and thus close to the kinase domain in the full-length protein) and features 19 interchain protein–protein hydrogen bonds, hydrophobic interactions, and several water-mediated hydrogen bonds. *Part I* of the interface therefore allows for more variability in the relative arrangement of the two monomers, whereas *part II* functions as a more tightly tethered hinge. Together, the two parts allow the monomers’ relative positions and orientations to be quite well defined and controlled near the heme sites while also permitting a highly dynamic arrangement, especially in the *part I* region (Fig. 2C).

Heme surroundings—The heme is bound in a hydrophobic pocket formed by residues from helices H2–H7. The 6-coordi-

Protein structures of a heme-based oxygen sensor kinase AfGcHK

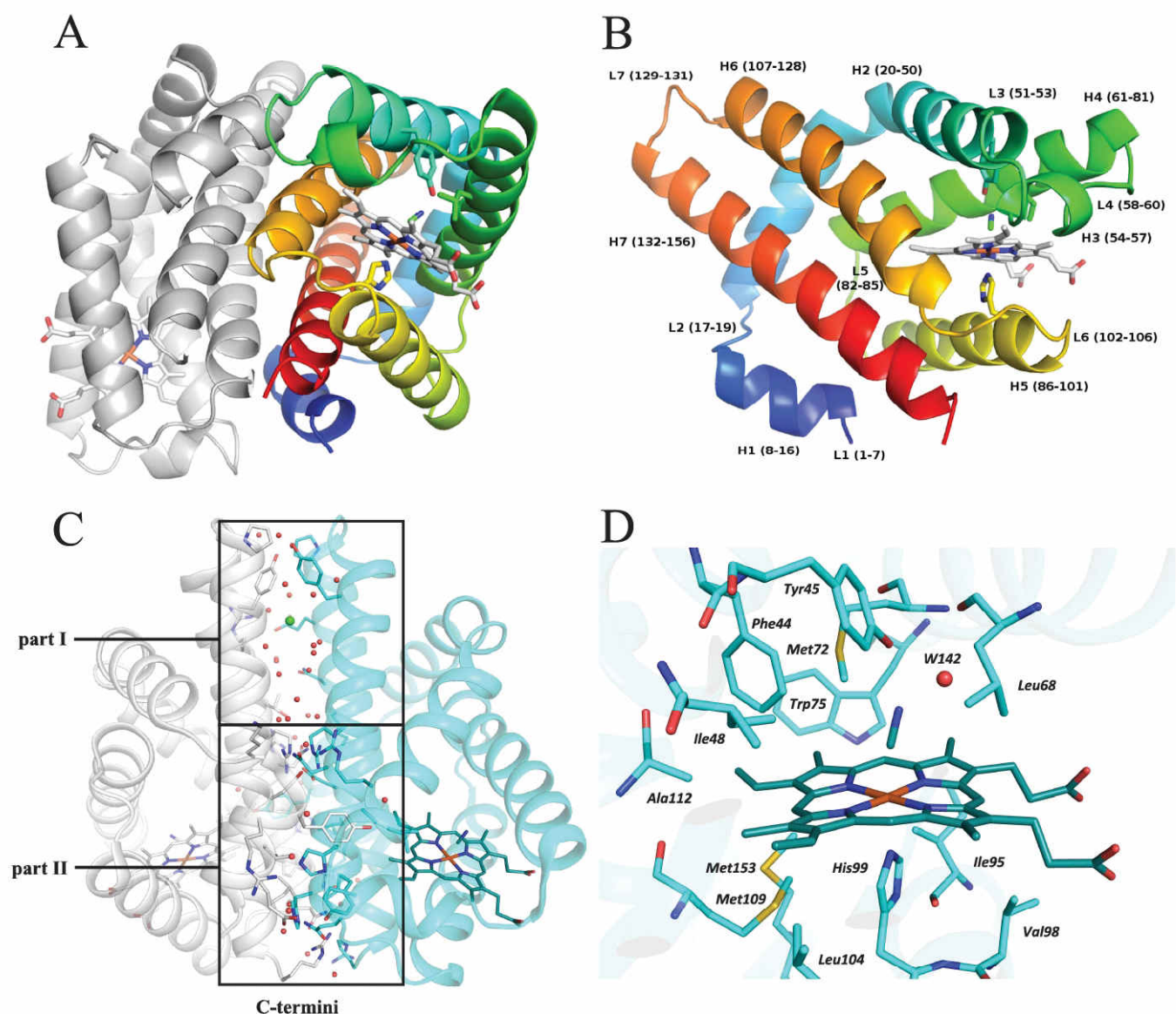


Figure 2. Crystal structure of a dimer of the globin domain of AfGcHK with an Fe(III)-CN⁻ heme complex (active state, PDB code 5OHE) and a close-up view of the heme surroundings. *A*, secondary structure representation of the dimer with the N terminus of chain A in blue, the C terminus of chain A in red, and chain B in gray. The heme, selected neighboring residues, and bound cyanide molecule are shown using a stick representation. *B*, close-up view of the molecular architecture of protein chain A, using the same color coding and representations as in *A*; individual α -helices, loops, and the corresponding residue numbers are marked. *C*, dimerization interface of the isolated globin domain dimer, showing its division into parts I and II; part I is situated opposite the kinase domain in the full-length protein and relies only on van der Waals interactions and water-mediated hydrogen bonds, with no direct protein–protein hydrogen bonds, whereas part II is near the C terminus (close to the kinase domain in the full-length protein) and features 19 interchain protein–protein hydrogen bonds, hydrophobic interactions, and several water-mediated hydrogen bonds. Red dots, water molecules; green sphere, a chloride ion. *D*, the heme pocket residues (whose carbon atoms are shown in cyan), the heme group (carbon atoms shown in dark cyan), and the cyanide ligand (carbon atom shown in dark cyan) are shown in a stick representation with color coding according to atom type. The graphics were generated using PyMOL (Schrödinger, LLC, New York).

nate Fe(III) ion is stabilized by direct interactions with His⁹⁹ (belonging to H5) at the proximal side and Tyr⁴⁵ (belonging to H2) at the distal side, with the latter interaction being mediated by a small ligand (Fig. 2*D*). In most chains, the small ligand can be interpreted as a CN⁻ ion, but the electron density maps for chains D and F lack the diatomic character and were interpreted as water molecules.

The distal side of the heme-binding pocket is formed from eight residues located within 4 Å of the heme: Phe⁴⁴, Tyr⁴⁵, Ile⁴⁸, Leu⁶⁸, Met⁷², Trp⁷⁵, Ala¹¹², and Met¹¹³. Additionally, Tyr¹⁵ from the neighboring chain completes the binding

pocket. The Leu⁶⁸ residue is located at the entrance to the heme-binding pocket and represents a “gate” for incoming ligand molecules. The proximal side is formed from residues Ile⁹⁵, Val⁹⁸, His⁹⁹ (which binds directly to the Fe(III) center), Ile¹⁰², Leu¹⁰⁴, Tyr¹⁰⁸, Met¹⁰⁹, and Met¹⁵³. As observed in our crystal structure, the distance between the Fe(III) center and the N^{ε2} center of His⁹⁹ is 2.1 Å.

The observed position of Tyr⁴⁵ is consistent with resonance Raman data on its interaction with O₂ bound to Fe(II) (1). In addition, mutation of Tyr⁴⁵ destabilizes the Fe(II)-O₂ complex, increasing its autoxidation rate several hundred-

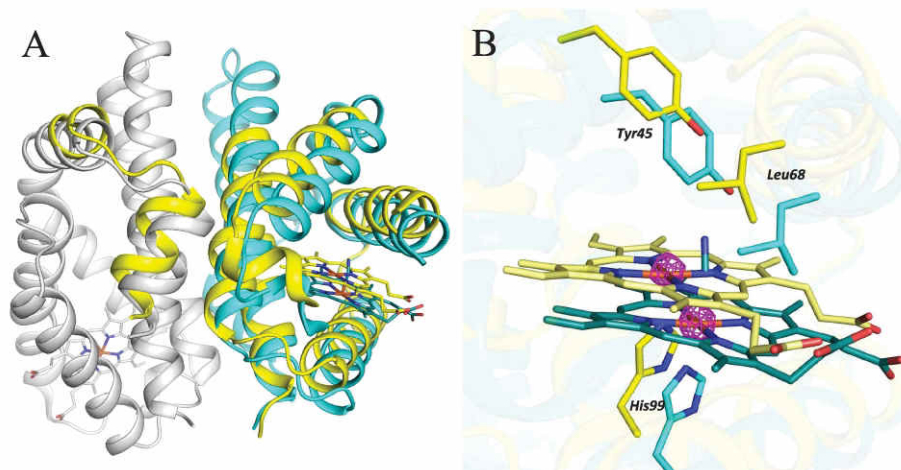


Figure 3. Structural changes induced by sodium dithionite soaking (PDB code 5OHF). A, chains G and H are shown using a secondary structure representation (in cyan and gray, respectively) except for their heme and CN^- moieties, which are shown using a stick representation (colored in dark cyan for chain G and dark gray for chain H). Alternative B is shown in yellow, and the position of its heme group is shown in light yellow using a stick representation. Most of the residues adopting different positions in alternative B are in chain G. B, detailed view of the shift of the heme group and the surrounding heme pocket upon dithionite soaking. The active Fe(III)-CN^- form is shown in cyan, and the inactive Fe(II) form is shown in yellow. The anomalous difference map (magenta, contoured at 5σ) confirms the presence of iron in two positions (observed in chain G only). The graphics were generated using PyMOL (Schrödinger, LLC).

fold (supplemental Table S1 and Figs. S2 and S3). The corresponding Tyr residue (Tyr⁴³) of the homologous GCS sensor protein, YddV, is also assumed to interact with O_2 bound to the heme Fe(II) center. Accordingly, mutation of this residue significantly changes the O_2 -binding behavior of YddV: the Y43A and Y43L mutants do not bind O_2 , and the autoxidation rates of the Y43F and Y43W mutants are more than 10 times higher than that of the wild type (supplemental Table S1) (1, 21–24). Leu⁶⁸, which is located between the small heme ligand and the bulk solvent, also has important effects on the activity of AfGcHK. Its role in stabilizing the Fe(II)-O_2 complex has been confirmed using site-directed mutagenesis; the L68G, L68N, and L68V mutations all significantly increased the heme iron autoxidation rate (supplemental Table S1 and Figs. S2 and S3).

Crystal structure of the AfGcHK globin domain after reduction with sodium dithionite (PDB code 5OHF)

To obtain a crystal structure of the AfGcHK globin domain with an Fe(II) heme complex, the crystal of the Fe(III)-CN^- -containing globin domain was soaked in a solution of the strong reductant sodium dithionite. The resulting diffraction data were processed at a resolution of 1.8 Å. The data processing parameters and structure characteristics for the reduced crystal are presented in Table 1.

The reduced crystal retains the unit cell and asymmetric unit ordering of the parent (non-soaked) crystal. However, the structure of protein chain G (which had the highest *B*-factors in the parent crystal) differs sharply from that in the parent crystal (Fig. 3A). The iron center of the heme group from chain G was found in two distinct positions, each having an occupancy of 0.5 (confirmed by anomalous scattering; see Fig. 3B). Similarly, the heme group and protein chain were also observed in two alternative positions designated A and B (supplemental Fig. S4). In alternative A, the structure of the G chain resembles that of the other chains, and the sixth ligand is visible above the heme; if the sixth ligand is not modeled, there is a positive difference peak in the position it would occupy. Alternative A thus repre-

sents an Fe(III)-CN^- -bound form. Omit electron density does not contain any significant positive difference peak that would justify building of a small ligand in the expected position above heme in alternative B. Therefore, alternative B contains a heme with no sixth ligand and thus represents a reduced heme iron complex formed by the action of dithionite. Based on the experimental conditions and the lack of a small axial ligand, we assume that the iron center in this alternative is 5-coordinate and exists in the Fe(II) oxidation state (Fig. 3B). In alternative A, the atomic coordinates for all amino acid residues in chain G and all of the other protein chains are consistent with those for the corresponding amino acids in the original 6-coordinate Fe(III)-CN^- structure. In alternative B, the positions of most residues in chain G and some in chain H (its dimerization partner protein chain) differed significantly from those in alternative A. In total, 93 residues in chain G were modeled in alternative positions: Pro³⁸–Leu⁵⁸, Gln⁶⁴–Leu¹²⁰, and Gly¹⁴³–Arg¹⁵⁸ at the end of the chain (residues Val⁵⁹–Ser⁶³ could not be localized and therefore were not modeled). Residues in chain H that required interpretation by two alternative positions were Thr⁷–Ala²⁵, located at the beginning of the chain (Fig. 3A). All residues built in two alternatives belong to helices H2–H7 of chain G and helices H1 and H2 of its partner chain H. The positional changes in chain H are clearly due to those in chain G rather than any redox process affecting the chain H heme complex. The heme and heme pocket in alternative B are shifted away from the globin dimer interface by 2.5 Å relative to their position in alternative A, and much of the positional difference between the protein chains in two alternatives is due to the displacement of residues to follow and accommodate this shift. The residue exhibiting the greatest displacement from its position in alternative A (3.6 Å) is Ile¹⁰², which forms van der Waals interactions with the heme.

The crystal structure presented in Fig. 3 is the best from a series of eight diffraction data sets obtained by soaking of the original crystals of the AfGcHK globin domain in sodium

Protein structures of a heme-based oxygen sensor kinase AfGCHK

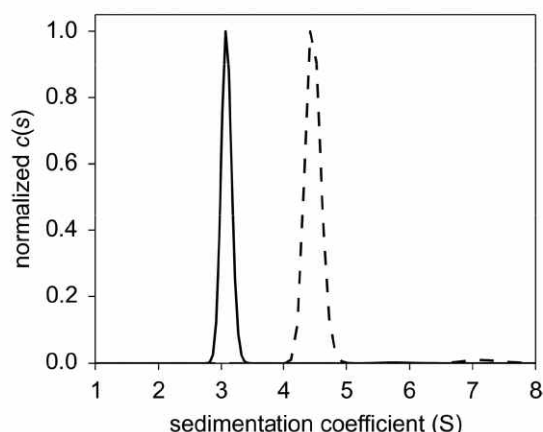


Figure 4. Sedimentation coefficient distributions for the isolated globin domain of AfGCHK (15 μM ; black solid line) and the full-length AfGCHK (15 μM ; black dashed line). The weight average sedimentation coefficients were calculated from the absorbance data. For further details, see "Experimental procedures." $c(s)$ denotes the continuous sedimentation coefficient distribution.

dithionite for various periods. All eight data sets were checked, and similar trends of structural changes were observed. The data set allowing the most accurate interpretation of the data in terms of structural changes was selected. For details, see the supplemental materials.

Determination of the oligomeric state of the isolated globin domain and the full-length protein in solution by analytical ultracentrifugation

The full-length AfGCHK protein forms a dimer in solution (Fig. 4) because its sedimentation coefficient of $s_{20,w} = 4.74$ S corresponds to a molecular mass of 82 kDa, but its molecular mass as computed from its amino acid sequence is 43 kDa. The isolated globin domain of AfGCHK also forms a dimer in solution (Fig. 4) because its sedimentation coefficient of $s_{20,w} = 3.20$ S corresponds to a molecular mass of 39 kDa, but its molecular mass as computed from its amino acid sequence is 19 kDa.

Similarities and differences between the active Fe(III)-OH⁻ and inactive Fe(II) forms of the full-length AfGCHK protein revealed by HDX-MS data

The structure of the isolated globin domain of AfGCHK containing Fe(III)-CN⁻ determined by X-ray crystallography in this work and our previously reported model structure of the isolated kinase domain (7) were used to visualize the changes in the functional states of AfGCHK that were observed by HDX-MS, which are summarized in Fig. 5.

Reduction of the Fe(III)-OH⁻ complex in AfGCHK changes the iron coordination number from 6 to 5 and is accompanied by changes in deuteration across the entire protein. This is shown in Fig. 6, which presents the relative differences in deuteration between the active full-length AfGCHK protein containing the Fe(III)-OH⁻ complex and the inactive 5-coordinate Fe(II) complex with no sixth ligand. The greatest decrease in deuteration was observed in the globin domain, and the magnitude and extent of the decrease observed 5 min after reduction were similar to those seen after 60 min (Fig. 6). Regions of the protein that were stabilized or more shielded from deutera-

tion included helices H2 and H3 (residues 44–72), and H5 and H6 (residues 89–120); these helices are shown in blue in the top left structure in Fig. 5B. On the other hand, heme iron reduction increased deuteration in part I of the globin dimerization interface, which is distant from the connection to the kinase domain. Regions exhibiting pronounced increases in deuteration included the end of H6, loop L7, and the beginning of H7 (residues 121–150); see the red areas in the top left structure in Fig. 5B. The HDX-MS results are consistent with the globin domain structure determined by X-ray crystallography (Fig. 2C); part I shows greater dynamics, whereas part II functions as a more tightly tethered hinge. This behavior was observed for the isolated globin domain with an Fe(III)-CN⁻ heme complex and is readily apparent in the HDX-MS results for the active and inactive forms of the full-length AfGCHK protein (compare the top left structures shown in Fig. 5, A and B). The structural data suggest that the globin dimerization interface undergoes a sort of scissor motion as the protein transitions from the active to the inactive state.

Interestingly, reduction of the heme iron center has little effect on the deuteration profile of the kinase domain outside two distinct regions: residues 221–231 of H9 and residues 284–296 of H11 (Figs. 5B (bottom left) and 6). The largest changes occur in the part of the kinase domain (helix H11) that forms the ATP binding site, which is more flexible and solvent-exposed in the inactive Fe(II)-bound form. It may be that heme iron reduction increases the separation of H9 and H11 (the ATP binding site), indirectly hindering His¹⁸³ (at H8) phosphorylation.

The differences in deuteration between the active Fe(III)-OH⁻ and inactive Fe(II) forms of the full-length AfGCHK protein were analogous in all tested incubation times. Data for the 5- and 60-min time points were selected as representative results (Fig. 6); the measurements for the other time points (0.5, 20, and 180 min) showed similar trends (supplemental Fig. S5).

Similarities and differences between the other active and inactive forms of the full-length AfGCHK protein revealed by HDX-MS data

To determine whether the changes in the deuteration profile of AfGCHK upon reduction of the active Fe(III)-OH⁻ globin domain heme complex to the inactive Fe(II) form are consistent with those observed for other active and inactive forms (supplemental Fig. S6), we performed HDX-MS experiments with three other full-length variants: the inactive heme-free apoprotein (the H99A mutant), the active Fe(III)-CN⁻ complex, and the active Fe(II)-O₂ complex (Fig. 7).

The differences in deuteration between the Fe(III)-OH⁻ form and the other active forms containing CN⁻ and O₂ were rather small and confined to the heme-distal side of the globin domain, specifically residues 30–60 and 120–130 in helices H2, H3, and H6 (represented as blue ribbons in the top left and central structures in Fig. 5A). It thus seems that the nature of the sixth heme ligand affects the protein's dynamics and the solvent accessibility in the vicinity of the heme prosthetic group on the heme-distal side but has little effect on the transduction of dynamic effects between the globin and kinase domains (repre-

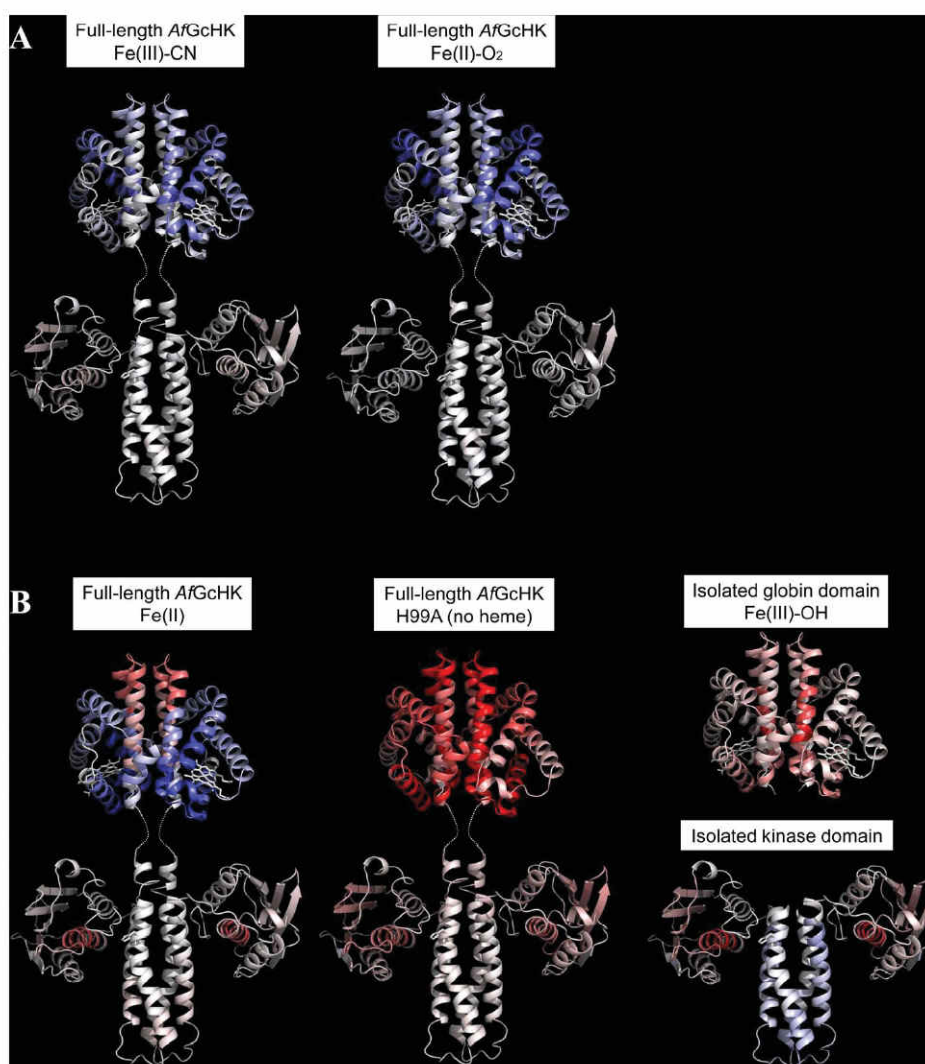


Figure 5. Conformational changes revealed by HDX-MS after 60 min of deuteration of the full-length AfGcHK proteins and the separated domains, visualized on the protein's structure. Differences between the Fe(III)-OH⁻ form and other active or inactive forms are color-coded; gray indicates no difference, whereas higher and lower levels of deuteration in the specified protein form are indicated by increasingly intense red and blue coloration, respectively. *A*, active full-length AfGcHK proteins with Fe(III)-CN⁻ (left) and Fe(II)-O₂ (center) heme complexes. *B*, inactive structures, including the full-length AfGcHK protein with an Fe(II) heme complex (left), the full-length heme-free (apo) H99A mutant (center), the isolated globin domain (top right), and the isolated kinase domain (bottom right). The globin domain structure is based on the X-ray crystal data (PDB code 5OHE) presented in this work, and the kinase domain was modeled as an asymmetric homodimer using subunits A and C of the sensor histidine kinase (HK853) from *Thermotoga maritima* (PDB code 3DGE). This approach was validated by experiments presented elsewhere (7).

sented as gray ribbons in the bottom left and central structures of Fig. 5A).

The HDX-MS patterns for the two inactive forms, the 5-coordinate Fe(II) complex and the H99A apo-mutant, differ significantly from those for the active forms. In particular, their globin domains have deuteration patterns very different from those of the active Fe(III)-OH⁻ form; the 5-coordinate Fe(II) complex is much less extensively deuterated on the heme-proximal side (helices H2, H3, and H5) but more strongly deuterated around the dimerization interface (helices H6 and H7) (see the top part of the left structure in Fig. 5B). On the other hand, the entire globin domain of the apo-form is completely deprotected (Fig. 5B, top part of the central structure). Interestingly, despite these differences in the globin domains, the kinase domains of the two inactive forms exhibit rather similar deuteration patterns, with sharply increased deuteration in helix H11(284–

296) (see the bottom parts of the left and central structures in Fig. 5B). Increases in the solvent accessibility and dynamic behavior of helix H11 were also identified as the major changes associated with domain separation and kinase inactivation (Fig. 5B, bottom right). This may indicate that this area is involved in intramolecular signal transduction. The deuteration patterns of the active and inactive forms of AfGcHK did not vary appreciably over the incubation times considered in this work.

Comparison of the full-length AfGcHK protein with its isolated globin and kinase domains based on HDX-MS data

We also compared the HDX-MS exchange profile of the Fe(III)-OH⁻ complex of the full-length AfGcHK protein with those of the isolated Fe(III)-OH⁻ globin domain and the isolated kinase domain (Fig. 8).

Protein structures of a heme-based oxygen sensor kinase AfGcHK

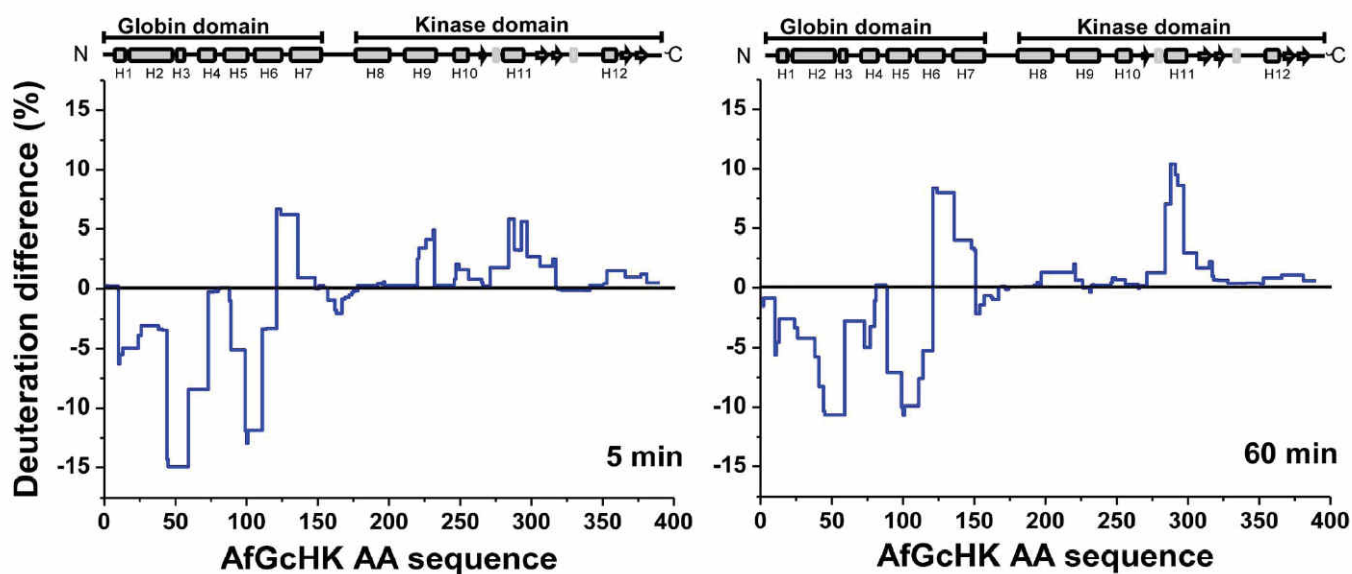


Figure 6. HDX-MS protection plots showing the differences in deuteration after 5 min (left) and 60 min (right) of exchange for the full-length Fe(III)-OH⁻ bound (active) and Fe(II)-bound (inactive) forms of AfGcHK. The deuteration levels of the active form were subtracted from those of the inactive form and plotted against the protein's sequence (x axis). The blue line thus represents the structural changes caused by reducing the heme iron center in the globin domain of the full-length protein.

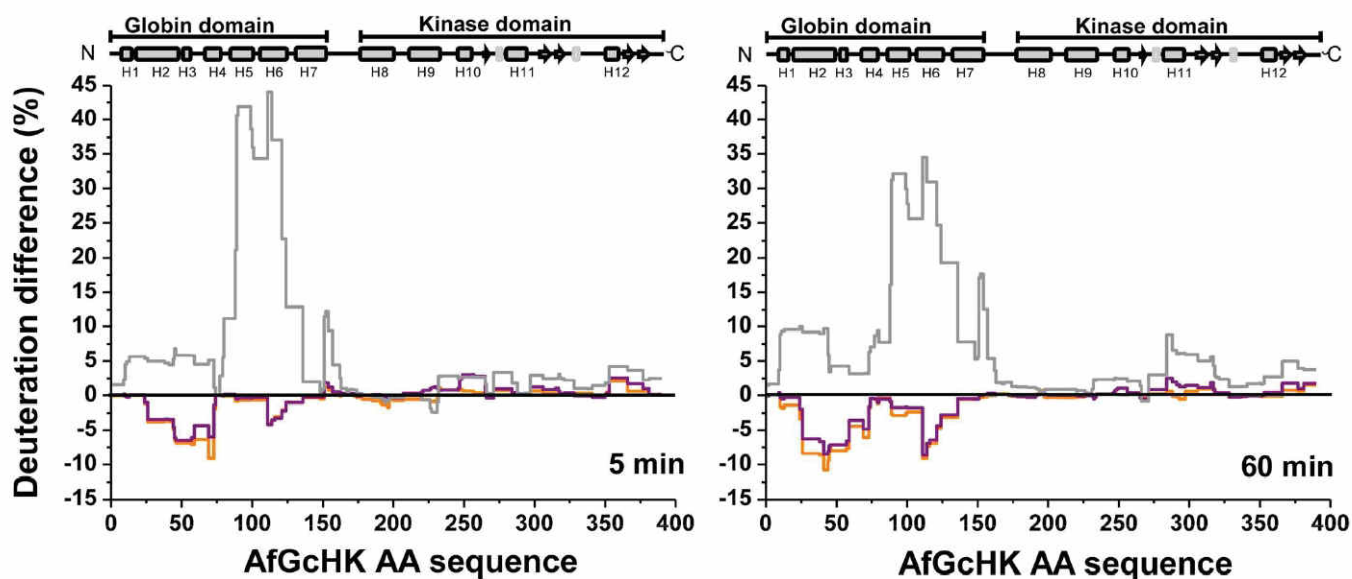


Figure 7. HDX-MS deuteration differences for the full-length active Fe(II)-O₂ (orange) and Fe(III)-CN (purple) forms of AfGcHK and the inactive full-length heme-free H99A mutant (gray) after 5 and 60 min of exchange. The deuteration differences for each form are computed relative to the deuteration of the full-length AfGcHK protein with the Fe(III)-OH⁻ heme complex.

The globin domain of the full-length protein is dimeric, and ultracentrifugation experiments showed that the isolated globin domain is too (Fig. 4). However, the absence of the covalently attached kinase domain increases the solvent accessibility of the globin domain contact interface (H6 and L7) in the isolated domain (Fig. 5B, top right structure). Interestingly, another region showing increased deuteration upon isolation of the globin domain was helix H5 on the heme-proximal side (shown in pink in the bottom parts of the top right structure in Fig. 5B; see also Fig. 8). This helix is in direct contact with both the heme and the C terminus of the globin domain, the latter of which is attached to the kinase domain via a short

linker. Therefore, H5 might be important in intraprotein signal transduction.

The separation of the kinase domain from the globin domain eliminates its autokinase activity, suggesting that the attachment of the globin domain in the full-length AfGcHK protein is required for the functioning of the kinase domain (supplemental Fig. S7). HDX-MS experiments indicated that the isolated kinase domain is more solvent-accessible than that in the full-length protein. The dark red ribbon in the bottom part of the right structure in Fig. 5B shows the significant structural destabilization of helix H11 (residues 284–292) associated with the isolation of the kinase domain in the full-length protein. The

Protein structures of a heme-based oxygen sensor kinase AfGcHK

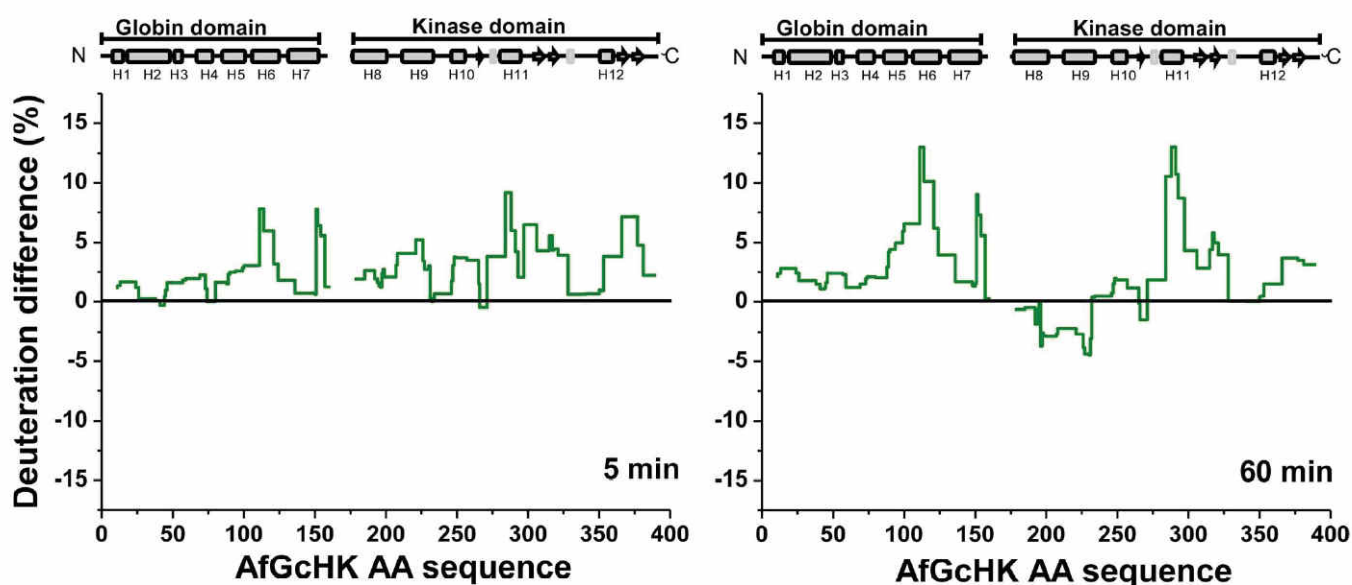


Figure 8. HDX–MS deuteration differences between the active full-length Fe(III)-OH[−] form of AfGcHK and a mixture of its isolated Fe(III)-OH[−]-bound globin domain with its isolated inactive kinase domain. Deuteration differences are shown for incubation times of 5 and 60 min lined in dark green, and the plotted values were obtained by subtracting the deuteration levels of the active full-length Fe(III)-OH[−] form from those for the isolated domains.

isolation of the kinase domain, which inactivates it, also affects helix H9, which is slightly deprotected over short deuteration times (Fig. 8) but moderately protected over longer deuteration times (see the *light blue ribbons* in the *bottom right structure* in Fig. 5B). Conversely, both incubation times make helix H11 more solvent-accessible. A slight increase in deuteration was also observed for the large β -sheet-forming solvent-exposed part of the ATP-binding subdomain (*pink arrows* in the *bottom right structure* in Fig. 5B).

The deuteration profiles of the isolated globin (Fig. 5B, *top right*) and kinase (Fig. 5B, *bottom right*) domains show several similarities to the inactive forms of the full-length protein (*i.e.* the 5-coordinate heme Fe(II) form and the H99A apo-form) (Figs. 5–8). Specifically, helices H6 and H11 behave similarly when the heme iron is reduced and when the domains are separated.

Characterization of the contact interface between the globin and kinase domains based on HDX–MS data for isolated domains and mixtures of isolated domains

HDX–MS can be used to map interaction interfaces between proteins or domains if they interact in a way that affects solvent accessibility and/or hydrogen bonding. However, as shown in [supplemental Fig. S8](#), the deuteration profiles of the isolated globin and kinase domains when measured in isolation (*dark green lines*) did not differ from those seen with an equimolar mixture of the two (*light green lines*). This implies that the domains are not in direct close contact with a clearly defined interaction interface. The absence of protection in a HDX–MS experiment does not necessarily mean the absence of a direct interaction; weak and/or transient interactions are not captured by this method (25–27). However, such weak interactions would probably not explain the efficient signal transduction between the sensor and kinase domains.

Discussion

Full-length heme-based gas sensor proteins are very difficult to crystallize. X-ray structures have been reported for a small full-length heme-based CO-sensing transcription activator, CooA (28, 29), but not for any full-length heme-based oxygen sensors. HDX–MS is a powerful complementary tool to crystallography for mapping the folding, interactions, and conformational changes of proteins in solution, including those that are not readily crystallized. For example, it was used to characterize significant conformational changes in the heme-based NO sensor soluble guanylate kinase induced by NO binding (30). In addition, we have previously studied the folding, interactions, and conformational changes of heme Fe(III) complexes of AfGcHK in the presence and absence of its response regulator partner protein (7). In this work, we determined the X-ray crystal structures of the isolated globin domain of AfGcHK with 6-coordinate Fe(III)-CN[−] and 5-coordinate Fe(II) complexes and compared these structures with conformational changes observed by HDX–MS.

X-ray structures of the AfGcHK globin domain in various forms

The X-ray structure of AfGcHK globin domain containing the Fe(III)-CN[−] complex (Fig. 2) revealed slight differences between the individual chains, mainly in the long loop (L3) connecting helices H3 and H4. This segment, which consists of residues Ala⁵⁷–Met⁷¹, has the highest absolute hydrogen/deuterium exchange level in both the isolated globin domain and the full-length AfGcHK protein, suggesting that it is very flexible and solvent-accessible. The large contact area observed between the two chains of the AfGcHK dimer supports the proposed physiological relevance of the dimerization of its globin domain, in keeping with the results of ultracentrifugation experiments (Fig. 4) and predictions based on earlier HDX–MS experiments (7). Moreover, all globin domains from homo-

Protein structures of a heme-based oxygen sensor kinase AfGcHK

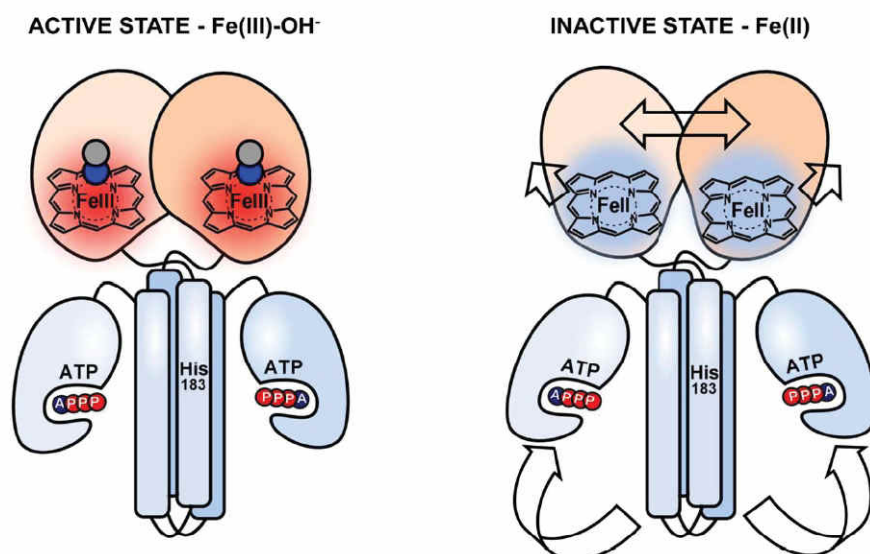


Figure 9. Proposed intramolecular signal transduction mechanism in the full-length AfGcHK protein that explains its catalytic inactivation upon heme reduction. Heme reduction induces conformational changes in the globin domain, simultaneously widening and splitting its internal dimeric interface, and making the initial residues of H7 accessible to the solvent. This signal is propagated down to the kinase domain via the linker, causing the ATP binding site to be separated from His¹⁸³, hindering the autophosphorylation of the latter residue. Data previously obtained by our group indicated that heme reduction increases the enzyme's K_m^{ATP} value and thus reduces the ATP affinity of the kinase domain (8).

logous GCS proteins with known structures form analogous dimers (16–18). The unique organization of the globin domain dimerization interface, with its flexible part I and tightly bound part II (see Fig. 2C), implies a high capacity for dynamic rearrangement (31). This is consistent with the HDX–MS data for active and inactive forms of the full-length AfGcHK protein (Figs. 5 (A and B), top parts in left structures), which suggest that the globin domain dimerization interface undergoes a “scissor” motion as the protein transitions between active and inactive forms (Fig. 9). A scissor-like dynamic motion was inferred for another oxygen sensor, EcDOS, based on the crystal structure of its dimeric isolated heme-bound PAS domain (11). A structural comparison of the isolated globin domains of AfGcHK with other GCSs is presented in the supplemental material.

Interestingly, reducing the heme iron in the crystallized Fe(III)-CN[−] form of the isolated globin domain induced a structural change (Fig. 3). The most significant changes were observed in chain G, in the chain with elevated temperature factors and weaker protein–protein contacts of the H3–L3 segment in the crystal. Surprisingly, only some heme iron molecules populating chain G were reduced upon soaking the original crystal in the dithionite solution, resulting in the observation of two different alternatives, A and B. Observations of alternative localization of protein atoms in crystal structures are common and can provide vital insights into how conformational changes enable proteins to function (32). Alternative A is consistent with the original atomic coordinates of the chains in the 6-coordinate Fe(III)-CN[−] structure, whereas alternative B represents the reduced state of the heme complex. Because this change occurred under strongly reducing conditions and the heme of the B alternative lacks a distal ligand, we conclude that the heme in chain G was partially reduced to form a 5-coordinate Fe(II) complex. Therefore, the two alternatives represent globin domain structures associated with one active form (Fe(III)-CN[−] complex) and one inactive form (Fe(II) complex).

The most important result is the observation that the heme and a significant part of the protein chain G and minor part of the protein chain H are shifted in the case of the heme iron reduction. There is thus a clear structural difference between the globin domains associated with the active and inactive forms. Conversely, Tarnawski *et al.* (16) found that heme iron reduction had no significant structural effect on the isolated globin domain of YddV from *Escherichia coli* (PDB entries 4ZVA and 4ZVB). They reached this conclusion by preparing two different crystals and superimposing their structures, whereas we prepared a single protein crystal containing AfGcHK in a mixture of two states. In our case, the four dimers in the asymmetric unit formed luckily a scaffold in which it is possible to see larger changes in one of the dimers without destroying the crystal. If all of the protein chains of this asymmetric crystal underwent similar reduction-induced changes, it would probably cause major structural changes in the crystal lattice; indeed, prolonged soaking in the dithionite solution led to macroscopic crystal reshaping. Based on the consistent experimental results for crystals soaked in the strong reducing agent and the adverse effects of long soaking times, we suggest that the concurrent observation of both states in the crystal was only possible because the heme of chain G in the asymmetric crystal reacts more rapidly than the hemes of the other chains.

Signal transduction in the full-length AfGcHK protein observed by HDX–MS

For the first time, we have observed conformational changes associated with signal transduction in a full-length heme-containing sensor protein. All known active forms of the full-length AfGcHK protein, namely the Fe(III)-CN[−], Fe(III)-OH[−] and Fe(II)-O₂-containing forms, exhibit very similar dynamic behavior and solvent accessibility, unlike the inactive Fe(II)- and heme-free forms (Fig. 5). The most important differences between the active and inactive forms were found 1) near the

heme in the globin domain; 2) in the dimerization interface (helices H6 and H7) of the globin domain, where the end of helix H6, loop L7, and the beginning of helix H7 are more solvent-accessible in the inactive forms; and 3) in helices H11 and (to a lesser extent) H9 in the kinase domain, which undergo faster hydrogen/deuterium exchange after heme iron reduction or in the absence of heme. The faster hydrogen/deuterium exchange in H11 and H9 could be caused by their opening or an increase in the mobility of this region, which is consistent with the hypothesis that the distance between the helices increases in the inactive states. These changes are probably significant because the HDX-MS results for the three active forms were similar, as were those for the two inactive forms, especially with respect to the kinase domain. The HDX-MS data thus highlighted the key regions involved in the molecular signal transduction mechanism and important structural differences between the active and inactive forms.

We have previously shown that the heme Fe(III)-OH⁻, Fe(III)-CN⁻, and Fe(II)-O₂-bound forms of full-length AfGcHK are active, whereas heme-free and heme Fe(II)-bound forms are inactive (1, 8). Here we reported for the first time that the isolated kinase domain is inactive, and its His¹⁸³ residue is not autophosphorylated (supplemental Fig. S7). Importantly, the HDX-MS profile of the isolated kinase domain (and especially that of H11) is similar to that of the kinase domain joined to the “inactive” Fe(II)-bound and heme-free globin domains in full-length AfGcHK (Fig. 5B).

Mechanism of signal transduction in AfGcHK

Two mechanisms have been proposed to explain how the kinase domain's autophosphorylation activity could be altered in response to signaling from the globin domain. The first is based on steric hindrance, with autophosphorylation being suppressed by physically blocking the autophosphorylation site (33). A similar mechanism was proposed to explain signal transduction in gas sensors; the protein surface of the heme-bound globin domain was suggested to directly contact the protein surface of the kinase domain such that signals from the globin domain could directly modulate the kinase domain's activity (34). The second mechanism involves indirect regulation of the autophosphorylation activity, with no direct blocking (“touching”) of the phosphorylation site in the kinase domain (35). The data presented here for AfGcHK strongly support this mechanism; there does not seem to be any direct interaction between the globin and kinase domains, which are only connected by a 15-residue-long covalent linker peptide in the full-length protein (supplemental Fig. S8).

The indirect mechanism of AfGcHK signal transduction loosely resembles that proposed for transmembrane signal propagation in membrane-bound two-component systems (3–6), although AfGcHK is not a membrane-bound protein.

In terms of dynamics, AfGcHK can be regarded as an ensemble of molecules sampling at least two conformational states. The kinase domains in these states feature different mutual arrangements of segments, including helices H11 (the ATP-binding site) and H9. In one state, the orientation of the H11 and H9 segments supports autophosphorylation; in the other, these segments occupy catalytically unfavorable positions. We

suggest that the oxygen-binding signal is propagated from the heme to the kinase domain via the globin dimerization interface and the long helices (H8 and H9) that form the dimerization interface of the kinase domain. The short and structurally undetermined linker sequence connecting the globin and kinase domains may also play some role. On the contrary, there was no difference in its behavior under the studied conditions; therefore, its functional significance is currently unknown. Finally, the signal is propagated throughout the kinase domain, reorienting helices H11 and H9 in a way that impairs autophosphorylation and possibly ATP binding, as suggested by an increase in the domain's K_m^{ATP} value (8). This signal transduction process may involve a scissor-like motion as was discussed above or a larger-scale dynamic rearrangement of the globin domain that transfers the signal to the kinase domain (Fig. 9). The X-ray crystallography and HDX-MS experiments performed in this study provided complementary information on the functional and structural behavior of AfGcHK. For the first time, the conformational changes associated with signal transduction were studied in a full-length globin-coupled oxygen sensor protein and linked to directly observed structural changes in the globin domain. As such, this work represents an important step toward a deeper understanding of the mechanism of heme-containing sensor regulation.

Experimental procedures

Materials

Ampicillin was obtained from P-lab (Prague, Czech Republic). Isopropyl β -D-thiogalactopyranoside, hemin, and acrylamide were obtained from Sigma-Aldrich. Water, doubly distilled over quartz, was purified using a Milli-Q Plus system (EMD Millipore, Billerica, MA). All glassware used for sample preparation was conditioned in advance by standing for 24 h in 10% (v/v) HCl Suprapur (Merck, Darmstadt, Germany). Phos-tag was from the Phos-tag consortium, Wako Pure Chemical Industries (Osaka, Japan). All chemicals used were of the highest purity grade available from commercial sources and used without further purification.

Protein production and purification

Cloning, overexpression in *E. coli*, and purification of the full-length wild-type, Y45F, Y45L, Y45W, L68N, L68F, L68G, L68W, and H99A AfGcHK proteins were performed as described previously (1, 7, 8). Briefly, His-tagged AfGcHK was expressed in BL21(DE3) (Novagen, Madison, WI) harboring the pET21c(+) plasmid. Cell lysates containing the His-tagged AfGcHK were isolated by affinity chromatography on a TALON[®] metal affinity resin column (Clontech), followed by size-exclusion chromatography on a Superdex Increase 200 GL 10/300 column (GE Healthcare). Protein and heme concentrations were determined using the BCA assay (Sunrise Absorbance Reader, TECAN, Männedorf, Switzerland) and the pyridine hemochromogen assay, respectively (36). Purified proteins were >90% homogeneous, as confirmed by SDS-PAGE.

The isolated globin domain of AfGcHK was prepared as follows. 500 ml of TB medium containing 100 μ g/ml ampicillin was inoculated with 500 μ l of O/N BL21(DE3) cells containing the appropriate pET21c(+) plasmid. Cells were grown at 37 °C

Protein structures of a heme-based oxygen sensor kinase AfGcHK

for 5 h (220 rpm), and then the temperature was lowered to 18 °C (160 rpm), and protein expression was initiated by adding 0.1 mM isopropyl 1-thio- β -D-galactopyranoside followed by further shaking for 18 h. Cells were then harvested by centrifugation at 4 °C and 5000 \times g, and stored at -80 °C. The pellets were resuspended in 50 mM Tris, 150 mM NaCl, pH 8, containing 1 mM PMSF, 1 mM EDTA, and 0.2 mg/ml lysozyme. After sonication (10 \times 1 min), reconstitution with 300 μ M hemin for 20 min, and 70 min of centrifugation at 50,000 \times g, the supernatant was applied to a TALON[®] metal affinity resin column (Clontech), and the protein was eluted using 200 mM imidazole. The eluted protein was concentrated to a volume of 2 ml and desalted on Sephadex G10 column equilibrated with 20 mM Tris, 150 mM NaCl, pH 8. The protein was then diluted to 0.5 mg/ml, and the His tag was cleaved with the tobacco etch virus protease (final concentration 0.05 mg/ml, 48 h at 10 °C). The tobacco etch virus protease and uncleaved protein were removed using a TALON[®] metal affinity resin column, leaving the isolated protein in the flow-through fraction. Finally, size-exclusion chromatography was performed using a Superdex Increase 200 GL 10/300 column (GE Healthcare), and the final protein preparation was frozen in liquid nitrogen for further use. SDS-PAGE experiments showed that the purified isolated globin domain of AfGcHK was >99% homogeneous.

The isolated kinase domain (Δ 161) of AfGcHK was prepared as follows. 500 ml of TB medium containing 100 μ g/ml ampicillin was inoculated with 500 μ l of O/N BL21(DE3) cells containing the appropriate pET21c(+) plasmid. Cells were grown at 37 °C for 5 h (220 rpm), and then the temperature was lowered to 18 °C (160 rpm), and protein expression was initiated by adding 0.1 mM isopropyl 1-thio- β -D-galactopyranoside followed by further shaking for 18 h. Cells were harvested by centrifugation at 4 °C and 5000 \times g and stored at -80 °C. Pellets were resuspended in 50 mM Tris, 150 mM NaCl, pH 8, containing 1 mM PMSF, 1 mM EDTA, and 0.2 mg/ml lysozyme. After sonication (5 \times 1 min) and 70 min of centrifugation at 50,000 \times g, the supernatant was applied to a TALON[®] metal affinity resin column (Clontech), and the protein was eluted using 200 mM imidazole. The protein was concentrated to a volume of 0.5 ml, size-exclusion chromatography was performed on a Superdex 200 GL 10/300 column (GE Healthcare), and the final protein preparation was frozen in liquid nitrogen for further use. SDS-PAGE experiments showed that the purified isolated kinase domain of AfGcHK was >70% homogeneous.

Crystallization of the isolated AfGcHK globin domain

A 5.4 mg/ml solution of the AfGcHK globin domain with the Fe(III)-OH⁻ complex in 150 mM NaCl, 20 mM Tris, pH 8.0, was crystallized using the hanging-drop vapor diffusion method at 25 °C. The drops contained 2 μ l of protein and 1 μ l of reservoir. The reservoir contained 20.7% (w/v) PEG 3350, 0.1 M MMT buffer (DL-malic acid, MES, and Tris base in a molar ratio of 1:2:2), pH 6.7, 0.2 M MgCl₂, 10 mM KCN, and 7.5% (v/v) glycerol. This yielded red wedge block-shaped crystals with dimensions of up to 80 \times 80 \times 300 μ m. The crystals were vitrified in liquid nitrogen without any cryoprotection. Before vitrification, the dithionite-soaked crystal was soaked for 15 min in a maternal drop containing 0.2 μ l of added 100 mM sodium dithionite (giv-

ing a final dithionite concentration of ~10 mM). Soaking did not cause any visible changes in the crystal.

Diffraction data collection, structure determination, and refinement

Data for the crystal with the Fe(III)-CN⁻ complex were collected at the Helmholtz-Zentrum Berlin (Bessy II) on beamline 14.1 equipped with a Dectris Pilatus 6M detector at 100 K, using wavelength 0.918409 Å, detector distance 0.375 m, $\Delta\phi$ 0.1° per image, and exposure time 0.5 s. Data for the sodium dithionite-soaked crystal were collected at the synchrotron light source Petra III in Hamburg on beamline PX13 equipped with a Dectris Pilatus 6M detector at 100 K using wavelength 0.92010 Å, detector distance 0.369 m, $\Delta\phi$ 0.05° per image, and exposure time 0.1 s.

The diffraction images were processed using XDS (37) and scaled using AIMLESS from the CCP4 program package (38). Data processing statistics are presented in Table 1. The phase problem was solved by molecular replacement using the MORDA program (39) and the structure of the globin domain of the globin-coupled sensor from *G. sulfurreducens* (PDB code 2W31 (17)). Structures were refined using REFMAC5 with manual editing using COOT (40), with 5% of reflections used as the testing set (the R_{free} set). The last cycle of the refinement was performed using all reflections. Structure quality was checked using the validation tools implemented in MOLPROBITY (41) and COOT.

The atomic coordinates and structure factors have been deposited in the Protein Data Bank under the codes 5OHE (globin domain of AfGcHK with cyanide) and 5OHF (globin domain of AfGcHK with cyanide, partially reduced).

HDX-MS

HDX-MS experiments using samples of full-length wild type AfGcHK (80 μ M), the globin domain of AfGcHK (80 μ M), the kinase domain of AfGcHK (80 μ M), and a 1:1 mixture of the globin and kinase domains with a total protein concentration of 160 μ M were initiated by 10-fold dilution in a deuterated buffer containing 20 mM Tris-HCl (pD 7.6), 150 mM NaCl, 50 mM KCl, and 5 mM MgCl₂ at 20 °C. Solutions of AfGcHK with different heme iron ligands in the globin domain were prepared as follows: Fe(III)-CN⁻, 1-h incubation of the protein in 10 mM KCN solution and use of a deuterated buffer containing 10 mM KCN; Fe(II)-O₂, 2-min incubation of the protein in 10 mM sodium dithionite followed by desalting on a Sephadex G10 column equilibrated with 20 mM Tris and 150 mM NaCl, pH 8; Fe(II), prepared in an anaerobic glove box (Jacomex GP-Concept; oxygen concentration <1 ppm) by 2-min incubation of the protein in 10 mM sodium dithionite followed by desalting on a Sephadex G10 column equilibrated with degassed 20 mM Tris, 150 mM NaCl, pH 8, buffer. All solutions used in this experiment were thoroughly degassed and equilibrated in the anaerobic box, and UV-visible spectra were recorded throughout the procedure to ensure the exclusive presence of the Fe(II) form.

Aliquots (25 μ l) were taken after 0.5, 5, 20, 60, and 180 min of exchange. The exchange reaction in the aliquots was immediately quenched by adding 25 μ l of 1 M glycine (pH 2.3), and the

samples were then rapidly frozen in liquid nitrogen. HPLC-MS analysis of deuterated samples was performed using a high-performance liquid chromatograph (1200 Agilent Technologies, Waldbronn, Germany) connected to an ESI-FT-ICR mass spectrometer (15T solariX XR, Bruker Daltonics, Billerica, MA). The analysis was initiated by rapidly thawing the sample, followed by digestion on a pepsin column (66- μ l bed volume, flow rate 100 μ l min⁻¹). The resulting peptides were desalted online using a Peptide MicroTrap (MichromBioresources, Auburn, CA) and separated on a C18 reversed phase column (0.5 \times 50 mm; Jupiter, Phenomenex, Torrance, CA) using a linear gradient of 10–45% (v/v) solvent B over 7 min, where solvent A was 2% (v/v) acetonitrile with 0.4% (v/v) formic acid in water and solvent B was 95% (v/v) acetonitrile, 5% (v/v) water with 0.4% (v/v) formic acid. The injector and switching valve, pepsin column, peptide trap, and analytical column were placed in an ice box to minimize back-exchange. Peptide identification (mapping, HPLC-MS/MS) was done using the system described above, and MASCOT was used to compare the obtained MS/MS spectra with a database containing a sequence for AfGcHK. Deuterated data were processed using an in-house program called DeutEx,⁴ which records the average mass for each peptide at each time point and each condition studied and calculates the percentage of deuteration relative to the maximum achievable deuteration based on the number of exchangeable amide hydrogens in each peptide. The deuterium content of each peptide was reported as a percentage of the maximum achievable deuteration based on the number of exchangeable amide hydrogens in each peptide (42).

Mass spectrometric analysis of AfGcHK phosphorylation at His¹⁸³

The above-mentioned LC-MS setup designed for HDX-MS samples was also used to analyze the phosphorylation status of His¹⁸³ in the full-length AfGcHK and the isolated kinase domain. Extracted ion chromatograms for non-phosphorylated and phosphorylated peptides including His¹⁸³ were plotted in Data Analysis (Bruker Daltonics).

UV-visible spectroscopy and autoxidation rate estimation

Optical absorption spectral data were obtained using an HP 8453 UV-visible spectrophotometer (Agilent Technologies) at 20 °C under aerobic conditions as described previously (1). Proteins were diluted to 300 μ l in 20 mM Tris/Cl, 150 mM NaCl, pH 8. A dithiothreitol solution (2 M) was then added to a final concentration of 0.5 M, and the protein sample was reduced for 60 min; the reduction was monitored by UV-visible spectrophotometry. Excess dithiothreitol was removed using a Sephadex G-25 desalting chromatography column, and the eluate was placed in a cuvette and diluted such that its absorbance at 413 nm was around 0.8. Spectra were collected every 15 or 30 min (depending on the protein) for 48 h at 25 °C (supplemental Fig. S2). The k_{ox} value was calculated under the assumption of first order kinetics based on the time-dependent decrease of the α band (577–580 nm) absorbance.

Enzyme activity of the isolated kinase domain of AfGcHK

A reaction mixture containing 10 μ M full-length wild-type AfGcHK or its isolated kinase domain, 50 mM Tris-HCl, pH 8.0, 50 mM KCl, and 5 mM MgCl₂ was preincubated for 5 min at 20 °C, and then the reaction was initiated by adding 1 mM ATP at 20 °C. At designated times, the autophosphorylation reaction was terminated by adding 100- μ l aliquots of termination buffer (125 mM Tris-HCl, pH 6.8, 4% (w/v) SDS, 10% (v/v) 2-mercaptoethanol, 20% (v/v) glycerol, 0.004% (w/v) bromophenol blue). Samples of the quenched reaction mixtures were then loaded on a 10% (w/v) SDS-polyacrylamide gel containing 75 μ M Phos-tag acrylamide and 0.2 mM MnCl₂. Each lane was loaded with a quantity of quenched reaction mixture containing 0.5 μ g of AfGcHK. Phosphorylated proteins in the sample interacted with the Phos-tag manganese complex in the gel, reducing their mobility relative to phosphate-free proteins (1, 43, 44). After electrophoresis, the proteins were visualized by staining with Coomassie Brilliant Blue R350, and the stained gels were imaged using a Scanjet G3010 (HP) scanner. The protein loadings were then quantified by analyzing the scanned images using ImageJ.

Analytical ultracentrifugation

Sedimentation velocity experiments were performed using a ProteomeLab XL-I (Beckman Coulter, Brea, CA) analytical ultracentrifuge at loading concentrations of 6–15 μ M for the isolated globin domain of AfGcHK and the full-length protein, at 20 °C and a rotor speed of 36,000 rpm. All data were collected using absorbance optics at 411 nm (selective for hemoproteins). Data analysis was performed with the SEDFIT, SEDPHAT, and Gussi packages (45–47). Sedimentation velocity data were analyzed using a continuous sedimentation coefficient distribution model, $c(s)$. The resulting apparent sedimentation coefficients were used to compute sedimentation coefficients in water at 20 °C ($s_{20,w}$).

Author contributions—M. S. planned experiments, performed experiments and analyzed data; P. M. planned, performed and interpreted MS experiments; T. S., P. K., and J. B. designed, performed, and analyzed the crystallization, diffraction data collection, structure determination, and refinement experiments; V. F. performed experiments; V. M. performed and interpreted protein models and discussed and interpreted data; J. D. performed interpretation and validation of structures and contributed to the manuscript; A. L. provided technical assistance and contributed to the preparation of the figures; M. R. provided technical assistance; T. S. discussed and interpreted data; M. M. discussed and interpreted data and wrote the paper. All authors reviewed the results and approved the final version of the manuscript.

Acknowledgments—We are grateful to Dr. Kenichi Kitanishi and Dr. Ondrej Vanek for technical assistance during the early stages of this work.

References

1. Kitanishi, K., Kobayashi, K., Uchida, T., Ishimori, K., Igarashi, J., and Shimizu, T. (2011) Identification and functional and spectral characterization of a globin-coupled histidine kinase from *Anaeromyxobacter* sp. Fw109-5. *J. Biol. Chem.* **286**, 35522–35534.

⁴ D. Kavan, P. Man, and G. Kruppa, unpublished data.

Protein structures of a heme-based oxygen sensor kinase AfGcHK

- Martínková, M., Kitanishi, K., and Shimizu, T. (2013) Heme-based globin-coupled oxygen sensors: linking oxygen binding to functional regulation of diguanylate cyclase, histidine kinase, and methyl-accepting chemotaxis. *J. Biol. Chem.* **288**, 27702–27711
- Gushchin, I., Melnikov, I., Polovinkin, V., Ishchenko, A., Yuzhakova, A., Buslaev, P., Bourenkov, G., Grudin, S., Round, E., Balandin, T., Borshchevskiy, V., Willbold, D., Leonard, G., Büldt, G., Popov, A., and Gordeliy, V. (2017) Mechanism of transmembrane signaling by sensor histidine kinases. *Science* 10.1126/science.aah6345
- Abriata, L. A., Albanesi, D., Dal Peraro, M., and de Mendoza, D. (2017) Signal sensing and transduction by histidine kinases as unveiled through studies on a temperature sensor. *Acc. Chem. Res.* **50**, 1359–1366
- Willett, J. W., and Crosson, S. (2017) Atypical modes of bacterial histidine kinase signaling. *Mol. Microbiol.* **103**, 197–202
- Zschiedrich, C. P., Keidel, V., and Szurmant, H. (2016) Molecular mechanisms of two-component signal transduction. *J. Mol. Biol.* **428**, 3752–3775
- Stranova, M., Martínek, V., Man, P., Fojtiková, V., Kavan, D., Vaněk, O., Shimizu, T., and Martinkova, M. (2016) Structural characterization of the heme-based oxygen sensor, AfGcHK, its interactions with the cognate response regulator, and their combined mechanism of action in a bacterial two-component signaling system. *Proteins* **84**, 1375–1389
- Fojtiková, V., Stranova, M., Vos, M. H., Liebl, U., Hranicek, J., Kitanishi, K., Shimizu, T., and Martinkova, M. (2015) Kinetic analysis of a globin-coupled histidine kinase, AfGcHK: effects of the heme iron complex, response regulator, and metal cations on autophosphorylation activity. *Biochemistry* **54**, 5017–5029
- Gong, W., Hao, B., and Chan, M. K. (2000) New mechanistic insights from structural studies of the oxygen-sensing domain of *Bradyrhizobium japonicum* FixL. *Biochemistry* **39**, 3955–3962
- Hao, B., Isaza, C., Arndt, J., Soltis, M., and Chan, M. K. (2002) Structure-based mechanism of O₂ sensing and ligand discrimination by the FixL heme domain of *Bradyrhizobium japonicum*. *Biochemistry* **41**, 12952–12958
- Kurokawa, H., Lee, D.-S., Watanabe, M., Sagami, I., Mikami, B., Raman, C. S., and Shimizu, T. (2004) A redox-controlled molecular switch revealed by the crystal structure of a bacterial heme PAS sensor. *J. Biol. Chem.* **279**, 20186–20193
- Park, H., Suquet, C., Satterlee, J. D., and Kang, C. (2004) Insights into signal transduction involving PAS domain oxygen-sensing heme proteins from the X-ray crystal structure of *Escherichia coli* Dos heme domain (Ec DosH). *Biochemistry* **43**, 2738–2746
- Cho, H. Y., Cho, H. J., Kim, Y. M., Oh, J. I., and Kang, B. S. (2009) Structural insight into the heme-based redox sensing by DosS from *Mycobacterium tuberculosis*. *J. Biol. Chem.* **284**, 13057–13067
- Podust, L. M., Ioanoviciu, A., and Ortiz de Montellano, P. R. (2008) 2.3 Å X-ray structure of the heme-bound GAF domain of sensory histidine kinase DosT of *Mycobacterium tuberculosis*. *Biochemistry* **47**, 12523–12531
- Yukl, E. T., Ioanoviciu, A., Nakano, M. M., de Montellano, P. R., and Moënn-Loccoz, P. (2008) A distal tyrosine residue is required for ligand discrimination in DevS from *Mycobacterium tuberculosis*. *Biochemistry* **47**, 12532–12539
- Tarnawski, M., Barends, T. R. M., and Schlichting, I. (2015) Structural analysis of an oxygen-regulated diguanylate cyclase. *Acta Crystallogr. D* **71**, 2158–2177
- Pesce, A., Thijs, L., Nardini, M., Desmet, F., Sisinni, L., Gourlay, L., Bolli, A., Coletta, M., Van Doorslaer, S., Wan, X., Alam, M., Ascenzi, P., Moens, L., Bolognesi, M., and Dewilde, S. (2009) HisE11 and HisF8 provide bis-histidyl heme hexa-coordination in the globin domain of *Geobacter sulfurreducens* globin-coupled sensor. *J. Mol. Biol.* **386**, 246–260
- Zhang, W., and Phillips, G. N. (2003) Structure of the oxygen sensor in *Bacillus subtilis*: signal transduction of chemotaxis by control of symmetry. *Structure* **11**, 1097–1110
- Krissinel, E., and Henrick, K. (2004) Secondary-structure matching (SSM), a new tool for fast protein structure alignment in three dimensions. *Acta Crystallogr. D* **60**, 2256–2268
- Krissinel, E., and Henrick, K. (2007) Inference of macromolecular assemblies from crystalline state. *J. Mol. Biol.* **372**, 774–797
- Nakajima, K., Kitanishi, K., Kobayashi, K., Kobayashi, N., Igarashi, J., and Shimizu, T. (2012) Leu65 in the heme distal side is critical for the stability of the Fe(II)-O₂ complex of YddV, a globin-coupled oxygen sensor diguanylate cyclase. *J. Inorg. Biochem.* **108**, 163–170
- Zhang, W., Olson, J. S., and Phillips, G. N. (2005) Biophysical and kinetic characterization of HemAT, an aerotaxis receptor from *Bacillus subtilis*. *Biophys. J.* **88**, 2801–2814
- Aono, S., Kato, T., Matsuki, M., Nakajima, H., Ohta, T., Uchida, T., and Kitagawa, T. (2002) Resonance Raman and ligand binding studies of the oxygen-sensing signal transducer protein HemAT from *Bacillus subtilis*. *J. Biol. Chem.* **277**, 13528–13538
- Springer, B. A., Sligar, S. G., Olson, J. S., and Phillips, G. N. J. (1994) Mechanisms of ligand recognition in myoglobin. *Chem. Rev.* **94**, 699–714
- Engen, J. R. (2003) Analysis of protein complexes with hydrogen exchange and mass spectrometry. *Analyst* **128**, 623–628
- Kadek, A., Kavan, D., Marcoux, J., Stojko, J., Felice, A. K. G., Cianféroni, S., Ludwig, R., Halada, P., and Man, P. (2017) Interdomain electron transfer in cellobiose dehydrogenase is governed by surface electrostatics. *Biochim. Biophys. Acta* **1861**, 157–167
- Rezabkova, L., Man, P., Novak, P., Herman, P., Vecer, J., Obsilova, V., and Obsil, T. (2011) Structural basis for the 14-3-3 protein-dependent inhibition of the regulator of G protein signaling 3 (RGS3) function. *J. Biol. Chem.* **286**, 43527–43536
- Lanzilotta, W. N., Schuller, D. J., Thorsteinsson, M. V., Kerby, R. L., Roberts, G. P., and Poulos, T. L. (2000) Structure of the CO sensing transcription activator CooA. *Nat. Struct. Biol.* **7**, 876–880
- Komori, H., Inagaki, S., Yoshioka, S., Aono, S., and Higuchi, Y. (2007) Crystal structure of CO-sensing transcription activator CooA bound to exogenous ligand imidazole. *J. Mol. Biol.* **367**, 864–871
- Underbakke, E. S., Iavarone, A. T., Chalmers, M. J., Pascal, B. D., Novick, S., Griffin, P. R., and Marletta, M. A. (2014) Nitric oxide-induced conformational changes in soluble guanylate cyclase. *Structure* **22**, 602–611
- Skálová, T., Dohnálek, J., Spiwok, V., Lipovová, P., Vondráčková, E., Petroková, H., Dusková, J., Strnad, H., Králová, B., and Hasek, J. (2005) Cold-active β -galactosidase from *Arthrobacter* sp. C2-2 forms compact 660 kDa hexamers: crystal structure at 1.9 Å resolution. *J. Mol. Biol.* **353**, 282–294
- Keedy, D. A., Fraser, J. S., and van den Bedem, H. (2015) Exposing hidden alternative backbone conformations in X-ray crystallography using qFit. *PLoS Comput. Biol.* **11**, e1004507
- Cunningham, K. A., and Burkholder, W. F. (2009) The histidine kinase inhibitor Sda binds near the site of autophosphorylation and may sterically hinder autophosphorylation and phosphotransfer to Spo0F. *Mol. Microbiol.* **71**, 659–677
- Shimizu, T., Huang, D., Yan, F., Stranova, M., Bartosova, M., Fojtiková, V., and Martínková, M. (2015) Gaseous O₂, NO, and CO in signal transduction: structure and function relationships of heme-based gas sensors and heme-redox sensors. *Chem. Rev.* **115**, 6491–6533
- Rao, M., Herzik, M. A., Jr., Iavarone, A. T., and Marletta, M. A. (2017) Nitric oxide-induced conformational changes govern H-NOX and histidine kinase interaction and regulation in *Shewanella oneidensis*. *Biochemistry* **56**, 1274–1284
- Antonini, E., and Brunori, M. (1971) *Hemoglobin and myoglobin in their reactions with ligands*, North-Holland Publishing Co., Amsterdam, The Netherlands
- Kabsch, W. (2010) XDS. *Acta Crystallogr. D* **66**, 125–132
- Winn, M. D., Ballard, C. C., Cowtan, K. D., Dodson, E. J., Emsley, P., Evans, P. R., Keegan, R. M., Krissinel, E. B., Leslie, A. G. W., McCoy, A., McNicholas, S. J., Murshudov, G. N., Pannu, N. S., Potterton, E. A., Powell, H. R., et al. (2011) Overview of the CCP4 suite and current developments. *Acta Crystallogr. D* **67**, 235–242
- Vagin, A., and Lebedev, A. (2015) MoRDa, an automatic molecular replacement pipeline. *Acta Crystallogr. A* **71**, s19
- Emsley, P., Lohkamp, B., Scott, W. G., and Cowtan, K. (2010) Features and development of Coot. *Acta Crystallogr. D* **66**, 486–501
- Chen, V. B., Arendall, W. B., 3rd, Headd, J. J., Keedy, D. A., Immormino, R. M., Kapral, G. J., Murray, L. W., Richardson, J. S., and Richardson, D. C.

Protein structures of a heme-based oxygen sensor kinase AfGCHK

- (2010) MolProbity: all-atom structure validation for macromolecular crystallography. *Acta Crystallogr. D* **66**, 12–21
42. Trcka, F., Durech, M., Man, P., Hernychova, L., Muller, P., and Vojtesek, B. (2014) The assembly and intermolecular properties of the Hsp70-Tomm34-Hsp90 molecular chaperone complex. *J. Biol. Chem.* **289**, 9887–9901
43. Yamada, S., Nakamura, H., Kinoshita, E., Kinoshita-Kikuta, E., Koike, T., and Shiro, Y. (2007) Separation of a phosphorylated histidine protein using phosphate affinity polyacrylamide gel electrophoresis. *Anal. Biochem.* **360**, 160–162
44. Igarashi, J., Murase, M., Iizuka, A., Pichierrri, F., Martinkova, M., and Shimizu, T. (2008) Elucidation of the heme binding site of heme-regulated eukaryotic initiation factor 2 α kinase and the role of the regulatory motif in heme sensing by spectroscopic and catalytic studies of mutant proteins. *J. Biol. Chem.* **283**, 18782–18791
45. Houtman, J. C. D., Brown, P. H., Bowden, B., Yamaguchi, H., Appella, E., Samelson, L. E., and Schuck, P. (2007) Studying multisite binary and ternary protein interactions by global analysis of isothermal titration calorimetry data in SEDPHAT: application to adaptor protein complexes in cell signaling. *Protein Sci.* **16**, 30–42
46. Schuck, P. (2000) Size-distribution analysis of macromolecules by sedimentation velocity ultracentrifugation and Lamm equation modeling. *Biophys. J.* **78**, 1606–1619
47. Brautigam, C. A. (2015) Calculations and publication-quality illustrations for analytical ultracentrifugation data. *Methods Enzymol.* **562**, 109–133

4.2 Disruption of the dimerization interface of the sensing domain in the dimeric heme-based oxygen sensor AfGcHK abolishes bacterial signal transduction

Skalova, T.; Lengalova, A.; Dohnalek, J.; Harlos, K.; Mihalcin, P.; Kolenko, P.; Stranova, M.; Blaha, J.; Shimizu, T.; Martínková, M.: *J. Biol. Chem.* (2020) 295, 1587–1597 (IF₂₀₁₉ 4,1).

Podíl předkladatelky na této práci: 60 % (*exprese a purifikace mutantních forem proteinu AfGcHK, kinetické a oligomerizační analýzy, spektroskopická měření, vyhodnocení a zpracování výsledků, příprava schémat*) - jedná se o sdílené spoluautorství s Dr. Skálovou potvrzeno korespondujícím autorem, doc. RNDr. Markétou Martínkovou, Ph.D.



Disruption of the dimerization interface of the sensing domain in the dimeric heme-based oxygen sensor AfGcHK abolishes bacterial signal transduction

Received for publication, October 23, 2019, and in revised form, December 30, 2019. Published, Papers in Press, December 30, 2019, DOI 10.1074/jbc.RA119.011574

Tereza Skalova^{‡1}, Alzbeta Lengalova^{§1}, Jan Dohnalek[‡], Karl Harlos[¶], Peter Mihalcin[§], Petr Kolenko^{‡||}, Martin Stranava[§], Jan Blaha^{§2}, Toru Shimizu[§], and Markéta Martínková^{‡§3}

From the [‡]Institute of Biotechnology of the Czech Academy of Sciences, v.v.i., Biocev, Vestec, 252 50 Czech Republic, the [§]Department of Biochemistry, Faculty of Science, Charles University, Prague 2, 128 43 Czech Republic, the [¶]Division of Structural Biology, The Wellcome Trust Centre for Human Genetics, University of Oxford, OX3 7BN Oxford, United Kingdom, and the ^{||}FNSPE, Czech Technical University in Prague, Brehova 7, Prague 1, 115 19 Czech Republic

Edited by F. Peter Guengerich

The heme-based oxygen sensor protein AfGcHK is a globin-coupled histidine kinase in the soil bacterium *Anaeromyxobacter* sp. Fw109-5. Its C-terminal functional domain exhibits autophosphorylation activity induced by oxygen binding to the heme-Fe(II) complex located in the oxygen-sensing N-terminal globin domain. A detailed understanding of the signal transduction mechanisms in heme-containing sensor proteins remains elusive. Here, we investigated the role of the globin domain's dimerization interface in signal transduction in AfGcHK. We present a crystal structure of a monomeric imidazole-bound AfGcHK globin domain at 1.8 Å resolution, revealing that the helices of the WT globin dimer are under tension and suggesting that Tyr-15 plays a role in both this tension and the globin domain's dimerization. Biophysical experiments revealed that whereas the isolated WT globin domain is dimeric in solution, the Y15A and Y15G variants in which Tyr-15 is replaced with Ala or Gly, respectively, are monomeric. Additionally, we found that although the dimerization of the full-length protein is preserved via the kinase domain dimerization interface in all variants, full-length AfGcHK variants bearing the Y15A or Y15G substitutions lack enzymatic activity. The combined structural and biophysical results presented here indicate that Tyr-15 plays a key role in the dimerization of the globin domain of AfGcHK and that globin domain dimerization is essential for internal signal transduction and autophosphorylation in this

protein. These findings provide critical insights into the signal transduction mechanism of the histidine kinase AfGcHK from *Anaeromyxobacter*.

Heme complexes play essential roles in many important physiological processes, including oxygen transport and storage, electron transport, oxidative stress protection, and signaling. They are also vital components of heme-containing sensor proteins, a large group of biologically significant proteins that are represented in almost all living organisms and exhibits great functional diversity (1–6).

There is considerable interest in the structure-function relationships of heme-based oxygen sensors because the heme-iron complex serves as the signaling center (1, 7–14). Proteins of this type often act as one component of a two-component signal transduction system. These systems are associated with biofilm formation and virulence in certain pathogenic bacteria but also fulfil many other functions (15–18). The heme-based oxygen sensor AfGcHK⁴ is a globin-coupled histidine kinase from the soil bacterium *Anaeromyxobacter* sp. Fw109-5 (19). It has an N-terminal heme-bound globin domain and a C-terminal kinase domain. The binding of oxygen to a heme-Fe(II) complex in the oxygen-sensing globin domain induces autophosphorylation of its kinase domain via interdomain signal transduction (19). AfGcHK proteins containing a heme-Fe(II)-O₂ complex or an Fe(III)-OH⁻ complex formed by autoxidation are both enzymatically fully active (20). The *k*_{cat} values of the heme-Fe(II)-O₂ and Fe(III)-OH⁻-bound AfGcHK forms were

This work was supported in part by the grant agency of Charles University in Prague Grant 704217, Charles University Grant SVV260427/2018, ERDF fund Projects CZ.1.05/1.1.00/02.0109, CZ.02.1.01/0.0/0.0/16_013/0001776, and CZ.02.1.01/0.0/0.0/15_003/0000447, and MEYS CR Grant CZ.02.1.01/0.0/0.0/16_019/0000778. The authors declare that they have no conflicts of interest with the contents of this article.

M. M. dedicates this paper to Professor Marie Stiborová of the Dept. of Biochemistry at Charles University on the occasion of her 70th birthday, in recognition of her devotion to science and people.

This article contains Figs. S1–S4 and Tables S1 and S2.

The atomic coordinates and structure factors (code 6OTD) have been deposited in the Protein Data Bank (<http://www.pdb.org/>).

Diffraction data (code 715) have been deposited in the SBCGrid Data Bank (doi:10.15785/SBCGRID/715).

¹ Both authors contributed equally to this work.

² Present address: EMBL Hamburg, c/o DESY, Bldg. 25A, Notkestraße 85, Hamburg, 226 03 Germany.

³ To whom correspondence should be addressed. Tel.: 420-221951242; Fax: 420-221951283; E-mail: marketa.martinkova@natur.cuni.cz.

⁴ The abbreviations used are: AfGcHK, globin-coupled histidine kinase from the soil bacterium *Anaeromyxobacter* sp. Fw109-5; AvGReg, *Azotobacter vinelandii* globin-coupled oxygen sensor; BpeGReg, globin-coupled oxygen sensor with diguanylate cyclase activity from *Bordetella pertussis*; CusS, *E. coli* copper and silver ions sensor; DevS (DosS), heme-based oxygen sensor protein from *Mycobacterium tuberculosis*; EcDOS or EcDosP, heme-based oxygen sensor phosphodiesterase; HDX-MS, hydrogen deuterium exchange coupled with mass spectrometry; HemAT, globin-coupled oxygen sensor from *B. subtilis*; heme-Fe(II), Fe(II)-protoporphyrin IX complex; heme-Fe(III), Fe(III)-protoporphyrin IX complex or hemin; MPD, 2-methyl-2,4-pentanediol; PccGCS, globin-coupled oxygen sensor with diguanylate cyclase activity from *P. carotovorum*; PDB, Protein Data Bank; TEV, tobacco etch virus; YddV, globin-coupled oxygen sensor diguanylate cyclase from *E. coli*; RMSD, root mean square deviation.

Dimerization of heme-based oxygen sensor kinase AfGcHK

1.0–1.1 min⁻¹, and their K_m^{ATP} values were 18.9–23.0 μM (Table S1). However, the form with an Fe(II)-CO-heme complex had a k_{cat} of 1.0 min⁻¹ but a very high K_m^{ATP} of 357 μM . This high K_m^{ATP} suggests that in addition to causing pronounced changes in the structure of the sensing site, CO coordination dramatically altered the structure of the kinase domain (20). The inactive AfGcHK forms either contain a heme-Fe(II) complex, lack the heme complex altogether (20), or lack the whole sensing domain (21).

Several studies have investigated the structure-function relationships of AfGcHK (19–22). As a result, the X-ray crystal structure of the isolated AfGcHK globin domain dimer has been solved and the full-length protein has been studied by hydrogen-deuterium exchange coupled with MS (HDX-MS) (21). These studies have revealed that changes in the heme redox state and axial ligand binding to the heme-iron complex induce large changes in the protein's structure in the vicinity of the heme, which in turn cause profound structural changes in the wider protein. It was suggested that these structural changes occur primarily within the dimerization interface of the globin domain and are linked to the regulation of the kinase domain's catalytic activity (21). Here, we present X-ray crystallographic investigations and a thorough biophysical analysis including a kinase activity study that were conducted to determine how the oligomerization state of the globin (sensing) domain affects the autophosphorylation activity of AfGcHK. The crystal structure of the monomeric sensing domain co-crystallized with imidazole was solved, and inspection of this structure suggested that Tyr-15 is involved in the domain dimerization process and also forms important contacts with the neighboring heme group. Therefore, the oligomeric states and functions of Tyr-15 mutant proteins were investigated. Based on the results of these investigations, we suggest that the interaction of Tyr-15 with the heme-binding pocket of the neighboring globin domain in the AfGcHK dimer is critical for the sensing domain's dimerization, and that the sensing domain's dimerization is required to enable signal transduction between the sensing and functional domains and the functional domain's autophosphorylation activity.

Results

Crystal structure of the monomeric imidazole-bound globin domain of AfGcHK

Overall crystal structure of the AfGcHK globin domain

A new crystal structure of the globin (sensing) domain of AfGcHK in the presence of imidazole was solved at a resolution of 1.8 Å (Fig. 1 and Table 1). The globin domain is monomeric in this structure. It has a globin-fold and consists of seven helices and seven loops. Additionally, it contains a heme molecule and three small ligands: two imidazole molecules and one molecule of 2-methyl-2,4-pentanediol (MPD). The MPD molecule (which originates from the crystallization solution) is bound at a crystal contact of two protein molecules, forming hydrogen bonds to Glu-62 and Arg-139 residues from neighboring protein chains; it has no biological significance. The binding of imidazole (also originating from the crystallization solution) is discussed in detail below. The data processing and

structure refinement parameters are shown in Table 1. All residues of the protein chain fit well to the observed electron density. 98.1% of the residues lie in the favored regions of the Ramachandran plot and there are no outliers. The atomic coordinates and structure factors have been deposited in the Protein Data Bank (PDB) under the code 6OTD.

The heme-binding pocket contains two imidazole molecules

The heme is located in its standard position and interacts directly with His-99 on the proximal side (Fig. 1A). On the distal side, an imidazole molecule (IMD203) occupies a typical ligand-binding position, binding to the heme-iron via N3; the Fe-N3 distance is 2.2 Å. The imidazole nitrogen N1 forms a hydrogen bond with the main chain carbonyl group of Leu-68 (2.7 Å). The His-67 side chain projects toward the heme molecule and forms a hydrogen bond to its propionate group (ND1 of His-67 and O2D of the heme are within a distance of 2.7 Å), making the heme inaccessible to the bulk solvent. This propionate group also makes a crystal contact with Phe-110 of an adjacent protein molecule. The heme's second propionate group makes a crystal contact with Arg-158, the last localized residue at the C terminus of the same crystal mate.

Another imidazole molecule (IMD204) is bound approximately in the plane of the heme (Fig. 1A), with a distance of 4.1 Å between the imidazole's C2 carbon and the heme's CMC carbon. This is the position occupied by Tyr-15 from the neighboring chain in the dimeric globin structure (Fig. 1B) (21). IMD204 is positioned in a small cavity with direct access to the solvent; there is no protein-protein crystal contact in this area of monomeric protein. Although the first imidazole molecule, IMD203, is well-localized in the electron density, IMD204 is relatively free within its cavity and forms no hydrogen bonds, so it is much less well-localized. Its position was therefore verified by generating a Polder map (Fig. S1) (23).

Structural differences between the monomeric imidazole-bound AfGcHK globin domain (6OTD) and the previously solved dimeric structures (5OHE and 5OHF)

Two crystal structures of the AfGcHK globin domain (PDB codes 5OHE and 5OHF) have been solved previously (21). Here we compare these structures to the new one (PDB code 6OTD). To this end, the globin domains (6OTD chain A, 5OHE chain G, and 5OHF chain G) were superimposed on the four nitrogen atoms of their heme groups. Structure 5OHE represents a dimeric CN-bound Fe(III) form of the AfGcHK globin domain, whereas structure 5OHF (in which chains G and H comprise the dimerization interface and exist in an alternative "B" configuration, denoted here as 5OHF-ligand-free) represents a dimeric form of the AfGcHK globin domain in the inactive state caused by treatment with sodium dithionite (21).

Comparison of monomeric imidazole-bound and dimeric CN-bound [Fe(III)-CN] forms

The monomeric imidazole-bound structure has some unique structural features including relaxation of the dimer-forming helices (due to its monomeric form), a more accessible heme, and differences in the architecture of the heme-binding site (Fig. 1B).

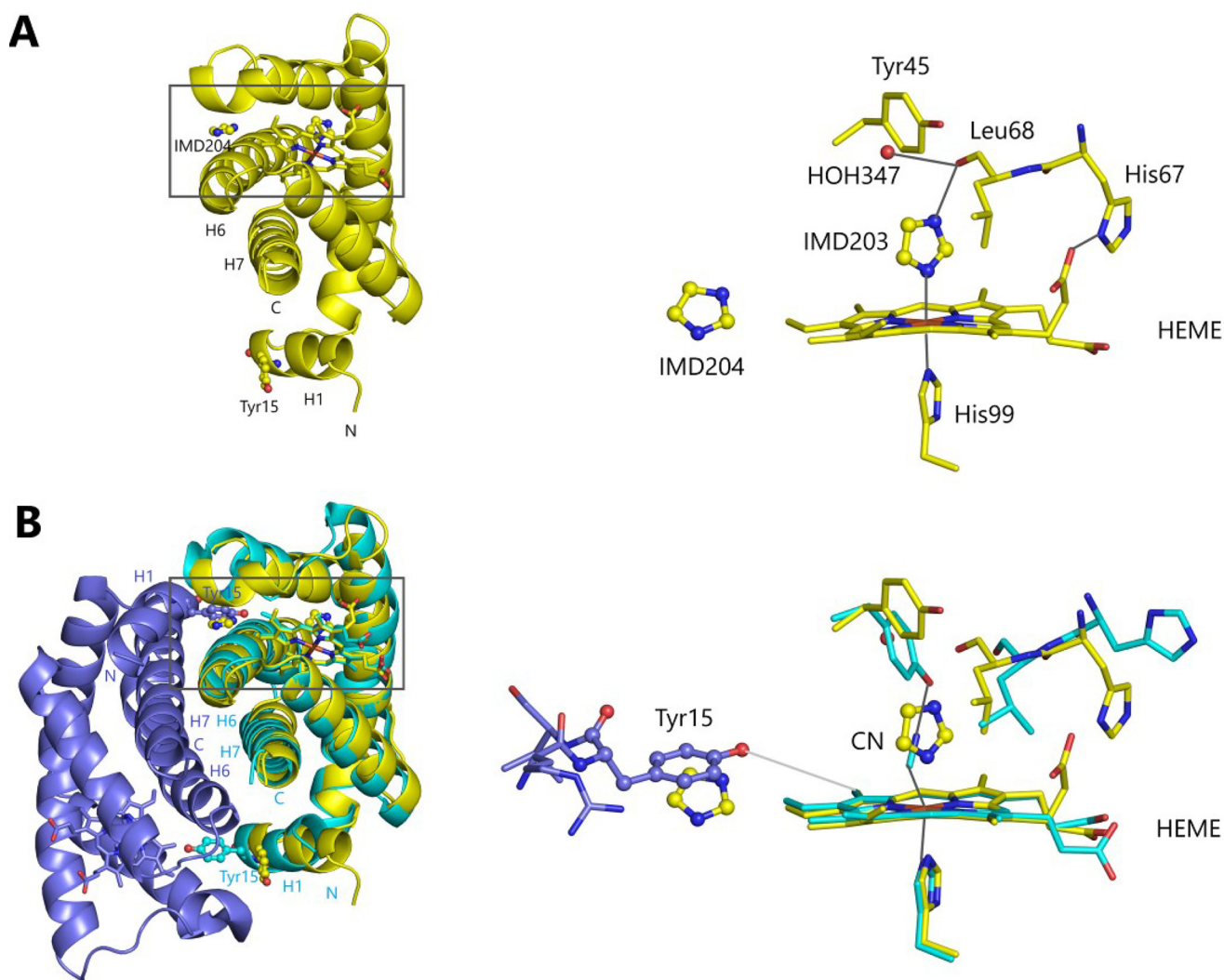


Figure 1. *A*, structure of the monomeric imidazole-bound AfGCHK globin domain (yellow chain, PDB code 6OTD) and *B*, a comparison of the imidazole-bound AfGCHK globin domain (yellow) to its dimeric cyanide-bound counterpart (cyan and dark blue; PDB code 5OHE, chains G and H). The rectangular boxes in the left-hand images enclose the heme-binding pockets, which are shown in expanded form in the right-hand images. The Tyr-15 residues (two in the dimeric complex and one in the monomer) and the two bound imidazole molecules (in the monomeric case only) are shown in ball-and-stick form. Helices H1, H6, and H7, which form the globin domain dimerization interface, are labeled. The chain termini are labeled N and C. The kinase domain of the full-length protein (not shown in the figure) would be located in front of the C terminus of helix H7.

The monomer's helices are relaxed—In the dimer (5OHE), Tyr-15 is immersed in the second chain's heme-binding cavity. This enables the residue to form part of the heme pocket and to protect the heme's equatorial region against interactions with the solvent, but requires the residue to adopt another conformation in which the torsion angle χ_1 is -165° . As a result, the position of the Tyr-15 C α is shifted by 2.5 Å relative to that in the monomeric structure, creating tension in the helix (H1) containing this residue. Conversely, in the monomeric structure 6OTD, the Tyr-15 side chain adopts the most common rotamer ($\chi_1 = -65^\circ$) and helix H1 is straight and relaxed. Similar behavior is seen for the two long helices H6 and H7, which form the main part of the dimerization interface: both are straightened up and relaxed in the monomeric structure (Fig. 2).

The monomer has a new access tunnel—In the monomeric globin domain, the absence of Tyr-15 from a neighboring chain opens a new access tunnel to the heme pocket. This makes the

heme more accessible to solvent molecules and oxygen, which is probably why the monomeric mutants Y15A and Y15G have high autoxidation rates (see below). In the monomeric crystal structure, this tunnel is occupied by the imidazole molecule IMD204, which is bound about 1 Å closer to the heme plane than the aromatic ring of Tyr-15 in the dimer.

Changes in the 6OTD heme-binding pocket—The Tyr-45 χ_1 angles of the monomer and dimer differ by 113° (Fig. 1B). In the monomer, the bulky imidazole molecule IMD203 binds to the heme distal side, pushing away the side chain of Tyr-45, which forms a hydrogen bond to the cyanide ligand in the dimeric structure (21). No such hydrogen bond exists between Tyr-45 and IMD203 in the monomeric structure, which is unsurprising because Tyr-45 interacts with the signal molecule O₂ (19) and other small heme ligands; imidazole is much bulkier than these species. The space occupied by the Tyr-45 side chain in the dimeric structure is in the monomeric structure occupied by water (HOH347) and partially by Leu-68, which relaxes into a

Dimerization of heme-based oxygen sensor kinase AfGcHK

Table 1

Data collection statistics and structure refinement parameters for the isolated AfGcHK globin domain

Values in parentheses refer to the highest resolution shell.

Data processing statistics	
Space group	P6 ₁ 22
Unit cell parameters <i>a</i> , <i>b</i> , <i>c</i> (Å)	69.4, 69.4, 113.4
Resolution range (Å)	41.25–1.80 (1.84–1.80)
No. of observations	213,525 (12,820)
No. of unique reflections	15,414 (902)
Data completeness (%)	99.2 (99.9)
Average redundancy	13.9 (14.2)
Mosaicity (°)	0.2
Average <i>I</i> / σ (<i>I</i>)	18.3 (2.0)
Solvent content (%)	43
Matthews coefficient (Å ³ /Da)	2.2
<i>R</i> _{merge} [†]	0.073 (1.320)
<i>R</i> _{pim} [§]	0.028 (0.506)
<i>CC</i> _{1/2}	0.999 (0.703)
Structure refinement parameters	
<i>R</i> _{work} [‡]	0.182
<i>R</i> _{free}	0.231
<i>R</i> _{all}	0.186
Average <i>B</i> -factor (Å ²)	35
RMSD bond lengths from ideal (Å)	0.017
RMSD bond angles from ideal (°)	1.7
Number of non-hydrogen atoms	1,404
Number of water molecules	68
Ramachandran statistics: residues in favored region (%)	98.1
PDB code	6OTD

[†] $R_{\text{merge}} = \frac{\sum_h \sum_i |I_{hi} - \langle I_h \rangle|}{\sum_h \sum_i I_{hi}}$
[§] $R_{\text{pim}} = \frac{\sum_h \sum_i (n_h - 1)^{-1/2} |I_{hi} - \langle I_h \rangle|}{\sum_h \sum_i I_{hi}}$ and
[‡] $R = \frac{\sum_n |F_{h,\text{obs}} - |F_{h,\text{calc}}||}{\sum_n |F_{h,\text{obs}}|}$, where I_{hi} is the observed intensity, $\langle I_h \rangle$ is the mean intensity of multiple observations of symmetry-related reflections, and $F_{h,\text{obs}}$ and $F_{h,\text{calc}}$ are the observed and calculated structure factor amplitudes. R_{work} is the *R* factor calculated on 95% of reflections excluding a random subset of 5% of reflections marked as “free”. The final structure refinement was performed on all observed structure factors.

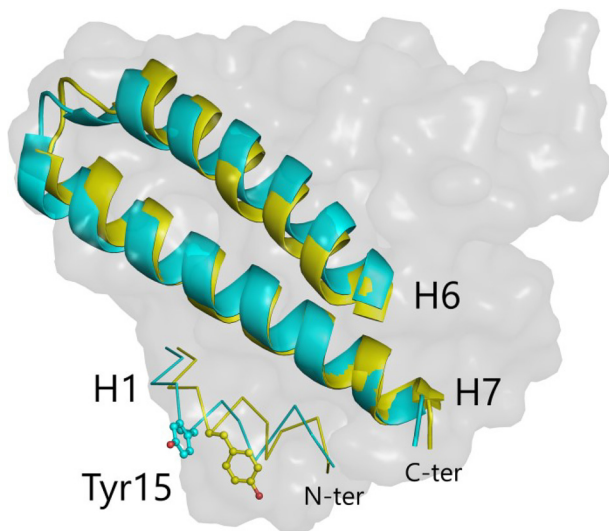


Figure 2. Changes in the conformations of helices H1, H6, and H7 (which form the AfGcHK globin domain dimerization interface) after the break of the dimer. The monomer (6OTD) is shown in yellow, the corresponding parts of the dimer (5OHE) are shown in cyan, and the surface of the remaining part of the monomer is shown in gray.

position closer to the axis above the heme center. This allows its main chain carbonyl oxygen to form hydrogen bonds with imidazole IMD203 (2.7 Å) and HOH347 (3.1 Å). In concert with the shift of Leu-68, His-67 changes its position and also changes its side chain rotamer (resulting in a χ_1 difference of 115°), forming a hydrogen bond with one of the heme’s propionate groups (Fig. 1A).

Comparison of monomeric imidazole-bound and dimeric ligand-free [Fe(II)] forms

Overall protein structure—The conformations of the distal helices of the globin domain in 5OHF ligand-free, which lacks an axial heme ligand, differ from those in the ligand-bound (CN[−] or imidazole) domains. The largest shift is observed for helix H2 (residues 20–50), which is located in similar positions in the CN[−] and imidazole-bound structures but is shifted away from the heme in the inactive ligand-free protein.

Heme-binding pocket—The fine structure of the heme-binding pocket primarily depends on the volume of the heme distal ligand. Therefore, the architecture of the active CN-bound state represents something of an intermediate between those of the imidazole-bound monomer (6OTD) and the ligand-free dimer (5OHF-ligand-free).

The effect of Tyr-15 on the oligomeric state of full-length AfGcHK and the isolated globin domain

Because the crystal structure of the Fe(III)-imidazole complex of the isolated monomeric globin domain of AfGcHK showed that Tyr-15 plays an important role in the protein’s architecture, we prepared Tyr-15 mutants (Y15A, Y15G, Y15F, and Y15W) of both the full-length protein and the isolated globin domain, and performed detailed functional (biophysical) studies on them.

Oligomeric state of WT and mutant full-length AfGcHK

The WT full-length AfGcHK protein and the tested Tyr-15 mutants all had similar elution volumes (from 13.2 to 13.4 ml, respectively) during size exclusion chromatography on a Superdex 200 Increase 10/300 GL column (Fig. 3A). The theoretical molecular mass of full-length AfGcHK in monomeric, dimeric, and tetrameric forms is 43, 86, and 172 kDa, respectively. Calibration experiments indicated that the column would clearly separate protein complexes of these masses (Fig. S2). The experiments confirmed that the full-length AfGcHK WT exists as a dimer in solution (Table 2) and showed that all the tested Tyr-15 mutants of the full-length AfGcHK protein are also dimeric (Table 2).

Oligomeric state of WT and mutant isolated globin domains of AfGcHK

The size exclusion elution volumes of the isolated globin domains of WT AfGcHK and the tested Tyr-15 mutants varied significantly, ranging from 16.0 to 17.3 ml (Fig. 3B). The theoretical molecular mass of the isolated globin domain of AfGcHK in the monomeric, dimeric, and tetrameric forms is 19, 38, and 76 kDa, respectively. Calibration experiments indicated that the column would clearly separate protein complexes of these masses (Fig. S2). The results confirmed that the isolated WT globin domain of AfGcHK forms a dimer in solution (Table 2), and demonstrated that the Y15F and Y15W mutants behave in the same way. Conversely, the Y15A and Y15G mutants of the isolated globin domain exist as monomers in solution (Figs. 3B and Table 2).

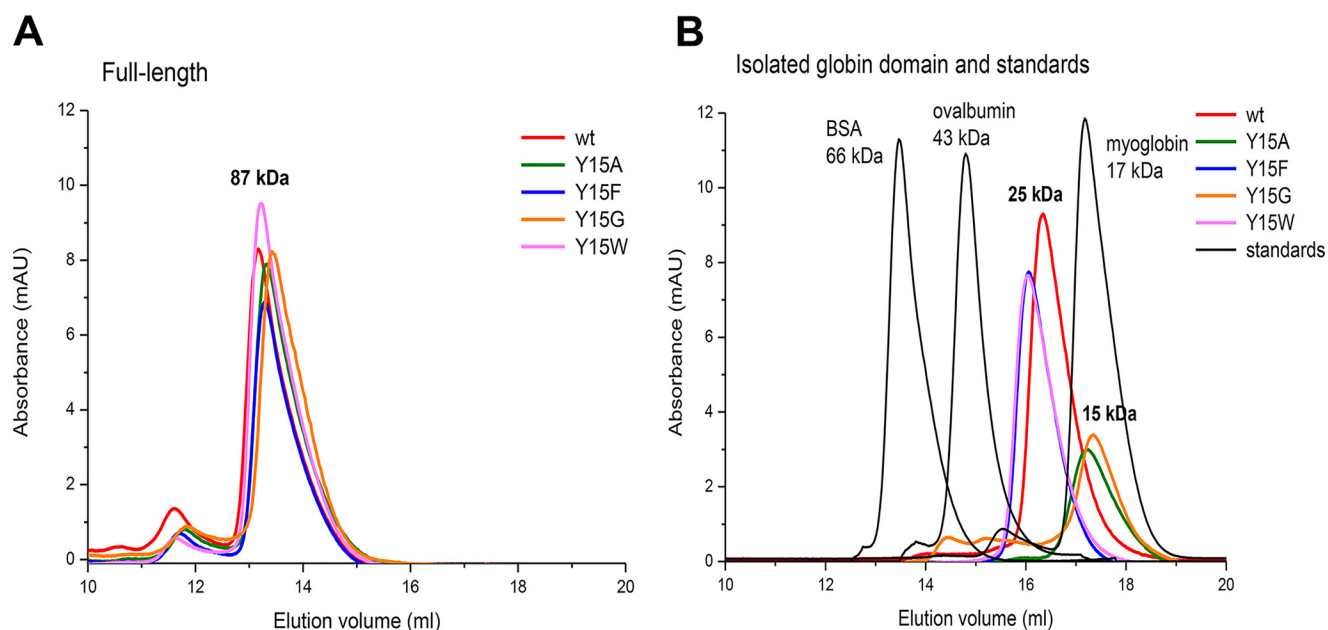


Figure 3. Oligomeric states of the WT and Tyr-15 mutant forms of the full-length AfGCHK protein and the isolated globin domain. A, size exclusion chromatography results for the full-length WT protein (red line) and its Y15A (green line), Y15F (blue line), Y15G (orange line), and Y15W (pink line) mutants at a concentration of 10 μM in 20 mM Tris-HCl, 150 mM NaCl, pH 8.0 (for further details, see “Experimental procedures”). B, size exclusion chromatography results for the isolated globin domain of WT AfGCHK (red line) and its Y15A (green line), Y15F (blue line), Y15G (orange line), and Y15W (pink line) mutants with overlaid calibration profiles of the standards BSA, ovalbumin and myoglobin (black lines) at 10 μM in 20 mM Tris-HCl, 150 mM NaCl, pH 8.0 (for further details, see “Experimental procedures”).

Table 2

Oligomeric states of the full-length AfGCHK protein and its isolated globin domain in their WT and Tyr-15 mutant forms

	Elution volume	Molecular mass calculated from calibration curve	Molecular mass, one protein chain according to AA sequence	Estimated oligomerization state
	<i>ml</i>	<i>kDa</i>		
AfGCHK full-length				
WT	13.2	91	43	Dimer
Y15A	13.3	87	43	Dimer
Y15F	13.3	87	43	Dimer
Y15G	13.4	83	43	Dimer
Y15W	13.2	91	43	Dimer
AfGCHK-isolated globin domain				
WT	16.3	23	19	Dimer
Y15A	17.2	15	19	Monomer
Y15F	16.1	25	19	Dimer
Y15G	17.3	15	19	Monomer
Y15W	16.0	26	19	Dimer

The effect of Tyr-15 on the heme axial environment of full-length AfGCHK and its isolated globin domain

UV-visible spectroscopy was used to study the effect of Tyr-15 on the heme axial environment of full-length AfGCHK and its isolated globin domain. Both the full-length proteins and the isolated globin domains of the Y15A and Y15G mutants in the Fe(II)-O₂ form exhibited very high autoxidation rates (>10 min⁻¹), making it impossible to obtain clear spectra of these species. Remarkably, the autoxidation rates of the full-length Y15A and Y15G mutants were approximately twice those of the corresponding isolated globin domain mutants. However, the Y15A and Y15G mutations had little effect on the absorption bands in the spectra of the Fe(III)-OH⁻, Fe(II), and Fe(II)-CO complexes, causing minor changes that were most pronounced in the visible region (Table 3 and Fig. S3). The spectra of the Y15F and Y15W mutants were identical to those for the WT protein

independently of the coordination and redox state of the heme-iron center, indicating that replacing Tyr-15 with an aromatic amino acid (Phe or Trp) does not greatly change the heme binding environment of the full-length protein or the isolated globin domain (Table 3 and Fig. S3).

The effect of Tyr-15 on the enzyme activity of full-length AfGCHK

A detailed kinetic analysis of the full-length AfGCHK protein in its WT and mutant variants of their Fe(III)-OH⁻ forms (Table 4 and Fig. S4) showed that the Y15A and Y15G mutations completely abolish its catalytic activity. However, the *k*_{cat} values of the Y15F and Y15W mutants are comparable with that of the WT. Additionally, the *K*_m value of Y15W is comparable with that of the WT but that of Y15F is approximately twice as high (Table 4 and Fig. S4).

Dimerization of heme-based oxygen sensor kinase AfGCHK

Table 3

Wavelength of absorption maxima (nm) in the UV-visible spectra of the Fe(III)-OH⁻, Fe(II), Fe(II)-O₂, and Fe(II)-CO complexes of the full-length WT and mutant AfGCHK proteins, and the corresponding isolated globin domains

λ (nm)	Fe(III)-OH ⁻	Fe(II)	Fe(II)-O ₂	Fe(II)-CO
AfGCHK full-length				
WT ^a	411, 538 ^a	431, 559 ^a	413, 545, 580 ^a	420, 541, 565 ^a
WT	410, 539	430, 556	415, 545, 580	420, 544, 566
Y15A	410, 536	423, 557	- ^b	420, 533, 565
Y15F	410, 541	425, 550	415, 545, 580	420, 545, 572
Y15G	410, 536	428, 556	- ^b	420, 535, 566
Y15W	410, 537	425, 553	415, 545, 580	420, 544, 570
AfGCHK-isolated globin domain				
WT	410, 539	430, 554	415, 545, 580	420, 543, 565
Y15A	410, 535	430, 559	- ^b	420, 540, 565
Y15F	410, 540	430, 551	415, 545, 580	420, 544, 566
Y15G	410, 535	430, 560	- ^b	420, 535, 564
Y15W	410, 539	430, 550	415, 545, 580	420, 541, 566

^a As described in Ref. 19.

^b Fast autoxidation, the spectra of the full-length AfGCHK mutants indicated that the Fe(III)-OH⁻ form predominated, with the Fe(II)-O₂ species being only a minor component. Autoxidation was slower in the corresponding isolated globin domain mutants (autoxidation rate > 10 min⁻¹), so mixed spectra of the Fe(III)-OH⁻ and Fe(II)-O₂ forms were observed (Fig. S3). Note that both the Fe(II)-O₂ form of the full-length AfGCHK enzyme and its autoxidation product, the Fe(III)-OH⁻ form, are catalytically fully active (20) (Table S1).

Table 4

Kinetic analysis of the autophosphorylation activity of WT and mutant full-length AfGCHK

Protein in its native Fe(III)-OH ⁻ form	K_m^{ATP} μM	k_{cat} min^{-1}
WT ^a	18.9 ± 2.3 ^a	1.08 ± 0.03 ^a
Y15A	No enzyme activity	
Y15F	28.5 ± 3.9	0.94 ± 0.11
Y15G	No enzyme activity	
Y15W	18.7 ± 3.1	1.05 ± 0.03

^a As described in Ref. 20.

Discussion

The structural role of Tyr-15 in AfGCHK

In the previously reported structure (21) of the CN-bound Fe(III) form of the dimeric AfGCHK globin domain (PDB code 5OHE), the side chain of Tyr-15 from one chain of the globin dimer forms part of the neighboring chain's heme-binding pocket: the distance between the heme CMC carbon and the O of the Tyr-15 OH group is between 3.8 and 4.2 Å (21). The imidazole-bound globin domain in this work was monomeric (PDB code 6OTD). Because Tyr-15 has no neighboring chain to interact with in the monomer, it adopts a different side chain conformation and its main chain position is relaxed, leading to the relaxation of helices H1, H6, and H7 (Fig. 2). This drew our attention to Tyr-15's possible role in the globin domain dimerization interface. We therefore performed a detailed functional analysis of selected Tyr-15 mutants to determine how Tyr-15 affects the full-length protein's oligomerization, oxygen-sensing ability, and enzymatic activity.

Biophysical characterization of Tyr-15's role in AfGCHK

The isolated globin domain of WT AfGCHK is dimeric in solution. If Tyr-15 is replaced with an aromatic residue (phenylalanine or tryptophan), the globin domain still forms a dimer, although the size exclusion chromatography results suggest that these dimers are somewhat more bulky than the WT dimer (Table 2 and Fig. 3). Conversely, if Tyr-15 is replaced with a nonaromatic residue, as in the Y15A and Y15G mutants, the globin domain becomes monomeric in solution (Table 2 and Fig. 3B).

The globin domain variants that are monomeric in solution (Y15A and Y15G) exhibit much higher rates of autoxidation than those that form dimers (Table 3, Fig. S3). This is probably because the inability to form a dimer causes profound changes in protein structure near the heme group, destabilizing the Fe(II)-O₂ state. Additionally, as noted above, the absence of the aromatic amino acid from the neighboring chain in the monomers opens a new tunnel allowing water and oxygen to access the heme pocket. Note that both the Fe(II)-O₂ form of the full-length AfGCHK enzyme and its autoxidation product, the Fe(III)-OH⁻ form, are catalytically fully active (20) (Table S1). Therefore, the increased autoxidation rates of the nonaromatic Tyr-15 mutants cannot explain their loss of enzyme activity.

The biophysical characteristics of the full-length mutants are similar to those of the corresponding isolated globin domains other than with respect to their oligomeric states (Tables 2 and 3 and Fig. 3A). All the full-length Tyr-15 mutants form dimers, but it is reasonable to speculate that the globin domains of the full-length Y15A and Y15G mutants are dissociated in the same way as in the cases of the isolated globin domains. The preservation of the oligomeric state of the full-length mutants is understandable because the kinase domain's dimerization interface is probably larger than that of the globin domain (21, 22).

Finally, it should be noted that UV-visible spectroscopy indicated that the protein structural changes caused by replacing Tyr-15 with another aromatic residue did not significantly alter the heme environment (including the neighboring chain and the tethering protein structure linking the globin and functional domains), and that kinetic studies showed that the Y15F and Y15W mutations did not significantly affect the enzyme's full-length activity (Table 4, Fig. S4).

Dimerization interfaces in the structures of other heme-containing oxygen sensors

There are four heme-containing oxygen sensor proteins with heme-bound globin-folds (7, 10, 11, 13, 14) for which the structure of the sensing domain has been solved: a globin-coupled sensor from *Geobacter sulfurreducens* (PDB code 2W31) (24), the HemAT protein from *Bacillus subtilis* (PDB codes 1OR4

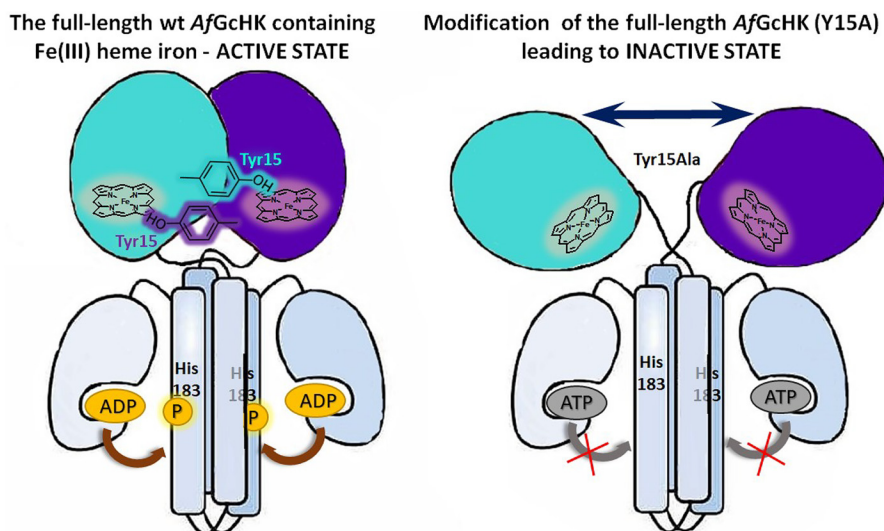


Figure 4. Schematic depiction of the deactivation of AfGcHK autophosphorylation by the disruption of globin domain dimerization induced by the Y15A mutation. When globin domain dimerization is prevented, the protein loses its capacity for signal transduction, making it enzymatically inactive.

and 1OR6) (25), the *Azotobacter vinelandii* globin-coupled oxygen sensor AvGReg (PDB code 4UII), and the *Escherichia coli* protein YddV or DosC (PDB codes 4ZVA–4ZVH) (26). All these globin domains are dimeric but none has an amino acid from one subunit that interacts as strongly with its partner subunit as does Tyr-15 in the AfGcHK globin domain dimer. Therefore, the results of the mutation experiments presented here are unlikely to be directly applicable to these proteins, and their dimerization interfaces may behave differently to that of AfGcHK.

Effect of imidazole binding in structures of similar proteins with globin-folds

Three-dimensional structural changes in globin domains and other globins induced by the binding of imidazole to the heme have been reported previously. For example, imidazole binding significantly changed the heme environment of the Fe(III) form of sperm whale myoglobin (PDB code 1MBI) because it caused the His-64 side chain (which otherwise acts as the distal site ligand) to swing outwards (27). This is similar to the changes observed for Tyr-45 in AfGcHK. Structural changes induced by imidazole binding have also been identified by comparing the structure of the imidazole-bound globin-coupled sensor from *Bordetella pertusis* (PDB code 4UIQ) to its imidazole-free counterpart (4UII). Unfortunately, because these structures have not yet been discussed in any publication, it is difficult to say anything further about them. Conversely, the protoglobin from *Methanosarcina acetivorans* (PDB code 3ZJP) exhibited only small changes in the conformations of two heme-distal site residues (Tyr-61 and Phe-93) following imidazole binding (28).

Mechanism of signal transduction in full-length AfGcHK

It has been challenging to determine the signal transduction mechanisms of various histidine kinases and globin-coupled oxygen sensors because the conformational flexibility of their WT (full-length) forms makes it difficult to resolve their structures.

Here, we show for the first time that Tyr-15 is necessary for the dimerization of the AfGcHK globin domain. When this residue is replaced with a nonaromatic amino acid, the isolated globin domain dimer dissociates into monomers. As discussed above, it is reasonable to assume that although the full-length aliphatic Tyr-15 mutants exist as dimers, their sensing domains would be dissociated into monomers in the same way as the isolated sensing domains. It thus seems that a dimerization process involving intimate contact between the heme group and the side chain of a residue from the neighboring side chain of the dimer is essential for the dynamic properties and/or conformation of the system that permit signal transduction between the sensing and functional domains. The conformational changes of helix H1 upon dimer formation and the development of tension within the globin dimerization interface probably contribute to the fine-tuning of the dimer's dynamic properties and signal transduction. We therefore suggest the following model of signal transduction in AfGcHK: the receipt of a signal in the heme-sensing site of the globin domain (*i.e.* the binding of a suitable ligand to the heme) influences the properties of the globin domain dimerization interface. Changes in the dimerization interface (or changes that act indirectly via the interface) in turn affect the functional domain, switching its catalytic activity on or off. Therefore, when globin domain dimerization is hampered, the protein becomes incapable of signal transduction and is enzymatically inactive, as also occurs when the heme or the entire sensor domain is missing (20–22). A schematic representation of this model is shown in Fig. 4.

As discussed above, the loss of enzyme activity observed for the aliphatic Tyr-15 mutants of the full-length AfGcHK protein is not due to increased autoxidation of these mutants. Both the Fe(II)-O₂ form of the WT full-length enzyme and its autoxidation product, the Fe(III)-OH⁻ form, are catalytically fully active (20) (Table S1). Moreover, the enzyme activities of all mutants were determined using their

Dimerization of heme-based oxygen sensor kinase AfGcHK

Fe(III)-OH⁻ forms to avoid complications resulting from the presence of mixtures of Fe(II)-O₂ and Fe(III)-OH⁻ species formed by autoxidation. Therefore, it is reasonable to conclude that the observed changes in AfGcHK kinase activity were due to changes in the monomeric/dimeric status of the sensing domain caused by the Tyr-15 mutations.

Signal transduction in the full-length AfGcHK compared with other histidine kinases or other heme-containing sensor proteins

Several mechanisms have been proposed to explain how the functional domains of various histidine kinases might be altered in response to signaling from the sensing domain (1, 9, 29–32). The results presented here together with some previously reported findings (21) strongly suggest that in AfGcHK, signal transduction is regulated without direct contact between the sensing and functional domains, probably via a short peptide linker between the two domains. This signal transduction mechanism (see paragraph above) resembles that proposed for transmembrane signal propagation in membrane-bound two-component systems (15–18), although AfGcHK is not a membrane-bound protein. In particular, a similar mechanism involving sensing domain dimerization that is subsequently propagated to a histidine kinase functional domain has been suggested for the *E. coli* copper and silver ion sensor CusS (33). Moreover, oligomerization plays an important role in signal transduction in the heme-based oxygen sensor protein DevS (DosS) from *Mycobacterium tuberculosis*. In this protein, the ability to rapidly change the oligomerization state based on the status of the heme in the sensing domain is directly connected to the catalytic activity of the functional domain (9). In addition, the equilibrium between oligomeric states in globin-coupled oxygen sensor proteins from *B. pertussis* (*BpeGReg*) and *Pectobacterium carotovorum* (*PccGCS*) was shown to depend on both O₂ binding to the sensing domain heme and *c*-di-GMP binding to the functional domain. These shifts in the position of equilibrium in turn affected the sensors' catalytic activity (10, 13). The catalytic activity of these two proteins was also sensitive to heme distortion modes and heme-protein interactions (8). In keeping with the results obtained for AfGcHK, it has been suggested that the globin dimerization interface may be involved in regulating the properties and catalytic behavior of the full-length *BpeGReg* and *PccGCS* proteins (11). A similar set of global interactions within the N-terminal dimeric heme-binding domain was proposed to explain the signal transduction process in the heme-based oxygen sensor phosphodiesterase *EcDOS* (also known as *EcDosP*), which has a heme-bound PAS (34).

Summary

Several artificial inactive variants of AfGcHK have been prepared, including monomeric isolated heme-bound oxygen-sensing globin domains and dimeric full-length variants whose heme-bound globin domains are probably monomeric. Analyses of these variants suggested that monomerization of the heme-bound globin domain entirely abolishes the protein's catalytic activity by impairing internal signal transduction, indicating that the dimerization of the heme-bound globin domain

is vital for signal transduction to the functional domain. This is consistent with our previously reported crystallographic and HDX-MS studies on the molecular mechanism of AfGcHK (21), which suggested that the globin domain's dimerization interface is crucial for inter-domain signal transduction between the globin and functional domains.

Experimental procedures

Materials

Ampicillin was obtained from P-lab (Prague, Czech Republic). Isopropyl β-D-thiogalactopyranoside, hemin, and acrylamide were obtained from Sigma-Aldrich. Water, doubly distilled over quartz, was purified using a Milli-Q Plus system (EMD Millipore, Billerica, MA). All glassware used for sample preparation was conditioned in advance by standing for 24 h in 10% HCl suprapur (Merck, Darmstadt, Germany). Phos-tag was from the Phos-tag consortium Wako Pure Chemical Industries (Osaka, Japan). All chemicals used were of the highest purity grade available from commercial sources and used without further purification.

Protein production and purification

Tyr-15 mutants of AfGcHK were prepared using a site-directed mutagenesis kit (Agilent Technologies, CA) (Table S2). Cloning, overexpression in *E. coli*, and purification of the full-length WT AfGcHK proteins and its Tyr-15 mutant proteins were performed as previously described (19). Briefly, His-tagged AfGcHK was expressed in BL21(DE3) (Novagen, Madison, WI) harboring the pET-21c(+) plasmid. Cell lysates containing His-tagged AfGcHK were isolated by affinity chromatography on TALON[®] Metal Affinity Resin (Clontech Laboratories) followed by size exclusion chromatography on a Superdex 200 GL 10/300 column (GE Healthcare, Amersham Biosciences, UK). Protein and heme concentrations were determined using the BCA assay (Sunrise Absorbance Reader, TECAN, Männedorf, Switzerland) and the pyridine hemochromogen assay, respectively. Purified proteins were >90% homogenous, as confirmed by SDS-PAGE.

Tyr-15 mutants of the isolated AfGcHK globin domain were prepared by In-Fusion cloning (Clontech Laboratories). For this purpose, Tyr-15 mutants of full-length AfGcHK were shortened by PCR using the primers 5'-GAAGGAGATATACATATGCATCATCATCATCATACCGGTGTTCCAGAAACTGTG-3' and 5'GTGGTGGTGTCTCGAGTCACAGATCTTCACGATAGGTGTGCAG-3'.

The sequence obtained by PCR was then inserted into the pET-21c(+) vector using standard cloning techniques. The isolated globin domain of AfGcHK and its Tyr-15 mutants were prepared by inoculating 500 ml of TB media containing 100 μg/ml of ampicillin with 500 μl of overnight BL21(DE3) cells containing the appropriate pET-21c(+) plasmid. The cells were grown at 37 °C for 4 h (170 rpm), then the temperature was lowered to 18 °C (140 rpm) and protein expression was initiated by adding 0.1 mM isopropyl 1-thio-β-D-galactopyranoside followed by further shaking for 20 h. Cells were harvested by centrifugation at 4 °C, 3,000 × g, and stored at -80 °C. Pellets were resuspended in 50 mM Tris, 100 mM NaCl, pH 8, containing

1 mM PMSF, 1 mM EDTA, and 0.2 mg/ml of lysozyme. The desired proteins were isolated and purified by sonication 6×1 min, reconstitution with 300 μM hemin for 20 min, centrifugation for 70 min at $50,000 \times g$, incubation of the supernatant with TALON[®] Metal Affinity Resin (Clontech Laboratories) for 1 h at 4 °C, and elution of the protein using 200 mM imidazole. Finally, the protein was concentrated to a volume of 1 ml and desalted on a Superdex 200 GL 10/300 column equilibrated with 20 mM Tris, 150 mM NaCl, pH 8. In the case of the WT globin domain of AfGCHK, the protein was diluted to 0.5 mg/ml and tobacco etch virus (TEV) protease was added to a final concentration of 0.05 mg/ml. Cleavage was performed at 10 °C for 48 h. TEV protease and uncleaved protein were removed using a TALON[®] Metal Affinity Resin column and the isolated protein was collected in the flow-through fraction. Finally, size exclusion chromatography on a Superdex 200 GL 10/300 column (GE Healthcare, Amersham Biosciences, UK) was applied and the final protein preparation was frozen in liquid nitrogen for further use. Tyr-15 mutants were analyzed without the TEV cleavage procedure. The purified isolated globin domain of AfGCHK was >99% homogenous, as confirmed by SDS-PAGE.

Determination of the oligomeric state of the full-length and isolated globin domains of WT and Tyr-15 mutant proteins of AfGCHK

The oligomerization states of the prepared proteins were determined by size exclusion chromatography on a Superdex 200 Increase 10/300 GL column (GE Healthcare). The mobile phase consisted of 20 mM Tris-HCl, pH 8.0, and 150 mM NaCl, and the flow rate was 0.5 ml/min with an injection volume of 100 μl . Eluted proteins were detected by monitoring the absorbance at 280 nm. The globular proteins thyroglobulin (669 kDa), apoferritin (481 kDa), BSA (66 kDa), ovalbumin (43 kDa), and myoglobin (17 kDa) were used as molecular mass standards and analyzed on the same column. The resulting calibration curve is shown in Fig. S2B. The theoretical molecular masses (calculated based on amino acid sequences) of the monomeric and dimeric forms of AfGCHK were 43 and 86 kDa for the full-length protein, and 19 and 38 kDa for the isolated globin domain, respectively. Samples for analysis were prepared by dissolving the appropriate AfGCHK protein in 50 mM Tris-HCl, 150 mM NaCl, pH 8.0, to a final concentration of 10 μM .

Optical absorption spectroscopy

Optical absorption spectral data were obtained at 24 °C using a Cary 60 UV-visible spectrophotometer (Agilent Technologies, CA). To ensure that the solution was maintained at an appropriate temperature, the reaction mixture was incubated for 5 min prior to spectroscopic measurement. After purification, spectra of the full-length and the isolated globin domain proteins with the Fe(III)-OH⁻ heme of AfGCHK were obtained. The corresponding heme-Fe(II) species were prepared by placing a 5 μM solution of the Fe(III)-OH⁻ protein in a quartz cuvette and reducing it using 1 mM sodium dithionite. Fe(II)-CO complexes were then prepared by gently bubbling gaseous carbon monoxide (Linde, Wiesbaden, Germany) through the cuvette for ~ 2 min. The Fe(II)-O₂ complex was prepared by removing sodium dithionite using PD Minitrap[™]

G-25 Desalting columns (GE Healthcare) and exposing the Fe(II) species to air for 5 min.

Enzyme activity of AfGCHK

The reaction mixture contained the appropriate full-length AfGCHK protein at a concentration of 10 μM , 50 mM Tris-HCl, pH 8.0, 50 mM KCl, and 5 mM MgCl₂. The reaction mixture was preincubated for 5 min at 20 °C, and the reaction was initiated by adding ATP at a concentration between 0 and 1 mM. All experiments were performed at 20 °C. At predetermined times, the AfGCHK autophosphorylation assay reaction was terminated by adding a 100- μl aliquot of termination buffer (125 mM Tris-HCl, pH 6.8, 4% SDS, 10% 2-mercaptoethanol, 20% glycerol, 0.004% bromophenol blue). Samples of the quenched reaction mixtures were then loaded on a 10% SDS-polyacrylamide gel containing 75 μM Phos-tag acrylamide and 0.2 mM MnCl₂. Each lane was loaded with a quantity of quenched reaction mixture containing 0.5 μg of the AfGCHK proteins. Phosphorylated proteins in the sample interacted with the Phos-tag manganese complex in the gel, reducing their mobility relative to phosphate-free proteins (19, 35, 36). After electrophoresis, proteins were visualized by staining with Coomassie Brilliant Blue R-350 and the stained gels were imaged using a Scanjet G3010 (HP, USA) scanner. The protein loadings were then quantified by analyzing the scanned images using ImageJ.

Crystallization of the AfGCHK globin domain

The crystallization solution contained the AfGCHK globin domain at a concentration of 5.4 mg/ml in 150 mM NaCl, 20 mM Tris, pH 8.0. Droplets (100 nl of reservoir solution and 100 nl of crystallization solution) were set up using a Cartesian Honeybee 961 robot (Genomic Solutions) at 21 °C. The crystal grew under C4 Morpheus conditions without any optimization. The C4 Morpheus condition contained 0.09 M ligand stock (NaNO₃, Na₂HPO₄, (NH₄)₂SO₄), 0.1 M buffer system, pH 6.5 (imidazole, 2-ethanesulfonic acid), and 37.5% precipitant stock MPD_P1K_P3350 (MPD, PEG 1000 and PEG 3350).

Diffraction data collection

Data were collected at the Diamond Light Source using the I02 beamline and a Pilatus 6 M-F detector. The wavelength was 0.97 Å, the crystal-detector distance was 350 mm, the exposure time per image was 0.05 s, and the oscillation width was 0.1°. The diffraction images were processed using XDS (37) and scaled using AIMLESS from the CCP4 program package (38). Finally, the best images (numbers 1100–1800 and 3000–3600) were selected based on their batch R_{merge} values and overall statistics. Final data processing statistics are shown in Table 1.

Structure solution and refinement

The phase problem was solved by molecular replacement with the program MOLREP (39) based on the previously reported structure of the protein, one monomer of the dimer was used as a model (PDB code 5OHF). The asymmetric unit of the structure presented here contains a monomer, and inspection of the interfaces within the crystal lattice confirmed the

Dimerization of heme-based oxygen sensor kinase AfGCHK

monomeric form of the protein in the crystal. The structure was refined using REFMAC5 (40) with manual editing using COOT (41) and using 5% of reflections as a test set (R_{free} set). The last refinement cycle was performed using all reflections. Structure quality was checked using the validation tools implemented in MOLPROBITY (42) and REFMAC5 (40).

Author contributions—A. L., J. D., and P. M. investigation; P. K. methodology; M. M. conceptualization; M. M. writing—original draft; T. Skalova, J. D., P. K., M. S., and J. B. designed, performed and interpreted the X-ray crystallographic investigations; A. L. performed the biophysical analysis including a kinase activity study; K. H. helped with the X-ray crystallographic data collection; T. Shimizu participated in the results discussion; M. M. designed and interpreted the biophysical analysis including a kinase activity study.

Acknowledgments—We thank Diamond Light Source for beamtime (proposal MX10627) and the staff of beamline I02 for assistance with data collection. The Wellcome Centre for Human Genetics is supported by Wellcome Trust Centre grant 203141/Z/16/Z. We also acknowledge the support and the use of resources of InStruct, a part of the European Strategy Forum on Research Infrastructures (ESFRI) and supported by national member subscriptions (1066).

References

- Shimizu, T., Huang, D., Yan, F., Stranova, M., Bartosova, M., Fojtiková, V., and Martinková, M. (2015) Gaseous O₂, NO, and CO in signal transduction: structure and function relationships of heme-based gas sensors and heme-redox sensors. *Chem. Rev.* **115**, 6491–6533 [CrossRef Medline](#)
- Kühl, T., and Imhof, D. (2014) Regulatory Fe(II/III) heme: the reconstruction of a molecule's biography. *Chembiochem* **15**, 2024–2035 [CrossRef Medline](#)
- Tsiftoglou, A. S., Tsamadou, A. I., and Papadopoulou, L. C. (2006) Heme as key regulator of major mammalian cellular functions: molecular, cellular, and pharmacological aspects. *Pharmacol. Ther.* **111**, 327–345 [CrossRef Medline](#)
- Ponka, P., Sheftel, A. D., English, A. M., Scott Bohle, D., and Garcia-Santos, D. (2017) Do mammalian cells really need to export and import heme? *Trends Biochem. Sci.* **42**, 395–406 [CrossRef Medline](#)
- Roumenina, L. T., Rayes, J., Lacroix-Desmazes, S., and Dimitrov, J. D. (2016) Heme: modulator of plasma systems in hemolytic diseases. *Trends Mol. Med.* **22**, 200–213 [CrossRef Medline](#)
- Shimizu, T., Lengalova, A., Martinek, V., and Martinková, M. (2019) Heme: emergent roles of heme in signal transduction, functional regulation and as catalytic centres. *Chem. Soc. Rev.* **48**, 5619–5808 [CrossRef](#)
- Martinková, M., Kitanishi, K., and Shimizu, T. (2013) Heme-based globin-coupled oxygen sensors: linking oxygen binding to functional regulation of diguanylate cyclase, histidine kinase, and methyl-accepting chemotaxis. *J. Biol. Chem.* **288**, 27702–27711 [CrossRef Medline](#)
- Rivera, S., Young, P. G., Hoffer, E. D., Vansuch, G. E., Metzler, C. L., Dunham, C. M., and Weinert, E. E. (2018) Structural insights into oxygen-dependent signal transduction within globin coupled sensors. *Inorg. Chem.* **57**, 14386–14395 [CrossRef Medline](#)
- Lobão, J. B. D. S., Gondim, A. C. S., Guimarães, W. G., Gilles-Gonzalez, M.-A., Lopes, L. G. F., and Sousa, E. H. S. (2019) Oxygen triggers signal transduction in the DevS (DosS) sensor of *Mycobacterium tuberculosis* by modulating the quaternary structure. *FEBS J.* **286**, 479–494 [CrossRef Medline](#)
- Burns, J. L., Rivera, S., Deer, D. D., Joynt, S. C., Dvorak, D., and Weinert, E. E. (2016) Oxygen and bis(3',5')-cyclic dimeric guanosine monophosphate binding control oligomerization state equilibria of diguanylate cyclase-containing globin coupled sensors. *Biochemistry* **55**, 6642–6651 [CrossRef Medline](#)
- Rivera, S., Burns, J. L., Vansuch, G. E., Chica, B., and Weinert, E. E. (2016) Globin domain interactions control heme pocket conformation and oligomerization of globin coupled sensors. *J. Inorg. Biochem.* **164**, 70–76 [CrossRef Medline](#)
- Burns, J. L., Jariwala, P. B., Rivera, S., Fontaine, B. M., Briggs, L., and Weinert, E. E. (2017) Oxygen-dependent globin coupled sensor signaling modulates motility and virulence of the plant pathogen *Pectobacterium carotovorum*. *ACS Chem. Biol.* **12**, 2070–2077 [CrossRef Medline](#)
- Burns, J. L., Deer, D. D., and Weinert, E. E. (2014) Oligomeric state affects oxygen dissociation and diguanylate cyclase activity of globin coupled sensors. *Mol. Biosyst.* **10**, 2823–2826 [CrossRef Medline](#)
- Walker, J. A., Rivera, S., and Weinert, E. E. (2017) Mechanism and role of globin-coupled sensor signalling. *Adv. Microb. Physiol.* **71**, 133–169 [CrossRef Medline](#)
- Gushchin, I., Melnikov, I., Polovinkin, V., Ishchenko, A., Yuzhakova, A., Buslaev, P., Bourenkov, G., Grudin, S., Round, E., Balandin, T., Borshchevskiy, V., Willbold, D., Leonard, G., Büldt, G., Popov, A., and Gordeliy, V. (2017) Mechanism of transmembrane signaling by sensor histidine kinases. *Science* **356**, eaah6345 [CrossRef Medline](#)
- Abriata, L. A., Albanesi, D., Dal Peraro, M., and de Mendoza, D. (2017) Signal sensing and transduction by histidine kinases as unveiled through studies on a temperature sensor. *Acc. Chem. Res.* **50**, 1359–1366 [CrossRef Medline](#)
- Zschiedrich, C. P., Keidel, V., and Szurmant, H. (2016) Molecular mechanisms of two-component signal transduction. *J. Mol. Biol.* **428**, 3752–3775 [CrossRef Medline](#)
- Willett, J. W., and Crosson, S. (2017) Atypical modes of bacterial histidine kinase signaling. *Mol. Microbiol.* **103**, 197–202 [CrossRef Medline](#)
- Kitanishi, K., Kobayashi, K., Uchida, T., Ishimori, K., Igarashi, J., and Shimizu, T. (2011) Identification and functional and spectral characterization of a globin-coupled histidine kinase from *Anaeromyxobacter* sp. Fw109-5. *J. Biol. Chem.* **286**, 35522–35534 [CrossRef Medline](#)
- Fojtikova, V., Stranova, M., Vos, M. H., Liebl, U., Hranicek, J., Kitanishi, K., Shimizu, T., and Martinkova, M. (2015) Kinetic analysis of a globin-coupled histidine kinase, AfGCHK: effects of the heme iron complex, response regulator, and metal cations on autophosphorylation activity. *Biochemistry* **54**, 5017–5029 [CrossRef Medline](#)
- Stranova, M., Man, P., Skálová, T., Kolenko, P., Blaha, J., Fojtikova, V., Martinek, V., Dohnálek, J., Lengalova, A., Rosúlek, M., Shimizu, T., and Martinková, M. (2017) Coordination and redox state-dependent structural changes of the heme-based oxygen sensor AfGCHK associated with intraprotein signal transduction. *J. Biol. Chem.* **292**, 20921–20935 [CrossRef Medline](#)
- Stranova, M., Martinek, V., Man, P., Fojtikova, V., Kavan, D., Van[caron]ek, O., Shimizu, T., and Martinkova, M. (2016) Structural characterization of the heme-based oxygen sensor, AfGCHK, its interactions with the cognate response regulator, and their combined mechanism of action in a bacterial two-component signaling system. *Proteins* **84**, 1375–1389 [CrossRef Medline](#)
- Liebschner, D., Afonine, P. V., Moriarty, N. W., Poon, B. K., Sobolev, O. V., Terwilliger, T. C., and Adams, P. D. (2017) Polder maps: improving OMIT maps by excluding bulk solvent. *Acta Crystallogr. D Struct. Biol.* **73**, 148–157 [CrossRef Medline](#)
- Pesce, A., Thijs, L., Nardini, M., Desmet, F., Sisinni, L., Gourlay, L., Bolli, A., Coletta, M., Van Doorslaer, S., Wan, X., Alam, M., Ascenzi, P., Moens, L., Bolognesi, M., and Dewilde, S. (2009) HisE11 and HisF8 provide bis-histidyl heme hexa-coordination in the globin domain of *Geobacter sulfurreducens* globin-coupled sensor. *J. Mol. Biol.* **386**, 246–260 [CrossRef Medline](#)
- Zhang, W., and Phillips, G. N. (2003) Structure of the oxygen sensor in *Bacillus subtilis*: signal transduction of chemotaxis by control of symmetry. *Structure* **11**, 1097–1110 [CrossRef Medline](#)
- Tarnawski, M., Barends, T. R., and Schlichting, I. (2015) Structural analysis of an oxygen-regulated diguanylate cyclase. *Acta Crystallogr. D Biol. Crystallogr.* **71**, 2158–2177 [CrossRef Medline](#)
- Lionetti, C., Guanziroli, M. G., Frigerio, F., Ascenzi, P., and Bolognesi, M. (1991) X-ray crystal structure of the ferric sperm whale myoglobin: imid-

- azole complex at 2.0 Å resolution. *J. Mol. Biol.* **217**, 409–412 [CrossRef](#) [Medline](#)
28. Pesce, A., Tilleman, L., Donné, J., Aste, E., Ascenzi, P., Ciaccio, C., Coletta, M., Moens, L., Viappiani, C., Dewilde, S., Bolognesi, M., and Nardini, M. (2013) Structure and haem-distal site plasticity in *Methanosarcina acetivorans* protoglobin. *PLoS ONE* **8**, e66144 [CrossRef](#) [Medline](#)
 29. Cunningham, K. A., and Burkholder, W. F. (2009) The histidine kinase inhibitor Sda binds near the site of autophosphorylation and may sterically hinder autophosphorylation and phosphotransfer to Spo0F. *Mol. Microbiol.* **71**, 659–677 [CrossRef](#) [Medline](#)
 30. Rao, M., Herzik, M. A., Jr., Iavarone, A. T., and Marletta, M. A. (2017) Nitric oxide-induced conformational changes govern H-NOX and histidine kinase interaction and regulation in *Shewanella oneidensis*. *Biochemistry* **56**, 1274–1284 [CrossRef](#) [Medline](#)
 31. Dikiy, I., Edupuganti, U. R., Abzalimov, R. R., Borbat, P. P., Srivastava, M., Freed, J. H., and Gardner, K. H. (2019) Insights into histidine kinase activation mechanisms from the monomeric blue light sensor EL346. *Proc. Natl. Acad. Sci. U.S.A.* **116**, 4963–4972 [CrossRef](#) [Medline](#)
 32. Jacob-Dubuisson, F., Mechaly, A., Betton, J.-M., and Antoine, R. (2018) Structural insights into the signalling mechanisms of two-component systems. *Nat. Rev. Microbiol.* **16**, 585–593 [CrossRef](#) [Medline](#)
 33. Affandi, T., and McEvoy, M. M. (2019) Mechanism of metal ion-induced activation of a two-component sensor kinase. *Biochem. J.* **476**, 115–135 [CrossRef](#) [Medline](#)
 34. Kurokawa, H., Lee, D.-S., Watanabe, M., Sagami, I., Mikami, B., Raman, C. S., and Shimizu, T. (2004) A redox-controlled molecular switch revealed by the crystal structure of a bacterial heme PAS sensor. *J. Biol. Chem.* **279**, 20186–20193 [CrossRef](#) [Medline](#)
 35. Igarashi, J., Murase, M., Iizuka, A., Pichierri, F., Martinkova, M., and Shimizu, T. (2008) Elucidation of the heme binding site of heme-regulated eukaryotic initiation factor 2 α kinase and the role of the regulatory motif in heme sensing by spectroscopic and catalytic studies of mutant proteins. *J. Biol. Chem.* **283**, 18782–18791 [CrossRef](#) [Medline](#)
 36. Yamada, S., Nakamura, H., Kinoshita, E., Kinoshita-Kikuta, E., Koike, T., and Shiro, Y. (2007) Separation of a phosphorylated histidine protein using phosphate affinity polyacrylamide gel electrophoresis. *Anal. Biochem.* **360**, 160–162 [CrossRef](#) [Medline](#)
 37. Kabsch, W. (2010) XDS. *Acta Crystallogr. D Biol. Crystallogr.* **66**, 125–132 [CrossRef](#) [Medline](#)
 38. Winn, M. D., Ballard, C. C., Cowtan, K. D., Dodson, E. J., Emsley, P., Evans, P. R., Keegan, R. M., Krissinel, E. B., Leslie, A. G., McCoy, A., McNicholas, S. J., Murshudov, G. N., Pannu, N. S., Potterton, E. A., Powell, H. R., Read, R. J., Vagin, A., and Wilson, K. S. (2011) Overview of the CCP4 suite and current developments. *Acta Crystallogr. D Biol. Crystallogr.* **67**, 235–242 [CrossRef](#) [Medline](#)
 39. Vagin, A., and Teplyakov, A. (2010) Molecular replacement with MOLREP. *Acta Crystallogr. D Biol. Crystallogr.* **66**, 22–25 [CrossRef](#) [Medline](#)
 40. Murshudov, G. N., Skubák, P., Lebedev, A. A., Pannu, N. S., Steiner, R. A., Nicholls, R. A., Winn, M. D., Long, F., and Vagin, A. A. (2011) REFMAC5 for the refinement of macromolecular crystal structures. *Acta Crystallogr. D Biol. Crystallogr.* **67**, 355–367 [CrossRef](#) [Medline](#)
 41. Emsley, P., Lohkamp, B., Scott, W. G., and Cowtan, K. (2010) Features and development of Coot. *Acta Crystallogr. D Biol. Crystallogr.* **66**, 486–501 [CrossRef](#) [Medline](#)
 42. Chen, V. B., Arendall, W. B., 3rd, Headd, J. J., Keedy, D. A., Immormino, R. M., Kapral, G. J., Murray, L. W., Richardson, J. S., and Richardson, D. C. (2010) MolProbity: all-atom structure validation for macromolecular crystallography. *Acta Crystallogr. D Biol. Crystallogr.* **66**, 12–21 [CrossRef](#) [Medline](#)

Disruption of the dimerization interface of the sensing domain in the dimeric heme-based oxygen sensor AfGcHK abolishes bacterial signal transduction
Tereza Skalova, Alzbeta Lengalova, Jan Dohnalek, Karl Harlos, Peter Mihalcin, Petr Kolenko, Martin Stranova, Jan Blaha, Toru Shimizu and Markéta Martínková

J. Biol. Chem. 2020, 295:1587-1597.

doi: 10.1074/jbc.RA119.011574 originally published online December 30, 2019

Access the most updated version of this article at doi: [10.1074/jbc.RA119.011574](https://doi.org/10.1074/jbc.RA119.011574)

Alerts:

- [When this article is cited](#)
- [When a correction for this article is posted](#)

[Click here](#) to choose from all of JBC's e-mail alerts

This article cites 0 references, 0 of which can be accessed free at <http://www.jbc.org/content/295/6/1587.full.html#ref-list-1>

Supporting Information for

Disruption of the dimerization interface of the sensing domain in the dimeric heme-based oxygen sensor *AfGcHK* abolishes bacterial signal transduction

Tereza Skalova, Alzbeta Lengalova, Jan Dohnalek, Karl Harlos, Peter Mihalcin, Petr Kolenko, Martin Stranova, Jan Blaha, Toru Shimizu and Markéta Martínková

Running title: *Dimerization of heme-based oxygen sensor kinase AfGcHK*

Table S1. Kinetic parameters for the autophosphorylation of various forms of the full-length *AfGcHK* protein (20) and its isolated kinase domain (21) showing how the enzyme's catalytic activity is affected by changes in the oxidation state and ligand coordination of the sensing domain's heme iron complex.

Heme iron state in the sensing domain of <i>AfGcHK</i>	K_m^{ATP} [μ M]	k_{cat} [min^{-1}]	k_{cat}/K_m^{ATP} [$\text{M}^{-1} \text{s}^{-1}$]	
Fe(III)-OH ⁻	18.9 ± 2.3	1.08 ± 0.03	1000	FULL ENZYME ACTIVITY
Fe(II)-O ₂	23.0 ± 1.3	0.96 ± 0.01	700	FULL ENZYME ACTIVITY
Fe(II)-CO	357.0 ± 28.0	1.04 ± 0.03	50	LOW ENZYME ACTIVITY
Fe(II)	78.0 ± 4.7	0.42 ± 0.02	90	LOW ENZYME ACTIVITY
no heme	33.6 ± 1.7	0.25 ± 0.01	120	LOW ENZYME ACTIVITY
no sensing domain	NO ENZYME ACTIVITY			

Dimerization of heme-based oxygen sensor kinase AfGcHK

Table S2. Primer sequences used to prepare *AfGcHK* Tyr-15 full-length mutants by site-directed mutagenesis.

Primer type	Primer sequence
Y15A Forward primer	5-TTCGAAGAGCTGAAACGCGCTGTTGGTTGGGGTGATGG-3
Y15A Reverse primer	5-CCATCACCCCAACCAACAGCGCGTTTCAGCTCTTCGAA-3
Y15F Forward primer	5-TCGAAGAGCTGAAACGCTTTGTTGGTTGGGGTG-3
Y15F Reverse primer	5-CACCCCAACCAACAAAGCGTTTCAGCTCTTCGA-3
Y15W Forward primer	5-CGAAGAGCTGAAACGCTGGGTTGGTTGGGGTGATGG-3
Y15W Reverse primer	5-CCATCACCCCAACCAACCCAGCGTTTCAGCTCTTCG-3
Y15G Forward primer	5-TTCGAAGAGCTGAAACGCGGTGTTGGTTGGGGTGATGG-3
Y15G Reverse primer	5-CCATCACCCCAACCAACACCGCGTTTCAGCTCTTCGAA-3

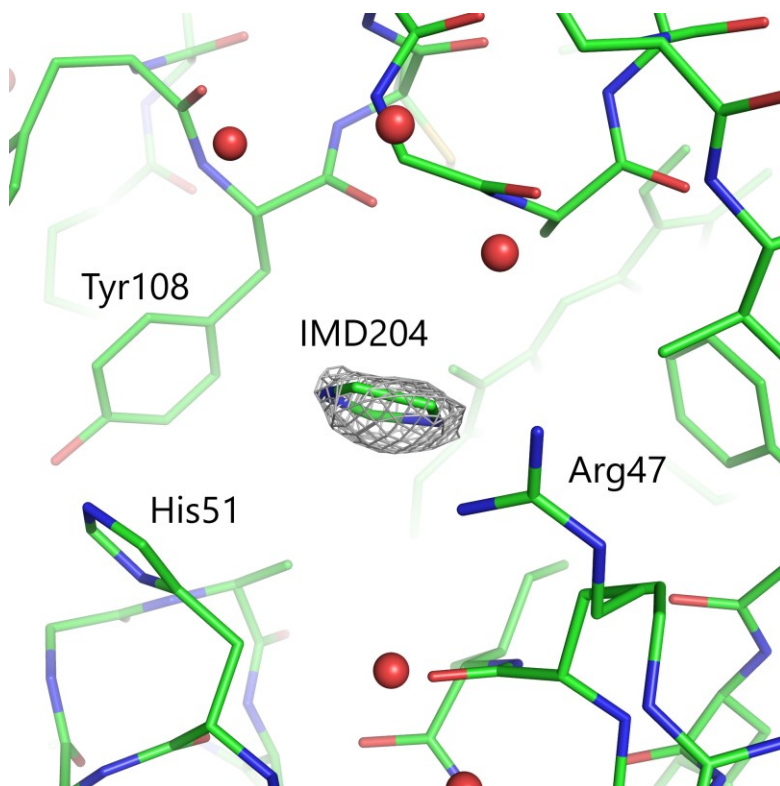


Figure S1. Electron density map for imidazole IMD204. In the monomeric structure of the AfGcHK globin domain, imidazole IMD204 occupies the position of Tyr-15 from the second protein chain in the dimeric structure. It is localized freely in the access tunnel and forms no hydrogen bonds. The Polder map for the ligand, contoured in grey mesh at 4.2σ , confirms its presence here.

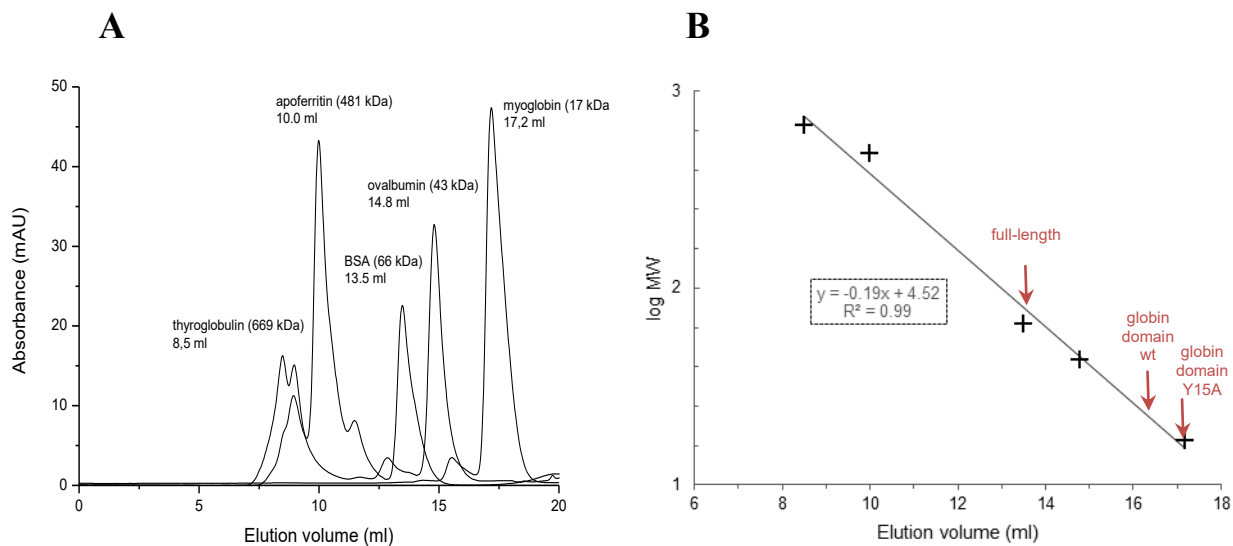
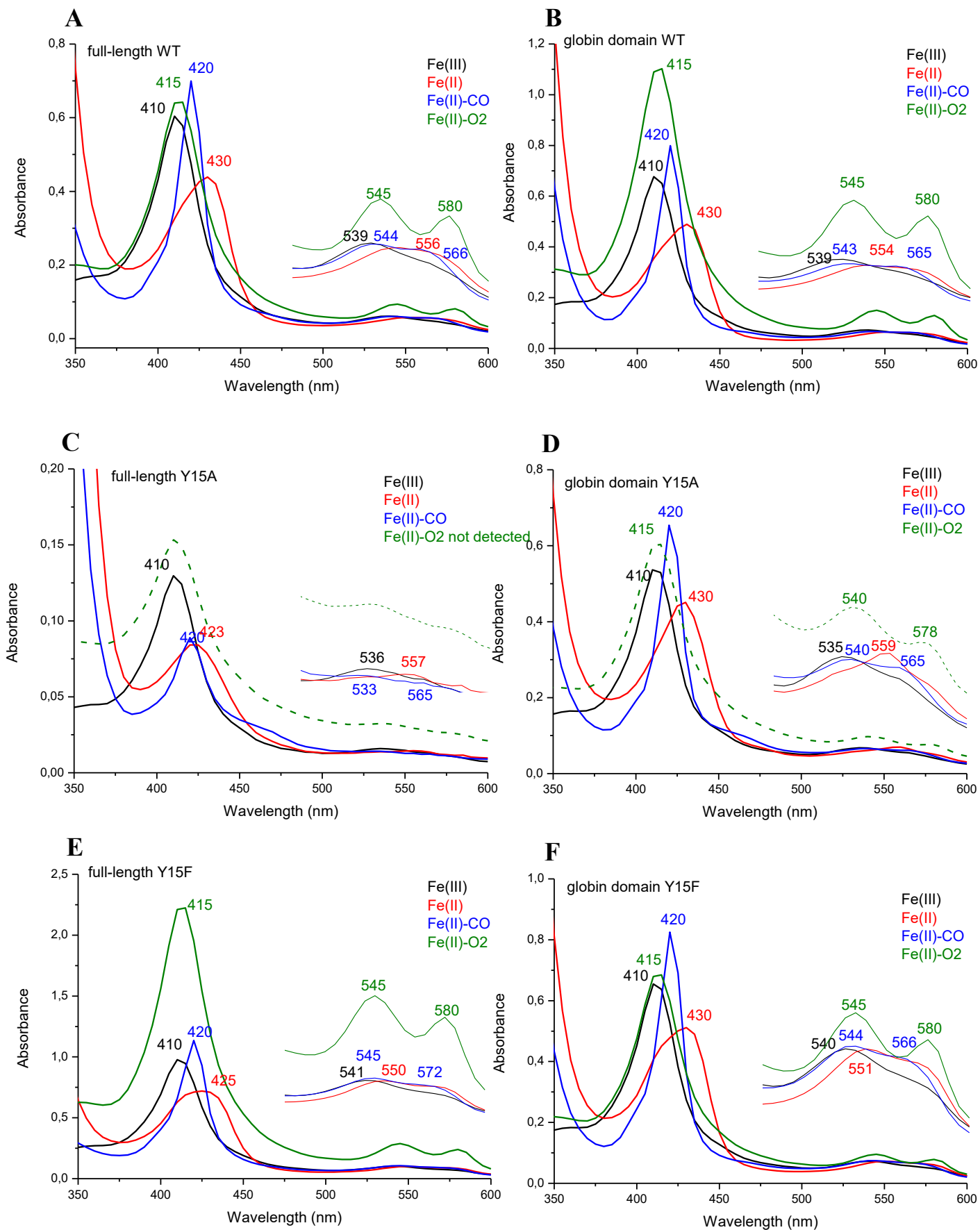


Figure S2 Calibration of the Superdex 200 Increase 10/300 GL column. (A) The globular proteins thyroglobulin (669 kDa), apoferritin (481 kDa), bovine serum albumin (66 kDa), ovalbumin (43 kDa) and myoglobin (17 kDa) were used as molecular weight standards and analyzed on the Superdex 200 Increase 10/300 GL column. (B) Calibration curve of the Superdex 200 Increase 10/300 GL column under the conditions used in this study (for further details, see Experimental Procedures). Log MW values are given in kDa.

Dimerization of heme-based oxygen sensor kinase AfGcHK



Dimerization of heme-based oxygen sensor kinase AfGcHK

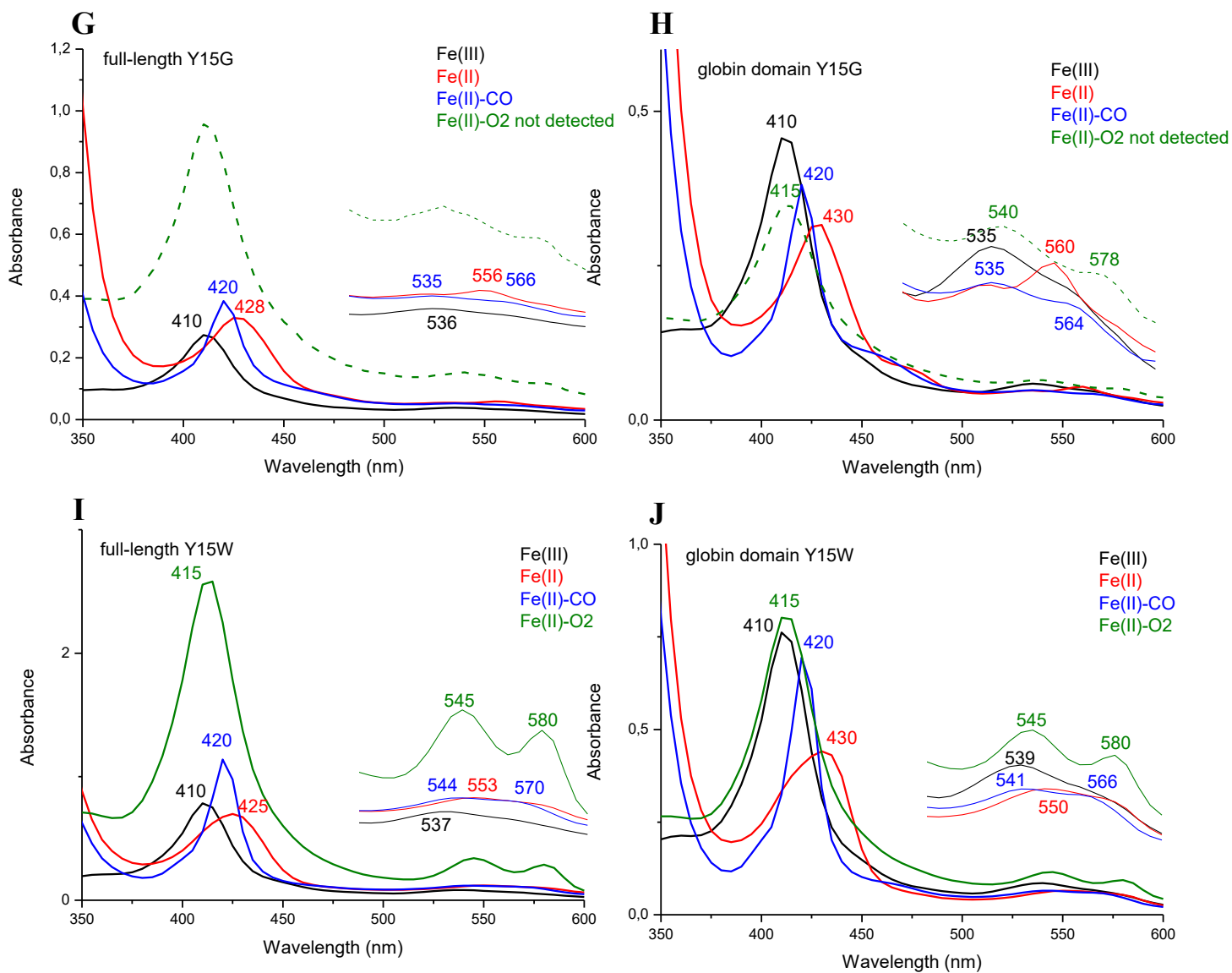


Figure S3. UV-Vis spectra of the full-length *AfGcHK* and its isolated globin domain. Wavelengths of maxima are indicated. (A) full-length wild type; (B) isolated wt globin domain; (C) full-length Y15A; (D) isolated Y15A globin domain; (E) full-length Y15F; (F) isolated Y15F globin domain; (G) full-length Y15G; (H) isolated Y15G globin domain; (I) full-length Y15W; (J) isolated Y15W globin domain.

Dimerization of heme-based oxygen sensor kinase *AfGcHK*

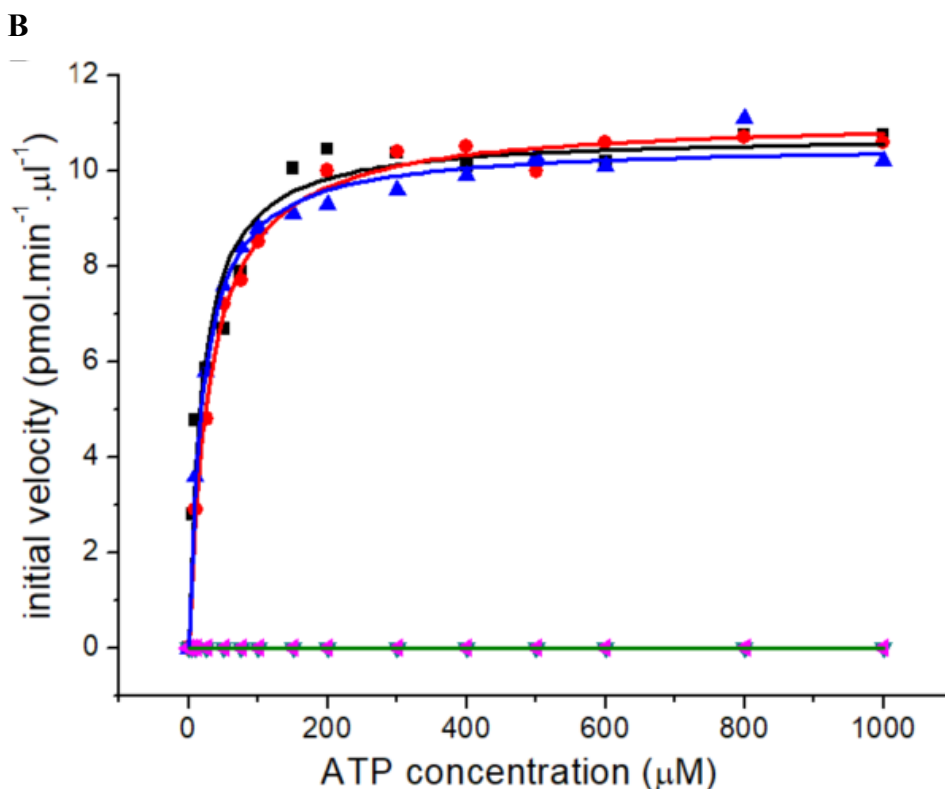
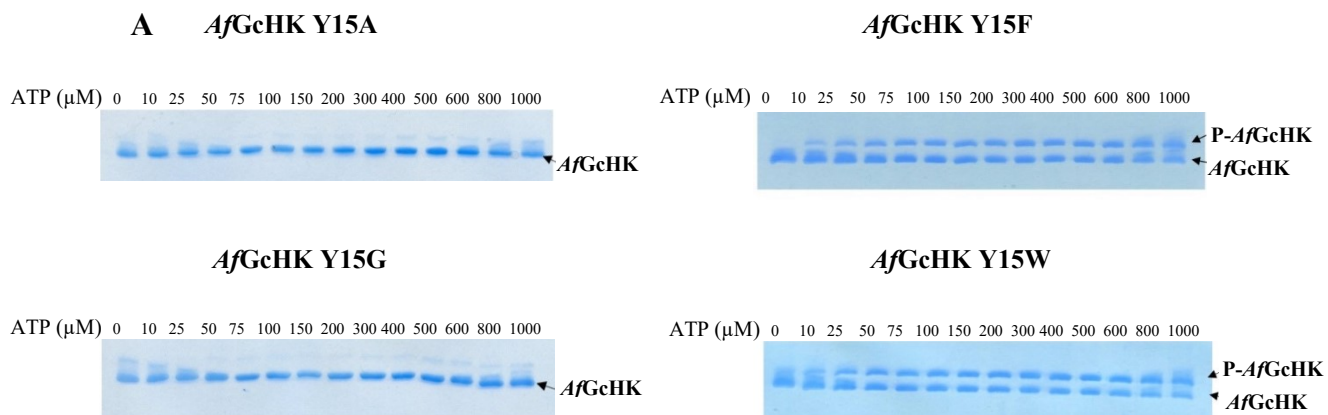


Figure S4. The effect of the mutations at Tyr-15 in the globin domain on the Michaelis-Menten kinetics of the autophosphorylation reaction catalyzed by *AfGcHK*. (A) Phos-tag PAGE separation of *AfGcHK* and P-*AfGcHK* formed by the autophosphorylation of Y15A, Y15F, Y15G, and Y15W *AfGcHK* at different ATP concentrations and (B) graphical representation of the results for each *AfGcHK* mutant; wt - black line and squares, Y15A - green line and triangles, Y15F - red line and circles, Y15G - pink line and triangles, Y15W - blue line and triangles; In each run, a reaction mixture containing 10 μM *AfGcHK*, 0 -1000 μM ATP, 50mM Tris-HCl (pH 8.0), 50mM KCl, and 5mM MgCl₂ was incubated in a total volume of 100 μl for 30 s (for further details, see Experimental Procedures).

4.3 Kinetic analysis of a globin-coupled diguanylate cyclase, YddV: Effects of heme iron redox state, axial ligands, and heme distal mutations on catalysis

Lengalova, A.; Fojtikova-Proskova, V.; Vavra, J.; Martínek, V.; Stranava, M.; Shimizu, T.; Martinkova, M.: *J. Inorg. Biochem.* (2019) 201, 110833–110842 (**IF**₂₀₁₆ **3,3**).

Podíl předkladatelky na této práci: 65 % (*exprese a purifikace mutantních forem proteinu MBP-YddV, příprava wt MBP-YddV, spektroskopická měření, oligomerizační studie, zpracování a vyhodnocení výsledků, příprava obrázků*)

potvrzeno korespondujícím autorem, doc. RNDr. Markétou Martínkovou, Ph.D.



Kinetic analysis of a globin-coupled diguanylate cyclase, YddV: Effects of heme iron redox state, axial ligands, and heme distal mutations on catalysis

Alzbeta Lengalova¹, Veronika Fojtikova-Proskova¹, Jakub Vavra, Václav Martínek, Martin Stranava, Toru Shimizu, Marketa Martinkova*

Department of Biochemistry, Faculty of Science, Charles University, Hlavova (Albertov) 2030/8, Prague 2, Czech Republic

ARTICLE INFO

Keywords:

Heme-based oxygen sensor
Intramolecular catalytic regulation
Signal transduction
Diguanylate cyclase
Globin-coupled oxygen sensor

ABSTRACT

Heme-based oxygen sensors allow bacteria to regulate their activity based on local oxygen levels. YddV, a globin-coupled oxygen sensor with diguanylate cyclase activity from *Escherichia coli*, regulates cyclic-di-GMP synthesis based on oxygen availability. Stable and active samples of the full-length YddV protein were prepared by attaching it to maltose binding protein (MBP). To better understand the full-length protein's structure, the interactions between its domains were examined by performing a kinetic analysis. The diguanylate cyclase reaction catalyzed by YddV-MBP exhibited Michaelis-Menten kinetics. Its pH optimum was 8.5–9.0, and catalysis required either Mg^{2+} or Mn^{2+} ; other divalent metal ions gave no activity. The most active form of YddV-MBP had a 5-coordinate Fe(III) heme complex; its kinetic parameters were $K_m^{GTP} 84 \pm 21 \mu M$ and $k_{cat} 1.2 \text{ min}^{-1}$. YddV-MBP with heme Fe(II), heme Fe(II)-O₂, and heme Fe(II)-CO complexes had k_{cat} values of 0.3 min^{-1} , 0.95 min^{-1} , and 0.3 min^{-1} , respectively, suggesting that catalysis is regulated by the heme iron's redox state and axial ligand binding. The k_{cat} values for heme Fe(III) complexes of L65G, L65Q, and Y43A YddV-MBP mutants bearing heme distal amino acid replacements were 0.15 min^{-1} , 0.26 min^{-1} and 0.54 min^{-1} , respectively, implying that heme distal residues play key regulatory roles by mediating signal transduction between the sensing and functional domains. Ultracentrifugation and size exclusion chromatography experiments showed that YddV-MBP is primarily dimeric in solution, with a sedimentation coefficient around 8. The inactive heme-free H93A mutant is primarily octameric, suggesting that catalytically active dimer formation requires heme binding.

1. Introduction

Heme-based oxygen sensor proteins give many bacteria unique ways to continuously monitor the composition of their surroundings and regulate intracellular processes to adapt to changing conditions. These proteins have at least two domains: an N-terminal sensing domain and a C-terminal functional domain [1,2]. The heme iron complex is located in the sensing domain and is the oxygen sensing site. Signals generated by the heme's interactions with molecular oxygen are transduced from the sensing domain to the functional domain, causing structural changes in the functional domain that enhance or suppress the protein's catalytic activity, switching it on or off as appropriate [1–3]. A detailed kinetic analysis of heme-based oxygen sensors with different heme iron redox and/or coordination states could shed more light on the molecular mechanism of signal transduction, but few such analyses have been reported.

In general, the sensing domains of heme-based oxygen sensor

proteins can adopt diverse conformations and the functional domains can exhibit various catalytic activities [1]. This work focuses on YddV (or EcDosC), a globin-coupled diguanylate cyclase sensor from *E. coli* [4–6]. Globin-coupled oxygen sensors with diguanylate cyclase activity have also been identified in *Pectobacterium carotovorum* (PccGCS) [7], *Bordetella pertussis* (BpeGReg) [7–11], *Desulfotalea psychrophila* (HemDGC) [12], *Azotobacter vinelandii* (AvGreg) [13], and *Shewanella putrefaciens* (SpDosD) [14]. Another protein of this class with putative diguanylate cyclase activity has been found in *Geobacter sulfurreducens* (GsGCS), but its activity has yet to be assessed [15].

Cyclic-di-guanosine-5'-monophosphate (c-di-GMP) is an important bacterial second messenger that regulates many key physiological functions including cell motility, differentiation, development, virulence, biofilm formation, cell–cell communication, and environmental persistence [16–18]. Two heme-based oxygen sensors play central roles in c-di-GMP signaling cascades in *E. coli*. As noted above, YddV consists of an N-terminal heme-bound oxygen sensing domain with a globin fold

* Corresponding author.

E-mail address: marketa.martinkova@natur.cuni.cz (M. Martinkova).

¹ Both authors contributed equally to this work.

and a C-terminal functional domain that catalyzes the formation of *c*-di-GMP from guanosine-5'-triphosphate (GTP). YddV acts in tandem with another heme-based oxygen sensor phosphodiesterase, *EcDOS* (or *EcDosp*), which has an N-terminal heme-bound oxygen sensing domain with a PAS fold (named for the proteins Per - *Drosophila* period clock protein, Arnt - vertebrate aryl hydrocarbon receptor nuclear translocator, and Sim - *Drosophila* single-minded protein) and a C-terminal functional domain that catalyzes the conversion of *c*-di-GMP to linear di-GMP [4,19,20]. The phosphodiesterase activity of *EcDOS* is substantially enhanced by O₂ binding to the heme Fe(II) complex in the sensing domain. It was found that YddV and *EcDOS* associate to form a functional complex and are translated from a polycistronic operon [21]. Accordingly, the two proteins were co-purified. Their interaction is probably based on hydrophobic forces [4].

The structure and function of the isolated YddV heme-binding domain have been studied extensively [6,22–26]. However, because of the difficulty of preparing a catalytically active version of the full-length YddV protein, only preliminary kinetic analyses of the full-length protein have been reported. These studies revealed that the Fe(III) form of YddV is the most active, while the Fe(II)-O₂ and Fe(II)-CO forms are less active [4–6]. It was also suggested that the Fe(II) form of YddV was significantly less active than other forms [5,6]. However, these studies only analyzed the catalytic activity of the full-length protein in terms of the initial rate of product formation (in micromoles of *c*-di-GMP per micromole of YddV per minute) [4–6]. One of these investigations also indirectly examined the diguanylate cyclase activity of YddV in the presence of the coupled enzyme *EcDOS* [4].

Here we report the first successful preparation of stable and active full-length YddV, which was achieved by attaching it to maltose binding protein (MBP). To better understand the structure of the full-length protein, the interactions between its sensing and functional domains were examined by performing a detailed kinetic analysis based on its *K_m*, *V_{max}* and *k_{cat}* values. The effects of the heme iron redox state and/or ligand coordination on its catalytic activity were investigated, along with the dependence of the enzyme's kinetic parameters on amino acid residues located on the heme distal side of the Fe(III) complex. The effects of divalent metal cations other than Mg²⁺ on catalysis were also studied. We analyze the interactions between the sensing and functional domains of YddV in terms of changes in the kinetic parameters of its diguanylate cyclase activity under diverse conditions. Specifically, we studied the impact of changes in the heme-containing sensing domain on the diguanylate cyclase activity of the YddV functional domain. Clarifying the relationship between signal transduction, protein conformation, and the functional state of the sensor protein should help explain the molecular mechanism of its sensing activity.

2. Experimental procedures

2.1. Materials

Ampicillin was obtained from P-lab (Prague, Czech Republic). Isopropyl β-D-thiogalactopyranoside, hemin, sodium dithionite, Na₂S, *c*-di-GMP, tris(hydroxymethyl)aminomethane (Tris) and acrylamide were obtained from Sigma-Aldrich (St. Louis, MO, USA) and GTP from GE Healthcare. Water, doubly distilled over quartz, was purified using a Milli-Q Plus system (EMD Millipore, Billerica, MA, USA). All glassware used for sample preparation was conditioned in advance by standing for 24 h in 10% HCl suprapur (Merck, Darmstadt, Germany). All chemicals used were of the highest purity grade available from commercial sources and used without further purification.

2.2. Overexpression and purification of the wild type (WT) and mutant proteins

Nine YddV-MBP protein expression vectors were constructed: pMAL-c5e/WT, R365A, Y43A, Y43F, L65G, L65M, L65Q, L65T and

H98A. The previously reported pET21c(+)/YddV plasmid [5] was digested with *NdeI* and *XhoI*, and subcloned into the pMAL-c5e vector (New England Biolabs, USA), leading to the introduction of an MBP protein tag at the N-terminus of the desired protein. The following oligonucleotides were designed to extract the inserts of previously reported YddV mutants (L65 and Y43) from the corresponding pET28a/YddV mutant vectors [5]. Nucleotides for *NdeI* and *XhoI* restriction sites were inserted into the oligonucleotide sequences.

Forward: 5'-AGATACATATGGAGATGTATTTTAAAAGAATG-3' and reverse: 5'-AGATACTCGAGCTAAAGACTGGCTTCCAG-3'.

To obtain the YddV-MBP H98A plasmid, the pMAL-c5e/YddV WT plasmid was mutated using the QuikChange II Site-Directed Mutagenesis Kit (Agilent). The following oligonucleotides were used for polymerase chain reaction:

Forward: 5'-CATACCGTCGCGGAAGTGGCTGCCCGCATAGGAATCC-3'

Reverse: 5'-GGAATTCTATGCGGGCAGCCACTTCCGCGACGGTATG-3'.

To obtain the gene encoding the YddV-MBP R365A mutant, gene splicing overlap extension polymerase chain reaction was performed using the following oligonucleotides:

Forward pMAL: 5'-CTCGGGGATGACGATG-3'

Reverse pMAL: 5'-CTCTCCTGAGTAGGACAAATC-3'

Forward R365A: 5'-TTATGACAACGTCGCCAGTAGTG-3'

Reverse R365A: 5'-CACTACTGGCGACGTTGTCAATAA-3'

Full-length wild-type and mutant variants of YddV-MBP were expressed in *E. coli* BL21(DE3) (Novagen) harboring the pMAL-c5e expression vector. Briefly, *E. coli* BL21(DE3) was transformed with the required plasmid, plated on Luria-Bertani (LB) agar containing 100 µg/ml ampicillin, and incubated at 37 °C overnight. On the following day, a single colony was inoculated in LB containing 100 µg/ml ampicillin and shaken overnight at 200 rpm and 37 °C. The culture medium was added to Terrific Broth medium (1:1000 dilution) containing the above antibiotics and shaken at 120 rpm and 37 °C for 4 h. Subsequently, the medium was cooled to 15 °C and protein expression was induced by adding 0.1 M isopropyl β-D-thiogalactopyranoside, followed by further shaking for 20 h. *E. coli* cells were harvested by centrifugation for 10 min at 6750 g and 4 °C, frozen in liquid nitrogen, and stored at -80 °C until purification. *E. coli* cells frozen at -80 °C were suspended in buffer A (50 mM Tris-HCl, pH 8.0, 150 mM NaCl), 1 mM phenylmethanesulfonyl fluoride, 1 mM ethylenediaminetetraacetic acid, and 0.2 mg/ml lysozyme. The solution was sonicated, centrifuged at 100,000g for 30 min and incubated for 20 min with hemin (300 µM) in dimethyl sulfoxide solution. Supernatant fractions were applied to an amylose column (Qiagen, Hilden, Germany) pre-equilibrated with buffer A. Subsequently, the column was washed with buffer A and YddV-MBP fractions were eluted with buffer A containing 10 mM maltose. Protein fractions were pooled and applied to a Superdex 200 10/300 GL column (GE Healthcare, UK) equilibrated with 20 mM Tris-HCl pH 8.0 buffer containing 150 mM NaCl. The desired eluates (identified by monitoring at 280 nm) were collected and concentrated with Amicon® Ultra Centrifugal Filters (Millipore, Billerica, MA, USA). Finally, the purified proteins were quickly frozen in liquid nitrogen and stored at -80 °C until use. All proteins were > 95% homogenous as confirmed by SDS-PAGE (sodium dodecyl sulfate polyacrylamide gel electrophoresis). Protein concentrations were determined using the bicinchoninic acid assay with bovine serum albumin as a standard (Sunrise Absorbance Reader, TECAN).

Expression and purification procedures for *EcDOS* are described in an earlier report [27]. The protein was > 95% homogenous as confirmed by SDS-PAGE. Protein and heme concentrations were determined using the bicinchoninic acid assay with bovine serum albumin as a standard (Sunrise Absorbance Reader, TECAN) and the pyridine hemochromogen assay, respectively.

2.3. Optical absorption spectroscopy

Optical absorption spectral data were obtained at 24 °C using a Cary 60 UV–Vis spectrophotometer (Agilent Technologies, CA, USA). To ensure that the solution was maintained at an appropriate temperature, the reaction mixture was incubated for 5 min prior to spectroscopic measurement.

2.4. Kinetic analysis of the diguanylate cyclase reaction

The diguanylate cyclase activity of YddV-MBP was assayed under various conditions. Unless stated otherwise, the enzymatic reaction was performed at 24 °C, in 50 µl reaction mixtures containing 10 µM YddV-MBP, 50 mM KCl, 5 mM MgCl₂, and 50 mM Tris buffer (pH 8.0). The reaction mixture was pre-incubated for 5 min and the reaction was initiated by adding 1 mM GTP (dissolved in Tris buffer, pH 8.0). The incubation time was usually 2.5 min. The reaction was stopped by incubation at 100 °C for 3 min. Each incubation was performed at least in triplicate. The samples were analyzed by HPLC (high-performance liquid chromatography) using Buffer A (0.1 M KH₂PO₄, 4 mM tetrabutyl ammonium hydrogen sulfate, pH 6.0) and Buffer B (75% Buffer A, 25% methanol) at a flow rate of 0.7 ml/min. Elution was performed using 60% A/ 40% B for the first 15 min then 100% B for 6 min before returning to 60% A/40% B. The absorbance of GTP and *c*-di GMP was monitored at 254 nm as reported previously [19].

The effect of pH on the diguanylate cyclase activity of YddV-MBP was tested in reaction mixtures containing various buffers. Reactions at pH 5.5, 6.0, 6.5 and 7.0 were performed using 100 mM phosphate buffer with an appropriate ratio of Na₂HPO₄ and NaH₂PO₄. Incubations at pH 7.5, 8.0, 8.5, and 9.0 were performed in 100 mM Tris buffer (Tris-HCl), and incubations at pH 9.5, 10.0 and 10.5 were performed using 100 mM glycine (glycine-NaOH) buffer.

The effects of divalent metal ions on YddV-MBP diguanylate cyclase activity were investigated using reaction mixtures containing solutions of metal salts other than MgCl₂. Specifically, 5 mM MgCl₂ was replaced with 5 mM MnCl₂, 5 mM CaCl₂, 5 mM CoCl₂, 5 mM NiCl₂, 5 mM ZnSO₄, or 5 mM CdCl₂ as appropriate. To assess the enzyme's activity in the absence of divalent metal cations, reactions were performed with no added metal salt. Kinetic constants were determined by fitting the kinetics using the tight-binding (Morrison) equation [28].

The time course of the diguanylate cyclase reaction catalyzed by WT YddV-MBP was assayed at 24 °C in a reaction mixture containing 10 µM WT YddV-MBP, 50 mM Tris-HCl (pH 8.0), 50 mM KCl, and 5 mM MgCl₂. The reaction mixture was preincubated for 5 min, and then the reaction was initiated by adding 1 mM GTP at 24 °C. The state of the reaction was determined at 0, 0.5, 1, 2, 3, 5, 15, 30, 45, and 60 min after initiation.

The kinetic parameters of the diguanylate cyclase activity of YddV-MBP were investigated using 50 µl reaction mixtures containing 10 µM YddV-MBP, 0–1000 µM GTP (0, 10, 25, 50, 100, 300, 500, 750, or 1000 µM dissolved in Tris buffer, pH 8.0), 50 mM Tris-HCl (pH 8.0), 50 mM KCl, and 5 mM MgCl₂. The reaction was started by adding GTP. On the basis of the previously determined (see the preceding paragraph) time course for the diguanylate cyclase reaction catalyzed by WT YddV-MBP, the amount of reaction product formed per minute over the first 3 min of the reaction was taken as the initial velocity of the enzymatic reaction (Fig. S1). Therefore, the reaction mixtures used to determine kinetic parameters were incubated at 24 °C for 2.5 min; the reaction during this period was assumed to proceed under initial velocity conditions because of the reaction's linearity over the first 3 min. The reaction was stopped by incubation at 100 °C for 3 min. The YddV-MBP diguanylate cyclase reaction is a condensation process (two molecules of the substrate, GTP, are combined to form the product, *c*-di-GMP). Kinetic constants were determined by nonlinear least-squares regression based on the Michaelis–Menten equation. At least three replicate experiments were performed for each set of reaction

conditions. Kinetic parameters were determined by fitting based on individual measurements and then averaged and grand standard deviations were calculated from the fit error and discrepancies between individual measurements.

The effects of the heme iron and its redox and coordination state on the Michaelis–Menten kinetics of the diguanylate cyclase reaction were investigated by varying the configuration of the sensing domain heme of YddV-MBP. After purification, the heme iron of the native YddV-MBP protein was in the Fe(III) state. Heme Fe(II) species were prepared by placing a 20 µM solution of the Fe(III) protein in a quartz cuvette and reducing it using 10 mM sodium dithionite in an anaerobic box. Fe(II)-CO complexes were then prepared by gently bubbling gaseous carbon monoxide (Linde, Wiesbaden, Germany) through the cuvette for 5 min. No spectral changes indicative of heme oxidation over time were detected during this process. Sodium dithionite was removed from the preparations containing the Fe(II) and Fe(II)-CO complexes using Sephadex G-25 in PD-10 desalting columns (GE Healthcare), although separate experiments demonstrated that the presence of sodium dithionite did not affect the measured kinetic parameters. The Fe(II)-O₂ complex was prepared by removing sodium dithionite using Sephadex G-25 in PD-10 desalting columns (GE Healthcare) and exposing the Fe(II) species to air for 10 min. After the kinetic experiments, we characterized the samples by UV–Vis spectroscopy to verify that the heme iron species remained in the Fe(II)-O₂ form. These studies revealed no evidence of heme iron autoxidation over the course of the experiment in the case of WT YddV-MBP. The Fe(III)-CN[−] and Fe(III)-imidazole forms of YddV-MBP were produced by mixing a 20 µM solution of the native YddV-MBP protein in its Fe(III) form with 0.1 M KCN and 0.1 M imidazole, respectively. The KCN was used in 100 mM Tris buffer (pH 8.0), and the solution's pH was monitored. Heme-free experiments were performed using the H98A YddV-MBP mutant instead of the WT protein.

The effects of key amino acids on the heme distal side of the sensing domain on the Michaelis–Menten kinetics of the diguanylate cyclase reaction catalyzed by YddV-MBP were investigated by testing mutant proteins in which selected amino acids of WT YddV-MBP were replaced, namely Y43A, Y43F, L65G, L65 M, L65Q, and L65 T. The heme iron was in the oxidation state (forming the Fe(III) complex) in all these proteins. At least three replicate experiments were performed for each mutant. As before, kinetic parameters for each mutant were determined by fitting based on individual measurements then averaging, and grand standard deviations were calculated from the fit error and discrepancies between individual measurements.

To test for possible feedback inhibition of diguanylate cyclase activity by the reaction product, *c*-di-GMP, the activity of YddV-MBP R365A mutant was investigated under the conditions used to study WT YddV-MBP, with the mutant replacing the WT protein. The heme iron center in this protein was in the oxidized state (forming the Fe(III) complex).

2.5. Analytical ultracentrifugation

Sedimentation velocity experiments were performed using a ProteomLab XL-I (Beckman Coulter, Brea, CA) analytical ultracentrifuge at loading concentrations of 1–10 µM YddV-MBP WT, 20 °C, and a rotor speed of 36,000 rpm. Samples were dialyzed against a buffer containing 20 mM Tris-HCl (pH 8.0) containing 150 mM NaCl prior to analysis. All data were collected using interference optics (used for weight average sedimentation coefficient calculations) and absorbance optics at 390 nm (selective for hemoproteins). Sedimentation velocity data were analyzed using a continuous sedimentation coefficient distribution model, *c*(*s*). The resulting apparent sedimentation coefficients were used to compute sedimentation coefficients in water at 20 °C (*s*_{20,w}).

2.6. Size exclusion chromatography

The oligomerization states of YddV-MBP WT and its mutants were determined by size exclusion chromatography using a Superdex 200 Increase 10/300 GL column (GE Healthcare). The mobile phase consisted of 20 mM Tris-HCl (pH 8.0), and 150 mM NaCl. The flow rate was 0.75 ml/min and the injection volume was 100 μ l. Eluted proteins were detected by their absorbance at 280 nm. The globular proteins thyroglobulin (669 kDa), apoferritin (481 kDa), aldolase (158 kDa), bovine serum albumin (66 kDa) and ovalbumin (43 kDa) were used as molecular weight standards, and were analyzed on a Superdex 200 Increase 10/300 GL column (GE Healthcare). The calibration data are shown in Fig. S2C and D. The theoretical molecular weights (calculated molecular weights based on amino acid sequences) of YddV-MBP in its monomeric, dimeric, and tetrameric forms are 96 kDa, 192 kDa and 384 kDa, respectively. The calibration data indicate that the column should adequately separate these forms under the conditions applied. The ratios of the content of each oligomeric form were calculated from the peak areas observed in the size exclusion chromatograms.

Samples for analysis were prepared as follows. YddV-MBP WT and mutants in their Fe(III) and other forms (see below) were dissolved in 50 mM Tris-HCl, pH 8.0, 50 mM KCl and 5 mM MgCl₂ to a final concentration of 10 μ M and incubated at 24 °C for 30 min prior to analysis. The native proteins were in their Fe(III) forms, as they were when isolated. The Fe(II)-O₂ complexes were prepared by incubating proteins with sodium dithionite (0.1 M), removing excess sodium dithionite using a Sephadex G-25 in PD-10 Desalting Column (GE Healthcare), and exposing the resulting Fe(II) species to air for 10 min. The Fe(III)-CN⁻ and Fe(III)-imidazole forms of YddV-MBP were produced by mixing a 10 μ M solution of the native YddV-MBP protein with 10 mM KCN (10 min incubation) and 10 mM imidazole (1 min incubation), respectively. The KCN was used in 50 mM Tris buffer (pH 8.0), and the solution's pH was monitored. After the size exclusion chromatography experiments, we characterized the samples by UV-Vis spectroscopy to verify that the heme iron species remained in the desired form. The samples of YddV-MBP in the presence of *c*-di-GMP were prepared by incubating 10 μ M protein with 1 mM GTP, 50 mM KCl, and 5 mM MgCl₂ to maximize completion of the diguanylate cyclase reaction (or 0.1 mM *c*-di-GMP for 5 min at 24 °C. In experiments on the effect of *Ec*DOS on the oligomeric state of YddV-MBP, both proteins were mixed together, each at 10 μ M, in 20 mM Tris-HCl (pH 8.0) and 150 mM NaCl, and the mixture was incubated for 30 min at 24 °C prior to analysis.

3. Results

The active full-length YddV protein has proven to be difficult to purify, resisting several standard methods of protein purification. The most efficient approach was to make a chimeric form of the full-length YddV protein fused with maltose binding protein (MBP) at its N-terminus. Removing the MBP from the purified YddV-MBP construct caused the immediate precipitation of the liberated YddV protein. Therefore, all studies presented here were conducted with the full-length YddV construct including the MBP tag (YddV-MBP). The UV-Vis spectral properties of the YddV-MBP construct (Supporting Table S1) are virtually identical to those of the isolated globin domain of YddV (YddV-heme) [5,22]. Based on the positions of the Soret band and other peaks in the visible region, the heme iron complex in purified YddV-MBP is a 5-coordinate high-spin Fe(III) complex.

I. The effect of the heme iron redox state and ligand coordination in the sensing domain on the kinetic parameters of the diguanylate cyclase reaction catalyzed by YddV-MBP

The time course of the reaction catalyzed by YddV-MBP indicated that the concentration of the reaction product (*c*-di-GMP) increased linearly during at least the first 3 min (Fig. S1). The reaction rate did

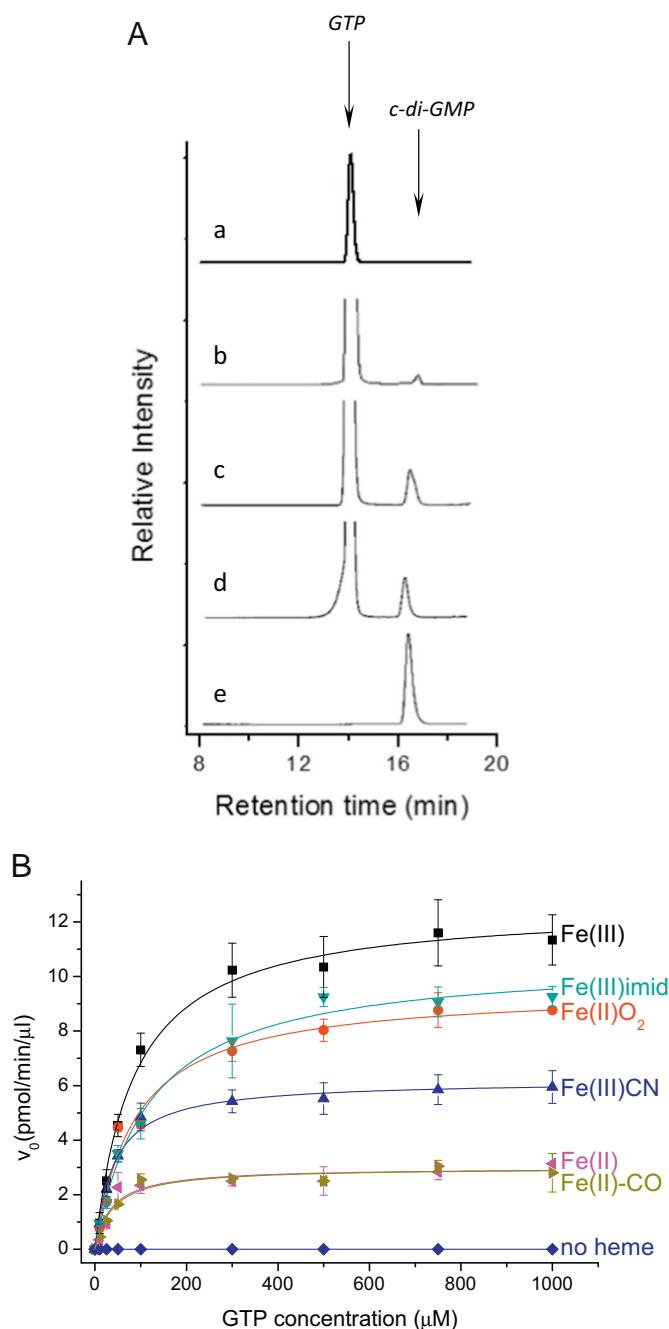


Fig. 1. A HPLC profiles showing the relative abundance of the substrate (GTP) and product (*c*-di-GMP) of the diguanylcyclase reaction catalyzed by YddV-MBP under various conditions. (a): GTP in enzyme-free buffer. (b): GTP after treatment with YddV-MBP in its Fe(II) form. (c): GTP after treatment with YddV-MBP in its Fe(III)-CN form. (d): GTP after treatment with YddV-MBP in its Fe(III) form. (e): *c*-di-GMP in enzyme-free buffer.

B. Effects of the heme iron center's redox state and coordination, and the presence of the heme iron in the sensing domain, on the Michaelis-Menten kinetics of the diguanylate cyclase reaction catalyzed by YddV-MBP. Results for the different forms of YddV-MBP are plotted using the following colors and symbols: Fe(III) (native form; black line and squares), Fe(III)-imidazole (green line and triangles), Fe(II)-O₂ (red line and circles), Fe(III)-CN⁻ (blue line and triangles), Fe(II)-CO (brown green line and triangles), Fe(II) (pink line and triangles), and heme-free form (H98A; dark blue line and diamonds). In each run, a reaction mixture containing 10 μ M of the appropriate YddV-MBP species, 0–1000 μ M GTP, 50 mM Tris-HCl (pH 8.0), 50 mM KCl, and 5 mM MgCl₂ in a total volume of 100 μ l was incubated for 2.5 min (for further details, see Experimental procedures). (For interpretation of the references to color in this figure legend, the reader is referred to the web version of this article.)

Table 1

Effects of the heme iron redox state, heme iron ligand coordination, and the presence of the heme iron in the sensing domain on the kinetic parameters of the diguanylate cyclase reaction catalyzed by YddV-MBP.

Heme iron state in the sensing domain of YddV-MBP	K_m^{GTP} (μM)	V_{max}^{GTP} (pmol <i>c</i> -di-GMP $\cdot\text{min}^{-1}\cdot\mu\text{l}^{-1}$)	k_{cat} (min^{-1})	k_{cat}/K_m^{GTP} ($\mu\text{M}^{-1}\cdot\text{min}^{-1}$)
Fe(III)	84 \pm 21	12 \pm 1	1.2 \pm 0.1	0.014
Fe(III)-CN ⁻	41 \pm 8	6.2 \pm 0.5	0.62 \pm 0.05	0.015
Fe(III)-imidazole	131 \pm 34	12 \pm 0.6	1.2 \pm 0.06	0.009
Fe(II)-O ₂	87 \pm 17	9.5 \pm 0.5	0.95 \pm 0.05	0.011
Fe(II)-CO	39 \pm 12	3.0 \pm 0.3	0.3 \pm 0.03	0.008
Fe(II)	38 \pm 19	3.0 \pm 0.3	0.3 \pm 0.03	0.008
No heme (H98A)		No reaction		

not change appreciably during extended incubations (Fig. S1), suggesting that YddV-MBP is not subject to significant feedback inhibition by the reaction product, *c*-di-GMP. The initial velocities of catalysis were calculated from the slopes of plots of product concentration against time over the first 2.5 min. The reaction kinetics were then analyzed at various GTP concentrations (Fig. 1). Each data set was curve-fitted to the Michaelis-Menten equation using the Hill coefficient ($n = 1$), revealing that the reactions of all the various YddV-MBP species exhibited Michaelis–Menten kinetics.

To determine whether the heme iron complex in the globin domain is essential for the activity of YddV-MBP, the His98 residue that acts as the proximal axial ligand of the heme Fe(III) complex was replaced with Ala. This led to the formation of heme-free YddV-MBP, as demonstrated by UV–Vis spectroscopy [5]. The heme-free YddV-MBP is inactive, indicating that the heme iron complex is essential for the catalytic activity of YddV-MBP (Fig. 1 and Table 1).

The purified YddV-MBP has a 5-coordinate high-spin Fe(III) complex that is stable under aerobic conditions. This enzyme exhibits high activity, with an apparent Michaelis-Menten constant (K_m^{GTP}) of 84 \pm 21 μM , an apparent reaction rate constant or maximal turnover number (k_{cat}) of 1.2 min^{-1} , a catalytic efficiency (k_{cat}/K_m^{GTP}) of 0.014 $\mu\text{M}^{-1}\cdot\text{min}^{-1}$ (Table 1), and a V_{max}^{GTP} of 12 pmol *c*-di-GMP $\cdot\text{min}^{-1}\cdot\mu\text{l}^{-1}$. The Fe(II) and Fe(II)-CO species have much lower V_{max}^{GTP} values (0.3 pmol *c*-di-GMP $\cdot\text{min}^{-1}\cdot\mu\text{l}^{-1}$) than the Fe(III) species but their K_m^{GTP} values (38–39 μM) were within \pm 50% of that for the Fe(III) species (Table 1, Fig. 1). The heme redox and/or coordination state significantly affected the k_{cat} values. For example, the enzymes with Fe(II) and Fe(II)-CO complexes had a k_{cat} of 0.3 min^{-1} , around 4 times lower than that of the enzyme with the Fe(III) complex (1.2 min^{-1}). Consequently, these enzymes had the lowest k_{cat}/K_m^{GTP} (0.008 $\mu\text{M}^{-1}\cdot\text{min}^{-1}$) values of the studied WT YddV-MBP species (the highest k_{cat}/K_m^{GTP} observed in this work was 0.015 $\mu\text{M}^{-1}\cdot\text{min}^{-1}$). When the enzyme with the Fe(II) complex was exposed to O₂, its catalytic activity increased significantly, suggesting that YddV is an oxygen sensing enzyme (Table 1, Fig. 1). The kinetic parameters of the enzyme with the Fe(II)-O₂ complex closely resemble those of the Fe(III) species.

The K_m^{GTP} (41 μM) and V_{max}^{GTP} (6.2 pmol *c*-di-GMP $\cdot\text{min}^{-1}\cdot\mu\text{l}^{-1}$) of the enzyme with the Fe(III)-CN⁻ complex were around half those for the Fe(III) species. Conversely, the K_m^{GTP} of the enzyme with the Fe(III)-imidazole complex (131 μM) was almost twice that of the Fe(III) species, although its V_{max}^{GTP} (12 pmol *c*-di-GMP $\cdot\text{min}^{-1}\cdot\mu\text{l}^{-1}$) was similar to that of the Fe(III) species (Table 1, Fig. 1). The k_{cat} (0.62 min^{-1}) of the Fe(III)-CN⁻ enzyme was half that for the Fe(III) species, but that for the Fe(III)-imidazole enzyme was similar to that for the Fe(III) species. Therefore, the catalytic efficiency (k_{cat}/K_m^{GTP}) (0.015 $\mu\text{M}^{-1}\cdot\text{min}^{-1}$) of the Fe(III)-CN⁻ species was comparable to that of the Fe(III) species, whereas that (0.009 $\mu\text{M}^{-1}\cdot\text{min}^{-1}$) of the Fe(III)-imidazole species was lower than that of the Fe(III) species. These differences in catalytic efficiency between the Fe(III)-CN⁻ and Fe(III)-imidazole species are due to their significantly different Michaelis constants (K_m^{GTP}) and k_{cat} values (Table 1, Fig. 1). The protein

structural changes at the heme binding site caused by imidazole binding would be larger than those due to cyanide binding. Structural changes in the vicinity of the sensing domain are presumably transduced through the protein's structure to the functional domain, explaining the greater impact of imidazole on the enzyme's K_m^{GTP} .

II. The effect of the Tyr43 and Leu65 residues in the sensing domain on the kinetic parameters of the diguanylate cyclase reaction catalyzed by YddV-MBP

Tyr43 and Leu65 are highly conserved amino acid residues on the heme distal side of the YddV sensing domain. Tyr43 interacts with an oxygen molecule coordinated to the heme Fe(II) complex [5], while Leu65 is critical for restricting the access of water molecules to the heme distal side to avoid rapid YddV autooxidation [22] (Fig. 2A). Mutating these key heme distal amino acids had significant effects on the kinetic parameters of YddV-MBP (Table 2, Fig. 2B). For example, the K_m^{GTP} (22 μM), V_{max}^{GTP} (1.5 pmol *c*-di-GMP $\cdot\text{min}^{-1}\cdot\mu\text{l}^{-1}$), and k_{cat} (0.15 min^{-1}) of L65G were the lowest of those for any of the YddV variants studied in this work, including the WT. While the K_m^{GTP} (101 μM) of L65Q was higher than those of other variants, its V_{max}^{GTP} (2.6 pmol *c*-di-GMP $\cdot\text{min}^{-1}\cdot\mu\text{l}^{-1}$) and k_{cat} (0.26 min^{-1}) were the second lowest after those of L65G, giving it the lowest k_{cat}/K_m^{GTP} (0.003 $\mu\text{M}^{-1}\cdot\text{min}^{-1}$) of the proteins studied here. The spectroscopic characteristics of L65G also differed substantially from those of the WT and other Leu65 mutants, indicating differences in structure and the rates of O₂ binding and autooxidation. These results suggest that the water molecule is bound near the heme distal side in both the Fe(III) and Fe(II)-O₂ L65G species [22]. The globin domain structure near the heme prosthetic group of the L65G mutant is probably the most different from the other tested mutants. All of the protein structure changes in the vicinity of the YddV-MBP heme caused by mutations at Leu65 markedly affect the heme Fe(III) enzyme's catalytic kinetics.

The kinetic parameters of the Tyr43 mutants were less striking than those of the Leu65 mutants. The comparatively modest impact of Tyr43 mutations is unsurprising because Tyr43 interacts with the bound O₂ molecule in the Fe(II)-O₂ complex [5]. Therefore, its side chain would be expected to project in a different direction or the residue would be expected to be positioned relatively far from the heme in the Fe(III) form of the enzyme.

III. Effects of other factors (pH, Mg²⁺, Mn²⁺, Ca²⁺, Co²⁺, Ni²⁺, Zn²⁺, and Cd²⁺ ions) on the kinetic parameters of the diguanylate cyclase reaction catalyzed by YddV-MBP

The enzyme was inactive below pH 6.0 and above pH 10.0 (Fig. 3A). Within this range, its activity exhibited an asymmetric bell-shaped dependence upon pH. Its optimal pH was around 8.5–9.00; the rate of catalysis at pH 7.0 was around half that at the optimal pH, while at pH 8.0, it was around 80% of the optimal rate. We conducted our experiments at pH 8.0 because these mildly alkaline conditions are optimal for preserving the conformation and stability of YddV-MBP and

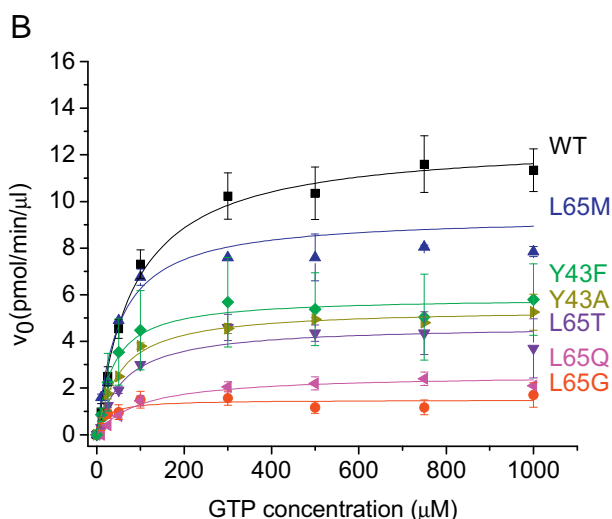
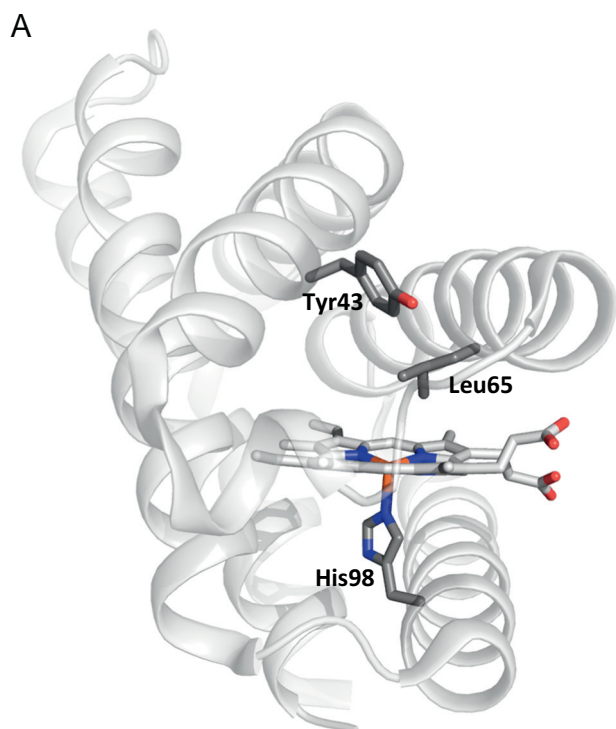


Fig. 2. A. Structure of the YddV sensing domain adopting the globin fold with the heme iron in its Fe(III) form based on PDB coordinates 4ZVA [6]. Heme and sidechains of important residues are shown as sticks.

B. Effects of key amino acids on the heme distal side of the sensing domain on the Michaelis–Menten kinetics of the diguanylate cyclase reaction catalyzed by YddV-MBP. Results for the wild type YddV-MBP are selected mutants plotted using the following colors and symbols: Fe(III) (wild type; black line and squares), L65G (red line and circles), L65M (blue line and triangles), L65T (purple line and triangles), L65Q (pink line and triangles), Y43A (brown line and triangles), and Y43F (green line and diamonds). In each run, a reaction mixture containing 10 μM YddV-MBP WT or mutant, 0–1000 μM GTP, 50 mM Tris-HCl (pH 8.0), 50 mM KCl, and 5 mM MgCl_2 in a total volume of 100 μl was incubated for 2.5 min (for further details, see Experimental procedures). (For interpretation of the references to color in this figure legend, the reader is referred to the web version of this article.)

are close to the optimal pH.

We tested the effects of several divalent metal cations (Mg^{2+} , Mn^{2+} , Ca^{2+} , Co^{2+} , Ni^{2+} , Zn^{2+} , and Cd^{2+}) on catalysis under the same conditions (Fig. 3B). No reaction was observed in the absence of divalent metal cations. Of the divalent cations investigated, Mn^{2+} was by far the

Table 2

Effects of key amino acid residues on the heme distal side of the sensing domain on the kinetic parameters of the diguanylate cyclase reaction catalyzed by YddV-MBP.

Mutant of YddV-MBP Fe(III)	K_m^{GTP} (μM)	$V_{\text{max}}^{\text{GTP}}$ (pmol <i>c</i> -di-GMP $\cdot\text{min}^{-1}\cdot\mu\text{l}^{-1}$)	k_{cat} (min^{-1})	$k_{\text{cat}}/K_m^{\text{GTP}}$ ($\mu\text{M}^{-1}\cdot\text{min}^{-1}$)
WT	84 ± 21	12 ± 1	1.2 ± 0.1	0.014
L65G	22 ± 19	1.5 ± 0.3	0.15 ± 0.03	0.007
L65M	42 ± 8	8.5 ± 0.4	0.85 ± 0.04	0.020
L65T	63 ± 25	4.7 ± 0.8	0.47 ± 0.08	0.007
L65Q	101 ± 33	2.6 ± 0.2	0.26 ± 0.02	0.003
Y43A	54 ± 11	5.4 ± 0.3	0.54 ± 0.03	0.010
Y43F	29 ± 10	6.9 ± 0.8	0.69 ± 0.08	0.024

most effective at stimulating catalysis: the $k_{\text{cat}}/K_m^{\text{GTP}}$ values in the presence of Mn^{2+} and Mg^{2+} were $0.067 \mu\text{M}^{-1}\cdot\text{min}^{-1}$ and $0.016 \mu\text{M}^{-1}\cdot\text{min}^{-1}$, respectively. Kinetic constants were determined by fitting the kinetics using the tight-binding (Morrison) equation [28]. The apparent K_m^{GTP} value in the presence of Mn^{2+} ($15 \pm 4 \mu\text{M}$) was approximately 5 times lower than that in the presence of Mg^{2+} ($76 \pm 5 \mu\text{M}$), while the $V_{\text{max}}^{\text{GTP}}$ (10 ± 0.4 pmol of *c*-di-GMP $\cdot\text{min}^{-1}\cdot\mu\text{l}^{-1}$) and k_{cat} (1.0 min^{-1}) values in the presence of Mn^{2+} were slightly lower than those (12 ± 0.2 pmol of *c*-di-GMP $\cdot\text{min}^{-1}\cdot\mu\text{l}^{-1}$ and 1.2 min^{-1}) in the presence of Mg^{2+} (Table 1 and Fig. 3B). Since both Mg^{2+} and Mn^{2+} form metal-GTP complexes, these results suggest that the enzyme's affinity for the Mn^{2+} -GTP complex and the orientation of GTP in its active site differ from those for the Mg^{2+} -GTP complex. Replacing Mg^{2+} with Ca^{2+} , Co^{2+} , Ni^{2+} , Zn^{2+} , or Cd^{2+} completely suppressed the enzyme's activity (Fig. 3B).

IV. Oligomeric state of YddV-MBP

Because the catalytic activities of other globin-coupled oxygen sensors (*PccGCS* and *BpeGReg*) depend on their oligomerization [7,8], the oligomeric state of YddV-MBP was examined. Ultracentrifugation experiments revealed that WT YddV-MBP predominantly exists as a dimer with a sedimentation coefficient ($s_{20,w}$) of around 8. A tetrameric form with a sedimentation coefficient of around 12 was also present in solution as a minor contributor (Fig. S2A). To study the oligomeric states of YddV-MBP under various conditions, size exclusion chromatography was used as a faster alternative to ultracentrifugation (Fig. S2B). The theoretical molecular weights of YddV-MBP in its monomeric, dimeric, and tetrameric forms are 96 kDa, 192 kDa and 384 kDa, respectively. The chromatographic experiments confirmed that YddV-MBP exists mainly as a dimer, in keeping with the results obtained by ultracentrifugation (Fig. S2A), and indicated that the oligomeric state of YddV-MBP is almost completely independent of the presence or absence of *c*-di-GMP (Fig. S2B). The protein containing the heme iron in its Fe(III) is fully enzymatically active and therefore forms *c*-di-GMP in the presence of GTP (and the other necessary compounds mentioned in the Experimental Procedures). The dimer to tetramer ratios for YddV-MBP in the presence and absence of GTP (and therefore of *c*-di-GMP) were 3.7:1 and 4.3:1, respectively (Fig. S2B).

The effect of the heme iron's oxidation state and ligand coordination on the oligomeric state of YddV-MBP as revealed by size exclusion chromatography is shown in Fig. S3A. Like the Fe(II) form, the Fe(II)- O_2 , Fe(III)- CN^- , and Fe(III)-imidazole forms of YddV-MBP exist primarily as dimers, with tetramers being minor components (Fig. S3A). This suggests that changes in the heme iron's oxidation state and ligand coordination have little effect on the protein's oligomerization. Unfortunately, efforts to perform size exclusion chromatography with Fe(II) species under anaerobic conditions were unsuccessful. Importantly, the enzymatically inactive YddV-MBP apoform (H98A) exists predominantly as an octamer (its dimer/tetramer/octamer ratio

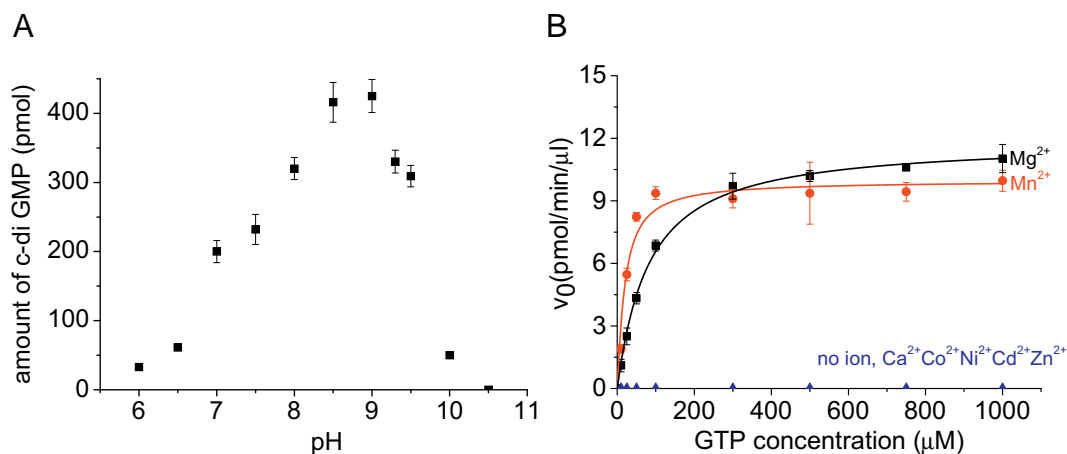


Fig. 3. Effect of pH and divalent metal ions on the diguanylate cyclase reaction catalyzed by WT YddV-MBP [in its Fe(III) form] (A) Effect of pH on the diguanylate cyclase reaction. In each run, a reaction mixture containing 10 μM YddV-MBP, 1 mM GTP, 50 mM KCl, 5 mM MgCl₂, and an appropriate pH buffer (100 mM) in a total volume of 100 μl was incubated for 2.5 min (for further details, see Experimental Procedures). (B) Effects of different divalent metal ions on the diguanylate cyclase reaction, plotted using the following colors and symbols: Mg²⁺ (black line and squares; $K_m^{GTP} = 76 \pm 5 \mu\text{M}$ and $V_{max}^{GTP} = 12 \pm 0.2 \text{ pmol of } c\text{-di-GMP}\cdot\text{min}^{-1}\cdot\mu\text{l}^{-1}$), Mn²⁺ (red line and circles; $K_m^{GTP} = 15 \pm 4 \mu\text{M}$ and $V_{max}^{GTP} = 10 \pm 0.4 \text{ pmol of } c\text{-di-GMP}\cdot\text{min}^{-1}\cdot\mu\text{l}^{-1}$), Ca²⁺, Co²⁺, Ni²⁺, Zn²⁺, and Cd²⁺, and no divalent cations (blue line and diamonds). In each run, a reaction mixture containing 10 μM YddV-MBP, 5–1000 μM GTP, 50 mM Tris-HCl (pH 8.0), 50 mM KCl, and 0 or 5 mM MgCl₂, 5 mM MnCl₂, 5 mM CaCl₂, 5 mM CoCl₂, 5 mM NiCl₂, 5 mM ZnSO₄, or 5 mM CdCl₂ in a total volume of 100 μl was incubated for 2.5 min (for further details, see Experimental Procedures). (For interpretation of the references to color in this figure legend, the reader is referred to the web version of this article.)

was 1/0/8.4) (Fig. S3A), suggesting that the heme iron complex plays an important role in dimer formation, which may stabilize the enzyme and maximize its catalytic activity.

The effects of key sensing domain amino acids on the oligomeric state of YddV-MBP are shown in Fig. S3B and C. The key amino acids in the sensing domain have stronger effects on the oligomerization of YddV-MBP than the heme iron oxidation and ligand coordination state (Fig. S3B and C). The mutants have a much greater propensity to exist as octamers than the WT protein, for which the abundance of this oligomer was negligible. The relative abundance of the octamer is highest for the Y43F mutant, followed by the L65G mutant (Fig. S3B). It is also interesting that no tetramers were detected in the cases of the L65G, L65Q, and L65T mutants. The calculated dimer:tetramer:octamer ratios are 4.3:1:~0 for the WT; 3.6:1:1.7 for Y43A; 1.5:1:2.5 for Y43F; 1:~0:1 for L65G; 2.5:~0:1 for L65Q; 1.8:~0:1 for L65T; and 5.2:1:1.2 for L65M. Experiments were also performed using the Fe(III), Fe(II)-O₂, and Fe(III)-CN⁻ complexes of the Tyr43 (Y43A, Y43F) and Leu65 (L65G, L65M, L65Q, L65T) mutants. However, the results obtained were very similar to those for the Fe(III) forms, so only results for the latter are shown (Fig. S3C). The presence or absence of *c*-di-GMP has no detectable effect on the protein's oligomerization state.

The effect of *Ec*DOS on the oligomerization of YddV was also investigated because it appears that YddV (a *c*-di-GMP synthesizing enzyme) and *Ec*DOS (a *c*-di-GMP degrading enzyme) work together to regulate *c*-di-GMP levels in *E. coli* [4]. However, *Ec*DOS has no detectable effect on the oligomerization state of YddV-MBP when both proteins are present in equimolar quantities (data not shown). Under our experimental conditions, changes in the oligomerization of YddV-MBP would only be observed if the two proteins formed a complex with very high affinity. Our results therefore do not exclude the possibility that *Ec*DOS and YddV interact.

4. Discussion

The molecular mechanism of signal transduction in YddV has remained unclear because of the difficulty of obtaining a catalytically active version of the full-length YddV protein [5,6]. We investigated several approaches to obtain a stable and active form of the full-length YddV protein. The most successful approach involved attaching maltose

binding protein (MBP) to full-length YddV at the *N*-terminus. However, it was impossible to remove the MBP tag because the YddV protein precipitated immediately upon doing so. Fortunately, the attachment of MBP to the heme-bound sensing domain has no discernible effect on the UV-Vis spectra of YddV-MBP, which are virtually identical to those of the isolated YddV sensing domain, suggesting that the heme sensing domain of the fusion protein adopts the native structure [5,22] (Supporting Table S1). In addition, the enzyme activities observed in this study for YddV-MBP are significantly higher than those reported previously [4–6]. It thus seems that the MBP tag does not affect the sensing or catalytic activity of YddV, making YddV-MBP a suitable model for studying YddV's kinetics.

Previous studies analyzed the catalytic activity of YddV only in terms of the initial rate of product formation (in micromoles of *c*-di-GMP per micromole of YddV per minute) [4–6]. Those investigations suggested that the Fe(III) form of YddV is more active than the Fe(II)-O₂ and Fe(II)-CO forms [4–6], and that the Fe(II) form is either completely inactive [5] or much less active than the other forms [6]. The initial rates of *c*-di-GMP formation for the Fe(III), Fe(II), Fe(II)-O₂, and Fe(II)-CO species were estimated to be 0.066–0.124 min⁻¹, < 0.001 min⁻¹, 0.022–0.066 min⁻¹, and 0.022 min⁻¹, respectively [5,6]. In this work, we performed detailed kinetic analyses of YddV's catalytic activity and determined the K_m , V_{max} and k_{cat} values of its various forms, allowing us to investigate how changes in the sensing domain affected its kinetics. We also demonstrated that its catalytic activity exhibits Michaelis-Menten kinetics, that the pH optimum for the process is about 8.5–9.0, and that its activity requires the presence of either Mg²⁺ or Mn²⁺; no diguanylate cyclase activity was observed in the presence of other common divalent metal cations (Ca²⁺, Co²⁺, Ni²⁺, Zn²⁺, and Cd²⁺).

In agreement with previous studies, we found that the most active heme iron oxidation and/or coordination form of YddV-MBP is its Fe(III) form. YddV-MBP was isolated in this form under aerobic conditions. However, it may be that the Fe(II) form predominates under anaerobic conditions, and that O₂ binding to this form stimulates catalysis transiently in certain microenvironments. It is possible that YddV acts as both an O₂ sensor and a redox sensor in the cell. In this context, it should be noted that the oxygen-binding affinity of YddV is relatively low (dissociation constant $K_d = 15 \mu\text{M}$) [22], supporting the possibility

that it may act as a redox sensor. The k_{cat} values of the less active forms of YddV-MBP are around 4 times lower than that of the Fe(III) form, but their catalytic efficiency is only around 2 times lower. The comparatively modest reduction in efficiency is due to a decrease in the K_m^{GTP} value, suggesting that the less active forms have a greater affinity for GTP than the most active form. This may be because of a complex rearrangement of the functional domain associated with the signal transduction process. Interestingly, the less-active Fe(II) form is activated by the binding of O_2 , but not by that of CO. It thus seems that the heme distal side of the sensing domain distinguishes between these diatomic molecules. The oxygen sensor AfGcHK can also discriminate between these molecules [29], but the oxygen sensor protein EcDOS cannot [19]. The introduction of a sixth axial ligand on the heme iron Fe(III) center also had interesting effects on the enzyme's activity: the small diatomic CN^- ion reduced the K_m^{GTP} value, suggesting an increase in the enzyme's affinity for its substrate (GTP). The difference in affinity between these two forms is comparable to that observed for the Fe(II) and Fe(II)-CO forms. In contrast, the more sterically demanding ligand imidazole caused the K_m^{GTP} value to increase, indicating a reduction in substrate affinity. However, the maximum velocity of the Fe(III)-imidazole form was identical to that of the Fe(III) form. The detailed kinetic analysis thus sheds more light on the changes in the sensing and functional domains (in terms of GTP affinity) caused by the signal transduction process. The importance of these results is amplified by the fact that the full-length protein's low solubility has prevented the acquisition of reliable structural data.

The cyclase activity of the other enzymatically characterized globin-coupled diguanylate cyclases (*PccGCS* and *BpeGReg*) depends on the heme iron's oxidation state and ligand binding to the heme, in keeping with our conclusions regarding YddV [7,8]. Additionally, the K_m^{GTP} values of these sensors in their active and less active forms are comparable to the corresponding values estimated for YddV-MBP: the K_m^{GTP} values for the active Fe(II)- O_2 forms of *PccGCS* and *BpeGReg* were $31 \pm 6 \mu M$ and $57 \pm 8 \mu M$, respectively. The k_{cat} values for *PccGCS* Fe(II)- O_2 and *BpeGReg* were 0.73 min^{-1} and 0.59 min^{-1} , respectively. The less active Fe(II) forms of these enzymes exhibited K_m^{GTP} values of $62 \pm 3 \mu M$ and $120 \pm 11 \mu M$, respectively, and k_{cat} values of 0.29 min^{-1} and 0.18 min^{-1} , respectively [7,8]. Although V_{max}^{GTP} values were not estimated for other globin-coupled diguanylate cyclases, the initial rates reported for these enzymes can be compared to the k_{cat} values presented here. The initial velocities for the active Fe(II)- O_2 form and less active Fe(II) forms of the globin-coupled diguanylate cyclases from *Shewanella putrefaciens* (*SpDosD*) were 1.68 min^{-1} and 0.52 min^{-1} , respectively; the K_m^{GTP} and V_{max}^{GTP} for this protein were not measured [14]. All these values are similar to those estimated for the active and less active forms of YddV-MBP. However, the initial velocity of the active Fe(II)- O_2 form of another globin-coupled oxygen sensor diguanylate cyclase, HemDGC, is 6.9 min^{-1} – almost an order of magnitude higher than that of similar sensors. Additionally, all other redox and ligand-bound forms of this enzyme exhibited negligible activity [12]. These findings revealed that some organisms with globin-coupled diguanylate cyclases having similar sensing properties [7,8] are probably relatively closely related (*E. coli*, *Bordetella pertussis*, *Pectobacterium carotovorum*), while others are more evolutionarily distant (*Desulfotalea psychrophila*) [12].

Both O_2 binding to the heme within the globin (sensing) domain and *c*-di-GMP binding to a product-binding inhibitory site (I-site) within the cyclase domain control the oligomerization states of *PccGCS* and *BpeGReg* [7,8]. We observed no such oligomerization-dependent differences in activity for YddV-MBP *in vitro*. YddV-MBP exists primarily as a dimer independently of its heme redox state, the heme's ligand coordination, and the presence or absence of the reaction product, *c*-di-GMP. However, mutations of heme distal residues increased the relative abundance of the tetramer and decreased that of the dimer (Figs. S2 and S3). Although globin-coupled diguanylate cyclases from *E. coli*, *Bordetella pertussis* and *Pectobacterium carotovorum* exhibit some notable

similarities [7,8], we showed that there are also significant differences in their behavior.

The functional domain of the YddV-MBP H98A mutant, which lacks a heme in its sensing domain, is catalytically inactive (Table 1 and Fig. 1). Similarly, the activity of a YddV construct without the globin domain was approximately four times lower than that of the Fe(III) form of the full-length protein [6]. These results are consistent with those obtained for a heme-based oxygen sensor phosphodiesterase from *Acetobacter xylinum*, AxPDEA [30], a heme-based oxygen sensor adenylate cyclase from *Leishmania*, HemAC-Lm [31], and globin-coupled histidine kinase from *Anaeromyxobacter sp.* Fw109–5, AfGcHK [29]. The heme-free forms of AxPDEA and HemAC-Lm exhibited very low activity. The binding of heme to the sensing domain presumably causes significant and profound structural changes in the active site that enables the efficient activation of these heme-based oxygen sensors. However, the functional effects of heme removal differ from those in the heme-based oxygen sensor phosphodiesterase EcDOS, whose heme-free forms have appreciable catalytic activity. It was suggested that the heme iron complexes of EcDOS may suppress catalysis, and that O_2 binding to the heme iron complex relieves this suppression [20]. Conversely, the YddV-MBP apoform (*i.e.* the H98A mutant) has no heme-binding capacity, exists primarily as an octamer rather than a dimer, and lacks catalytic activity (Table 1, Figs. 1 and S3). This suggests that the dimeric form adopts a fold or conformation that is required for catalysis.

Experiments involving mutating key amino acids in the sensing domain of YddV-MBP yielded remarkable results (Table 2 and Fig. 2B). Leu65 on the heme distal side probably restricts the access of water molecules to the heme iron complex in the WT protein, while the OH side chain of Tyr43 appears to interact directly with O_2 bound to the heme Fe(II) on the heme distal side [22,26]. The activities of Leu65 and Tyr43 mutants seemed to be partially related to the autooxidation rates of the corresponding mutants of the isolated YddV globin domain: mutations that cause high rates of autooxidation in the isolated domain [22] caused low activity in the intact protein, even when only the Fe(III) forms were considered (Supporting Table S2). In addition, the relative abundance of tetramers appeared to be higher for YddV-MBP variants bearing mutations that reduce activity (Table 2 and Fig. S3B and C).

Taking all these results together, we studied the impact of changes in the heme-containing sensing domain on the diguanylate cyclase activity of the YddV functional domain. The results obtained expand our general knowledge of the relationships between signal transduction, protein conformation, and the functional state of YddV, which is important given the lack of robust structural data on the full-length protein.

Moreover, we note that the intracellular concentration of GTP in *E. coli* ranges from 0.2 to 1.2 mM depending on the carbon source present in the growth medium [32]. Therefore, the GTP concentration will always significantly exceed the K_m^{GTP} values for the YddV-MBP diguanylate cyclase enzyme reported here. This implies that the rate-limiting step is not substrate recognition (and so K_m^{GTP} is not the most useful kinetic parameter for analyzing trends in YddV's activity) even though the signal transduction process apparently involves some appreciable conformational changes. Instead, the limiting step is probably one of the chemical reactions associated with GTP cyclization. The diguanylate cyclase chemical reaction can be characterized in terms of the V_{max}^{GTP} (or the k_{cat} , which is calculated from V_{max}^{GTP}). Therefore, V_{max}^{GTP} is the most useful kinetic parameter when analyzing the diguanylate cyclase process catalyzed by YddV in the *E. coli* cells.

There are many heme-based oxygen sensors. There are also several different classes of heme domain with different protein folds that bind oxygen and regulate the activity of the catalytic domain. For example, the heme domains of YddV and other globin-coupled oxygen sensors have the globin fold, while those of FixL and EcDOS have the PAS fold, and those of DevS and DevT have the GAF fold (named for the proteins cGMP-specific and -stimulated phosphodiesterase, adenylate cyclase,

and *E. coli* formate hydrogen lyase transcriptional activator) [1–3]. Some of the observed functional differences between the studied proteins may thus be due to differences in protein fold and function.

The diguanylate cyclase enzyme activity of YddV should also be considered in relation to that of the PAS domain-coupled phosphodiesterase *EcDOS* because these two proteins act together to regulate intracellular *c*-di-GMP levels. The activity of YddV species decreases in the order Fe(III) > Fe(II)-O₂ > > Fe(II)-CO and Fe(II), while that of *EcDOS* species increases in the order Fe(II)-CO > Fe(II)-O₂ > > Fe(II) > Fe(III) [19,20]. Because we already know that the substrate concentration in *E. coli* cells substantially exceeds the K_m^{GTP} values for the different YddV-MBP species, the overall rate of the process is determined by V_{max}^{GTP} . While the kinetic parameters of the reaction catalyzed by *EcDOS* are unknown, it is likely that the concentration of its substrate, *c*-di-GMP, is much lower than that of GTP. Therefore, the rate of the phosphodiesterase process may be governed by the affinity of *c*-di-GMP for individual *EcDOS* species, unlike in the case of YddV. Moreover, there are probably other factors in the cells that influence the oxygen sensing process and the concentration of *c*-di-GMP. Local milieu- and time-dependent changes/differences in the O₂ concentration in cells will affect the *c*-di-GMP concentration because the O₂ affinities of YddV (K_d : 14 μM) [5] and *EcDOS* (K_d : 340 μM) [33] differ markedly.

Finally, it should be noted that H₂S is another important signaling gas molecule in bacteria that interacts with the hemes of some heme-based oxygen sensors (including *EcDOS*, and *AfGcHK*) and affects their catalytic activities [34–37]. We therefore investigated its effect on the UV-Vis spectra and catalytic activities of the heme Fe(III) form of YddV-MBP. Adding H₂S to solutions of this protein caused spectral changes indicative of redox and coordination changes but had no significant effect on its catalytic activity (See Supporting data).

5. Summary

A catalytically active form of the full-length YddV protein was prepared by attaching it to maltose-binding protein (MBP) and subjected to rigorous kinetic analysis. This revealed that:

1. The diguanylate cyclase reaction catalyzed by YddV-MBP exhibits Michaelis-Menten kinetics, has a pH optimum of around 8.5–9.0, and requires the presence of either Mg²⁺ or Mn²⁺. The most catalytically active form of YddV-MBP was that with a 5-coordinate heme Fe(III) complex; the kinetic parameters determined for this species were K_m^{GTP} 84 ± 21 μM, V_{max}^{GTP} 12 ± 1 pmol of *c*-di-GMP·min⁻¹·μl⁻¹, k_{cat} 1.2 min⁻¹, and k_{cat}/K_m^{GTP} 0.014 μM⁻¹·min⁻¹.

2. The k_{cat} values of YddV-MBP species with heme Fe(II), heme Fe(II)-O₂, and heme Fe(II)-CO complexes were 0.3 min⁻¹, 0.95 min⁻¹ and 0.3 min⁻¹, respectively, suggesting that catalysis is regulated by the heme iron center's redox state and axial ligand binding.

3. The k_{cat} values of the heme Fe(III) forms of YddV-MBP variants bearing the L65G, L65Q, and Y43A mutations at heme distal sites were 0.15 min⁻¹, 0.26 min⁻¹ and 0.54 min⁻¹, respectively, implying that heme distal amino acid residues play key roles in the catalytic mechanism of YddV because they mediate signal transduction between the sensing and functional domains.

4. Ultracentrifugation and size exclusion chromatography experiments indicated that YddV-MBP predominantly exists as a dimer in solution, with a sedimentation coefficient ($s_{20,w}$) around 8. Conversely, the catalytically inert heme-free mutant H93A was predominantly octameric, suggesting that heme binding is important for formation of the catalytically active dimer.

The results presented here improve our knowledge about the effects of various heme iron redox and axial coordination states on the diguanylate cyclase activity of YddV. Since the heme iron is localized in the protein's sensing domain while the diguanylate cyclase activity is localized in its functional domain, we learned more about the relationship between the domains and the signal transduction process.

The approach used in this work provided useful insights into the signaling mechanism of YddV, which is particularly important given the lack of structural data on the full-length protein.

Table of abbreviations

AfGcHK	a globin-coupled histidine kinase from <i>Anaeromyxobacter sp.</i> Fw109–5
AxPDEA	a heme-based oxygen sensor phosphodiesterase of <i>Acetobacter xylinum</i>
BpeGReg	a globin-coupled oxygen sensor with diguanylate cyclase activity from <i>Bordetella pertussis</i>
<i>c</i>-di-GMP	cyclic-di-GMP
EcDOS	a heme-based oxygen sensor phosphodiesterase or <i>EcDosP</i>
<i>E. coli</i>	<i>Escherichia coli</i>
Fe(II)	Fe(II)-protoporphyrin IX complex
Fe(III)	Fe(III)-protoporphyrin IX complex, or hemin
GAF	protein domain named after three proteins: cGMP-specific and -stimulated phosphodiesterase, adenylate cyclase, and <i>E. coli</i> formate hydrogen lyase transcriptional activator
GMP	guanosine-5'-monophosphate
GTP	guanosine-5'-triphosphate
HemAC-Lm	a heme-based oxygen sensor adenylate cyclase of <i>Leishmania</i>
HemDGC	a globin-coupled oxygen sensor with diguanylate cyclase activity from <i>Desulfotalea psychrophila</i>
HPLC	high-performance liquid chromatography
MBP	maltose binding protein
PAS	protein domain named after three proteins (<i>Per-Arnt-Sim</i>)
PccGCS	a globin-coupled oxygen sensor with diguanylate cyclase activity from <i>Pectobacterium carotovorum</i>
SDS-PAGE	sodium dodecyl sulfate polyacrylamide gel electrophoresis
SpDosD	a globin-coupled oxygen sensor with diguanylate cyclase from <i>Shewanella putrefaciens</i>
Tris	tris(hydroxymethyl)aminomethane
WT	wild type
YddV	a globin-coupled oxygen sensor diguanylate cyclase or <i>Ec-DosC</i>
YddV-heme	an isolated heme-bound globin domain of YddV
YddV-MBP	a full-length YddV protein containing a MBP tag

Acknowledgments

This work was supported in part by Charles University, Czech Republic (SVV260427/2018) and the Grant Agency of Charles University, Czech Republic (grant 704217). CIISB research infrastructure project LM2015043 funded by MEYS CR is gratefully acknowledged for the financial support of the measurements at the CMS.

Appendix A. Supplementary data

Supplementary data to this article can be found online at <https://doi.org/10.1016/j.jinorgbio.2019.110833>.

References

- [1] M. Martínková, K. Kitanishi, T. Shimizu, Heme-based globin-coupled oxygen sensors: linking oxygen binding to functional regulation of diguanylate cyclase, histidine kinase, and methyl-accepting chemotaxis, *J. Biol. Chem.* 288 (2013) 27702–27711, <https://doi.org/10.1074/jbc.R113.473249>.
- [2] T. Shimizu, D. Huang, F. Yan, M. Stranova, M. Bartosova, V. Fojtíková, M. Martínková, Gaseous O₂, NO, and CO in signal transduction: structure and function relationships of heme-based gas sensors and heme-redox sensors, *Chem. Rev.* 115 (2015) 6491–6533, <https://doi.org/10.1021/acs.chemrev.5b00018>.
- [3] J.A. Walker, S. Rivera, E.E. Weinert, Mechanism and role of globin-coupled sensor signalling, *Adv. Microb. Physiol.* 71 (2017) 133–169, <https://doi.org/10.1016/bb.ampbs.2017.05.003>.
- [4] J.R. Tuckerman, G. Gonzalez, E.H.S. Sousa, X. Wan, J.A. Saito, M. Alam, M.-

- A. Gilles-Gonzalez, An oxygen-sensing diguanylate cyclase and phosphodiesterase couple for c-di-GMP control, *Biochemistry* 48 (2009) 9764–9774, <https://doi.org/10.1021/bi901409g>.
- [5] K. Kitanishi, K. Kobayashi, Y. Kawamura, I. Ishigami, T. Ogura, K. Nakajima, J. Igarashi, A. Tanaka, T. Shimizu, Important roles of Tyr43 at the putative heme distal side in the oxygen recognition and stability of the Fe(II)-O₂ complex of YddV, a globin-coupled heme-based oxygen sensor diguanylate cyclase, *Biochemistry* 49 (2010) 10381–10393, <https://doi.org/10.1021/bi100733q>.
- [6] M. Tarnawski, T.R.M. Barends, I. Schlichting, Structural analysis of an oxygen-regulated diguanylate cyclase, *Acta Crystallogr. D Biol. Crystallogr.* 71 (2015) 2158–2177, <https://doi.org/10.1107/S139900471501545X>.
- [7] J.L. Burns, D.D. Deer, E.E. Weinert, Oligomeric state affects oxygen dissociation and diguanylate cyclase activity of globin coupled sensors, *Mol. Biosyst.* 10 (2014) 2823–2826, <https://doi.org/10.1039/c4mb00366g>.
- [8] J.L. Burns, S. Rivera, D.D. Deer, S.C. Joynt, D. Dvorak, E.E. Weinert, Oxygen and bis(3',5')-cyclic dimeric guanosine monophosphate binding control oligomerization state equilibria of diguanylate cyclase-containing globin coupled sensors, *Biochemistry* 55 (2016) 6642–6651, <https://doi.org/10.1021/acs.biochem.6b00526>.
- [9] X. Wan, J.R. Tuckerman, J.A. Saito, T.A.K. Freitas, J.S. Newhouse, J.R. Denery, M.Y. Galperin, G. Gonzalez, M.-A. Gilles-Gonzalez, M. Alam, Globins synthesize the second messenger bis-(3'-5')-cyclic diguanosine monophosphate in bacteria, *J. Mol. Biol.* 388 (2009) 262–270, <https://doi.org/10.1016/j.jmb.2009.03.015>.
- [10] S. Rivera, J.L. Burns, G.E. Vansuch, B. Chica, E.E. Weinert, Globin domain interactions control heme pocket conformation and oligomerization of globin coupled sensors, *J. Inorg. Biochem.* 164 (2016) 70–76, <https://doi.org/10.1016/j.jinorgbio.2016.08.016>.
- [11] S. Rivera, P.G. Young, E.D. Hoffer, G.E. Vansuch, C.L. Metzler, C.M. Dunham, E.E. Weinert, Structural insights into oxygen-dependent signal transduction within globin coupled sensors, *Inorg. Chem.* 57 (2018) 14386–14395, <https://doi.org/10.1021/acs.inorgchem.8b02584>.
- [12] H. Sawai, S. Yoshioka, T. Uchida, M. Hyodo, Y. Hayakawa, K. Ishimori, S. Aono, Molecular oxygen regulates the enzymatic activity of a heme-containing diguanylate cyclase (HemDGC) for the synthesis of cyclic di-GMP, *Biochim. Biophys. Acta* 1804 (2010) 166–172, <https://doi.org/10.1016/j.bbapap.2009.09.028>.
- [13] L. Thijs, E. Vinck, A. Bolli, F. Trandafir, X. Wan, D. Hoogewijs, M. Coletta, A. Fago, R.E. Weber, S. Van Doorslaer, P. Ascenzi, M. Alam, L. Moens, S. Dewilde, Characterization of a globin-coupled oxygen sensor with a gene-regulating function, *J. Biol. Chem.* 282 (2007) 37325–37340, <https://doi.org/10.1074/jbc.M705541200>.
- [14] C. Wu, Y.-Y. Cheng, H. Yin, X.-N. Song, W.-W. Li, X.-X. Zhou, L.-P. Zhao, L.-J. Tian, J.-C. Han, H.-Q. Yu, Oxygen promotes biofilm formation of *Shewanella putrefaciens* CN32 through a diguanylate cyclase and an adhesin, *Sci. Rep.* 3 (2013) 1945, <https://doi.org/10.1038/srep01945>.
- [15] A. Pesce, L. Thijs, M. Nardini, F. Desmet, L. Sisinni, L. Gourlay, A. Bolli, M. Coletta, S. Van Doorslaer, X. Wan, M. Alam, P. Ascenzi, L. Moens, M. Bolognesi, S. Dewilde, HisE11 and HisF8 provide bis-histidyl heme hexa-coordination in the globin domain of *Geobacter sulfurreducens* globin-coupled sensor, *J. Mol. Biol.* 386 (2009) 246–260, <https://doi.org/10.1016/j.jmb.2008.12.023>.
- [16] R. Hengge, Principles of c-di-GMP signalling in bacteria, *Nat. Rev. Microbiol.* 7 (2009) 263–273, <https://doi.org/10.1038/nrmicro2109>.
- [17] T. Schirmer, U. Jenal, Structural and mechanistic determinants of c-di-GMP signalling, *Nat. Rev. Microbiol.* 7 (2009) 724–735, <https://doi.org/10.1038/nrmicro2203>.
- [18] J.R. Tuckerman, G. Gonzalez, M.-A. Gilles-Gonzalez, Cyclic di-GMP activation of polynucleotide phosphorylase signal-dependent RNA processing, *J. Mol. Biol.* 407 (2011) 633–639, <https://doi.org/10.1016/j.jmb.2011.02.019>.
- [19] A. Tanaka, H. Takahashi, T. Shimizu, Critical role of the heme axial ligand, Met95, in locking catalysis of the phosphodiesterase from *Escherichia coli* (Ec DOS) toward cyclic diGMP, *J. Biol. Chem.* 282 (2007) 21301–21307, <https://doi.org/10.1074/jbc.M701920200>.
- [20] A. Tanaka, T. Shimizu, Ligand binding to the Fe(III)-protoporphyrin IX complex of phosphodiesterase from *Escherichia coli* (Ec DOS) markedly enhances catalysis of cyclic di-GMP: roles of Met95, Arg97, and Phe113 of the putative heme distal side in catalytic regulation and ligand binding, *Biochemistry* 47 (2008) 13438–13446, <https://doi.org/10.1021/bi8012017>.
- [21] L. Tagliabue, A. Maciag, D. Antoniani, P. Landini, The yddV-dos operon controls biofilm formation through the regulation of genes encoding curli fibers' subunits in aerobically growing *Escherichia coli*, *FEMS Immunol. Med. Microbiol.* 59 (2010) 477–484, <https://doi.org/10.1111/j.1574-695X.2010.00702.x>.
- [22] K. Nakajima, K. Kitanishi, K. Kobayashi, N. Kobayashi, J. Igarashi, T. Shimizu, Leu65 in the heme distal side is critical for the stability of the Fe(II)-O₂ complex of YddV, a globin-coupled oxygen sensor diguanylate cyclase, *J. Inorg. Biochem.* 108 (2012) 163–170, <https://doi.org/10.1016/j.jinorgbio.2011.09.019>.
- [23] J.-C. Lambry, M. Stranova, L. Lobato, M. Martinkova, T. Shimizu, U. Liebl, M.H. Vos, Ultrafast spectroscopy evidence for picosecond ligand exchange at the binding site of a heme protein: heme-based sensor YddV, *J. Phys. Chem. Lett.* 7 (2016) 69–74, <https://doi.org/10.1021/acs.jpclett.5b02517>.
- [24] A. Pavlou, M. Martinková, T. Shimizu, K. Kitanishi, M. Stranova, A. Loullis, E. Pinakoulaki, Probing the ligand recognition and discrimination environment of the globin-coupled oxygen sensor protein YddV by FTIR and time-resolved stepscan FTIR spectroscopy, *Phys. Chem. Chem. Phys.* 17 (2015) 17007–17015, <https://doi.org/10.1039/c5cp01708d>.
- [25] P. Anzenbacher, S. Marchal, J. Palacký, E. Anzenbacherová, T. Domaschke, R. Lange, T. Shimizu, K. Kitanishi, M. Stranova, M. Stiborová, M. Martinkova, Pressure effects reveal that changes in the redox states of the heme iron complexes in the sensor domains of two heme-based oxygen sensor proteins, EcDOS and YddV, have profound effects on their flexibility, *FEBS J.* 281 (2014) 5208–5219, <https://doi.org/10.1111/febs.13060>.
- [26] M. Stranova, M. Martinková, M. Stiborová, P. Man, K. Kitanishi, L. Muchová, L. Vítek, V. Martínek, T. Shimizu, Introduction of water into the heme distal side by Leu65 mutations of an oxygen sensor, YddV, generates verdoheme and carbon monoxide, exerting the heme oxygenase reaction, *J. Inorg. Biochem.* 140 (2014) 29–38, <https://doi.org/10.1016/j.jinorgbio.2014.06.010>.
- [27] Y. Sasakura, S. Hirata, S. Sugiyama, S. Suzuki, S. Taguchi, M. Watanabe, T. Matsui, I. Sagami, T. Shimizu, Characterization of a direct oxygen sensor heme protein from *Escherichia coli*. Effects of the heme redox states and mutations at the heme-binding site on catalysis and structure, *J. Biol. Chem.* 277 (2002) 23821–23827, <https://doi.org/10.1074/jbc.M202738200>.
- [28] D.J. Murphy, Determination of accurate KI values for tight-binding enzyme inhibitors: an in silico study of experimental error and assay design, *Anal. Biochem.* 327 (2004) 61–67, <https://doi.org/10.1016/j.ab.2003.12.018>.
- [29] V. Fojtikova, M. Stranova, M.H. Vos, U. Liebl, J. Hranicek, K. Kitanishi, T. Shimizu, M. Martinkova, Kinetic analysis of a globin-coupled histidine kinase, AfGCHK: effects of the heme iron complex, response regulator, and metal cations on autophosphorylation activity, *Biochemistry* 54 (2015) 5017–5029, <https://doi.org/10.1021/acs.biochem.5b00517>.
- [30] A.L. Chang, J.R. Tuckerman, G. Gonzalez, R. Mayer, H. Weinhouse, G. Volman, D. Amikam, M. Benziman, M.A. Gilles-Gonzalez, Phosphodiesterase A1, a regulator of cellulose synthesis in *Acetobacter xylinum*, is a heme-based sensor, *Biochemistry* 40 (2001) 3420–3426, <https://doi.org/10.1021/bi0100236>.
- [31] F. Roy, S. Sen Santara, M. Bose, S. Mukherjee, R. Saha, S. Adak, The ferrous-dioxy complex of *Leishmania major* globin coupled heme containing adenylate cyclase: the role of proximal histidine on its stability, *Biochim. Biophys. Acta* 1844 (2014) 615–622, <https://doi.org/10.1016/j.bbapap.2014.01.004>.
- [32] M. Morikawa, K. Izui, M. Taguchi, H. Katsuki, Regulation of *Escherichia coli* phosphoenolpyruvate carboxylase by multiple effectors in vivo. Estimation of the activities in the cells grown on various compounds, *J. Biochem.* 87 (1980) 441–449.
- [33] S. Taguchi, T. Matsui, J. Igarashi, Y. Sasakura, Y. Araki, O. Ito, S. Sugiyama, I. Sagami, T. Shimizu, Binding of oxygen and carbon monoxide to a heme-regulated phosphodiesterase from *Escherichia coli*. Kinetics and infrared spectra of the full-length wild-type enzyme, isolated PAS domain, and Met-95 mutants, *J. Biol. Chem.* 279 (2004) 3340–3347, <https://doi.org/10.1074/jbc.M301013200>.
- [34] H. Takahashi, M. Sekimoto, M. Tanaka, A. Tanaka, J. Igarashi, T. Shimizu, Hydrogen sulfide stimulates the catalytic activity of a heme-regulated phosphodiesterase from *Escherichia coli* (Ec DOS), *J. Inorg. Biochem.* 109 (2012) 66–71, <https://doi.org/10.1016/j.jinorgbio.2012.01.001>.
- [35] Y. Du, G. Liu, Y. Yan, D. Huang, W. Luo, M. Martinkova, P. Man, T. Shimizu, Conversion of a heme-based oxygen sensor to a heme oxygenase by hydrogen sulfide: effects of mutations in the heme distal side of a heme-based oxygen sensor phosphodiesterase (Ec DOS), *Biomaterials* 26 (2013) 839–852, <https://doi.org/10.1007/s10534-013-9640-4>.
- [36] F. Yan, V. Fojtikova, P. Man, M. Stranova, M. Martinková, Y. Du, D. Huang, T. Shimizu, Catalytic enhancement of the heme-based oxygen-sensing phosphodiesterase EcDOS by hydrogen sulfide is caused by changes in heme coordination structure, *Biomaterials* 28 (2015) 637–652, <https://doi.org/10.1007/s10534-015-9847-7>.
- [37] V. Fojtikova, M. Bartosova, P. Man, M. Stranova, T. Shimizu, M. Martinkova, Effects of hydrogen sulfide on the heme coordination structure and catalytic activity of the globin-coupled oxygen sensor AfGCHK, *Biomaterials* 29 (2016) 715–729, <https://doi.org/10.1007/s10534-016-9947-z>.

4.4 Heme: emergent roles of heme in signal transduction, functional regulation and as catalytic centres

Shimizu, T.; Lengalova, A.; Martínek, V.; Martinkova, M.: *Chem. Soc. Rev.* (2019) 48, 5624–5657 (**IF₂₀₁₈ 40,4**).

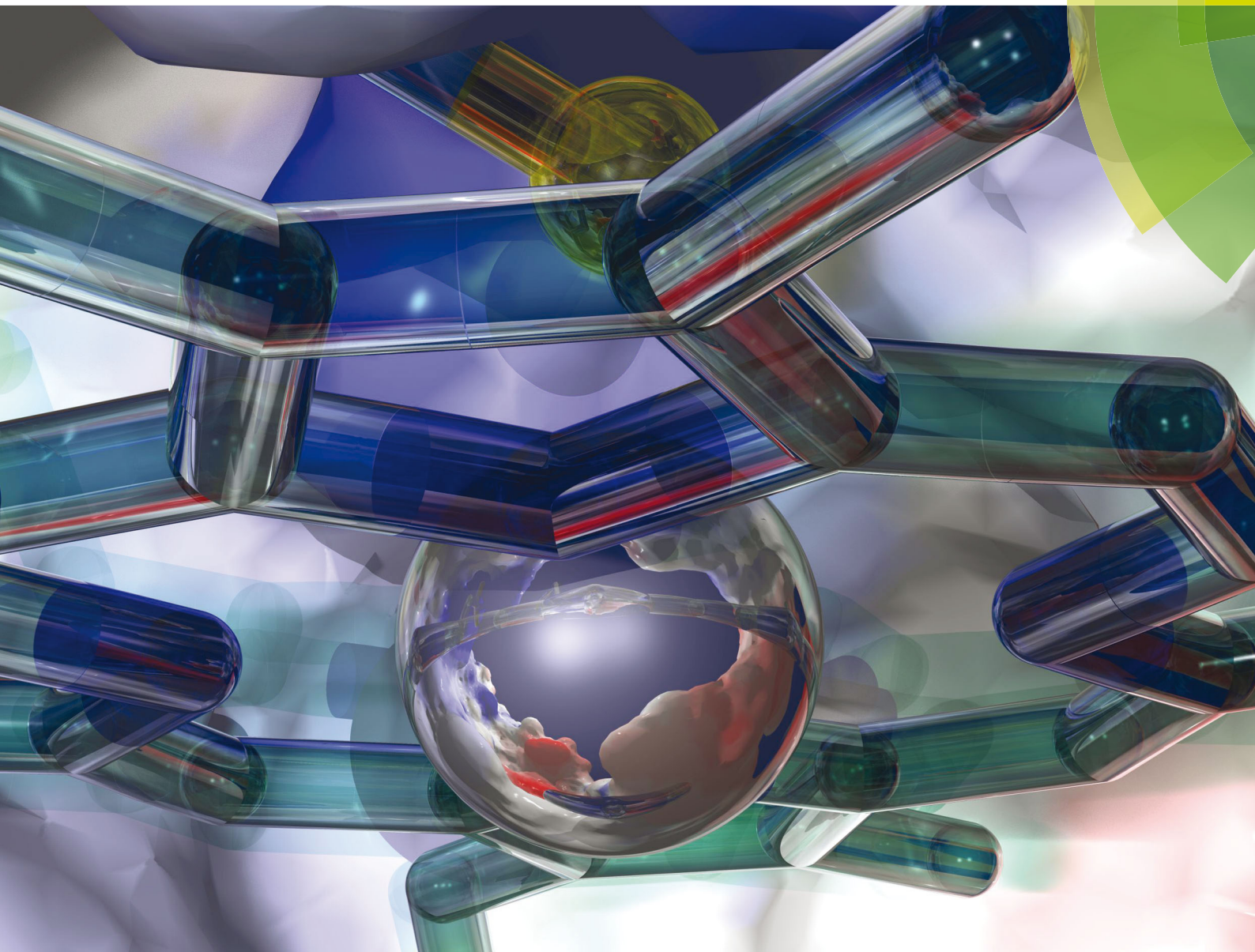
Podíl předkladatelky na této práci: 25 % (*řešerše týkající se proteinů Bach1 a HRI, technická asistence, příprava obrázků a schémat*)

potvrzeno korespondujícím autorem, doc. RNDr. Markétou Martínkovou, Ph.D.

Chem Soc Rev

Chemical Society Reviews

rsc.li/chem-soc-rev



ISSN 0306-0012



ROYAL SOCIETY
OF CHEMISTRY

Celebrating
IYPT 2019





REVIEW ARTICLE

Toru Shimizu, Markéta Martínková *et al.*
Heme: emergent roles of heme in signal transduction,
functional regulation and as catalytic centres



Cite this: *Chem. Soc. Rev.*, 2019, 48, 5624

Heme: emergent roles of heme in signal transduction, functional regulation and as catalytic centres

Toru Shimizu, *^{ab} Alzbeta Lengalova, ^a Václav Martínek ^a and Markéta Martínková *^a

Protoporphyrin IX iron complex (heme) is an important cofactor for oxygen transfer, oxygen storage, oxygen activation, and electron transfer when bound to the heme proteins hemoglobin, myoglobin, cytochrome P450 and cytochrome c, respectively. In addition to these prototypical heme proteins, there are emergent, critical roles of exchangeable/labile heme in signal transduction. Specifically, it has been shown that association/dissociation of heme to/from heme-responsive sensors regulates numerous functions, including transcription, DNA binding, microRNA splicing, translation, protein kinase activity, protein degradation, heme degradation, K⁺ channel function, two-component signal transduction, and many other functions. In this review, we provide a comprehensive overview of structure–function relationships of heme-responsive sensors and describe new, additional roles of exchangeable/labile heme as functional inhibitors and activators. In order to complete the description of the various roles of heme in heme-bound proteins, we also mention heme as a novel chemical reaction centre for aldoxime dehydratase, *cis*–*trans* isomerase, N–N bond formation, hydrazine formation and S–S formation, and other functions. These unprecedented functions of exchangeable/labile heme and heme proteins should be of interest to biological chemists. Insight into underlying molecular mechanisms is essential for understanding the new role of heme in important physiological and pathological processes.

Received 27th June 2019

DOI: 10.1039/c9cs00268e

rsc.li/chem-soc-rev

^a Department of Biochemistry, Faculty of Science, Charles University, Hlavova (Albertov) 2030/8, Prague 2, 128 43, Czech Republic.

E-mail: marketa.martinkova@natur.cuni.cz

^b Research Center for Compact Chemical System, National Institute of Advanced Industrial Science and Technology (AIST), Sendai 983-8551, Japan.

E-mail: toru.shimizu.e5@tohoku.ac.jp

1. Introduction

Metal cations are involved in numerous significant functions and make structural contributions to biological substances and proteins, and thus are very important for the survival of living creatures.^{1–3}



Toru Shimizu

has expertise in the structure–function relationships of heme-responsive sensors and heme-based oxygen sensors.

Toru Shimizu received his BS, MS and PhD degrees in chemistry from Tohoku University (Sendai, Japan). He held the positions of Associate Professor and Full Professor at Tohoku University before retiring in 2012. He is now a Professor Emeritus of Tohoku University, Visiting Professor of Charles University (Prague, Czech Republic) and Visiting Researcher of AIST (Sendai). He is a recipient of the Academic Award from the Chemical Society of Japan. He



Alzbeta Lengalova

Alžběta Lengalová received her MS degree in biochemistry from Charles University (Prague, Czech Republic) in 2016. Her Master's thesis was dedicated to anticancer drugs and their transport when incorporated into nanoparticles. Currently, she is a PhD student in the laboratory of Markéta Martínková in the Department of Biochemistry, Charles University in Prague. Her main research interests are heme-containing sensor proteins such as Bach1, HRI, YddV and AfGCHK.

Among important transition metal cations is the iron cation.^{4,5} The free iron cation itself is very toxic and unstable.^{6,7} Siderophore molecules (*e.g.*, enterobactin, mycobactin, bacillibactin)^{8–10} and many proteins (*e.g.*, ferritin, transferrin, hepcidin, ferroportin) are involved in the storage, transfer, export, and/or uptake (acquisition) of iron cations and regulate transcription during iron metabolism and homeostasis, including ferroptosis.^{11–14}

Many iron cations exist as an iron-bound protoporphyrin IX (b-type porphyrin) complex called the heme iron complex. The redox state of iron in heme complexes can vary. Among redox states, the two most common are the heme Fe(III) complex (or ferric protoporphyrin IX), termed hemin, and the heme Fe(II) complex (or ferrous protoporphyrin IX). The heme iron complex itself is practically insoluble in aqueous solution and is toxic.¹⁵ This toxicity manifests as reactive oxygen species (ROS) generation, as is the case for the free iron cation. Thus, the concentration of labile hemin is very low in the cytosol (as low as 20–40 nM) of *Saccharomyces cerevisiae*,¹⁶ and even lower in mitochondria and the nucleus (<2.5 nM).¹⁷ By contrast, the concentration of labile cytosolic heme in the malaria parasite is ~1.6 μM.¹⁸

Some proteins harbor hemin in a manner that precludes hemin contact with O₂ in aqueous solutions. These proteins, which include heme scavengers such as helminth defense molecule (HDM), heme chaperone proteins such as hemopexin and other heme-binding proteins (*e.g.*, DNA protecting protein, Pgdps), hold hemin so as to limit its interaction with O₂ and prevent subsequent generation of ROS, thereby protecting the cell against their toxic effects.^{12,19–24}

Numerous heme-binding proteins, such as HasA, IsdB, PhuR, ShuA, HRG-1/2 and FLVCR1a/1b, among others, act as heme carriers, and transfer and/or take up proteins that cross the membrane into and/or out of the cytosol and nucleus during heme iron metabolism.^{1,25–33}

Prototypical hemeproteins that harbor a bound heme iron complex play numerous important physiological roles as O₂

carriers (hemoglobin), O₂ storage molecules (myoglobin), activators of molecular O₂ (cytochrome P450), mediators of electron transfer (cytochrome *c*) and many other important functions required for cell survival. Heme proteins classified as b-type hemes, such as hemoglobin, myoglobin, cytochrome P450 enzymes, catalases, peroxidases, NO synthases and soluble guanylate cyclase, among others, are major players in physiology; other proteins with non b-type heme include cytochrome *c* (heme *c*), cytochrome *c* oxidase (heme *a3*), cytochrome *d* (heme *d1*), and cytochrome *o* oxidase (heme *o*).^{34–36}

In addition to these prototypical and better-known roles of the heme iron complex in physiological functions, new roles of the heme iron complex are emerging. Two prominent non-prototypical roles of the heme iron complex include (1) a “heme-responsive sensor” function, where the exchangeable/labile heme iron complex acts as the first signal for subsequent successive signal transduction, and (2) a “heme-based gas sensor” function, in which the heme iron complex acts as the sensing site of a gas (O₂, NO, CO).³⁷

For most “heme-based gas sensors”, functional domain activities, including phosphodiesterase, diguanylate cyclase and histidine kinase, among others, are switched on/off in response to gas (O₂, NO and CO) binding to the heme iron complex in the sensing domain.^{37–41} In the present review, we provide an in-depth description of “heme-responsive sensors”. For heme-responsive sensors, exchangeable/labile hemin (Fe(III) protoporphyrin IX complex) plays a significant role in regulating important physiological functions, such as transcription, microRNA processing, translation, protein phosphorylation, protein degradation, heme iron degradation, K⁺ channel function and many others. Specifically, association/dissociation of exchangeable/labile hemin switches these functions on/off; thus, impairment of these sensing functions in eukaryotes and even in (patho)bacteria may be linked to serious diseases.

In Section 2. Heme-responsive sensors, we emphasize the various heme-sensing motifs that exist beyond the prototypical,



Václav Martínek

Václav Martínek received his PhD degree from Charles University (Prague, Czech Republic) in 2003 for his work on azo-dye metabolism mediated by cytochromes P450 and peroxidases and identification of their DNA adducts. During a postdoctoral fellowship in the laboratory of Jan Florian at Loyola University, Chicago, he studied the mechanism of DNA polymerase beta. Subsequently he returned to Charles University, where his work has

focused on hemoproteins and their interactions with other proteins and lipids. Currently, he is an Associate Professor of Biochemistry at the Departments of Biochemistry and Chemical Education, both in the Faculty of Science, Charles University.



Markéta Martínková

Markéta Martínková received her PhD degree from Charles University (Prague, Czech Republic) in 2003 for her work on the cytochromes P450 and peroxidases from an enzymology viewpoint. In 2004, she was awarded a postdoctoral fellowship by the JSPS to work on heme-containing sensor proteins in the laboratory of Toru Shimizu at Tohoku University (Sendai, Japan). In 2006 she returned to Charles University. Her research interests

lie in the characterization of various hemoproteins. Currently, she is an Associate Professor of Biochemistry in the Department of Biochemistry, Faculty of Science, Charles University and a Vice-Dean of the same faculty.

canonical Cys-Pro (CP) motif, and highlight how they differ from classic concepts of heme sensing. Importantly, we discuss overlapping or duplicate roles of heme-responsive sensors and heme-based CO sensors that remain unresolved. These distinctions, which tend to have been obscure in previous papers, often misconstrue differences between changes caused by CO binding and those induced by alterations in the heme redox state. In the Section 3. Heme-regulated inhibition, activation and non-canonical heme active sites of heme proteins, we describe the exchangeable/labile heme iron complex's inhibitory and regulatory functions and heme proteins that contain a non-canonical heme active site; in these latter proteins, heme serves unprecedented functions that are totally unlike those of the well-known prototypical heme proteins, such as hemoglobin, cytochrome *c*, and cytochrome P450s. In Conclusions, we summarize the significance of heme-responsive sensors as well as expected outcomes and future directions of heme-responsive sensors in terms of their potential pharmaceutical and medical benefits, focusing particularly on understanding the molecular mechanisms of heme-stimulated signaling functions.

2. Heme-responsive sensors (Tables 1 and 2)

2.1. General concepts, principles and mechanisms of heme-responsive sensors, and their heme iron complex sensing/binding sites (Fig. 1)

[1] Concept of heme sensing: hemin (heme Fe(III) complex) acts as the first signal in a heme-responsive sensor in that the association/dissociation of hemin to/from the heme-sensing/binding site of the protein regulates important physiological functions, including transcription, translation, protein degradation, heme degradation, ion channel function, and other important functions operating at other sites/domains within the same protein.

[2] Cys-Pro motif (CP motif) as the sensing/binding site for hemin (Fig. 1A and Tables 1, 2): the Cys thiolate of the CP motif is the prototypical sensing/binding site for hemin in many heme-responsive sensors. The importance of the Pro residue adjacent to the Cys residue lies probably in its steric regulation of the protein structure in the neighborhood of the heme-sensing/binding site, which serves to facilitate sensing/binding of hemin by the adjacent Cys residue.^{42–47}

[3] Stand-alone Cys of non-CP motifs as a sensing/binding site for hemin (Fig. 1B and Tables 1, 2): There are several cases of heme-responsive sensors in which a stand-alone Cys residue in a non-CP motif performs heme sensing/binding.⁴⁷ These include Cys612/His616 (612CXX615C616H motif) in the Ca²⁺-sensitive large-conductance K⁺ (BK) channel,^{48,49} Cys13/His16 + His35 (13CXX16H motif) in the voltage-dependent K⁺ (K_v1.4) channel,⁵⁰ Cys628/His648 (628CXXHX648H motif) in the K_{ATP}-channel⁵¹ and His119/Cys170 in NPAS2 (neuronal PAS domain protein 2).⁵²

[4] His or other non-Cys amino acid residues can serve as the sensing/binding site for hemin (Fig. 1C and Table 1): it is important

to note that Cys and/or the CP motif may not always be the binding site for hemin in the heme-responsive sensor. Instead, His or another non-Cys amino acid residue can serve this function, for example, in HrtR,^{53,54} Rev-erb α ,^{55–57} Rev-erb β ,^{56,58–62} CLOCK,⁶³ TRpRS⁶⁴ and PGRM1.^{65,66} Although the most common protein arrangement for heme binding is a helical scaffold, other conformations are also possible. For example, the β -hairpin conformation is a possible heme-binding site, as demonstrated by artificially constructed heme-binding β -hairpin peptides.⁶⁷

[5] The affinity of hemin for the heme-responsive sensor varies depending on the cell and subcellular environment: For the heme-sensing nuclear receptor Rev-erb β to regulate transcription, its affinity for hemin should be very high, with a K_d value on the same order as the concentration of heme in the nucleus ($\sim 10^{-9}$ M).^{17,60} In contrast, the affinity of hemin for heme-regulated eukaryotic initiation factor 2 α kinase (HRI), a heme-responsive sensor in red blood cells, where the hemin concentration is approximately 10^{-6} M,⁶⁸ is rather low, with K_d values around 10^{-5} M.⁶⁹

[6] The hemin-binding/sensing site in a heme-responsive sensor is generally very flexible: global rearrangement of the heme-responsive sensor protein occurs upon binding of hemin to HRI,⁴³ just as in the case of heme binding to Gis1.⁷⁰ In addition, in the heme-regulated transcription factors Bach1 and Bach2, the binding site(s) of the whole protein molecule is (are) very flexible.^{71,72} The hemin-binding sites at the thiol/disulphide switching regions of HO2,^{73,74} the BK channel,^{49,74} ALAS⁷⁵ and CLOCK⁶³ are very flexible in the absence of hemin, but are likely to become structured in the presence of hemin. However, note that most of the heme-regulated-motif region of heme sensors remains unstructured, although it is true that a local structure develops around the heme binding site.

[7] In some heme-responsive sensors, a stand-alone Cys or CP motif ceases to serve as the binding site for the heme Fe(II) complex—the reduced form of hemin (Fig. 1A and B): Importantly, the axial ligand (sensing/binding site) Cys thiolate for hemin is dissociated from the heme Fe(II) complex upon reduction of the heme Fe(III) complex (hemin), because the interaction of the anionic Cys thiolate with the heme iron complex is hampered when hemin is reduced to values that are less positive than those of the heme Fe(III) complex.^{44,76,77} Therefore, the heme Fe(II) complex binds to sites different from those for hemin, or the coordination structure of the heme Fe(II) bound to the heme-responsive sensor differs from that of hemin in the heme-responsive sensor. Thus, for such heme-responsive sensors, a heme-redox-dependent ligand switch occurs in that the Cys thiolate bound to hemin is switched to the His imidazole, neutral thiol (protonated Cys)⁷⁶ or another amino acid residue upon reduction of hemin to the heme Fe(II) complex. Accordingly, several studies have emphasized that this type of heme-responsive sensor should instead be considered a heme redox sensor^{38,78–81} (see Section 2.6. Heme redox sensors).

This situation is in contrast to other heme proteins containing a Cys-bound heme Fe(III) complex, such as cytochrome P450 enzymes and NOS (nitric oxide synthase).^{35,36,44} In these heme proteins, Cys thiolate is still the axial ligand for the heme Fe(II) complex, even when the heme Fe(III) complex is reduced to the

Table 1 Heme-responsive sensors associated with transcriptional regulation, DNA binding, tRNA synthesis, miRNA processing and translational regulation. Note that DnrF is also a heme-based NO sensor. E75s of *D. melanogaster*, *B. mori* are heme-based NO/CO sensors, and E75 of *O. fasciatus* is possibly a heme-based NO sensor

Name	Functions	Hemin-sensing/binding site	Hemin K_d , k_{off} or redox potential	Partner	Origin	Ref.
Hap1	Hemin binding activates transcription of genes encoding cytochromes	5-Coordinated Cys1193 (7th of seven CP motifs, located at the C-terminus distant from the zinc-cluster motif and dimerization element)	$K_d < 20 \mu\text{M}$ (with peptide)	Hsp90	<i>S. cerevisiae</i> (yeast)	42 and 82
NPAS2	Hemin and heme Fe(II) regulate NPAS2-BMAL1 heterodimer formation and DNA binding in association with transcription of circadian rhythm-related genes; hemin binding to NPAS2 facilitates NPAS2 DNA binding	6-Coordinated His119/Cys170 for hemin (non-CP motif) 6-Coordinated His119/His171 for heme Fe(II) , located in the PAS-A domain downstream of the N-terminal bHLH domain	$k_{off} \approx 5.3 \times 10^{-3} \text{ s}^{-1}$ $K_d \approx 10^{-4} \mu\text{M}$	BMAL1	Mouse	52 and 83–87
All4978	Hemin binding facilitates DNA binding (heme redox sensor)	6-Coordinated Cys92/His97 or His99 (CP motif: Cys92-Pro93-X-His95-X-His97-X-His99, in 1st of three GAF domains) for hemin and His95 for heme Fe(II)	$K_d < 20 \mu\text{M}$ (redox potential: -445 to -453 mV)		<i>Nostoc</i> sp. PCC7120 (cyanobacterium)	78
DnrF	Binding of heme Fe(II) or 5-coordinated Fe(II) -NO enhances DNA binding, leading to transcriptional activation of the NO reductase gene and repression of the nitrate reductase gene (heme-based NO sensor)	Not identified	$K_d < 28 \mu\text{M}$ for heme Fe(II)	RNA polymerase	<i>D. shibae</i> DFL12 ^T (marine bacterium)	88
Bach1	Hemin inhibits DNA binding, leading to initiation of transcription of HO1, ferritin and ferroportin, and ultimately inducing nuclear export and polyubiquitination	5-Coordinated CP3, CP4, CP5 and CP6 (C-terminal side) out of 6 total CP motifs	$K_d \approx 0.1 \mu\text{M}$	Mafk, HOIL-1	Human	89–93
Bach2	Hemin binding regulates immune response signaling cascades; also regulates transcription of Bach1	Not known which of the five CP motif(s) senses/binds hemin		Mafk	Human	71, 72 and 92–95
p53	Hemin interferes with DNA binding and triggers nuclear export and cytosolic degradation	5-Coordinated Cys275-Ala-Cys277-Pro (C-terminal DNA-binding domain; one of three total CP motifs)	$K_d \approx 1.2 \mu\text{M}$	PER2	Human	96 and 97
Gis1	Hemin enhances demethylase and transcription	5-Coordinated binding of two hemin complexes to two CP motifs: Cys250-Pro (N-terminal JmjN + JmjC domain) and Cys859-Pro (C-terminal Zn-finger domain)	$K_d > 20 \mu\text{M}$	Unknown proteins	Yeast	70
PpsR	Hemin inhibits DNA binding and increases transcription of a subset of target genes involved in photosynthesis and tetrapyrrole biosynthesis	6-Coordinated His275 (2nd PAS)/Cys424 (C-terminal HTH DNA-binding domain) (non-CP motif; one heme per protein)	$K_d \approx 1 \mu\text{M}$		<i>Rhodobacter sphaerooides</i> (purple photosynthetic bacterium)	98
HrtR	Hemin prevents DNA binding and increases the expression of heme-efflux system proteins, HrtA and HrtB, which alleviate heme toxicity (cytoplasmic heme-sensing system)	6-Coordinated His72 (DNA binding domain)/His149			<i>Lactococcus lactis</i>	53 and 54
Rev-erb α	Hemin binding facilitates interaction with NCoR-HDAC3 and suppresses the expression of glucose metabolism- and circadian rhythm-related genes	to heme binding has not been directly confirmed	$K_d \approx 2\text{--}3 \mu\text{M}$	NCoR-HDAC3 complex	Human	55 and 56
Rev-erb β	Hemin binding has functional effects similar to those for Rev-erb α ; also promotes degradation through the ubiquitin-proteasome pathway; disulphide/free thiol redox switch in the CP motif regulates heme status, suggesting that the CP motif acts as a redox sensor	6-Coordinated Cys384-Pro385/His568 (CP motif) or X/His568 for hemin; CP motif acts as a redox sensor	Reduced heme binding domain: $K_d < 0.1 \text{ nM}$ and $> 10 \text{ nM}$ for hemin and heme Fe(II) , respectively; oxidized heme binding domain: $K_d > 10 \text{ nM}$ for hemin; full-length protein: $K_d \approx 0.1 \text{ nM}$ for hemin, $k_{off} \approx 10^{-6} \text{ s}^{-1}$	NCoR-HDAC3 complex	Human	56, 58–62 and 74

Table 1 (continued)

Name	Functions	Hemin-sensing/binding site	Hemin K_d , k_{off} or redox potential	Partner	Origin	Ref.
FurA	Hemin binds to FurA bound to DNA sequences (iron-boxes) of the promoter of iron-responsive gene and dissociates its DNA binding; disulphide/free thiol redox switch might regulate hemin binding	6-Coordinated Cys141 (CP motif)/X for hemin	$K_d < 1 \mu\text{M}$	HU, Alr4123, All1140	<i>Anabaena</i> sp. PCC 7120 (cyanobacterium)	99 and 100
SbnI	Hemin binding prevents DNA binding and decreases synthesis of staphyloferrin B (a siderophore)		$K_d < 1 \mu\text{M}$		<i>S. aureus</i>	101 and 102
E75	Hemin or heme Fe(II) forms a heterodimer with DHR3, leading to DNA binding of DHR3 and suppresses activation of target genes; NO and CO can abolish the inhibitory effect of heme Fe(II) (heme-based NO/CO sensor)	His364/His574 for hemin for <i>D. melanogaster</i> ; 6-coordinated Cys/His (non-CP motif) for hemin for <i>B. mori</i>		DHR3	<i>D. melanogaster</i> , <i>B. mori</i>	61, 103 and 104
E75	Heme-based NO sensor, c-type heme	E75 has covalently bound heme and possibly acts as an NO sensor			<i>O. fasciatus</i>	105
DHR51	<i>Drosophila</i> hormone receptor, homologous to human photoreceptor cell-specific nuclear receptor	6-Coordinated Cys/His (non-CP motif)	$K_d \approx 0.43 \mu\text{M}$		<i>D. melanogaster</i>	106
Per2	Transcriptional regulator associated with circadian rhythms; hemin binding leads to ubiquitin-dependent protein degradation	5-Coordinated Cys215 (non-CP motif in PAS-A domain) and His454 (in PAS-B) for mouse Per2; 5-coordinated Cys841/Pro842 (1st of two CP motifs) for human Per2		CRY, p53	Mouse, human	84, 97 and 107–110
CLOCK	Transcriptional regulator associated with circadian rhythms. Hemin binding disrupts binding CLOCK to its E-box DNA target	6-Coordinated His/His144 Additional His/Cys at 20k	$K_d \approx 1.05 \mu\text{M}$, 4.2 μM	BMAL1	Human	63 and 111
CRY1	Transcriptional regulator associated with circadian rhythms	5-Coordinated Cys414/Pro415 (CP motif)		Per	Mouse	112
TrpRS	Hemin induces activation of aminoacylation <i>HcArgRS</i>	5-Coordinated His Hemin induces oligomerization and inhibits catalysis in the N-end role pathway	5-Coordinated Cys115 (non-CP motif)		Human	64
113 <i>Pf</i> RRS	Hemin induces dimerization and inhibits catalysis		$K_d \approx 2 \mu\text{M}$		<i>P. falciparum</i>	114
GluRS	Hemin inhibits catalysis				<i>Acidithiobacillus ferrooxidans</i>	115
GDCR8	Hemin promotes dimerization and activates mRNA splicing, or induces a conformational switch that enables binding to the terminal loop with high specificity	5-Coordinated Pro351–Cys352 (CP motif) for hemin; no cysteine interactions with heme Fe(II)	$k_{off} < 10^{-6} \text{ s}^{-1}$ for hemin; $k_{off} > 10^2 \text{ s}^{-1}$ for heme Fe(II)	DrosHa	Human	46 and 116–120
HRI	Hemin deficiency activates Ser/Thr/Tyr kinase activity, thereby suppressing translation of globin	6-Coordinated His119 (or His120)/Cys409–Pro410 (1st of two CP motifs)	$k_{off} \approx 10^{-3} \text{ s}^{-1}$	eIF2 α		43, 69 and 121–126

Table 2 Heme-responsive sensors associated with protein degradation, heme degradation, cation channel, two-component signal transduction, redox sensing and protein–protein interaction. Proteins in [] are already described above in Table 1. Note that the isolated AA584–717 linker region of the BK channel is also a heme-based CO sensor

Name	Functions	Hemin sensing/binding site	Hemin K_d , k_{off} or redox potential	Partner	Origin	Ref.
IRP2	Hemin binding triggers ubiquitination and proteasome-mediated degradation; heme-dependent oxidative modification triggers protein degradation	5-Coordinated Cys201-Pro-Phe-His204 (single CP motif); heme binds Cys201, heme Fe(II) binds His204		HOIL-1, FBXL5	Human	5, 128 and 130–132
ALAS1	Hemin-dependent oxidative modification triggers protein degradation	5-Coordinated Cys108–Pro109 (3rd of three CP motifs)		ClpXP, LONP1	Human	133
Arginyl transferase (N-end rule pathway) UBR1	Hemin inhibits arginyl-transferase, induces proteasome-dependent degradation, and inhibits UBR1	5-Coordinated Cys71–Cys72–Pro73 (2nd of five CP motifs)		UBR1	Mouse <i>S. cerevisiae</i>	134–137
[Bach1]	Hemin inhibits E3 ubiquitin ligase activity (inhibition of protease activity within the N-end rule pathway of protein degradation)			CUP9	Mouse <i>S. cerevisiae</i>	134–137
[Rev-erb β]	Proteasome-dependent protein degradation	5-Coordinated CP3, CP4, CP5 and CP6 motifs (C-terminal side) out of six total CP motifs		MafK HOIL-1	Mouse	90
[Per2]	Proteasome-dependent protein degradation	6-Coordinated Cys384–Pro385/His568 (CP motif) or X/His568 for heme; CP motif acts as a redox sensor		NCoR-HDAC3	Human	59 and 60
Irr	Proteasome-dependent protein degradation Heme degradation triggers protein degradation	5-Coordinated Cys841–Pro842 (1st of three CP motifs) Two heme binding sites: 5-coordinated Cys (Cys29-Pro-X-His; CP motif), and 6-coordinated bis His-bound low-spin complex		CRY, p53	Human	97 and 108
Slo1 BK channel	Both heme and heme Fe(II) binding inhibit channel activity	6-Coordinated Cys615 and/or His616 (Cys612-X-X-Cys615-His616 non-CP motif) for heme	$K_d \approx 45\text{--}120$ nM		<i>B. japonicum</i> (nitrogen-fixing bacterium), Gram-negative bacteria generally Human Slo1 BK channel	48
Isolated AA584–717 linker region of the BK channel	Hemin binding inhibits channel activity and CO recovers channel activity (heme-based CO sensor)	5-Coordinated His616 (Cys612-X-X-Cys615-His616 non-CP motif)	$K_d \approx 2.8$ μM for oxidized disulphide form, $K_d \approx 0.21$ μM for reduced disulphide form	HO2	Human BK channel	49
Kv1.4	Hemin binding enhances channel activity	6-Coordinated bis-His with His16 (Cys13-X-X-His16) and His35	$K_d \approx 20$ nM		Rat	50
K _{ATP} channel	Hemin binding enhances channel activity	6-Coordinated Cys628/His648 (Cys628-X-X-His(X ₁₆)-His648 non-CP motif)	$K_d \approx 100$ nM based on K _{ATP} currents; $K_d \approx 8$ μM for isolated SUR2A subunit		Human	51 and 141
HssS	TCS; heme phosphorylates HssS-HssR and increases transcription of HrtAB (p-HssR binds to the <i>hrtAB</i> promoter) and alleviates heme toxicity	Localizes to the extracellular part of the transmembrane protein		HssR	<i>S. aureus</i>	142 and 143
ChrS	TCS; heme binding influences ChrS-ChrA, increasing transcription of HO and ABC-type heme exporter			ChrA	<i>C. diphtheria</i>	144 and 145
Fre-MsrQ	TCS (non-classical): heme-mediated electron transfer system, but not a heme-responsive sensor	5-Coordinated b-type; two hemes through histidine residues		MsrP	<i>E. coli</i>	146

Table 2 (continued)

Name	Functions	Hemin sensing/binding site	Hemin K_d , k_{off} or redox potential	Partner	Origin	Ref.
MA4561	TCS: heme redox sensor (c-type heme); active with hemin, inactive with heme Fe(II) TCS: Heme redox sensor; inactive with hemin, active with heme Fe(II) Redox sensor (c-type heme)	5-Coordinated Cys656 (2nd GAF domain, non-CP motif); heme is covalently bound via a vinyl side chain Hemin binds to the PAS domain of NtrY	Redox potential: -95 to -75 mV	Not known	<i>M. acetivorans</i>	79
NtrY	TCS: Heme redox sensor; inactive with hemin, active with heme Fe(II) Redox sensor (c-type heme)	Hemin binds to the PAS domain of NtrY	Redox potential: -255 mV	NtrX	<i>Brucella</i> spp.	80
TL10287	Redox sensor (c-type heme)	6-Coordinated Cys668/His145 (PAS domain, Cys-X-X-Cys-His non-CP motif)	Redox potential: -255 mV		<i>T. elongatus</i> (thermophilic cyanobacterium)	81
[All4978]	Redox sensor: heme binding facilitates DNA binding, heme Fe(II) binding does not	6-Coordinated Cys92/His97 or His99 (Cys92-Pro93-X-His95-X-His97-XHis99 CP motif in one of 3 GAF domains) for heme or His95 for heme Fe(II) 5-Coordinated Tyr113	$K_d < 20 \mu\text{M}$; redox potential: -445 mV to -453 mV		<i>Nostoc</i> sp. PCC7120 (cyanobacterium)	78
PGRM1	Hemin binding recruits EGFR and cytochrome P450 enzymes	5-Coordinated Tyr113	Redox potential: -331 mV; $K_d \approx 50 \text{ nM}$	EGFR, cytochrome P450 enzymes, ferrochelatase	Human	65, 66 and 147
HO2	Disulphide/free thiol redox switch in CP motifs regulates heme affinity in association with heme degradation	5-Coordinated His45 at the catalytic core under oxidative conditions 6-Coordinated His256/Cys265 (CP motif) and 5-coordinated Cys282 (CP motifs) at regulatory sites under reduced conditions; CP motifs act as redox sensors	$K_d \approx 0.014 \mu\text{M}$ (His45) under oxidative conditions $K_d \approx 0.09 \mu\text{M}$ (His256/Cys265) and $K_d \approx 0.9 \mu\text{M}$ (Cys282) under reduced conditions	Slo1 BK channel	Human	73, 74 and 148-153

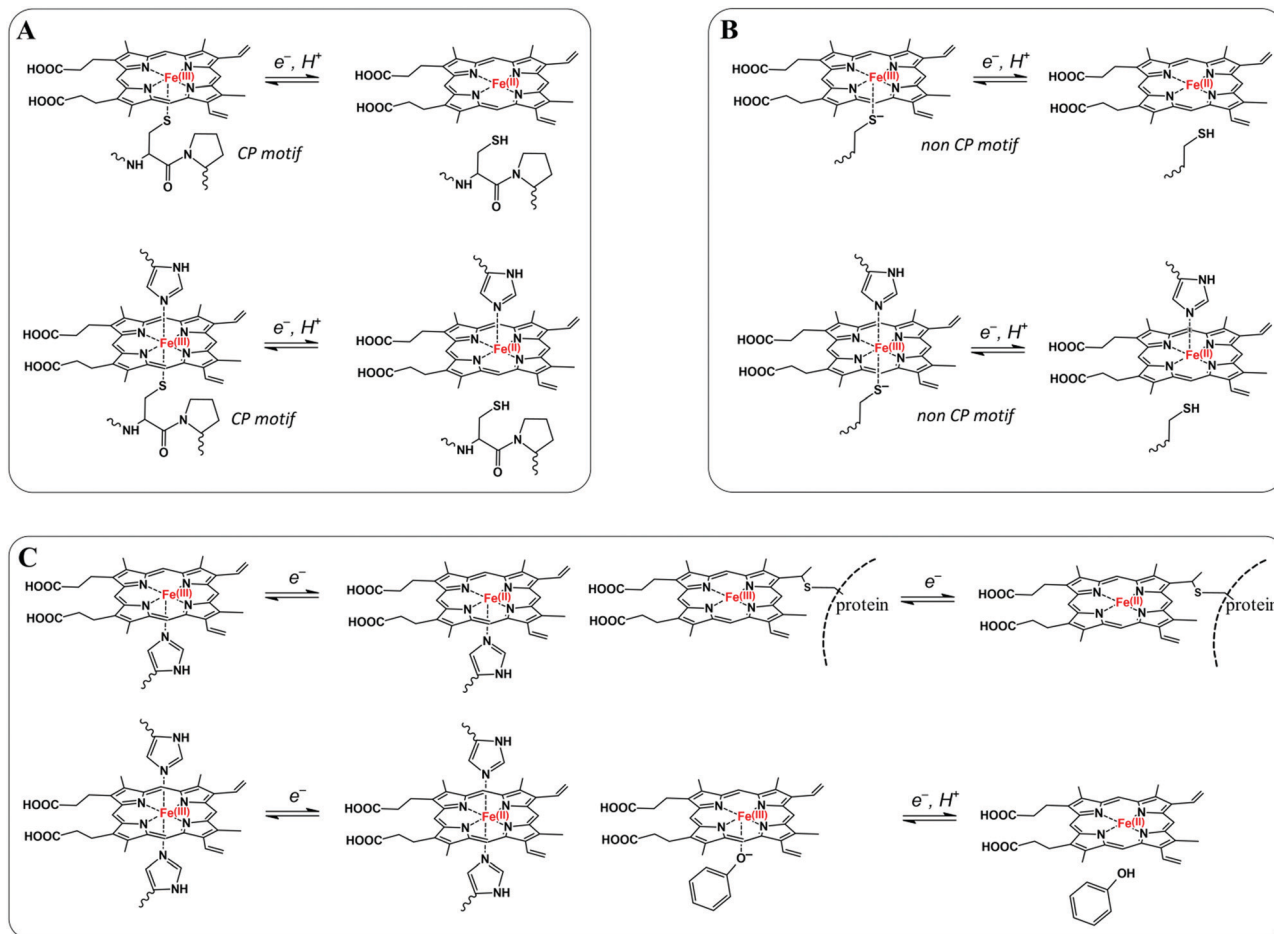


Fig. 1 Coordination structures of heme iron/protoporphyrin IX iron complexes bound to heme-sensing/binding sites in heme-responsive sensors. (A) 5-Coordinated CP-hemin complex (upper): Hap1, Bach1, p53, Gris1, Per2 (human), CRY1, GDCR8, IRP2, HO2 (sensing site under reduced conditions with low affinity), ALAS1, N-end rule pathway/arginyl transferase and Irr (1st site). 6-Coordinated CP-hemin-His complex (lower): All4978, Rev-erba, Rev-erb β , HO2 (sensing site under reduced conditions with low affinity) and HRI. (B) 5-Coordinated Cys (non-CP)-hemin complex (upper): Per2 (PAS-A domain, mouse), HcArgRS, porphobilinogen deaminase, PgDps and STEAP1 (1st site). 6-Coordinated Cys (non-CP)-hemin-His complex (lower): NPAS2, PpsR, E75 (*D. melanogaster*), DHR51, Slo1 BK channel, K_{ATP} channel, ALAS and Z-ISO (1st site). (C) First reaction (left-handed upper): 5-coordinated His-hemin complex: TrpRS, BK channel (isolated linker), HO2 (catalytic core under oxidized conditions with high affinity), Fre-MsrQ, OxdB and KtzT. Second reaction (left-handed lower): 6-coordinated His-hemin-His complex: HrtR, CLOCK, Irr (2nd site), Kv1.4, OxdA, Z-ISO (2nd site), STEAP1 (2nd site), STEAP3 and Dcyl. Third reaction (right-handed upper): cytochrome c-type heme covalently bound to the protein *via* vinyl or Met and used in redox sensors: E75 (*O. fasciatus*), MA4561, Tll0287, TsdA and hydrazine synthase. Fourth reaction (right-handed lower): 5-coordinated Tyr-hemin complex: PGRM1. Note that Cys residues of CP and non-CP motifs bound to heme dissociate from the heme iron complex upon heme reduction; thus, the thiolate does not bind to the heme Fe(II) complex. Also, coordination structures for heme Fe(II) complexes and functions of sensors with bound heme Fe(II) described here are, in most cases, not well characterized, although those for heme have been the focus of considerable research.

heme Fe(II) complex. This is because axial ligation of the Cys residue to the heme Fe(II) complex is supported by hydrogen bonds from neighboring amino acids, preventing the anionic Cys thiolate from dissociating from the less positive heme Fe(II) complex.

Importantly, the redox-dependent ligand switching of a heme-responsive sensor casts significant doubt on the proposed eukaryotic heme-based CO sensors, as described later (see Section 2.9).

2.2. Heme-responsive sensors involved in DNA binding, transcriptional regulation, tRNA synthesis, microRNA splicing and protein synthesis (Table 1)

Binding of heme to a transcriptional regulatory protein switches on/off transcription of various enzymes and proteins that are critical for cell survival.

2.2.1 Hemin binding facilitates transcription or DNA binding by Hap1, NPAS2, All4978, and DnrF (Fig. 2A).

HAP1 is a heme-sensing transcriptional regulator involved in heme iron metabolism; upon heme binding, its DNA binding is facilitated and its mitochondrial import of δ -aminolevullinate synthase is inhibited.⁴² It was originally proposed that the CP motif constituted the consensus binding site for heme among all heme-responsive sensors that had been identified.

The 7th of seven CP motifs in the HAP1 protein was found to be the single binding site for heme that activated transcription.⁸² HAP1 forms a higher-order complex composed of HAP1 and other cellular proteins, mainly heat shock proteins, such as Hsp90. Upon heme binding, Hsp90 interacts with HAP1, causing structural changes that are optimal for full activation of HAP1.⁸²

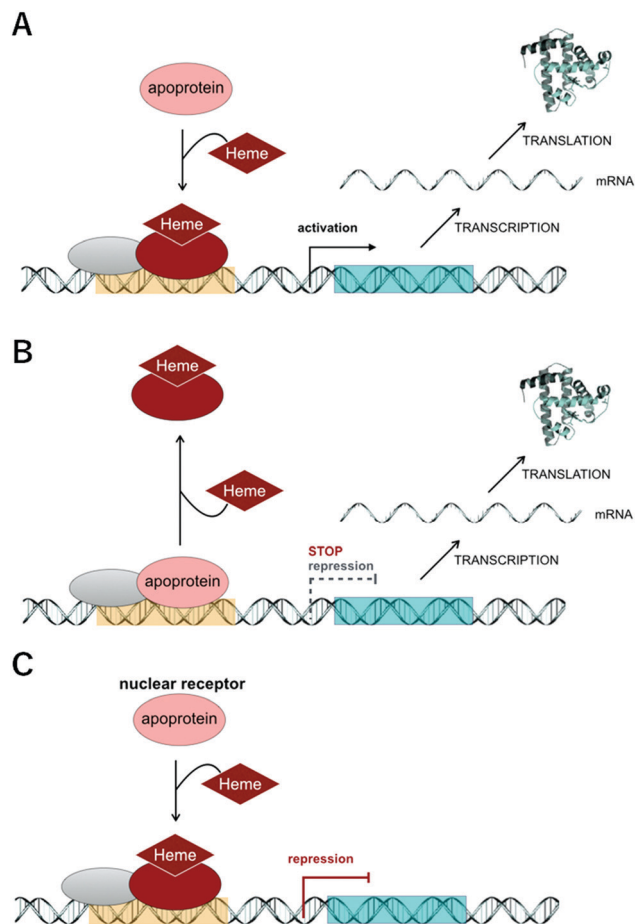


Fig. 2 (A) Hemin binding facilitates transcription or DNA binding: Hap1, NPAS2, All4978 and DnrF. Hemin binds to the free apoprotein, promoting binding of the heme-bound protein to DNA and stimulating transcriptional activation. (B) Hemin binding interferes with DNA–protein interactions, leading to transcriptional activation: Bach1, Bach2, p53, Gis1, PpsR, HrtR, Rev-erb α , Rev-erb β , FurA and CLOCK. The apoprotein is constitutively bound to DNA and represses transcription; hemin binding to the apoprotein activates transcription by dissociating the protein from DNA. (C) Hemin binding inhibits transcription through binding to a nuclear receptor: E75, DHR51, Per1, Per2, CLOCK and possibly CRY. Hemin binds to a free nuclear receptor protein and regulates gene transcription by promoting binding of the heme-bound protein to DNA.

NPAS2 is a transcriptional regulator associated with circadian rhythms.⁸³ It is composed of N-terminal bHLH, PAS-A and PAS-B domains, the latter two of which both bind heme. His119 and Cys170 were found to be the heme-binding sites for the isolated PAS-A domain of NPAS2.⁵² A heterodimeric protein composed of NPAS2 and BMAL1 (brain and muscle Arnt-like protein-1) interacts with E-box DNA.^{83,84} Both heme-free and heme-bound forms of the NPAS2–BMAL1 heterodimer bind to DNA in the presence of 3–5 mM NADPH.⁸³ Binding of heme to the isolated basic helix-loop-helix (bHLH)-PAS domains of NPAS2 significantly facilitates NPAS2 DNA binding ability in the absence of BMAL1, suggesting that NPAS2 is a prototypical heme-responsive sensor.⁸⁵ It was also proposed that NPAS2 is a heme-based CO sensor, since CO binding to the heme-bound heterodimer in the presence of NADPH disrupts its

DNA binding.⁸³ Although CO binds only to the heme Fe(II) complex, and not to hemin, the conversion of hemin, bound to the isolated PAS domain of the NPAS2 protein, to the heme Fe(II) complex significantly changes the heme binding site or the heme coordination structure from the axial ligand His119/Cys170 to His119/His171.⁵² This has led to questions about whether CO binding is solely responsible for disrupting its DNA binding. Consistent with this latter concern, mutations at His119 or His171 in the binding site of the heme Fe(II) of NPAS2 were shown to impair NPAS2–BMAL1 heterodimer formation and remarkably reduce its DNA binding activity in the absence of CO, suggesting that the heme redox state and/or heme binding status is involved in the DNA binding and transcriptional activity of the NPAS2–BMAL1 heterodimer.⁸⁶

Moreover, NADPH significantly enhances the DNA-binding ability of the NPAS2–BMAL1 heterodimer even in the absence of heme iron.^{87,127} The molecular mechanism underlying the function of NPAS2 in response to CO will be discussed in detail later (see Section 2.9).

All4978 of cyanobacterium *Nostoc* sp. PCC7120, encoding a putative heme-binding GAF (cGMP-specific phosphodiesterase, adenylyl cyclase, and FhlA) protein, has three GAF domains; Cys92 and His97 or His99 in the Cys92XXHis95XHis97XHis99 motif in one of the three GAF domains constitutes the heme binding site in All4978.⁷⁸ Binding of heme to All4978 facilitates its DNA binding at a helix-turn-helix motif.⁷⁸ However, since reduction of hemin to the heme Fe(II) complex switches the axial ligand or heme binding site from the Cys residue to a His residue, thereby abolishing DNA binding, it has also been suggested that All4978 is a redox sensor, as described later (see Section 2.6. Heme redox sensors).

Under oxygen-limiting conditions, the marine bacterium *Dinoroseobacter shibae* DFL12^T generates energy through denitrification, and the resulting accumulation of nitric oxide (NO) may cause cytotoxic effects. The response to this nitrosative (NO-triggered) stress is controlled by the Crp/Fnr-type transcriptional regulator, DnrF,⁸⁸ which in its dimeric form binds one molecule of heme per subunit. DnrF senses NO through its bound cofactor, heme Fe(II), by forming a 5-coordinated NO–heme Fe(II) complex. Addition of a heme Fe(II) or heme Fe(II)–NO complex to apo-DnrF protein, together with the aid of RNA polymerase, induces up to a 5-fold increase in the affinity of the holo-DnrF for its specific binding motif on the NO reductase gene promoter, leading to activation of NO reductase genes and promotion of NO consumption. The same treatment also represses the expression of nitrate reductase genes, hampering NO production. Whether the result is transcriptional activation or repression depends on the position of the DnrF-binding site within the corresponding promoter.

2.2.2 Hemin binding interferes with protein–DNA interactions of the heme-responsive transcription factors Bach1, Bach2, p53, Gis1, PpsR, HrtR, Rev-erb α , Rev-erb β , FurA and CLOCK and siderophore regulator SbnI, leading to transcriptional activation and decreased siderophore synthesis, respectively (Fig. 2B). Many heme-responsive transcriptional regulators form a heterodimer or hetero-oligomeric complex with partner proteins that bind to

specific DNA sequences, resulting in transcriptional suppression of genes. Binding of hemin to a regulator changes interactions with partner proteins and disrupts protein–DNA interactions, leading to initiation of transcription and subsequent protein expression.

Bach1 (BTB domain and CNC homolog 1) is the first mammalian transcription factor recognized as being regulated by hemin. Bach1 forms a heterodimer with small Maf family proteins, such as MafK. The Bach1/MafK heterodimer binds to the Maf-recognition element (MARE) in DNA and suppresses the expression of HO1 (heme oxygenase-1), ferritin and ferroportin genes.^{89,91,92}

Hemin binds to four of six CP motifs in the C terminus of Bach1, causing a marked decrease in DNA binding affinity and dissociation of the heterodimer, leading to expression of *HMOX1* and other genes.^{89,91} Hemin binding to Bach1 also induces its nuclear export and polyubiquitination, after which Bach1 binds to a ubiquitin-protein ligase or HOIL-1 (heme-oxidized IRP2 ubiquitin ligase-1) and is subsequently degraded *via* the proteasome.^{90,128} However, it is not clear which specific CP motif(s) is (are) involved in the regulation of Bach1 DNA binding and/or polyubiquitination, although CP motifs CP3 and CP4 are likely responsible for inducing nuclear export. Consistent with this, there are two modes of heme binding to Bach1: one with six-coordinated hemin and one with five-coordinated hemin.

Bach2 has five CP motifs and its transcriptional regulation is similar to that of Bach1.⁹⁴ However, binding of hemin to Bach2 may additionally regulate immune responses through its involvement in a signaling cascade that induces plasma cell differentiation.^{92,93,95} Results of a charge-stage-distribution analysis suggest that the binding region for hemin is intrinsically disordered.^{71,72}

The tumor-suppressor protein p53, which suppresses tumorigenesis and regulates DNA-damage repair, cell-cycle arrest and tumor responses to chemotherapy,^{96,97} also binds hemin. Similar to the case for Bach1 and Bach2, hemin binding interferes with p53–DNA interactions and triggers both nuclear export and cytosolic degradation of p53.^{92,96} A Cys residue in the third of three CP motifs (CACP motif: C275AC277P) in the C-terminus of the p53 protein is involved in binding hemin. The ubiquitin-dependent degradation of p53 is prevented by binding to period 2 (Per2), a circadian transcriptional regulatory factor that also binds heme,⁹⁷ as described in detail below. Interestingly, iron deprivation suppresses the growth and tumorigenicity of human colon carcinoma cells in a p53-dependent manner,⁹⁶ suggesting that the involvement of hemin in the p53–Per2 interaction is associated with heme iron metabolism.

The yeast Gis1 protein is a transcriptional regulator that belongs to the JMJD2/KDM4 subfamily of histone demethylases.⁷⁰ Gis1 contains two Jmj domains – JmjN and JmjC – in the N-terminus, and a zinc finger domain (ZnF) in the C-terminus.

Each domain contains a CP motif to which hemin binds. At low concentrations, hemin first partially binds to the high-affinity site in the CP motif of the paired JmjN + JmjC domains, enabling Gis1 to exhibit partial demethylase activity. At increased

concentrations, hemin binds to the CP motif in ZnF, inducing profound conformational changes and oligomerization of Gis1 and causing dissociation of unidentified cellular proteins that probably inhibit the transcriptional activity associated with their DNA binding. As a consequence, Gis1 histone demethylase and transcriptional activities are fully activated by hemin.⁷⁰ It has also been suggested that Gis1 is oxygen sensitive; consistent with this, oxygen signaling can be mediated by heme.⁷⁰

PpsR controls the synthesis of heme and bacteriochlorophyll in purple photosynthetic bacteria.⁹⁸ Both His275 in the second PAS domain and Cys424 (in a non-CP motif) in the C-terminal helix-turn-helix DNA-binding domain of PpsR are the hemin axial ligands; one molecule of heme interacts with a single molecule of PpsR. Binding of hemin to PpsR inhibits the ability of PpsR to form a higher-order PpsR–DNA complex, with hemin binding at Cys424 appearing to be more important in the hemin-induced DNA dissociation. Hemin binding to PpsR differentially induces the expression of a subset of PpsR-controlled photosynthetic and tetrapyrrole biosynthesis genes.⁹⁸

The transcriptional regulator HrtR of *Lactococcus lactis* interacts with a specific sequence in the promoter region of *hrtA* and *hrtB* genes (encoding the heme-regulated transporters, HrtA and HrtB) that is needed for transcriptional repression of *hrtA* and *hrtB*. HrtR binds hemin at His72 and His149, forming a 6-coordinated low-spin complex.^{53,54} Binding of hemin to HrtR abolishes HrtR–DNA interactions, allowing transcription and subsequent translation of the HrtA–HrtB transporters. Binding of hemin to HrtR causes a profound coil-to-helix transition of the $\alpha 4$ helix in the heme-sensing domain that triggers structural changes in the DNA-binding domain of HrtR, causing it to dissociate from the target DNA.⁵⁴ Therefore, HrtA–HrtB permease controls heme toxicity by directly and specifically controlling its efflux.

Rev-erb α , a nuclear receptor also known as NR1D1 (nuclear receptor subfamily 1, group D, member 1), acts as a constitutive transcriptional repressor that regulates circadian rhythm, glucose metabolism and energy metabolism in a tissue-specific manner.^{55,56,62} Given the high homology with the structurally better characterized Rev-erb β it can be assumed that hemin binds to Rev-erb α at Cys418/His602 and regulates its function by promoting its assembly with two proteins: nuclear receptor co-repressor (NCoR) and histone deacetylase 3 (HDAC3). The resulting complex represses the expression of genes encoding phosphoenolpyruvate carboxykinase and glucose 6-phosphatase, both of which control glucose metabolism. Heme also augments transcriptional repression of the core clock gene *Bmal1* by Rev-erb α . A spectral study of the binding of hemin to the isolated heme-binding domain of Rev-erb α revealed that His602 is the axial ligand for the hemin complex. However, the contribution of Cys418 to heme-binding affinity has not been directly confirmed. Moreover, it is not clear how hemin influences the interaction of Rev-erb α , alone or in a NCoR–HDAC3 complex, with the specific DNA sequence that is also bound by the retinoic acid receptor-related orphan receptor (ROR).

Rev-erb β , a nuclear receptor similar to Rev-erb α , is believed to function as a transcriptional silencer and negative regulator

of glucose metabolism and circadian rhythms.^{56,62} Hemin binds to Cys384/His568 of the isolated heme-binding domain of Rev-erb β .^{61,62} Crystal structures of the isolated heme-binding domain with hemin or heme Fe(II) have been determined.⁶² NO and CO also interact with the heme Fe(II) bound to Rev-erb β , additionally suggesting that Rev-erb β is a gas sensor.⁵⁸

Comprehensive biochemical studies have elegantly demonstrated a number of functional features of Rev-erb β .^{58–60} (1) The affinity of hemin for the reduced form of the isolated heme-binding domain of Rev-erb β is very high, with a $K_d < 0.1$ nM. Free Cys374 and Cys384 serve as the axial ligand in the reduced form, but in the oxidized form, the isolated heme-binding domain contains a Cys374–Cys384 disulphide bridge that changes the coordination structure of hemin, decreasing its affinity for the isolated heme-binding domain by nearly 100-fold. These observations suggest that oxidative stress is linked to circadian and/or metabolic imbalances and that Rev-erb β is a redox sensor. Hemin dissociation from this protein de-represses the expression of target genes in response to changes in intracellular redox conditions. (2) Changes in the coordination structure of the isolated heme-binding domain accompany the 100-fold lower affinity of heme Fe(II) that occurs upon reduction of hemin to heme Fe(II); thus, a Cys residue is no longer available to bind heme Fe(II) as the axial ligand, additionally implying that Rev-erb β is a redox sensor. (3) The rate constant and K_d of hemin dissociation from full-length Rev-erb β were found to be extremely slow ($\sim 10^{-6}$ s $^{-1}$) and very low (0.1 nM), respectively, values that are in accord with the very low concentration (<2.5 nM) of labile hemin in the nucleus.¹⁷ By contrast, the corresponding values for heme Fe(II) or the oxidized form of Rev-erb β are greater than the concentration of hemin. Thus, heme reduction or conversion to the disulphide form causes dissociation of heme. (4) Hemin binding to full-length Rev-erb β acts indirectly through unidentified cellular components to facilitate Rev-erb β interactions with HDAC3-bound NCoR, resulting in repression of Rev-erb β target genes. (5) Hemin binding to Rev-erb β leads to Rev-erb β degradation *in vivo*, likely through the proteasome-dependent pathway, and indirectly regulates its interaction with NCoR1. (6) These data support the hypothesis that Rev-erb β binds hemin too tightly to function as a direct heme-responsive sensor. However, the authors also expand on this idea by noting that Rev-erb β possesses qualities of a redox sensor, such that heme binding is coupled to the redox-sensing function and acts to poise the receptor for NCoR1 binding or degradation.

The cyanobacterial transcriptional repressor FurA (ferric uptake regulator) from *Anabaena* sp. PCC 7120 regulates iron metabolism.⁹⁹ FurA binds to DNA sequences (iron-boxes) in the promoter of iron-responsive genes. *In vitro*, one molecule of hemin binds to one molecule of FurA with high affinity ($K_d < 1$ μ M) and inhibits FurA–DNA interactions.¹⁰⁰ Cys141 within the CP motif of FurA should be an axial ligand for 6-coordinated low-spin hemin. On the other hand, FurA also exhibits disulphide reductase activity. FurA has two redox CXXC motifs. Cys101 and Cys104 in one redox motif form a disulphide that acts as a thiol/disulphide switch to regulate reductase activity.⁹⁹ In the second motif, interactions

between hemin and Cys141 of FurA are likely regulated by a thiol/disulphide switch, as observed for Rev-erb β (as shown above) and HO2 (as shown later). However, the physiological function of the FurA-hemin complex remains to be explored.

SbnI of *Staphylococcus aureus* is a hemin and iron sensor that controls the expression of genes involved in the synthesis of siderophores (mainly staphyloferrin B), which are involved in iron uptake during times of iron scarcity in infectious diseases.^{101,102} Under conditions of low hemin and low iron, the Sbn1 protein forms dimers in solution and binds to DNA within the *sbnC* coding region, promoting the expression of genes *sbnD-H*, which are involved in staphyloferrin B synthesis. Under conditions of high hemin and high iron, hemin binds to Sbn1 and prevents its DNA binding, thereby resulting in decreased expression of *sbnD-H* genes. Thus, it is possible that SbnI senses both the hemin complex and iron ion.

CLOCK, a transcriptional regulatory protein associated with circadian rhythms,⁸⁴ has a domain structure similar to that of NPAS in that its N-terminal site is composed of bHLH, PAS-A, and PAS-B domains. Spectroscopic studies of the characteristics of hemin binding to the isolated PAS-A domain of CLOCK¹¹¹ showed that hemin binds to the protein to form a 6-coordinated low-spin complex, whereas heme Fe(II) binds to the protein in an equilibrium between 5-coordinated high-spin and 6-coordinated low-spin states. In a separate study, hemin addition to CLOCK containing bHLH-PAS-A domains disrupted its bHLH domain-mediated DNA binding.⁶³ The hemin binding site was a low-spin complex with bis-His residues (His144 as one of the axial ligands) in the PAS-A domain. EPR spectra of the hemin bound to CLOCK indicate that additional His/Cys coordination exists at 20k, suggesting a conformationally mobile protein framework within the hemin binding site.

2.2.3 Hemin inhibits transcription by binding to the nuclear receptors E75, DHR51, Per1, Per2 and possibly CRY (Fig. 2C). The *Drosophila* transcriptional nuclear receptor, E75 (ecdysone-induced protein 75), acts as a repressor that tightly binds hemin to its His364 and His574 residues.¹⁰³ A second nuclear receptor, DHR3 (*Drosophila* hormone receptor 3), acts as a transcriptional activator that increases transcription by ~ 10 -fold over basal levels. Cotransfection of E75 with DHR3 reduces DHR3-induced activity by 3- to 4-fold. Providing supplemental hemin further reduces the level of reporter gene expression to near background levels owing to an increase in E75 stability and accumulation, suggesting that E75 is a heme-responsive sensor.¹⁰³ Addition of an NO donor to the culture media restores the activity of DHR3 to the levels observed in the absence of E75, suggesting that E75 is also a heme-based NO sensor in which NO acts to antagonize E75 repressor activity. The interaction of E75 with the DHR3-derived peptide, HR3 AF2, increases E75 stability, resulting in an increase in the denaturation transition temperature, suggesting that E75 directly interacts with DHR3. Interestingly, this thermostabilization only occurs when binding is carried out with the reduced Fe(II)-bound form of E75, suggesting that E75 is a redox sensor. Taken together, these observations indicate that E75 interacts with DHR3 and interferes with its activation. Reduction of

hemin in the E75–DHR3 dimer to heme Fe(II), a conversion that might occur in cells, reduces the transcriptional activity of E75–DHR3, probably because of significant structural changes in the protein caused by heme Fe(II). NO interacts with heme Fe(II) and restores the activity of DHR3, likely owing to a decrease in the interaction of E75 with DHR3. It has also been suggested that E75 is a CO sensor, given that addition of CO to E75 containing heme Fe(II) increases the transition temperature. However, roles of hemin and heme Fe(II) in functions were unclear, because both chemicals were not strictly distinct in the study. Further studies are needed to clarify the problem. We will discuss the CO sensor function of E75 later (see Section 2.9).

Spectrometric studies of hemin binding to the isolated heme-binding domains of E75 proteins from *Drosophila melanogaster* and *Bombyx mori* have shown that hemin bound to the heme binding domain forms a 6-coordinated low-spin complex with the axial ligands Cys and His.^{61,104,105} The Cys binding site for hemin is analogous to that in other heme-responsive sensors. Significant changes in the coordination structure are observed following reduction of hemin to heme Fe(II). It should be noted that the heme iron complex of E75 from *Oncopeltus fasciatus* is covalently bound to the protein, similar to the case in cytochrome *c*.¹⁰⁵ Biochemical and biophysical data suggest that E75 is a heme-based NO sensor.¹⁰⁵

DHR51, a *D. melanogaster* hormone receptor, is the homologue of the human photoreceptor cell-specific nuclear receptor that controls neuronal differentiation in the developing retina. Spectral characterization of the isolated ligand-binding domain of this protein revealed that hemin is bound to the protein through the axial ligands His and Cys, forming a 6-coordinated low-spin complex.¹⁰⁶

Period circadian protein (Per) is an important transcriptional regulatory factor involved in circadian rhythms. Per binds to cryptochrome (CRY) and the resultant Per/CRY heterodimer interacts with the NPAS2–BMAL1 heterodimer to inhibit the transcription of *Per* and *Cry*.⁸⁴ Heme shuttling between mouse Per2 (mPer2), which is a heme-binding protein, and NPAS2 may regulate the transcriptional activity of NPAS2–BMAL1.¹⁰⁷ Hemin was found to bind the isolated PAS-A domain of Per2 through Cys215.¹⁰⁹ Hemin is transferred from the isolated holo bHLH-PAS 2 domain of NPAS2 to the isolated apo PAS-A domain of mPer2, suggesting that mPer2 is a heme-responsive sensor.¹⁰⁹ The site in the isolated PAS-B domain of mPer2 to which hemin binds is found to be His454.¹¹⁰

Importantly, hemin binds to one of the two CP motifs located in the C-terminus of human PER2 and destabilizes the PER2/CRY heterodimer, leading to ubiquitin-dependent degradation of the protein.¹⁰⁸ In contrast, hemin binding to the N-terminal PAS domain leads to the formation of a stable PER2/CRY heterodimer. These observations have implications for the association of PER2 with p53, suggesting that the spatiotemporal organization of PER2–p53 interactions and the nature of their chemical modifications are critical for their time-dependent subcellular redistribution and potential biological functions.⁹⁷ Additional studies of the involvement of the heme iron complex in these functions are warranted.

As described above, CRY is an important transcriptional regulatory protein associated with circadian rhythms.⁸⁴ CRY contains a CP motif that is evolutionarily well conserved among divergent animals.¹¹² Transgenic mice overexpressing CRY1 containing a mutation in the CP motif were shown to display abnormal entrainment behavior, exhibiting markedly modified circadian activity. Surprisingly, this mutant also caused diabetes mellitus.¹¹² Although this study did not provide direct evidence for hemin binding to the CP motif of CRY, its results strongly suggest that hemin plays a significant role in circadian rhythms.

2.2.4 tRNA synthases as heme-responsive sensors (Fig. 3A and Table 1). Mammalian tryptophanyl-tRNA synthases (TrpRSs) are Zn²⁺-binding proteins that catalyze the aminoacylation of tRNA^{Trp}.⁶⁴ Biochemical analyses using purified human full-length TrpRS have revealed that hemin interacts strongly with Zn²⁺-depleted TrpRS, with a stoichiometric hemin:protein ratio of 1 : 1, and enhances aminoacylation activity by more than 10-fold.⁶⁴ His residues were suggested to be the axial ligand for the hemin complex bound to human TrpRS.⁶⁴ This study further showed that, in contrast, the Zn²⁺-bound form of TrpRS does not bind hemin. The enhancement of catalytic activity caused by association of heme is similar to that caused by Zn²⁺. Because Trp is the least abundant amino acid in humans, regulation of TrpRS activity by hemin could serve as a mechanism for protecting the cell against Trp starvation, reflecting hemin-mediated activation of the Trp degradation pathway through activation of indoleamine 2,3-dioxygenase. On the other hand, TrpRSs from mouse, zebrafish and *Arabidopsis* do not bind hemin.

Human cytoplasmic arginyl-tRNA synthase (HcArgRS) was reported to bind hemin, resulting in a decrease in its catalytic activity.¹¹³ This study showed that the addition of hemin did not influence K_m values for t-RNA^{Arg}, arginine or ATP, but dramatically reduced k_{cat} values. Hemin was shown to induce oligomerization of the enzyme, an effect that could account for the inhibition of its catalytic activity. Cys115 was identified as the specific binding site for hemin; however, a Cys115Ala mutant was also inhibited by hemin, suggesting that binding of hemin at Cys115 is not solely responsible for the inhibitory effect.

An analysis of the structure of arginyl-tRNA synthase (*PfRRS*) of *Plasmodium falciparum*¹¹⁴ showed that hemin drives *PfRRS* dimerization and inhibits its catalysis. Hemin interferes with interactions between *PfRRS* and its cognate tRNA^{Arg}. Excessive amounts of hemin in chloroquine-treated malaria parasites result in significantly reduced levels of charged tRNA^{Arg}, suggesting deceleration of protein synthesis.

Glutamyl-tRNA, formed by Glu-tRNA synthase (GluRS), is a substrate for protein biosynthesis and tetrapyrrole formation by the C₅ pathway.¹¹⁵ In *Acidithiobacillus ferrooxidans*, an acidophilic bacterium that expresses two forms of GluRS (GluRS1 and GluRS2) with different tRNA specificities, intracellular heme levels vary depending on growth conditions. Under respiration conditions, in which high concentrations of heme are required, the levels of GluRS and Glu-tRNA-reductase (GluTR), an enzyme responsible for transforming Glu-tRNA to

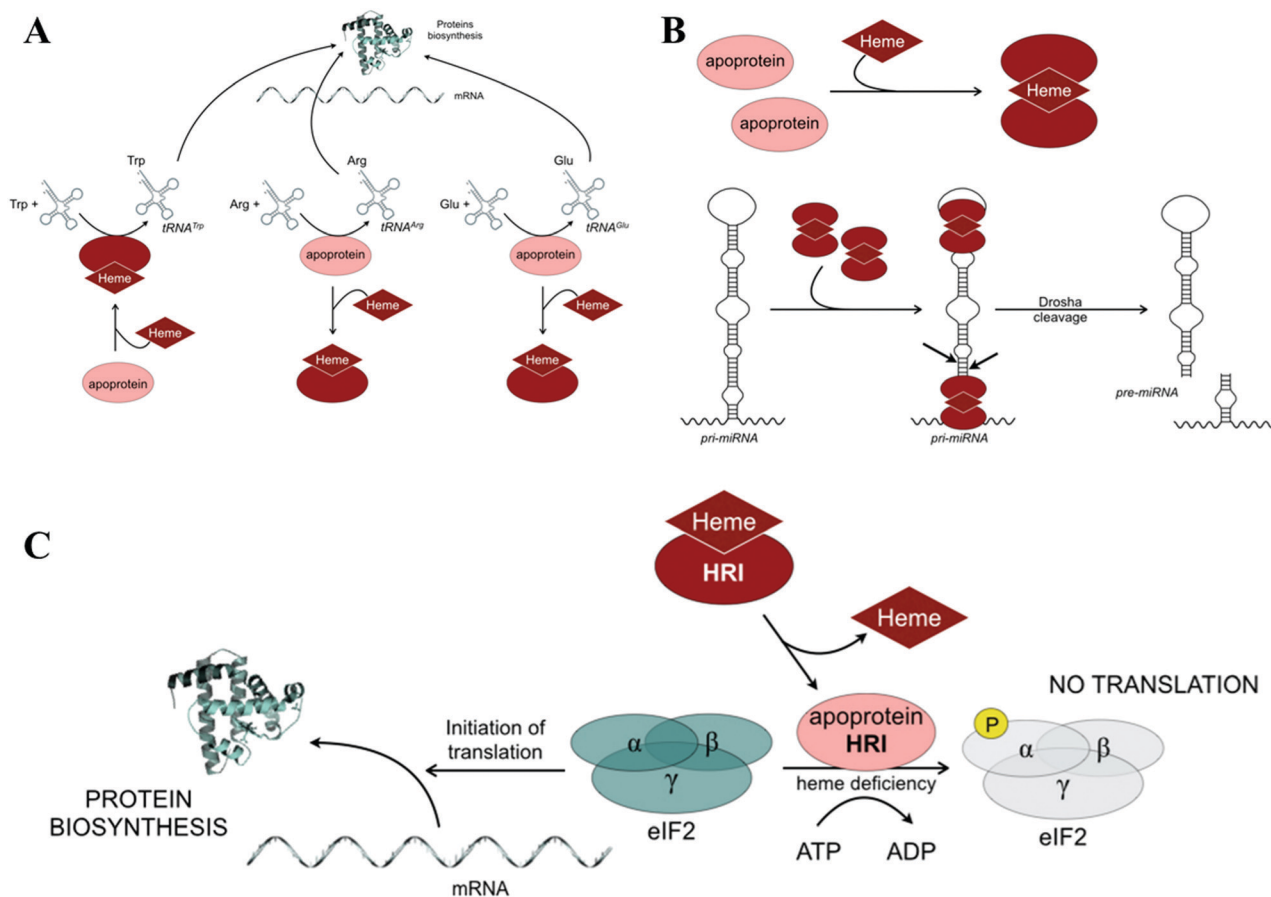


Fig. 3 (A) Hemin binding regulates tRNA synthase: TrpRS, *HcArgRS*, *PfRRS*, GluRS. Hemin binds to Trp tRNA synthase (TrpRS), leading to enhancement of its aminoacylation activity and thus protein biosynthesis, whereas for Arg t-RNA synthetases (*HcArgRS*, *PfRRS*) and Glu t-RNA (GluRS) synthase, hemin binding results in a decrease of catalytic activity. (B) Hemin binding regulates miRNA splicing: GDCR8. Hemin promotes dimerization of GDCR8 and activates mRNA splicing. (C) Hemin binding regulates protein translation: HRI. Hemin-bound HRI has no kinase activity, allowing initiation of translation (left side). In contrast, under conditions where hemin concentrations are low (e.g., in blood diseases) hemin dissociates from HRI, thereby activating HRI and allowing it to phosphorylate eIF2 α and thus terminate translation of globin in erythroid cells (right side). Note that GCN2, PERK, and PKR operate in the same fashion as HRI in that those sensor kinases phosphorylate Ser51 of eIF2 α and stop translation in response to various stimuli.

delta-aminolevulinic acid—the universal precursor of tetrapyrroles, including heme—are increased. However, when intracellular heme levels are in excess, the cells respond by dramatically decreasing GluRS activity and GluTR levels. These results suggest that GluRS plays a major role in regulating the cellular level of heme. Indeed, GluRS1 activity is inhibited by heme, but is restored by NADPH. Further biochemical studies are needed to elucidate the role of heme and heme Fe(II) in GluRS catalysis.

2.2.5 GDCR8: a heme-responsive sensor involved in microRNA (miRNA) splicing (Fig. 3B and Table 1). The RNA-binding protein DGCR8 (DiGeorge critical region 8) and its ribonuclease partner Drosha are essential for cleaving primary microRNA (pri-miRNAs) transcripts as part of the canonical miRNA-processing pathway.¹¹⁶ Mammalian DGCR8 forms a highly stable, active, dimeric complex with hemin in which two Cys residues serve as the axial ligands, one from each monomer.^{46,116} In addition to its double-stranded RNA-binding domain, DGCR8 has been reported to act through a dimeric heme-binding domain to directly contact pri-miRNA.¹¹⁸ This RNA-binding heme domain directs two DGCR8 dimers to bind each pri-miRNA hairpin.

However, another group suggested that heme induces a conformational change in DGCR8 that serves to activate DGCR8 and allows it to recognize pri-miRNAs by specifically binding the terminal loop near the 3' single-stranded segment.¹¹⁷ Incidentally, reduction of heme to heme Fe(II) abolishes pri-miRNA processing activity, accompanied by a marked decrease in affinity, implying that DGCR8 is a redox-sensitive regulator.¹¹⁹ Accordingly, the coordination structure of heme Fe(II) is significantly different from that of hemin in that Cys thiolate is no longer an axial ligand for heme Fe(II) in DGCR8.¹²⁰

2.2.6 HRI: a heme-responsive sensor involved in protein synthesis in red blood cells (Fig. 3C and Table 1). Eukaryotic initiation factor 2 α (eIF2 α) kinases are sensors that are activated under various stress conditions. These kinases, which include PKR (a double-stranded RNA sensor involved in detecting virus infection and mitochondria RNA), PERK (a sensor of endoplasmic reticulum (ER) stress associated with accumulation of denatured proteins) and GCN2 (a sensor for amino acid starvation), act by phosphorylating Ser51 in the α subunit of eIF2, a key regulatory translational initiation factor, thus terminating translation at the

initiation stage.^{122,123,129} In erythroid precursors, heme controls the translation of globins by modulating the activity of the heme-regulated eIF2 α kinase, HRI.¹²¹ The translational regulation of HRI is essential for reducing excessive synthesis of globin proteins and decreasing the severity of phenotypes associated with iron deficiency anemia, erythropoietic protoporphyria, and β -thalassemia.¹²¹

Under normal healthy conditions, the concentration of free heme in erythroid cells—between 0.1 and 10 μM ^{31,68}—is sufficient to allow heme binding to HRI, resulting in blockade of the catalytic site and prevention of eIF2 α phosphorylation. However, in the context of a heme deficiency caused by impaired heme biosynthesis (e.g., in blood diseases), heme dissociates from HRI, leading to opening of the catalytic site, followed by autophosphorylation, subsequent phosphorylation of eIF2 α , and ultimately a halt in globin translation that serves to balance the concentrations of heme and globin. An examination of the molecular mechanism of this heme-regulated function for the full-length HRI enzyme^{43,69,124–126} revealed that (1) heme binds to HRI with a heme : HRI ratio of 1 : 1 and inhibits catalysis; (2) heme binding to the protein through one of two axial ligands, Cys409, located at the C-terminus (the other axial ligand, His119/120, is located at the N-terminus), causes global structural changes in the protein; (3) the axial ligand, Cys409, is part of a CP motif in the protein in which Pro410 is important for the heme binding, as evidenced by abolition of heme binding to mutant HRI containing a Pro410Ala substitution; (4) added NO forms a 5-coordinated NO-heme Fe(II) complex in which catalysis inhibited by heme is restored; (5) the dissociation rate of heme from HRI ($k_{\text{off}} 10^{-3} \text{ s}^{-1}$) is much higher than that of myoglobin and hemoglobin (10^{-6} – 10^{-7} s^{-1}), suggesting that heme is not tightly bound to HRI, which probably has a K_{d} of about 10^{-5} M ; (6) Hg^{2+} strongly inhibits the function of HRI ($\text{IC}_{50} \approx 0.6 \mu\text{M}$), but NO fully reverses this inhibition, suggesting that a free Cys residue is involved in the inhibition and restoration of catalysis; and (7) autophosphorylation at Tyr193, Thr485, and Thr490 of HRI is important for the initial stage of catalysis.

2.3. Heme-responsive sensors involved in protein degradation *via* ubiquitination: IRP2, ALAS1, N-end rule pathway components, Bach1, Rev-erb β , and Per2 and a heme-responsive sensor involved in heme degradation and subsequent protein degradation, Irr (Fig. 4A and Table 2)

IRP2 (iron regulatory protein 2) is a post-transcriptional regulator of iron metabolism.^{5,130} When iron is depleted, IRP2 binds to mRNAs that encode proteins involved in iron homeostasis, promoting translation of the transferrin receptor and blocking translation of ferritin, with the net result being an increase in cytosolic iron levels through stimulation of iron uptake and use and mobilization of iron stores.

When iron levels are sufficient, IRP2 is targeted for degradation by the iron-stabilized E3 ligase component FBXL5 (F-Box and leucine-rich repeat protein 5) or HOIL-1.¹²⁸ As a result, translation of the transferrin receptor is blocked and translation of ferritin is facilitated, ultimately leading to a decrease in

the cytosolic iron level. Similar sequential reactions apply to the IRP2 homolog, IRP1.^{5,130} Heme binding to IRP2 triggers ubiquitination and degradation of IRP2.^{128,131} Both Cys201 and His204 residues in the Cys201-Pro-Phe-His204 cluster (CP motif) of the iron-dependent degradation domain are required for the heme-dependent degradation of IRP2. Oxidative modification of IRP2 mediated by heme binding triggers IRP2 ubiquitination, and the oxidized IRP2 is selectively recognized by FBXL5 (or HOIL-1). Cys201 binds heme, whereas His204 binds to the heme Fe(II) complex and might generate ROS when the heme Fe(II) complex is bound. Pulse radiolysis experiments on IRP2 have shown that a transient 5-coordinate His-ligated heme Fe(II) is a prerequisite for oxidative modification of heme-bound IRP2.¹³² Incidentally, IRP1 binds two molecular equivalents of heme, but does not have the Cys-Pro-X-His motif or the iron-dependent degradation domain ascribed to oxidative modification.¹³² Interestingly, bacterial iron regulatory protein (Irr) is degraded following heme degradation in a heme-dependent manner similar to IRP2 and has a similar heme-binding motif Cys-Pro-X-His,^{138,139} as described later.

In eukaryotic cells, heme production is tightly controlled by heme itself through negative feedback-mediated regulation of ALAS1, a nonspecific 5-aminolevulinic synthase that is the rate-limiting enzyme for heme biosynthesis.^{5,25,34,133} ALAS1 expression is suppressed by heme at the transcriptional, translational and post-translational levels. ALAS1 forms a complex with mitochondrial ATP-dependent protease (ClpXP) in a heme-dependent manner.¹³³ Heme binds to Cys108 and Pro109, the third of three CP motifs, located at the N-terminus of the mature ALAS1 protein, and forms an ALAS1/ClpXP complex within the mitochondrial matrix, leading to heme-dependent degradation of ALAS1. Heme binding to the CP motif is also necessary for the heme-dependent oxidative modification of ALAS1, which enables the recruitment of LONP1 (lon peptidase 1, mitochondrial), another ATP-dependent protease in the mitochondrial matrix, into the ALAS1/ClpXP complex. Thus, the degradation of ALAS1 maintains appropriate intracellular heme levels.

The N-end rule pathway is a set of proteolytic systems whose function is to recognize and polyubiquitylate proteins containing N-terminal degradation signals, thereby causing the proteasome-mediated degradation of these proteins.^{134–137} Regulated degradation of specific proteins by the N-end rule pathway mediates a legion of physiological functions, including heme, O₂ and NO sensing, and selective elimination of misfolded proteins. The conjugation of arginine by arginyl-transferase to N-terminal aspartate, glutamate, or oxidized Cys is a part of the N-end rule pathway of protein degradation. Heme functions in multiple ways: (1) it binds and inhibits arginyl-transferase of mice and the yeast, *Saccharomyces cerevisiae*.^{134,136} This inhibition by heme is mediated by a redox mechanism that involves the formation of a disulphide bond between Cys71 and Cys72 residues of the Cys71–Cys72–Pro73 sequence by heme. (2) It induces the proteasome-dependent degradation of arginyl-transferase *in vivo*. (3) It interacts with UBR1 (an E3 ubiquitin ligase of the N-end rule pathway) and blocks the activation of one of its substrate-binding sites, which targets the transcriptional

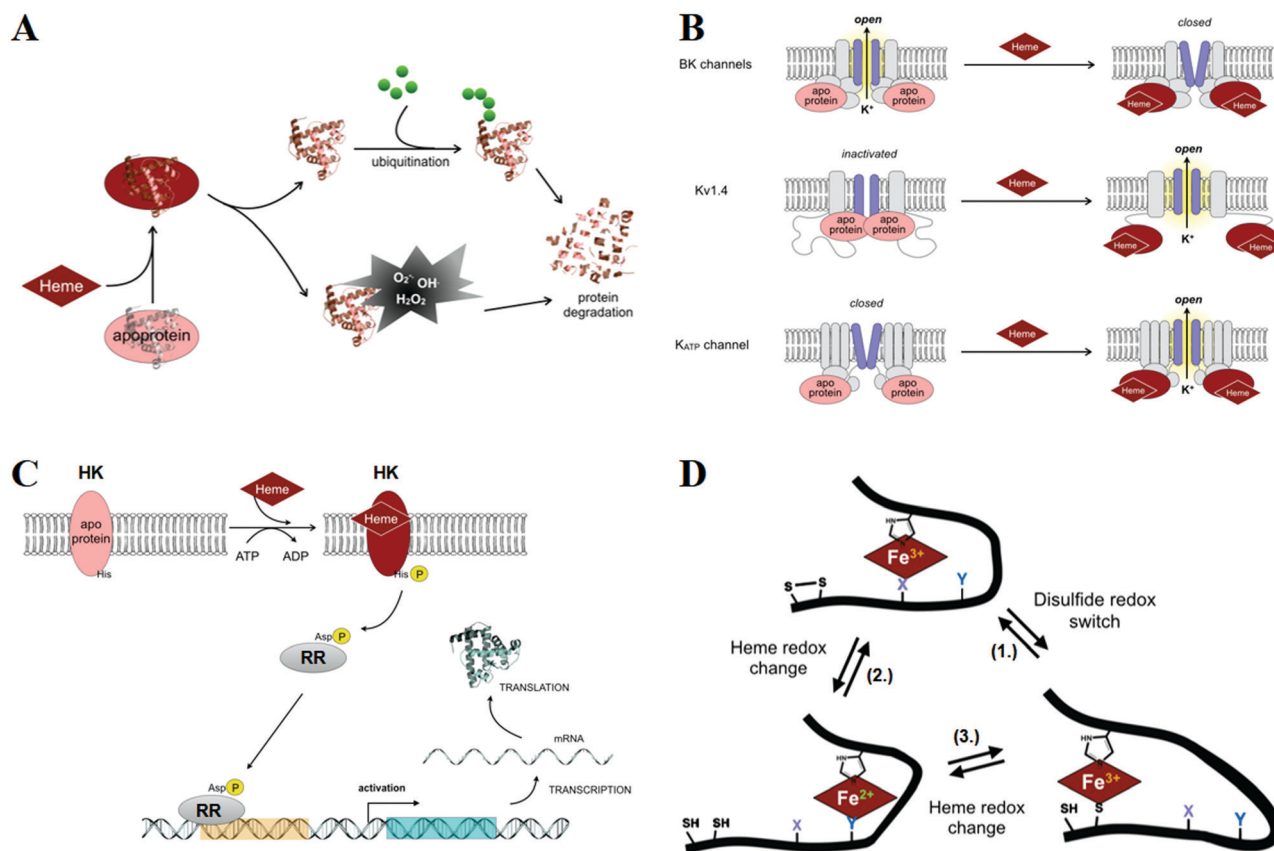


Fig. 4 (A) Hemin binding regulates protein degradation: IRP2, ALAS1, N-end rule pathway systems, [Bach1], [Rev-erb β], [Per2], and Irr. For IRP2, hemin triggers ubiquitination, leading to proteasome-dependent degradation (upper route); for Irr, hemin triggers formation of ROS, leading to protein degradation (lower route). (B) Hemin binding regulates K^+ channel function: BK channels, Kv1.4 channels, and K_{ATP} channels. In the case of BK channels, hemin binding activates the channels by causing their opening; in the case of Kv1.4 and K_{ATP} channels, hemin binding deactivates the channel by decreasing the frequency of channel opening. (C) Hemin binding regulates TCSs: HssS-HssR, ChrS-ChrA, Fre-MsrQ-MsrP, MA4561, and NtrY-NtrX. Hemin triggers autophosphorylation of histidine kinase (HK), then the activated HK transfers the phosphate group to Asp residues of a response regulator (RR), which further interacts with a transcriptional activator, leading to activation of transcription. (D) Hemin binding regulates heme-redox sensors: [MA4561], [NtrY-NtrX], TlI0287, and All4978. A thiol/disulfide redox switch (1) regulates heme affinity/redox and/or heme redox-mediated ligand switching (2), subsequently leading to heme degradation (HO-2) or transcriptional regulation (Rev-erb β). Reduction of heme to heme Fe(II) (3) changes the heme coordination structure and triggers various physiological functions, including autophosphorylation (MA4561, NtrY-NtrX), H_2S oxidation (TlI0287), and DNA binding (All4978) (see Fig. 2).

repressor, CUP9. Hemin binds UBR1 at a site different from the CUP9 binding site and thus allosterically blocks its interaction with CUP9, resulting in inhibition of protease reactions of CUP9. Thus, heme acts as both a “stoichiometric” and “catalytic” down-regulator of the N-end rule pathway. The molecular mechanism of the heme-induced degradation of arginyl-transferase remains to be elucidated.

As noted above, the heme-regulated mammalian transcriptional factor, Bach1, is degraded after heme-bound Bach1 interacts with the ubiquitin-protein ligase, HOIL-1, in a heme-dependent manner.

Rev-erb β is a heme-binding transcriptional regulatory protein, as described above (see Section 2.2).^{56,58–62} Hemin binding to Rev-erb β triggers its proteasome-mediated degradation *in vivo* and indirectly regulates its interaction with the partner protein NCoR1, probably resulting in a decrease in the repressor activity of the Rev-erb β -NCoR1 complex.^{59,60}

Per2 is a transcriptional regulator associated with circadian rhythms, as described above (see Section 2.2). Hemin binding

to the first of two CP motifs in the C-terminal domain of human PER2 triggers ubiquitination-dependent degradation of PER2 in the absence of interaction with CRY.¹⁰⁸ However, when human PER2 first interacts with CRY, heme or heme Fe(II) is bound to the PAS domain at the C-terminal side of PER2, leading to a stable complex. A model of this process proposes that heme-mediated oxidation triggers human PER2 degradation, thereby controlling heterodimerization and ultimately gene transcription.¹⁰⁸ The tumor-suppressor p53 is a heme-responsive sensor, as described above. The spatiotemporal organization of PER2-p53 interactions and the nature of their chemical modifications are critical for their time-dependent subcellular redistribution and potential biological functions.⁹⁷ Involvement of the heme iron complex in these interactions is anticipated.

Irr from the nitrogen-fixing bacterium, *Bradyrhizobium japonicum*, is a key transcriptional regulator of iron homeostasis that binds to target genes and represses the translation of genes encoding enzymes involved in heme biosynthesis.^{138–140}

In the presence of iron or hemin, Irr is degraded, thereby initiating the transcription of target genes. Irr has two heme binding sites, one with a 5-coordinated, Cys29 (CP motif)-bound high-spin complex, and the other with a 6-coordinated bis His (in a His cluster)-bound low-spin complex. Hemin binding to Irr and subsequent hemin degradation trigger Irr protein degradation. Irr protein degradation triggered by hemin proceeds according to the following steps: (1) hemin binding to the two heme-binding sites, (2) reduction of hemin to heme Fe(II), (3) O₂ binding to heme Fe(II), (4) H₂O₂ generation at heme Fe(II) binding sites, (5) heme degradation and free iron release, (6) “active site conversion” from heme iron to non-heme iron, (7) H₂O₂ activation to generate ROS such as •OH, and (8) oxidative protein modification at the iron binding site.¹³⁹ This heme-dependent Irr protein degradation mechanism is significantly different from that of IRP2 in which protein degradation is mediated by the ubiquitin-proteasome system.¹³¹

2.4. Heme-responsive sensors involved in K⁺ channel function: BK channels, K_v1.4 channels and K_{ATP} channels (Fig. 4B and Table 2)

The large-conductance Ca²⁺- and voltage-activated K⁺ channel (BK channel) complex contains four Slo1 (KCNMA1) subunits, each of which possesses the putative transmembrane segments, S0–S6.¹⁵⁴ Human and rat Slo1 BK channels bind both hemin and heme Fe(II), which profoundly inhibit transmembrane K⁺ currents by decreasing the frequency of channel opening.⁴⁸ The affinity of hemin for these channels is high, with IC₅₀ values of 45–120 nM. The inhibition by hemin persists at higher, more physiological concentrations of Ca²⁺. Hemin appears to bind to the heme-binding motif, CXXCH (specifically, C612KACH616), located between cytoplasmic putative RCK1 and RCK2 (regulators of conductance for K⁺) subdomains near the C-terminus. His616 is probably the heme axial ligand. It has been suggested that hemin binding to the channel interferes with allosteric interactions among the channel's gate, voltage sensors and Ca²⁺-binding segments.¹⁵⁴ However, it is still puzzling how heme Fe(II) interacts with BK channels, since the coordination structure for heme Fe(II) is, in general, significantly different from that for hemin.

Heme binding studies have been conducted for an isolated, putative heme-binding domain (HBD; residues 584–717) that forms a linker segment between RCK1 and RCK2.⁴⁹ This study focused on the control of HBD affinity for heme by a thiol/disulphide redox switch, as described above for Rev-erbβ^{58–60} and below for HO2.^{73,149} The HBD contains a CXXCH motif in which His616 serves as the axial ligand; the two Cys residues in the Cys612XXCys615His616 motif can form a reversible thiol/disulphide (Cys612–Cys615) redox switch. The reduced dithiol state binds hemin ($K_d \approx 210$ nM) ~14-fold more tightly than the oxidized disulphide state, suggesting that a thiol/disulphide redox switch system also operates in the BK channel system. The HBD was shown to tightly bind CO ($K_d \approx 50$ nM) with the Cys residues in the CXXCH motif regulating the affinity of HBD for CO. The normoxic/hypoxic-dependent affinity of heme and CO for HBD were rationalized based on an intrinsic mechanical interaction between the human BK channel and HO2.^{49,155}

Relationships between CO binding and hemin will be discussed later (see Section 2.9).

Inactivation of the K_v1.4 channel, an A-type voltage-gated K⁺ channel, is mediated by a “ball-and-chain” mechanism in which the distal N-terminal structure (ball) occludes the ion permeation pathway.⁵⁰ K_v1.4 channels are potently regulated by intracellular free hemin. Hemin binds to the N-terminal ball-and-chain inactivation domain and thereby impairs the inactivation process, thus enhancing K⁺ currents with an apparent EC₅₀ value of ~20 nM. The ball-and-chain domain contains a heme-responsive binding motif involving Cys13XXHis16 and a secondary His35. The N-terminus containing the heme-binding motif is predicted to be highly flexible and disordered, whereas the helix containing His35 is well defined. Binding of hemin to the N-terminal domain through formation of bis His coordination (His16/His35) might reduce the flexibility of the ball-and-chain machinery and induce a partial secondary structure that would make it impossible for the peptides comprising the ball to reach the channel's cavity.⁵⁰

Members of the K_{ATP} family of ion channels respond to intracellular ATP and play a pivotal role in linking cellular metabolism to excitability. Functions of cardiac K_{ATP} channels, which regulate the excitability of cardiac ventricular myocytes, are regulated by hemin.⁵¹ Hemin binds a cytoplasmic Cys628XXHis(X₁₆)His648 motif on the sulphonylurea receptor subunit (SUR2A) of the K_{ATP} channel by forming a Cys/His complex and increases cardiac K_{ATP} single-channel activity. The hemin-binding motif is located in an unstructured region between the first transmembrane domain and the first nucleotide-binding domain. Spectral evidence that the heme-binding form is composed of a 5-coordinated high-spin complex and a 6-coordinated low-spin complex suggests the flexibility or intrinsic mobility of the heme binding site or the protein structure. His648 is a potential ligand for the low-spin heme complex, whereas spectroscopic data for the Cys628 variant do not unambiguously confirm this residue as a ligand for the low-spin heme species. CO activates K_{ATP} channels, and hemin binding to the Cys628XXHis(X₁₆)His648 motif in SUR2A is required for the CO-dependent increase in channel activity.¹⁴¹ Molecular mechanisms of this CO-induced function will be discussed later (see Section 2.9).

2.5. Heme involvement in two-component signal transduction systems: HssS-HssR, ChrS-ChrA, Fre-MsrQ-MsrP, MA4561 and NtrY-NtrX (Fig. 4C and Table 2)

Organisms constantly sense and respond to extracellular signals so as to adapt to environmental changes and survive. For this, bacteria employ a large number of two-component signal transduction systems (TCSSs), which consist of paired sensor and response regulator (RR) proteins specific to different stimuli.^{156,157} The sensor protein of a typical TCS is a histidine kinase (HK), most often membrane-bound,^{158,159} that autophosphorylates a His residue at the C-terminal domain upon stimulation and then transfers its phosphate group to its cognate RR. The sensing mechanism should be coupled with the autophosphorylation from ATP and the phospho-transfer reaction from HK and RR.

Heme-based gas (O_2 , NO)-sensor kinase TCSs, such as FixL and AfGcHK, have been reported.³⁸ In addition to these gas sensors, several TCSs are reported in which heme binding or the heme redox state regulates HK function.¹⁵⁸

Heme is toxic at high concentrations and kills bacteria. On the other hand, the human pathogen *S. aureus* requires heme as a vital source of nutrient iron during infection. To maintain cellular heme homeostasis, *S. aureus* employs the coordinated actions of the heme-sensing two-component heme-responsive sensor system, HssS-HssR, and the heme-regulated transporter efflux pump, HrtAB.¹⁴² Binding of extracellular heme to the heme-responsive sensor, HssS, causes autophosphorylation (activation) of a bacterial membrane-localized HK, which transfers its phosphate group to the cognate RR, HssR. Phosphorylated HssR then binds to a direct-repeat DNA sequence within the heme-regulated transporter (*hrt*) efflux pump promoter genes, *hrtA* and *hrtB*, leading to expression and translation of the heme efflux pump proteins, HrtA and HrtB. Therefore, HssS-HssR dependent expression of HrtA and HrtB results in the alleviation of heme toxicity and tempered staphylococcal virulence. Since a role for bacterial NOS in bacterial survival in the host has been noted, NO synthesis and heme sensing are intertwined in *Staphylococci*.¹⁴³

The pathogen *Corynebacterium diphtheria* employs a TCS composed of the heme-sensing kinase, ChrS, and the cognate RR, ChrA, to regulate degradation and transport of heme.¹⁴⁵ ChrA consists of an N-terminal regulatory domain, a long linker region, and a C-terminal DNA-binding domain. When ChrS protein is incorporated into proteoliposomes, it catalyzes heme-dependent autophosphorylation by ATP.¹⁴⁴ The phosphorylated and activated ChrA specifically binds to either *hmuO* or *hrtAB* promoter regions to promote the transcription of genes encoding heme oxygenase and the ABC-type heme exporter, respectively. The crystal structure of ChrA revealed that the structural flexibility of the linker could be an important feature in rearranging the domain orientation to create a dimerization interface that binds DNA during heme-sensing signal transduction.¹⁴⁵

Fre-MsrQ-MsrP, a methionine sulphoxide reductase system found in *Escherichia coli*,¹⁴⁶ appears to be specifically involved in repairing the periplasmic protein, MsrP, for example following oxidation by hypochlorous acid (HOCl). Ferric reductase (Fre) is a cytosolic NAD(P)H flavin reductase and a potential soluble physiological dehydrogenase partner for MsrQ that delivers electrons to MsrQ. MsrQ is an integral membrane-spanning, b-type heme protein containing two b-type hemes, coordinated through His residues, that acts as a specific electron donor for MsrP. MsrP, a periplasmic protein, is a methionine sulphoxide reductase that shows structural similarities to the sulphide oxidase molybdenum-enzyme family. Thus, Fre and MsrQ proteins form a prokaryotic TCS for electron transfer through the membrane that could be structurally related to the eukaryotic NADPH oxidase system.¹⁴⁶ This system is not a typical heme-responsive sensor, but is a new heme-mediated two-component electron transfer system containing methionine sulphoxide reductase. Further detailed studies remain to be done in order to establish the molecular mechanism.

The protein MA4561 from the methanogenic archaeon *Methanosarcina acetivorans* contains a heme iron complex that is covalently attached to Cys656 via a vinyl side chain in the second GAF domain,⁷⁹ marking the first report of a covalently attached heme cofactor in a cytoplasmic sensor protein. MA4561 containing heme possesses strong autophosphorylation activity, whereas MA4561 containing heme Fe(II) does not show any such activity. It has been suggested that heme is bound to a large pocket in the protein that enables imidazole and dimethyl sulphoxide to bind to the heme iron complex. The intrinsic coordination structure of the heme is heterogeneous; thus, a clear identification of the axial ligands has not been feasible. Moreover, potential phosphorylated residues in the protein have not been identified. Given its genomic localization, it has been suggested that MA4561 is a redox-sensor kinase component of a TCS that affects the regulation of a set of three homologous corrinoid/methyltransferase fusion protein isoforms involved in methyl sulphide metabolism.⁷⁹ Further detailed studies remain to be done in order to establish the molecular mechanism.

The NtrY-NtrX TCS of *Brucella* spp. acts as a redox sensor to regulate the expression of the nitrogen respiration system.⁸⁰ *Brucella* spp. are facultative intracellular bacteria that are pathogenic for many mammalian species, including humans, causing a disease called brucellosis. The bacterium contains the TCS, NtrY-NtrX, in which heme is bound to the PAS domain of the NtrY HK and a phosphate group in a His residue of the kinase domain is transferred to the cognate RR, NtrX. NtrY containing heme Fe(II) exhibits autophosphorylation activity, whereas that containing heme does not. NO or CO binding to the enzyme containing heme Fe(II) does not change catalytic activity.

2.6. Heme redox sensors: [MA4561], [NtrY-NtrX], Tl10287, [All4978] (Table 2)

It has been suggested that some heme-responsive sensors are heme-redox sensors. Generally speaking, the coordination structure of the heme iron complex and the protein structures of the heme binding site are substantially changed upon reduction of heme to heme Fe(II) (Fig. 1). Accordingly, the functions of heme-responsive sensors that respond to heme would be significantly changed or abolished, when heme is reduced to heme Fe(II). Thus, it would be reasonable to suggest that the functions of heme-responsive sensors should overlap with those of heme-redox sensors.

As shown above, MA4561 contains a covalently-attached heme iron complex and is suggested to be the redox-heme sensor kinase of a TCS⁷⁹ (third reaction in Fig. 1C and 4C). MA4561 containing heme autophosphorylates, whereas MA4561 containing heme Fe(II) does not, suggesting that this enzyme is a heme-based redox sensor.

As described above (Fig. 4C), the heme-bound kinase, NtrY, of the *Brucella* NtrY-NtrX TCS system is a heme redox sensor in that NtrY containing heme Fe(II) exerts autophosphorylation activity, whereas that containing heme does not.⁸⁰ NO and CO binding to NtrY containing heme Fe(II) does not alter NtrY

activity. O₂ binding to NtrY containing heme Fe(II) rapidly oxidizes the heme iron and generates NtrY containing hemin, ruling out the possibility that NtrY is a heme-based O₂ sensor.

Hemin binds to Tll0287, which has a CXXCH motif characteristic of *c*-type cytochromes (third reaction in Fig. 1C), from the thermophilic cyanobacterium *Thermosynechococcus elongatus* in which Cys68 and His145 in the PAS domain serve as the axial ligands.⁸¹ The redox potential at pH values greater than 7.5 (−255 mV) dramatically increases to 57 mV at lower pH values, suggesting the involvement of a protonatable group with a $pK_{\text{red}} \approx 7.2$. It has been suggested that Tll0287 acts as a redox sensor under microaerobic conditions or as a cytochrome subunit of an H₂S-oxidizing system.⁸¹

As described above and shown in Table 1, hemin binds to All4978 and facilitates binding of its helix-turn-helix motif to DNA.⁷⁸ Reduction of hemin to heme Fe(II) abolishes DNA binding, suggesting that All4978 is not only a heme-responsive sensor associated with transcriptional regulation, but also a heme redox sensor.⁷⁸

Although other heme-redox sensors containing a covalently bound *c*-type heme, such as GSU582/GSU935, DcrA and insect E75, have been reported (third reaction in Fig. 1C), their intrinsic functions in relation to redox or electron transfer reactions are not well understood.³⁸

2.7. PGRMC1: a heme-responsive sensor involved in protein-protein interactions (Table 2)

PGRMC1 (progesterone receptor membrane component 1), a member of the membrane-associated progesterone receptor family, contains an N-terminal transmembrane domain and a putative C-terminal cytochrome *b*₅ domain.^{65,66,147} Apo-PGRMC1 exists as an inactive monomer. On binding to hemin, PGRMC1 forms a stable dimer through stacking interactions between the two protruding heme moieties. The hemin is 5-coordinated with Tyr113 as the proximal axial ligand, and the open surface of the heme mediates dimerization⁶⁶ (fourth reaction in Fig. 1C). Hemin binding to PGRMC1 enables the protein to interact with the epidermal growth factor receptor (EGFR) and cytochrome P450 enzymes, leading to enhanced proliferation and chemo-resistance of cancer cells. Binding of progesterone to hemin-bound PGRMC1 has also been suggested,⁶⁵ and CO binding to heme Fe(II) significantly decreases these functions.⁶⁶ However, heme coordination structures and the heme binding environment of heme Fe(II)-bound PGRMC1 are expected to be significantly different from those of hemin-bound PGRMC1. Therefore, there is a reason to doubt that CO acts through CO-sensor functions to affect PGRMC1, as discussed later (see Section 2.9).

On the other hand, the redox potential of heme-bound human PGRMC1 is very low—as low as −331 mV.⁶⁵ The axial ligand of many heme (hemin) transfer proteins is a Tyr residue, reflecting the fact that tyrosine as the axial ligand for hemin, similar to that for many heme-transfer proteins, would play a significant role in decreasing the redox potential so as to avoid heme reduction, which hampers the heme (hemin) transfer reaction.^{27,29} The low redox potential of the heme-bound PGRMC1, taken together with several lines of experimental

evidence, has led to a number of suggested potential roles of PGRMC1. These include the possibility that PGRMC1 serves as (1) a heme chaperone to deliver newly synthesized heme to hemo-proteins in different cellular locations, (2) a heme-responsive sensor that directly interacts with ferrochelatase and decreases ferrochelatase activity, (3) a heme-responsive sensor that regulates endosomal trafficking of iron to the mitochondria for heme synthesis, and (4) a heme-responsive sensor that regulates localization of the mitochondrial heme biosynthesis complex to inner and outer membrane junction points.¹⁴⁷

2.8. HO2: a heme-degrading enzyme containing a redox switch at two CP motifs, which act as a redox sensor to regulate the affinity of hemin (Fig. 4D and Table 2)

Heme oxygenase (HO), the only known mammalian enzyme capable of degrading heme, is a key player in heme homeostasis that catalyzes the conversion of hemin to biliverdin, CO, and free ions.^{73,148–152} Mammals contain two isoforms of this enzyme, HO1 and HO2, which share the same α -helical fold that forms the catalytic core and heme-binding site. Unlike HO1, HO2 contains three CP motifs: one CP motif includes Cys127, and the other two CP motifs include Cys265 and Cys282 near the C-terminus. These latter two CP motifs are located at positions distinct from the heme-binding site, His45, which serves as the axial ligand on the proximal side where heme degradation occurs at the catalytic core. They also act as a thiol/disulphide redox switch to regulate hemin binding. For the oxidized form of HO2, in which two thiolates form the disulfide bond S(Cys265)–S(Cys282), heme Fe(III) binds only at the catalytic core with high affinity ($K_{\text{d}} \approx 0.014 \mu\text{M}$; His45/H₂O). On the other hand, for the reduced form of HO2 in which two free Cys residues are formed, two heme Fe(III) bind with lower affinities to regulatory sites in the protein different from the catalytic core (His256/Cys265, $K_{\text{d}} \approx 0.09 \mu\text{M}$; Cys282, $K_{\text{d}} \approx 0.9 \mu\text{M}$).^{73,149}

Both K_{d} values (0.09 μM and 0.9 μM) of heme for HO2 under reducing conditions are higher than the normal concentration¹⁷ of labile heme in the cytoplasm of most cells (0.02–0.04 μM); thus, the disulphide switch of HO2 responds to cellular oxidative stress and reducing conditions.¹⁴⁸ Upon reduction of the C-terminal disulphide bond (Cys265 and Cys282) to free thiolates, the two Cys residues become available to ligate heme, suggesting that the CP motifs act as a redox sensor.^{149,150} However, heme bound to the C-terminus is not a substrate of HO2; thus, only heme bound to His45 in the N-terminal catalytic site is a substrate of HO.¹⁵¹ Spectroscopic studies have revealed that the heme regulatory motif of HO2 (containing a disulphide bond) is dynamically disordered under oxidative conditions and lacks heme binding, whereas under reducing conditions, the C-terminal region gains some structure in association with heme binding.¹⁵⁰ Note again that heme-regulatory CP motifs are located in an intrinsically disordered region. The main importance of the S–S bond is that the two Cys residues in the motif are involved in heme binding. Therefore, formation of the S–S bond causes a loss of the Cys ligand and destabilizes heme binding to the two heme-regulatory CP motifs.¹⁵² The disordered structure of the hemin binding site of HO2 is similar to that of Bach1, as described above. Functional

regulation through thiol/disulphide switches acting as redox sensors is also found in other motifs, such as the CXXC motif in the heme-binding domain of FurA⁹⁹ and the BK channel,⁴⁹ as described above.

2.9. Unresolved issues of heme-responsive sensors with a CO-sensing function or *vice versa*: NPAS2, CLOCK-BMAL1, E75, Rev-erb α , Rev-erb β , K⁺ channels, PGRMC1, and sGC/PKG

The heme iron complex serves as the sensing site for gaseous molecules (O₂, NO and CO) in gas sensors.³⁸ “CO sensor” is a very attractive term for both physiologists and pathologists. Numerous papers about CO sensors have been reported.³⁸ But the molecular mechanism of CO sensing is controversial, and several issues related to its biological chemistry remain unresolved.

For heme-responsive sensors, association/dissociation of hemin to/from the heme binding site of the sensor proteins regulates various important functions, such as transcription, DNA binding, tRNA synthesis, microRNA processing, protein translation, protein degradation, heme degradation, K⁺ channel activity, autophosphorylation and redox switching, among others (Table 1). In contrast, for CO sensors, CO binding to heme Fe(II) bound to the heme-responsive sensor further up- or down-regulates similar functions already observed for the heme-responsive sensor or allows new functions to be switched on. Importantly, CO binds only to heme Fe(II), and never binds hemin.^{160–162}

Most CO sensors hitherto reported are suggested to be both heme-responsive sensors and heme-based CO sensors. The exceptions include heme-based CO sensors such as CooA, RcoM and CBS, in which the heme iron complex is constitutively bound to the heme binding domain/site through distinct coordination, and CO binding to the heme Fe(II) complex regulates functions.

CO binds only to heme Fe(II), forming a stable heme Fe(II)–CO complex. This characteristic of CO is in contrast to that of O₂^{39,163–165} and NO.^{41,166–178} Specifically, O₂ binds only to heme Fe(II), forming a heme Fe(II)–O₂ complex, but the heme Fe(II)–O₂ complex is often oxidized and converted into hemin through generation of ROS, such as superoxide.^{38–40} ROS further interact with amino acid residues on the protein surface. NO binds to both hemin and heme Fe(II), forming the corresponding NO complexes. Additionally, NO and its oxidative derivatives further interact with amino acid residues on the protein surface and regulate numerous reactions.³⁸ Thus, there is rather straightforward rationale for understanding the role of CO in CO sensing within heme-responsive sensors.

The coordination structure of hemin bound to proteins differs significantly from that of heme Fe(II) bound to the same proteins. In particular, many heme-responsive sensors, though not all of them, have a cysteine or CP motif as the hemin binding/sensing site. Usually, thiolate residues that serve as the axial ligand or binding/sensing site for hemin are converted to His or other amino acid residues when hemin is reduced to heme Fe(II). This is partly because of ionic repulsion between the anionic character of the thiolate residue and the less positive character of heme Fe(II) compared with hemin. Thus, it is possible

that heme redox changes in heme-responsive sensors are accompanied by significant changes in the protein structure surrounding the heme. Those redox-dependent heme coordination or protein structural changes should occur before CO is bound to the heme Fe(II) in the heme-responsive sensor. In the case of the RNA-binding protein, GDCR8, redox-dependent changes in the coordination structure of the heme iron complex that accompany the loss of cysteines as axial ligands abolish its function.¹¹⁹

The presence of a reductant/reductase (or oxidant/oxidase) poses significant issues for the conversion from hemin to heme Fe(II) as well as changes in coordination and protein structure caused by the conversion from hemin to heme Fe(II), even in the absence of CO. Studies reported to date have provided circumstantial evidence that fails to unequivocally demonstrate that heme-responsive sensors are simultaneously heme-based CO sensors.

Let us consider each heme-responsive sensor with CO-sensing characteristics in turn.

NPAS2. NPAS2 is a transcriptional regulatory protein associated with circadian rhythms, as described above in Section 2.2.1 (Table 1). The heterodimer of NPAS2, both hemin-free and hemin-bound, with BMAL1 binds to DNA in the presence of 3–5 mM NADPH.⁸³ Importantly, NADPH alone facilitates the DNA-binding ability of the NPAS2–BMAL1 heterodimer, even in the absence of hemin, suggesting that hemin is not a prerequisite for DNA binding of the heterodimer.^{87,127} Addition of CO to the hemin-bound NPAS2–BMAL1 heterodimer in the presence of NADPH under anaerobic conditions abolishes the DNA-binding ability of the heterodimer.⁸³ CO binds only to heme Fe(II), and not to hemin, thus NADPH might help heme reduction. Mutations at the binding site of heme Fe(II) abolish the DNA-binding ability of the heterodimer as a result of cleavage of the NPAS2–BMAL1 heterodimer, suggesting that heme Fe(II) binding or the protein structure of the heme Fe(II)-bound pocket is important for these functions.⁸⁶ In contrast, mutations at the hemin binding site do not alter heterodimer formation or DNA-binding ability, suggesting that hemin is not important for these functions.

Taken together, these observations indicate that NADPH, but not hemin, is required for NPAS2–BMAL heterodimer formation and the DNA binding of the heterodimer. If it is assumed that heme iron is involved in heterodimer formation and DNA-binding ability, then hemin, which is bound to the NPAS2–BMAL1 heterodimer, would be reduced to heme Fe(II) with the aid of CO in the presence of NADPH under anaerobic conditions. CO-stimulated heme reduction in the presence of electron donors has been reported.¹⁷⁹ Redox changes in the heme iron cause striking changes in heme coordination and accompanying protein structures in the heme-binding pocket,⁵² leading to heterodimer dissociation and loss of DNA-binding ability⁸⁶ prior to CO binding to heme Fe(II). Unfortunately, however, spectral changes caused by adding CO to the heterodimer solution in the presence of NADPH under anaerobic conditions have not been reported, although spectral changes caused by adding CO to the heterodimer containing dithionite-reduced

heme Fe(II) have been observed.⁸³ Therefore, the NPAS2–BMAL1 system is unlikely a prototypical CO sensor.

Chelation of endogenous CO in mice by intraperitoneal administration of a selective CO scavenging agent promotes the binding of NPAS2 and CLOCK to E-box sites in DNA in the murine liver and causes disruption of circadian rhythms.¹⁸⁰ However, when CO is purposely removed from the cells or body, the heme-degrading enzyme, HO1, is abruptly overexpressed in cells, serving to compensate for the diminished intracellular CO concentration. Thus, free heme (a substrate of HO1), biliverdin and free Fe(II) (products of HO1), the concentration of NADPH (an essential cofactor for HO1 catalysis), and ROS (byproducts of uncoupled HO1 reactions) play significant roles in the effects of the CO scavenging system on circadian rhythms. Thus, the possibility that effects of these species account for the disruption in circadian rhythm caused by the CO scavenger cannot be ruled out.

CLOCK–BMAL1. HO1 depletion globally alters CLOCK-controlled transcription in hepatocytes.¹⁸¹ CO, a heme-degradation product, suppresses CLOCK–BMAL1 binding and transactivation of target genes. CLOCK binds both heme and heme Fe(II) (Section 2.2.3, Table 1).¹¹¹ Since CO binds to heme Fe(II), it is reasonable to suggest that heme Fe(II) is involved in those functions that are associated with circadian rhythms. However, questions similar to those that arose with respect to NPAS2 remain to be addressed. Specifically, how is heme converted into heme Fe(II)? How are CO, heme and heme Fe(II) involved in CLOCK–BMAL1 heterodimer formation? And how does the heterodimer interact with DNA?

E75. It has been claimed that the heme-binding nuclear receptor E75 from *Drosophila* is a gas (NO or CO) sensor,¹⁰³ as described above in Section 2.2.3 (Table 1). E75 containing heme Fe(II), but not heme, interacts with the peptide HR3 AF2 derived from a second nuclear receptor, DHR3. Addition of CO to E75 containing heme Fe(II) stabilizes the protein, as evidenced by an increase in its transition denaturation temperature. Interestingly, however, addition of HR3 AF2 to E75 containing heme Fe(II) has no further effect on E75 stability beyond the effect of CO alone. This lack of an additional effect suggests that E75 containing heme Fe(II) cannot interact with DHR3 in the presence of CO. Thus, although CO stabilizes the E75 protein, it appears to prevent binding of the DHR3-derived peptide. However, the authors of this study did not assess the effects of CO on transcriptional activity. Thus, these findings do not provide direct evidence that E75 is a heme-based CO sensor, since they only showed that the protein–peptide interacts with heme Fe(II)–CO. In an interesting study, the same group reported a significant effect of NO on the function of E75, although the involvement of heme and CO in function was not described.¹⁸²

Rev-erb α and Rev-erb β . Heme and heme Fe(II) bind to the human nuclear receptors Rev-erb α and Rev-erb β ⁵² both of which are suggested to be heme-responsive sensors (see Section 2.2.2; Table 1). NO and CO bind to the heme Fe(II) incorporated in Rev-erb proteins, suggesting that Rev-erb proteins are heme-based NO and CO sensors. However, it has been found that both Rev-erb proteins are transcriptional repressors whose

activities are reversed by NO binding; by contrast, the effects of CO are marginal. Transcriptional repression by Rev-erb proteins is augmented by binding NCoR, but this repression too is reversed by NO. Interactions of Rev-erb proteins with NCoR peptides, derived from the interaction interface of Rev-erb and NCoR proteins, are weakened by heme, an effect that is mitigated by NO. Here again, there is no direct evidence that Rev-erb proteins are heme-based CO sensors, although effects of NO on the transcriptional activity of these proteins and on Rev-erb–NCoR protein interactions are clear.

In a separate work, it was suggested that a thiol-disulphide switch between Cys374 and Cys384 controls the interaction of heme Fe(III) (bound *via* Cys384/His568) with the heme-binding domain of Rev-erb β .⁵⁸ The CO affinity for heme Fe(II) of the reduced switched state of Rev-erb β was found to be very high ($K_d \approx 60$ nM). Nevertheless, the authors of this report did not suggest that Rev-erb β is a heme-based CO sensor.

K⁺ channels. Ca²⁺-Dependent K⁺ channels have been reported to be heme-responsive sensors, such that binding of either heme or heme Fe(II) to human Slo1 BK channels profoundly inhibits transmembrane K⁺ currents,⁴⁸ as described above in Section 2.4 (Table 2). It has further been reported that HO2 is part of the BK channel complex and enhances channel activity under aerobic conditions. HO2 knockdown reduces channel activity, but CO, a product of HO2, rescues this loss of function.¹⁵⁵ Although these authors showed that CO binds to heme Fe(II), they did not propose that the K⁺ channel is a combined heme-responsive sensor and heme-based CO sensor; instead, they carefully avoided referring to the possibility of the involvement of heme iron in the functional inhibition by CO by suggesting that HO2 is an O₂ sensor.¹⁵⁵ There is clearly no direct evidence that the heme-bound K⁺ channel is a heme-based CO sensor. Under aerobic conditions, heme is degraded into Fe(II), CO, and biliverdin with the aid of HO2, but left unanswered is the question of how CO binds to heme Fe(II) when the heme iron complex is degraded by HO2. Moreover, the authors of this paper did not discuss the role of heme Fe(II) in CO-associated functions or how heme is reduced to heme Fe(II).

A group led by Hoshi, which first reported the important role of heme iron in the function of Slo1 BK channels,⁴⁸ examined the role of CO in the function of the same channel.¹⁸³ They reported that CO reliably and repeatedly activates Slo1 BK channels in excised membrane patches in the absence of Ca²⁺ in a voltage-sensor-independent manner. The stimulatory action of CO on the Slo1 BK channel requires an aspartate and two His residues located in the cytoplasmic RCK domain. Taking into account the involvement of heme iron, they examined the effects of mutations at the putative heme binding site, Cys612–Lys–Ala–Cys–His616, on CO-induced functional enhancement, but found no such effects. In addition, the current-enhancing effect of CO was completely absent when the intracellular Ca²⁺ concentration was increased to 120 μ M, suggesting that the effect of CO is dependent on the Ca²⁺ concentration. Mutations of His365, Asp367, and/or His394 at the putative Ca²⁺ binding site abolished the CO sensitivity of the channel, but failed to alter the sensitivity of the channel to heme. These results suggest that CO-induced

functional enhancement is mechanically different or exhibits distinct local features compared with heme-induced functional inhibition.

Yi *et al.*⁴⁹ identified a thiol/disulphide redox switch in the human BK channel that controls its affinity for heme and CO. The heme-binding domain of the BK channel has a Cys612XXCys615His motif in which histidine serves at the axial heme ligand and the two Cys residues form a reversible thiol/disulphide redox switch that regulates affinity of this domain for heme. This heme-binding domain was shown to interact with HO2. The reduced thiol state binds heme Fe(III) with a K_d of ~ 210 nM, which is 14-fold more tightly than the oxidized disulphide state binds heme Fe(III). Furthermore, heme Fe(II) in the domain tightly binds CO ($K_d \approx 50$ nM). Accordingly, it was proposed that a thiol/disulphide switch in the heme-binding domain is a mechanism by which the activity of the BK channel can respond quickly and reversibly to changes in the redox state of the cell, especially as it switches between hypoxic and normoxic conditions. Nevertheless, it remains unclear how CO regulates the function of the channel.

Al-Owais *et al.*¹⁸⁴ reported that CO mediates the anti-apoptotic effects of HO1 in medulloblastoma DAOY cells through inhibition of K^+ channel activity. The voltage-gated rectifier K^+ channel, $K_v2.1$, plays a significant role in neuronal apoptosis by permitting the K^+ efflux necessary to initiate caspase activation. Induction of HO1 markedly increases the resistance of DAOY cells to oxidant-induced apoptosis. CO generated from CORM-2 (30 μ M) was shown to inhibit voltage-gated K^+ currents in DAOY cells and largely reverse the oxidant-induced increase in K^+ channel activity. Thus, it was demonstrated that CO can protect central neurons against oxidative stress by inhibiting $K_v2.1$, thereby suppressing the pro-apoptotic effect of the loss of intracellular K^+ . Nevertheless, it is again unclear how CO inhibits the function of $K_v2.1$ and whether heme Fe(II) is involved in the process.

CO activates K_{ATP} channels, and heme binding to the Cys628XXHis631(X₁₆)His648 motif of the SUR2A K_{ATP} channel subunit is required for the CO-dependent increase in channel activity, as described above in Section 2. Heme-responsive sensors (Table 2). The affinity of heme for SUR2A, the kinetics of CO binding to heme Fe(II), and the resonance Raman spectrum of CO-heme Fe(II) bound SUR2A have been carefully examined, and the results themselves are not in doubt.¹⁴¹ However, in these studies, heme was reduced to heme Fe(II) in solution by adding sodium dithionite, but this does not automatically result in the reduction of heme. It is not clear why or how heme added to the K_{ATP} channel solution is converted into heme Fe(II), only that it accepts CO as its axial ligand. A spectroscopic study is needed to demonstrate that heme bound to the K_{ATP} channel is converted into heme Fe(II) under certain conditions to generate CO-accepting heme Fe(II). Is a reductase or reducing agent needed for heme reduction? Or is it possible that CO facilitates the heme reduction?

At this point, an interesting and important proposal regarding the “heme-independent interplay between iron and CO in Slo1 BK channels” is worth noting.¹⁸⁵ In this critical review

article, the author emphasized the importance of considering whether contaminating free iron in media used for overexpressing the channel plays a role in the CO-dependent functional regulation of the channel. The author claims that free iron is always present in an overexpressed, purified protein. CO repeatedly stimulates the human Slo1 BK channel, possibly by binding to an iron site. It has been suggested that CO acts as a small, strong iron (or Fe(II)) chelator that disrupts a putative iron bridge in ion channels, thereby tuning their activity. *In silico* structural models of Slo1 BK channels have been generated based on structures of the channel from human and *Aplysia californica*. It was assumed that in the human Slo1 BK channel, Fe(II) is located in a bowl containing the putative motifs, Trp524XXTyrTyr/Phe528 and Phe391XXHisPhe395, and further suggested that dynamic binding of His365/Asp367 to the first Fe(II) bowl or Gln970/Cys911 binding to the second Fe(II) bowl promotes channel closure. Accordingly, CO might act by outcompeting His365/Asp367 and Gln970/Cys911 for the first and second Fe(II) bowls to promote Ca^{2+} -independent and Ca^{2+} -dependent channel opening, respectively. Washout followed by CO stimulation was shown to reverse channel activity, indicating that the CO effect is repeatable. The author claimed that, because CO may target other metalloproteins to which transition metals are bound, the heme-independent regulation mode of CO may have significant and extensive implications for these metalloproteins.

On the assumption that the above-proposed role of free iron cations in functions impacted by CO is appropriate, we proposed an additional role of Fe(II) generated by constitutively expressed or overexpressed HO under aerobic conditions in the interaction with CO. The degradation products of heme by HO are free Fe(II), CO and biliverdin, the latter of which is further degraded to bilirubin, which has antioxidative properties. A number of papers have emphasized the critical effect of CO on important functions, making the claim that a protein acts as a CO sensor in cases where knockout of HO significantly up- or down-regulates these functions.¹⁵⁵ However, such effects do not rule out the idea that free Fe(II) generated from heme plays a role in interacting with CO, implying that free Fe(II) binds to numerous enzymes, including K^+ channels, and that Fe(II) bound to the protein further rebinds CO and exerts numerous CO-dependent functions. Whereas overexpression of HO in cells generates free Fe(II), the endogenous HO transcription/expression system regulated by Bach1/MafK is accompanied by expression of the iron-capturing protein ferritin, and other iron-removing proteins with a high affinity for free Fe(II).⁹² Under appropriate conditions, timely and synergistic expression of ferritin and other iron-removing proteins with HO might not occur, allowing cells to accumulate enough free Fe(II) for rebinding to proteins such as K^+ channels. Thus, free Fe(II) generated by HO, in addition to free iron present in culture medium, could significantly influence numerous CO effects that are interpreted as effects of CO and heme (or heme Fe(II)).

PGRMC1. The crystal structure of the heme-bound homodimeric form of PGRMC1 and the role of heme-bound PGRMC1 in recruiting proteins that interact with PGRMC1

were described above in Section 2. Heme-responsive sensors (Table 2). In a study reporting that CO binding to hemin-bound PGRMC1 dimers disrupts protein–protein interactions, it was claimed that the binding of hemin is essential for PGRMC1 dimer formation and interactions with several proteins.⁶⁶ However, although CO binds only to heme Fe(II), no results related to protein–protein interactions for the heme Fe(II)-bound protein were reported. The spectral features of the heme Fe(II)-bound protein generated by adding sodium dithionate, a strong reductant, are significantly different from those of the hemin-bound protein. In addition, the gel-filtration chromatography pattern of the protein containing sodium dithionate-induced heme Fe(II) is significantly different from that containing hemin in terms of the background level. Thus, it is possible that the protein structure and function of the heme Fe(II)-bound form are already significantly different before addition of CO to the solution. Importantly, the redox potential of hemin-bound PGRMC1 is very low (−331 mV),⁶⁵ suggesting that the redox state of hemin-bound PGRMC1 is very stable and difficult to reduce to heme Fe(II) under aerobic conditions. Thus, it is not clear how CO *per se* influences the structure and function of PGRMC1.

sGC/PKG. Yuan *et al.*¹⁸⁶ reported that CO inhibits the catalysis of cystathionine- γ -lyase (CSE), a non-heme-binding protein, through activation of sGC and subsequent stimulation of protein kinase G (PKG)-dependent phosphorylation of Ser377 in CSE. It has additionally been reported that an exogenously added excess of CO (concentration not reported) activates sGC. However, the affinity of CO for sGC is very low ($K_d \approx 10^{-4}$ M) compared with that of NO ($K_d \approx 10^{-12}$ M),^{187,188} and CO only enhances the catalytic activity of sGC by 4–5-fold¹⁸⁹ compared with the nearly 200-fold increase induced by NO.^{168,169,173,190,191} Therefore, the effects of CO on these functions will require further investigations.

3. Heme-regulated inhibition and activation, and non-canonical heme active sites of heme proteins (Table 3)

3.1. Heme-regulated inhibition and activation

Labile hemin *per se* acts as an inhibitor or an activator of several catalytic functions, although the roles of hemin in inhibition/activation may not be strictly distinct from those of heme-responsive sensors described in Section 2. Heme-responsive sensors. As described in that previous section, the N-end rule pathway is involved in regulating the *in vivo* half-life of a protein based on the identity of its N-terminal residue.¹³⁶ Hemin inhibits arginyl-transferase through a redox mechanism that involves the formation of a disulphide bond between the enzyme's Cys71 and Cys72 residues in the CP motif (Cys71Cys72Pro73).¹³⁴ Hemin also interacts with yeast and mouse E3 ubiquitin ligases (UBR1) of the N-end rule pathway.

YybT family proteins contain an N-terminal PAS domain and a C-terminus composed of a DHH/DHHA1 phosphodiesterase (PDE) domain that exhibits PDE activity toward c-di-AMP, and a GGDEF domain that possesses weak ATPase activity.¹⁹² Hemin

binds to the PAS domain of YybT, forming a typical heme-based gas sensor in which the enzyme is composed of an N-terminal heme-binding domain and a C-terminal functional domain.³⁸ Interestingly, the heme-free form has high PDE activity toward c-di-AMP, with a k_{cat}/K_m value of $0.42 \text{ s}^{-1} \mu\text{M}^{-1}$, whereas the hemin-bound form has a 276-fold lower k_{cat}/K_m value ($0.0015 \text{ s}^{-1} \mu\text{M}^{-1}$) than the heme-free form. YybT protein containing the heme Fe(II) complex has similarly low activity. However, YybT proteins containing a hemin–CN complex or heme Fe(II)–NO complex have 2–3-fold higher activity than those in a ligand-free form. This is a unique case in that heme binding significantly reduces the PDE activity of YybT, which has a domain structure typical of a heme-based sensor.^{38,192}

Elevated hemin levels impair the control of bacterial proliferation independently of heme-iron acquisition by pathogens. Hemin strongly inhibits phagocytosis and the migration of human and mouse phagocytes by disrupting actin cytoskeletal dynamics through activation of the GTP-binding Rho family protein, Cdc42, by the guanine nucleotide exchange factor, DOCK8.¹⁹³ Details of the molecular mechanisms involved in this inhibition remain to be determined.

Heme binds to porphobilinogen deaminase from *Vibrio cholera* with a dissociation constant of $0.33 \mu\text{M}$ and decreases its activity by $\sim 15\%$.¹⁹⁴ Spectral data suggest that the heme in this protein is a mixture of 5- and 6-coordinated states. Mutational studies have shown that the axial ligand of the 5-coordinated heme is Cys105 (part of a non-CP motif) and the axial ligand for the 6-coordinated heme is His227. The crystal structure of this protein suggests that coordination of His227 to heme induces reorientation of the domain containing Cys105, leading to a decrease in catalysis.

The activity of aminolevulinic acid synthase (ALAS) is negatively regulated by hemin through repression of ALAS gene expression, degradation of ALAS mRNA, and inhibition of mitochondrial translocation of the mammalian precursor protein, as shown above (see Section 2.3). It has been found that hemin directly binds to His340 and Cys398 of ALAS from *Caulobacter crescentus* (cALAS) and inhibits its activity by releasing the important coenzyme, pyridoxal phosphate (PLP), from the protein.⁷⁵

Hemin has been described as a potent proinflammatory molecule that is able to induce multiple innate immune responses. One cellular response induced by hemin is the formation of p62/SQTM1 aggregates containing ubiquitinated proteins in structures known as aggresome-like induced structures (ALISs), which are ultimately degraded by autophagy.¹⁹⁵ Heme degradation by HO1 is required for ALIS formation; thus, the free Fe(II) ion released upon heme degradation is necessary and sufficient to induce ALIS formation. Moreover, ferritin, a key protein in iron metabolism, prevents excessive ALIS formation. Thus, hemolysis delivers a free heme iron complex, which promotes an increase in ALIS formation in target tissues. This action is part of a defensive response to the excessive generation of ROS induced by heme iron, driven by the transcription factor NRF2 (nuclear factor erythroid 2-related factor 2).¹⁹⁵

Inflammation induces stress erythropoiesis through heme-dependent activation of the transcriptional factor SPI-C.

Table 3 Heme-regulated inhibition, activation and non-canonical heme active sites of heme proteins. Proteins in [] are already described above in Table 2

Name	Functions	Hemin-sensing/binding site	Hemin K_d or k_{off}	Partner	Origin	Ref.
[Arginyl-transferase]	Hemin inhibits activity (inhibition of arginylation within the N-end rule pathway of protein degradation)	5-Coordinated Cys71/Cys72/Pro73 (2nd of five CP motifs)		UBR1	Mouse, <i>S. cerevisiae</i>	134 and 136
[UBR1]	Hemin inhibits E3 ubiquitin ligase activity (inhibition of protease activity within the N-end rule pathway of protein degradation)			CUP9	Mouse, <i>S. cerevisiae</i>	134 and 136
YybT	Hemin inhibits PDE activity	Phe107 (in the PAS domain)			<i>S. aureus</i> , <i>Listeria monocytogenes</i> , <i>Bacillus subtilis</i> , <i>Geobacillus thermodentrificans</i>	38 and 192
Cdc42	Hemin inhibits phagocytosis	5-Coordinated Cys105 (non-CP motif); 6-coordinated Cys105/His227	$K_d \approx 0.33 \mu\text{M}$	DOCK8	<i>V. cholerae</i>	193
Porpho-bilinogen deaminase	Hemin inhibits activity	6-Coordinated His340/Cys398 (non-CP motif)			<i>C. crescentus</i>	194
ALAS	Hemin inhibits ALA synthesis					75
ALIS	Hemin induces formation of p62/SQTM1 aggregates containing ubiquitinated proteins, aggresome-like induced structure (ALIS), which is degraded by autophagy in response to excessive generation of ROS formed by heme iron			NRF2		195
Inflammation	Erythrophagocytosis, heme-regulated transcriptional factor SPI-C				Mice	196
Fibrinogen	Hemin assists in diTyr cross-linking of fibrinogen, leading to blood coagulation					68
PgDps	Hemin tightly binds PgDps and protects DNA from ROS formed by hemin or heme Fe(II)	5-Coordinated Cys101 (non-CP motif)	$K_d \approx 0.037 \mu\text{M}$		<i>P. gingivalis</i>	22
Amyloid- β	Hemin suppresses amyloid- β -mediated inflammatory activation by reducing expression of proinflammatory cytokines				Mouse	197
Heme-DNAzyme	Hemin catalyzes carbene insertion into styrene					198
DOG1	Hemin regulates dormancy and germination of plants	6-Coordinated His245/His249		AHG1, PP2C	<i>Arabidopsis</i>	199
Oxd (aldoxime dehydratase: OxdA from <i>Pseudomonas chlororaphis</i> B23; OxdB from <i>Bacillus</i> sp. Oxd-1; OxdRE from <i>Rhodococcus</i> sp. N-771)	Heme Fe(II) is the catalytic centre of aldoximes; dehydrated to form R-C \equiv N	OxdA: 5-coordinated His299 (assisted with His320) OxdB: 5-coordinated His306 OxdRE: 5-coordinated His299			<i>Pseudomonas chlororaphis</i> B23, <i>Bacillus</i> sp. OXB-1, <i>Rhodococcus</i> sp. N-771	200–202
TsdA	c-Type dihememes, catalyze tetrathionate S-S bond formation	6-Coordinated Cys138/His99 and Met255/His207 (<i>C. jejuni</i>); 6-coordinated His53/Cys96 and His164/Lys208 (<i>A. vinosum</i>); Cys330 (pupative) (<i>M. purpuratum</i>) (non-CP motifs) Tyr591			<i>C. jejuni</i> , <i>A. vinosum</i> , <i>M. purpuratum</i> , <i>Cupriavidus metallidurans</i> , <i>Thiomonas intermedia</i> , <i>Sideroxydans lithotrophicus</i>	203–206
HZS	c-Type heme, catalyzes N-N bond formation in hydrazine synthesis	5-Coordinated His65			<i>Kuonenia stuttgartensis</i>	207 and 208
KtzT	Hemin catalyzes N-N bond formation in the biosynthesis of piperazate				<i>Kutzneria</i> sp. 744	209
Z-ISO	Heme Fe(II) is involved in <i>cis-trans</i> isomerization of 9,15,9'- <i>cis-ζ</i> -carotene	6-Coordinated His150/Cys263 (non-CP motif); 6-coordinated His150/His266			<i>Zea mays</i> (plant)	210

Table 3 (continued)

Name	Functions	Hemin-sensing/binding site	Hemin K_d or k_{off}	Partner	Origin	Ref.
STEAP3 and STEAP1 (ferric reductase)	Electron transfer <i>via</i> heme iron to reduce free Fe(III) to Fe(II)	6-Coordinated His316/His409 for STEAP3; 5-coordinated Cys57 (non-CP motif); 6-coordinated His175/His268 for STEAP1			Human, rabbit	211 and 212
Dcytb	Electron transfer <i>via</i> heme iron to reduce free Fe(III) to Fe(II)	6-Coordinated His50/His120, His86/His159			Human	213
Myoglobin (artificial system, directed evolution)	Heme catalyzes carbene transfer to olefin in the synthesis of cyclopropanes					214
Cytochrome <i>c</i> (artificial system, directed evolution)	Heme catalyzes carbene transfer in the silylation reaction				<i>Rhodothermus marinus</i>	215
Cytochrome <i>c</i> (artificial system, directed evolution)	Heme catalyzes chiral organoborane synthesis				<i>Rhodothermus marinus</i>	216
Cytochrome P450s (artificial system, directed evolution)	Heme catalyzes direct anti-Markovnikov alkene oxidation				<i>Labrenzia aggregata</i>	217
Cytochrome P450s (artificial system, directed evolution)	Heme catalyzes syntheses of highly strained carbocycles, such as bicyclobutane and cyclopropene				<i>Bacillus megaterium</i>	218
Cytochrome P450s (artificial system, directed evolution)	Heme catalyzes C-C bond formation <i>via</i> iron-catalyzed sp^3 C-H functionalization				<i>Bacillus megaterium</i>	219
Cytochrome P450s (artificial system, directed evolution)	Heme catalyzes C-H amidation for synthesis of diverse lactams				<i>Bacillus megaterium</i>	220
Cytochrome P450s (substrate misrecognition by decoy)	Heme catalyzes hydroxylating reactions toward non-native substrates with the aid of decoy molecules				<i>Bacillus megaterium</i> , <i>Bacillus subtilis</i>	221 and 222
SOUL (HEBP2)	Heme metabolism, heme insertion into hemoglobin, import of coproporphyrinogen into mitochondria		$K_d \approx 0.003 \mu\text{M}$		Rat, mouse	223–225

Note: the functions exerted by the exchangeable/labile heme iron complex are, in general, believed to be conceptually different from those of heme-responsive sensors. However, strictly speaking, the functions partially overlap and thus are difficult to clearly differentiate.

Specifically, activation of Toll-like receptors (TLRs) by zymosan A results in an increase in erythrophagocytosis. Increased erythrophagocytosis leads to an increase in intracellular heme through breakdown of hemoglobin. This increase in heme, in turn, promotes induction of *Spi-c*, which encodes the heme-regulated transcription factor SPI-C.¹⁹⁶

Hemin assists dityrosine cross-linking of fibrinogen upon non-thermal plasma exposure and facilitates blood coagulation.⁶⁸ It has been suggested that fibrinogen, the most important coagulation protein, binds to hemin, and the resulting protein-hemin complex exhibits pseudo-peroxidase activity such that, in the presence of H₂O₂, the complex can induce dityrosine formation between fibrinogen molecules, leading to the formation of the fibrin network necessary for blood coagulation.

The widely expressed Dps (DNA-protective protein from starved-cells) family proteins are major contributors to prokaryotic resistance to stress.²² Dps from *Porphyromonas gingivalis* (PgDps), which was previously described as an iron-storage and DNA-binding protein, binds hemin with a high affinity ($K_d = 0.037 \mu\text{M}$). Hemin forms a 5-coordinated high-spin complex in which Cys101 serves as the axial ligand. Recombinant PgDps protein exists as a stable dodecamer that oligomerizes upon binding of hemin. Since the heme Fe(II) and/or free Fe(II) generated from hemin by HO promotes the production of ROS, which damage DNA, the ability of PgDps to sequester heme iron sequestration would protect DNA against ROS-mediated degradation and confer resistance to heme toxicity.²²

Hemin and hemoglobin act through dual mechanisms to function as potent modulators of astrocyte immune activity.¹⁹⁷ Hemin and hemoglobin suppress the immune activity of primary mouse astrocytes by reducing astrocyte expression of several proinflammatory cytokines and the scavenger receptor CD36, and by reducing fibril growth/aggregation of amyloid- β (1–42). Specifically, hemin (and hemoglobin) directly binds to highly inflammatory amyloid- β (1–42) oligomers and suppresses inflammation. Hemin also up-regulates phosphoprotein signaling in the phosphoinositide 3-kinase (PI3K)/Akt pathway, which regulates immune functions such as cytokine expression and phagocytosis.

Guanine-rich single-stranded DNAs and RNAs that fold into G-quadruplexes (GQs) are known to bind tightly to hemin and heme Fe(II). Heme-GQ (DNA) complexes, known as heme-DNAzymes, catalyze a variety of one-electron (peroxidase) and two-electron (peroxygenase) oxidation reactions.¹⁹⁸ Complexes of heme Fe(II) with GQ also catalyze carbene insertion into styrene.¹⁹⁸

Seed dormancy and germination of plants are controlled by a DOG1 (delay of germination1)-AHG1 (abscisic acid hypersensitive germination1)-PP2C (type 2C protein phosphatase) complex through binding of heme. DOG1 is an α -helical heme-binding protein. His245 and His249 are suggested to be axial ligands for 6-coordinated low-spin heme bound to DOG1.¹⁹⁹

3.2. Emergent novel roles of heme in non-stereotypical hemoprotein functions

In addition to classical heme-containing enzymes, such as cytochrome P450 and peroxidase, heme iron complex bound in non-canonical heme-containing proteins acts as an

active centre for several unique catalytic functions (Fig. 5 and Table 3).

Aldoxime dehydratase (Oxd), a heme-bound protein, catalyzes the dehydration of aldoximes (R-CH=N-OH) to their corresponding nitrile (R-C \equiv N)^{200–202} (Fig. 5A). Unlike other heme enzymes, the substrate is directly bound to the heme iron complex in Oxd. OxdA from *Pseudomonas chlororaphis* B23 contains heme Fe(II) with His299 as the proximal axial ligand and receives aldoxime as the substrate and catalyzes its conversion to nitrile and water with the aid of His320 located on the distal side of the heme iron complex. This distal His residue is a prerequisite for the catalysis, and its direct interaction with the OH group of aldoxime^{200,202} or the C atom of the C=N bond of aldoxime²⁰¹ facilitates the dehydration reaction. In contrast, Oxd containing hemin does not catalyze the dehydration reaction. The X-ray crystal structure of the Michaelis complex of OxdRE from *Rhodococcus* sp. N-771 demonstrates the unique substrate binding and activity-regulating properties of Oxd.²⁰²

Bifunctional thiosulphate dehydrogenases/tetrathionate reductases (TsdAs) are a distinct type of diheme *c*-type cytochromes that catalyze the reversible formation of a sulphur-sulphur bond between the sulphane atoms of two thiosulphate molecules ($^-\text{O}_3\text{S-S}^-$), yielding tetrathionate ($^-\text{O}_3\text{S-S-S-SO}_3^-$) and releasing two electrons^{203–206} (Fig. 5B). Both hemes (heme 1 and heme 2) are covalently bound to the protein through Cys residues. Heme 1 of TsdA from *Campylobacter jejuni* is a 6-coordinated complex with Cys138/His99 as the axial ligands, whereas heme 2 is a 6-coordinated complex with Met255/His207 as the axial ligands. Replacement of one (Cys138 for heme 1, Met255 for heme 2) of these axial ligand residues with another amino acid results in loss of heme binding and a virtually inactive enzyme. Heme 1 acts as the active centre, whereas heme 2 acts as an electron relay centre that wires the active site to the enzyme's redox partner.²⁰³ In TsdA from *Allochromatium vinosum*, heme 1 and heme 2 have His53/Cys96 and His164/Lys208, respectively, as the axial ligands.²⁰⁵ Cys96 is essential for catalysis, as evidenced by the fact that mutations at Cys96 completely abolish catalysis. A ligand switch from Lys208 to Met209 occurs upon reduction of heme 2. Binding of thiosulphate to hemin and reduction of hemin to heme Fe(II) cause dissociation of the axial ligand Cys96 from the heme iron complex.²⁰⁵ The crystal structure of a fusion protein composed of TsdA and TsdB (an electron receptor) from *Marichromatium purpuratum* revealed that Cys330, the putative axial ligand for heme 1 of TsdA in the fusion protein, is situated 2.9 Å from the heme iron, a distance that is too far for direct ligation. Importantly, thiosulphate is covalently bound to Cys330.²⁰⁴

Hydrazine synthase (HZS) is a multiprotein complex, each subunit of which contains two unique *c*-type heme-containing active sites, as well as an interaction point for a redox partner. HZS produces hydrazine (N₂H₄) from NO and ammonium (NH₃)^{207,208} (Fig. 5C). Electron transfer processes involving the *c*-type heme of HZS play a significant role in N-N bond formation. The crystal structure of HZS implies a two-step mechanism for hydrazine synthesis: (1) three-electron reduction

able to rotate to the thermodynamically more favorable *trans* orientation.

STEAP (six-transmembrane epithelial antigen of prostate metalloredutases) are the major ferric reductases in developing erythrocytes, where they are critical for metal homeostasis; they are also linked to multiple diseases.^{211,212} The single b-type heme, flavin-adenine dinucleotide (FAD), and iron-binding sites are located in the transmembrane domain. Bis-His residues are axial ligands for hemin, and two Tyr residues bind a free Fe(III) atom adjacent to heme.²¹¹ STEAP3 functions as a transmembrane electron shuttle, moving cytoplasmic electrons derived from NADPH across the lipid layers to the extracellular face, where they reduce free Fe(III) to free Fe(II) and potentially Cu²⁺ to Cu⁺. STEAP3 functions as a homodimer and utilizes an intrasubunit electron-transfer pathway through the single heme moiety rather than an intersubunit electron transfer pathway through a potential domain-swapped dimer. STEAP1 is likely to form a homotrimer and forms a heterotrimer when co-expressed with STEAP2. Heme Fe(II) of STEAP1 reacts readily with O₂.²¹² The sequence motifs in the transmembrane domain that are associated with the FAD and metal binding sites are present among STEAP1–STEAP4.

Duodenal cytochrome *b* (Dcytb), a ferric Fe(III) reductase, is an integral membrane protein that catalyzes reduction of non-heme Fe(III) by electron transfer from ascorbate across the membrane.²¹³ The resultant ferrous iron Fe(II) would be transported by divalent metal ion transporter 1 (DMT1). The function of Dcytb is similar to that of STEAPs. Crystal structures of Dcytb have revealed that the free metal cation, in this case Zn(II) instead of Fe(III), coordinates to two hydroxyl groups of apical ascorbate and a His residue, suggesting that Fe(III) uptake is promoted by ascorbate or relevant reducing agents.

Heme-based catalysis also operates in artificial synthetic pathways created by engineering prototypical heme proteins, such as myoglobin, cytochrome *c* and cytochrome P450, through directed evolution. Catalytic carbene transfer to olefins is a useful approach for synthesizing cyclopropanes, which are key structural motifs of many drugs and biologically active natural products.²¹⁴ Myoglobin promotes carbene-mediated cyclopropanation reactions with excellent catalytic activity and selectivity.²¹⁴ The crystal structure of a reactive iron porphyrin carbene intermediate for the carbene-transferring silylation reaction in the heme binding pocket of an engineered cytochrome *c* protein has been determined.²¹⁵ Taken together with computational methods, such structural insights into key catalytic intermediates should advance our understanding of the reaction mechanism of the “carbene transferase” of heme proteins.^{214,215} Effective chiral organoborane syntheses have also been achieved through directed evolution of cytochrome *c* mutants.²¹⁶ Applying directed evolution to engineering of cytochrome P450, a well-known monooxygenase,^{35,36} makes anti-Markovnikov alkene oxidation,²¹⁷ synthesis of highly strained carbocycles, such as bicyclobutane and cyclopropane,²¹⁸ C–C bond formation²¹⁹ and C–H amidation possible.²²⁰ Furthermore, hydroxylating reactions toward non-native substrates such as propane, butane, cyclohexane, benzene, styrene and

ethylbenzene mediated by cytochrome P450 with the aid of decoy molecules have been reported.^{221,222}

SOUL (heme-binding protein 2, also known as HEBP2) homologs constitute a superfamily of heme-binding proteins involved in heme biosynthesis/metabolism that are associated with a number of physiological processes.^{223–225} The SOUL protein is expressed in the retina and pineal gland in chicken and is solely expressed in the retina in mice. Recombinant murine SOUL exists as a dimer in the absence of heme iron, but it specifically binds one heme per monomer unit and becomes a hexamer upon binding heme.²²³ Murine p22HBP (p22 heme-binding protein), also known as HEBP1, is a heme protein ubiquitously expressed in numerous tissues that has been reported to exhibit 27%²²⁴ or 40%^{223,226} identity to murine SOUL. It also binds one heme per monomer, but its coordination to heme uses no specific axial ligand. SOUL binds heme through coordination with a His residue.^{223,224} Dissociation rate constants of heme from both SOUL and p22HBP are very high, with k_{off} values of $1.2 \times 10^3 \text{ s}^{-1}$ and $4.4 \times 10^{-3} \text{ s}^{-1}$, respectively, compared with $8.4 \times 10^{-7} \text{ s}^{-1}$ for myoglobin, suggesting that heme has a high affinity for these SOUL proteins.²²³ In contrast, similarly low affinity of heme for p22HBP ($K_{\text{d}} \approx 0.03 \text{ }\mu\text{M}$) has been demonstrated using a fluorescence quenching method.²²⁴ SOUL and p22HBP share what is likely to be a conserved tertiary fold, but NMR spectroscopy suggests that they bind heme at different sites within this fold.²²⁴ SOUL and p22HBP could either function as heme transporters or chaperones for heme insertion into hemoglobin or as mediators of coproporphyrinogen import into mitochondria.²²⁴

Note that a helical scaffold is not essential for heme binding, as heme can bind to a peptide composed predominantly of β -scaffold secondary structures.⁶⁷

4. Conclusions

Biochemistry textbooks describe the important role of the heme iron complex prosthetic group in physiology. In particular, it is said that the heme iron complex manifests its capabilities in hemeproteins, rather than as a free heme iron complex. For example, the heme iron complex in prototypical hemeproteins plays a key role in O₂ storage, O₂ transfer, O₂ activation, peroxide activation and electron transfer at the heme active site. However, new and totally different types of heme proteins—heme-responsive sensors—have emerged. In these proteins, the association/dissociation of heme regulates numerous intrinsic functions that are important physiologically and pathologically. In the present review, we have provided comprehensive coverage of heme-responsive sensors, with a focus on molecular mechanisms.

Heme-responsive sensors are critically involved in numerous important physiological functions, such as transcriptional regulation, tRNA syntheses, mRNA splicing, translational regulation, proteasome-dependent and -independent protein degradation, K⁺ channel regulation, autophosphorylation, and protein–protein interactions. Some functions are associated with the biosynthesis and metabolism of the heme iron complex. Interestingly, some

heme-sensing transcriptional regulations are associated with circadian rhythms. In addition, heme-responsive sensors act as scavengers that bind detrimental heme iron complexes so as to prevent their participation in the generation of ROS.

There are additional novel, emergent roles of the free heme iron complex and heme iron complexes in hemeproteins. For example, hemin inhibits PDE and deaminase activity, phagocytosis, and amyloid β -mediated inflammation, whereas hemin recruits EGFR and cytochrome P450 enzymes, forms aggregates with ubiquitinated proteins, and induces diTyr cross-linking of fibrinogen. Furthermore, aldoxime dehydration, *cis-trans* isomerization, N–N bond formation, S–S bond formation, and carbene-transfer reactions are directly catalyzed by the heme iron complex in heme proteins.

It is claimed that some heme-based CO sensors simultaneously act as heme-responsive sensors or *vice versa*. However, the molecular mechanisms of overlapping or duplicate roles of these sensors still remain unresolved, but hopefully will be adequately addressed in the near future.

Dysfunction of heme-responsive sensors is critical in various diseases. In particular, if functions associated with heme synthesis and heme metabolism are impaired, serious blood-related diseases can ensue. On the other hand, in pathobacteria, the heme iron complex is degraded to provide free iron for use as a bacterial nutrient. Since heme-sensing systems tend to precede heme-degradation reactions, impairment of the heme-sensing ability of bacteria would help cure infectious bacterial diseases.

It is certain that, in future, numerous physiologically important heme-sensing functions and heme-associated catalysis/reactions will be discovered. Many spectroscopic methods can be used to characterize the structure and functions of heme-responsive sensors. This will prove beneficial for biological chemists in advancing our understanding of the molecular mechanisms of numerous important reactions involving heme and heme-responsive sensors, and ultimately lead to clinically meaningful therapeutic targets in diverse diseases associated with ROS, NO, CO, iron, heme biosynthesis and metabolism, and/or bacteria.

Abbreviations

ALAS	Aminolevulinic acid synthase
ALAS1	Nonspecific 5-aminolevulinic acid synthase
ALIS	Aggresome-like induced structure
All4978	Protein from cyanobacterium <i>Nostoc</i> sp. PCC7120
Arnt	Aryl hydrocarbon receptor nuclear translocator
Bach1	BTB domain and CNC homolog 1
Bach2	BTB domain and CNC homolog 2
bHLH	Protein domain with a basic helix-loop-helix motif
BK channel	Ca ²⁺ -Sensitive large-conductance K ⁺ channel
BMAL1	Brain and muscle Arnt-like 1
cALAS	ALAS from <i>Caulobacter crescentus</i>

ChrA	Response regulator (RR) of ChrS protein
ChrS	Heme-sensing kinase of <i>Corynebacterium diphtheria</i>
CLOCK	Transcriptional regulatory protein associated with circadian rhythms
ClpXP	Mitochondrial ATP-dependent protease
CP motif	Cys-Pro motif
CRY	Cryptochrome
CSE	Cystathionine- γ -lyase
CUP9	Homeodomain-containing transcriptional repressor or homeobox protein
Dcylb	Duodenal cytochrome <i>b</i>
DGCR8	DiGeorge critical region 8
DHR3	Drosophila hormone receptor 3
DHR51	Drosophila hormone receptor 51
DnrF	Crp/Fnr-type transcriptional regulator
DOG1	Delay of germination1
Dps	DNA-protective protein from starved-cells
E75	Ecdysone-induced protein 75
EGFR	Epidermal growth factor receptor
eIF2 α	Eukaryotic initiation factor 2 α
FAD	Flavin-adenine dinucleotide
FBXL5	F-Box and leucine-rich repeat protein 5
Fre	Ferric reductase
Fre-MsrP-MsrQ	Methionine sulphoxide reductase system from <i>Escherichia coli</i>
FurA	Ferric uptake regulator from cyanobacteria <i>Anabaena</i> sp. PCC 7120.
GAF	Protein domain named after three proteins, cGMP-specific phosphodiesterase, adenylyl cyclase and FhlA
GCN2	General control nonderepressible 2
Gis1	Yeast histone demethylase
GlURS	Glutamyl-tRNA synthase
GlUTR	Glutamyl-tRNA reductase
GQ	Guanine-rich single-stranded DNA and RNA that fold into G-quadruplex
HAP1	Heme-sensing transcriptional regulator
HBD	Heme binding domain
HcArgRS	Human cytoplasmic arginyl-tRNA synthase
HDAC3	Histone deacetylase 3
HDM	Helminth defense molecule
HEBP1	Heme-binding protein 1 or p22HBP
HEBP2	Heme-binding protein 2 or SOUL
heme	Protoporphyrin IX iron complex
heme Fe(II) complex	Ferrous protoporphyrin IX
hemin	Heme Fe(III) complex or ferric protoporphyrin IX
HK	Histidine kinase
HO1	Heme oxygenase-1
HO2	Heme oxygenase-2
HOIL-1	Heme-oxidized IRP2 ubiquitin ligase-1
HR3 AF2	Peptide derived from DHR3 protein
HRI	Heme-regulated inhibitor (eukaryotic initiation factor 2 α kinase)

hrt	Gene for heme-regulated transporter	Rev-erb β	Nuclear receptor also known as NR1D2 (nuclear receptor subfamily 1, group D, member 2)
HrtA, HrtB	Heme-regulated transporters of <i>Lactococcus lactis</i>	ROR	Retinoic acid receptor-related orphan receptor
HrtAB	Heme-regulated transporter efflux pump	ROS	Reactive oxygen species
HrtR	Transcriptional regulator of <i>Lactococcus lactis</i>	RR	Response regulator
Hsp90	Heat shock protein 90	SbnI	Protein from <i>Staphylococcus aureus</i>
HssS-HssR	Heme-sensing two-component heme-responsive-sensor system	sGC	Soluble guanylate cyclase
HZS	Hydrazine synthase	Sim	Single-minded protein
IRP1	Iron-responsive element-binding protein-1 or iron regulatory protein 1	SOUL	Heme-binding protein 2 or HEBP2
IRP2	Iron-responsive element-binding protein-2 or iron regulatory protein 2	STEAP	Six-transmembrane epithelial antigen of prostate metalloredutase
Irr	Ferric uptake regulation protein from <i>Bradyrhizobium japonicum</i>	SUR2A	Sulphonylurea receptor subunit
KtzT	Protein from <i>Kutzneria</i> sp. 744	TCS	Two-component signal transduction system
K _v 1.4 channel	Voltage-dependent K ⁺ channel	Tll0287	Protein from <i>Thermosynechococcus elongatus</i>
LONP1	Lon peptidase 1, mitochondrial	TrpRS	Tryptophanyl-tRNA synthase
MA4561	Kinase protein from <i>Methanosarcina acetivorans</i>	TsdA	Thiosulphate dehydrogenase/tetrathionate reductase
Maf	Musculoaponeurotic fibrosarcoma	UBR1	E3 ubiquitin ligase of the N-end rule pathway
MafK	bZip Maf transcription factor protein	YybT	Stress signaling proteins from <i>Bacillus subtilis</i>
mPer2	Mouse period circadian protein homologue 2	Z-ISO	15- <i>cis</i> - ζ -Carotene isomerase
NADPH	Nicotinamide adenine dinucleotide phosphate (reduced form)	ZnF	Zinc finger domain
NCoR	Nuclear receptor co-repressor		
NOS	Nitric oxide synthase		
NPAS2	Neuronal PAS domain protein 2		
NRF2	Nuclear factor erythroid 2-related factor 2		
NtrY-NtrX	Redox sensor system of <i>Brucella</i> spp.		
Oxd	Aldoxime dehydrase		
p22HBP	p22 heme-binding protein or HEBP1		
p53	Tumor-suppressor protein		
PAS	Protein domain named after three proteins (Per-Arnt-Sim)		
PDE	Phosphodiesterase		
Per	Period circadian protein		
PERK	Protein kinase R (PKR)-like endoplasmic reticulum kinase		
PfRRS	<i>Plasmodium falciparum</i> arginyl-tRNA synthase		
PgDps	DNA protecting protein from <i>Porphyromonas gingivalis</i>		
PGRMC1	Progesterone receptor membrane component 1		
PKG	Protein kinase G		
PKR	Protein kinase R		
PpsR	Protein from <i>Rhodobacter sphaeroides</i>		
pri-miRNA	Primary microRNA		
RCK	Regulator of conductance for K ⁺		
Rev-erb α	Nuclear receptor also known as NR1D1 (nuclear receptor subfamily 1, group D, member 1)		

Conflicts of interest

There are no conflicts to declare.

Acknowledgements

This work was supported in part by Charles University (SVV260427/2018) and the Grant Agency of Charles University (grant 704217).

Notes and references

- 1 P. Chandrangsu, C. Rensing and J. D. Helmann, *Nat. Rev. Microbiol.*, 2017, **15**, 338–350.
- 2 Z. Ma, F. E. Jacobsen and D. P. Giedroc, *Chem. Rev.*, 2009, **109**, 4644–4681.
- 3 A. Chao, P. J. Sieminski, C. P. Owens and C. W. Goulding, *Chem. Rev.*, 2019, **119**, 1193–1220.
- 4 B. J. Crielgaard, T. Lammers and S. Rivella, *Nat. Rev. Drug Discovery*, 2017, **16**, 400–423.
- 5 M. U. Muckenthaler, S. Rivella, M. W. Hentze and B. Galy, *Cell*, 2017, **168**, 344–361.
- 6 D. L. Abeyawardhane, R. D. Fernández, C. J. Murgas, D. R. Heitger, A. K. Forney, M. K. Crozier and H. R. Lucas, *J. Am. Chem. Soc.*, 2018, **140**, 5028–5032.

- 7 J. A. Zinskie, A. Ghosh, B. M. Trainor, D. Shedlovskiy, D. G. Pestov and N. Shcherbik, *J. Biol. Chem.*, 2018, **293**, 14237–14248.
- 8 M. Sandy and A. Butler, *Chem. Rev.*, 2009, **109**, 4580–4595.
- 9 B. R. Wilson, A. R. Bogdan, M. Miyazawa, K. Hashimoto and Y. Tsuji, *Trends Mol. Med.*, 2016, **22**, 1077–1090.
- 10 B. Qi and M. Han, *Cell*, 2018, **175**, 571–582.
- 11 M. D. Knutson, *J. Biol. Chem.*, 2017, **292**, 12735–12743.
- 12 C. C. Philpott, M.-S. Ryu, A. Frey and S. Patel, *J. Biol. Chem.*, 2017, **292**, 12764–12771.
- 13 R. Coffey and T. Ganz, *J. Biol. Chem.*, 2017, **292**, 12727–12734.
- 14 B. R. Stockwell, J. P. Friedmann Angeli, H. Bayir, A. I. Bush, M. Conrad, S. J. Dixon, S. Fulda, S. Gascón, S. K. Hatzios, V. E. Kagan, K. Noel, X. Jiang, A. Linkermann, M. E. Murphy, M. Overholtzer, A. Oyagi, G. C. Pagnussat, J. Park, Q. Ran, C. S. Rosenfeld, K. Salnikow, D. Tang, F. M. Torti, S. V. Torti, S. Toyokuni, K. A. Woerpel and D. D. Zhang, *Cell*, 2017, **171**, 273–285.
- 15 L. T. Roumenina, J. Rayes, S. Lacroix-Desmazes and J. D. Dimitrov, *Trends Mol. Med.*, 2016, **22**, 200–213.
- 16 D. A. Hanna, R. Hu, H. Kim, O. Martinez-Guzman, M. P. Torres and A. R. Reddi, *J. Biol. Chem.*, 2018, **293**, 12378–12393.
- 17 D. A. Hanna, R. M. Harvey, O. Martinez-Guzman, X. Yuan, B. Chandrasekharan, G. Raju, F. W. Outten, I. Hamza and A. R. Reddi, *Proc. Natl. Acad. Sci. U. S. A.*, 2016, **113**, 7539–7544.
- 18 J. R. Abshire, C. J. Rowlands, S. M. Ganesan, P. T. C. So and J. C. Niles, *Proc. Natl. Acad. Sci. U. S. A.*, 2017, **114**, E2068–E2076.
- 19 I. Yanatori, D. R. Richardson, K. Imada and F. Kishi, *J. Biol. Chem.*, 2016, **291**, 17303–17318.
- 20 P. Hahl, R. Hunt, E. S. Bjes, A. Skaff, A. Keightley and A. Smith, *J. Biol. Chem.*, 2017, **292**, 13658–13671.
- 21 V. Martínez-Sernández, M. Mezo, M. González-Warleta, M. J. Perteguer, T. Gárate, F. Romarís and F. M. Ubeira, *J. Biol. Chem.*, 2017, **292**, 8667–8682.
- 22 J.-L. Gao, Y. Lu, G. Browne, B. C.-M. Yap, J. Trehwella, N. Hunter and K.-A. Nguyen, *J. Biol. Chem.*, 2012, **287**, 42243–42258.
- 23 T. Uchida, N. Kobayashi, S. Muneta and K. Ishimori, *Biochemistry*, 2017, **56**, 2425–2434.
- 24 E. A. Sweeny, A. B. Singh, R. Chakravarti, O. Martinez-Guzman, A. Saini, M. M. Haque, G. Garee, P. D. Dans, L. Hannibal, A. R. Reddi and D. J. Stuehr, *J. Biol. Chem.*, 2018, **293**, 14557–14568.
- 25 P. Ponka, A. D. Sheftel, A. M. English, D. Scott Bohle and D. Garcia-Santos, *Trends Biochem. Sci.*, 2017, **42**, 395–406.
- 26 A. R. Reddi and I. Hamza, *Acc. Chem. Res.*, 2016, **49**, 1104–1110.
- 27 R. Abe, J. M. M. Caaveiro, H. Kozuka-Hata, M. Oyama and K. Tsumoto, *J. Biol. Chem.*, 2012, **287**, 16477–16487.
- 28 C. F. M. Bowden, A. C. K. Chan, E. J. W. Li, A. L. Arrieta, L. D. Eltis and M. E. P. Murphy, *J. Biol. Chem.*, 2018, **293**, 177–190.
- 29 W. Huang and A. Wilks, *Annu. Rev. Biochem.*, 2017, **86**, 799–823.
- 30 T. Mourer, J.-F. Jacques, A. Brault, M. Bisailon and S. Labbé, *J. Biol. Chem.*, 2015, **290**, 10176–10190.
- 31 X. Yuan, N. Rietzschel, H. Kwon, A. B. Walter Nuno, D. A. Hanna, J. D. Phillips, E. L. Raven, A. R. Reddi and I. Hamza, *Proc. Natl. Acad. Sci. U. S. A.*, 2016, **113**, E5144–E5152.
- 32 Y. Naoe, N. Nakamura, A. Doi, M. Sawabe, H. Nakamura, Y. Shiro and H. Sugimoto, *Nat. Commun.*, 2016, **7**, 13411.
- 33 S. Peherstorfer, H. H. Brewitz, A. A. Paul George, A. Wißbrock, J. M. Adam, L. Schmitt and D. Imhof, *Biochim. Biophys. Acta*, 2018, **1862**, 1964–1972.
- 34 A. S. Tsiftoglou, A. I. Tsamadou and L. C. Papadopoulou, *Pharmacol. Ther.*, 2006, **111**, 327–345.
- 35 F. P. Guengerich and F. K. Yoshimoto, *Chem. Rev.*, 2018, **118**, 6573–6655.
- 36 X. Huang and J. T. Groves, *Chem. Rev.*, 2018, **118**, 2491–2553.
- 37 H. M. Girvan and A. W. Munro, *J. Biol. Chem.*, 2013, **288**, 13194–13203.
- 38 T. Shimizu, D. Huang, F. Yan, M. Stranova, M. Bartosova, V. Fojtíková and M. Martínková, *Chem. Rev.*, 2015, **115**, 6491–6533.
- 39 M. Martínková, K. Kitanishi and T. Shimizu, *J. Biol. Chem.*, 2013, **288**, 27702–27711.
- 40 H. Sawai and Y. Shiro, *Gas Sensing in Cells*, The Royal Society of Chemistry, 2018, pp. 47–83.
- 41 Y. Kang, R. Liu, J.-X. Wu and L. Chen, *Nature*, 2019, **574**, 206–210.
- 42 L. Zhang and L. Guarente, *EMBO J.*, 1995, **14**, 313–320.
- 43 J. Igarashi, M. Murase, A. Iizuka, F. Pichierri, M. Martinkova and T. Shimizu, *J. Biol. Chem.*, 2008, **283**, 18782–18791.
- 44 T. Shimizu, *J. Inorg. Biochem.*, 2012, **108**, 171–177.
- 45 T. Kühn, A. Wißbrock, N. Goradia, N. Sahoo, K. Galler, U. Neugebauer, J. Popp, S. H. Heinemann, O. Ohlenschläger and D. Imhof, *ACS Chem. Biol.*, 2013, **8**, 1785–1793.
- 46 I. Barr, A. T. Smith, R. Senturia, Y. Chen, B. D. Scheidemantle, J. N. Burstyn and F. Guo, *J. Biol. Chem.*, 2011, **286**, 16716–16725.
- 47 T. Omura, *Biochem. Biophys. Res. Commun.*, 2005, **338**, 404–409.
- 48 X. D. Tang, R. Xu, M. F. Reynolds, M. L. Garcia, S. H. Heinemann and T. Hoshi, *Nature*, 2003, **425**, 531–535.
- 49 L. Yi, J. T. Morgan and S. W. Ragsdale, *J. Biol. Chem.*, 2010, **285**, 20117–20127.
- 50 N. Sahoo, N. Goradia, O. Ohlenschläger, R. Schönherr, M. Friedrich, W. Plass, R. Kappl, T. Hoshi and S. H. Heinemann, *Proc. Natl. Acad. Sci. U. S. A.*, 2013, **110**, E4036–E4044.
- 51 M. J. Burton, S. M. Kapetanaki, T. Chernova, A. G. Jamieson, P. Dorlet, J. Santolini, P. C. E. Moody, J. S. Mitcheson, N. W. Davies, R. Schmid, E. L. Raven and N. M. Storey, *Proc. Natl. Acad. Sci. U. S. A.*, 2016, **113**, 3785–3790.

- 52 T. Uchida, E. Sato, A. Sato, I. Sagami, T. Shimizu and T. Kitagawa, *J. Biol. Chem.*, 2005, **280**, 21358–21368.
- 53 D. Lechardeur, B. Cesselin, U. Liebl, M. H. Vos, A. Fernandez, C. Brun, A. Gruss and P. Gaudu, *J. Biol. Chem.*, 2012, **287**, 4752–4758.
- 54 H. Sawai, M. Yamanaka, H. Sugimoto, Y. Shiro and S. Aono, *J. Biol. Chem.*, 2012, **287**, 30755–30768.
- 55 L. Yin, N. Wu, J. C. Curtin, M. Qatanani, N. R. Szwegold, R. A. Reid, G. M. Waitt, D. J. Parks, K. H. Pearce, G. B. Wisely and M. A. Lazar, *Science*, 2007, **318**, 1786–1789.
- 56 S. Raghuram, K. R. Stayrook, P. Huang, P. M. Rogers, A. K. Nosie, D. B. McClure, L. L. Burris, S. Khorasanizadeh, T. P. Burris and F. Rastinejad, *Nat. Struct. Mol. Biol.*, 2007, **14**, 1207–1213.
- 57 L. J. Everett and M. A. Lazar, *Trends Endocrinol. Metab.*, 2014, **25**, 586–592.
- 58 N. Gupta and S. W. Ragsdale, *J. Biol. Chem.*, 2011, **286**, 4392–4403.
- 59 E. L. Carter, N. Gupta and S. W. Ragsdale, *J. Biol. Chem.*, 2016, **291**, 2196–2222.
- 60 E. L. Carter, Y. Ramirez and S. W. Ragsdale, *J. Biol. Chem.*, 2017, **292**, 11280–11299.
- 61 K. A. Marvin, J. L. Reinking, A. J. Lee, K. Pardee, H. M. Krause and J. N. Burstyn, *Biochemistry*, 2009, **48**, 7056–7071.
- 62 K. I. Pardee, X. Xu, J. Reinking, A. Schuetz, A. Dong, S. Liu, R. Zhang, J. Tiefenbach, G. Lajoie, A. N. Plotnikov, A. Botchkarev, H. M. Krause and A. Edwards, *PLoS Biol.*, 2009, **7**, e43.
- 63 S. L. Freeman, H. Kwon, N. Portolano, G. Parkin, U. Venkatraman Girija, J. Basran, A. J. Fielding, L. Fairall, D. A. Svistunenko, P. C. E. Moody, J. W. R. Schwabe, C. P. Kyriacou and E. L. Raven, *Proc. Natl. Acad. Sci. U. S. A.*, 2019, **116**, 19911–19916.
- 64 K. Wakasugi, *Biochemistry*, 2007, **46**, 11291–11298.
- 65 D. Kaluka, D. Batabyal, B.-Y. Chiang, T. L. Poulos and S.-R. Yeh, *Biochemistry*, 2015, **54**, 1638–1647.
- 66 Y. Kabe, T. Nakane, I. Koike, T. Yamamoto, Y. Sugiura, E. Harada, K. Sugase, T. Shimamura, M. Ohmura, K. Muraoka, A. Yamamoto, T. Uchida, S. Iwata, Y. Yamaguchi, E. Krayukhina, M. Noda, H. Handa, K. Ishimori, S. Uchiyama, T. Kobayashi and M. Suematsu, *Nat. Commun.*, 2016, **7**, 11030.
- 67 D. Nagarajan, S. Sukumaran, G. Deka, K. Krishnamurthy, H. S. Atreya and N. Chandra, *J. Biol. Chem.*, 2018, **293**, 9412–9422.
- 68 Z. Ke and Q. Huang, *Sci. Rep.*, 2016, **6**, 26982.
- 69 M. Miksanova, J. Igarashi, M. Minami, I. Sagami, S. Yamauchi, H. Kurokawa and T. Shimizu, *Biochemistry*, 2006, **45**, 9894–9905.
- 70 S. Lal, J. M. Comer, P. C. Konduri, A. Shah, T. Wang, A. Lewis, G. Shoffner, F. Guo and L. Zhang, *Nucleic Acids Res.*, 2018, **46**, 215–228.
- 71 M. Watanabe-Matsui, T. Matsumoto, T. Matsui, M. Ikeda-Saito, A. Muto, K. Murayama and K. Igarashi, *Arch. Biochem. Biophys.*, 2015, **565**, 25–31.
- 72 T. Suenaga, M. Watanabe-Matsui, T. Uejima, H. Shima, T. Matsui, M. Ikeda-Saito, M. Shirouzu, K. Igarashi and K. Murayama, *J. Biochem.*, 2016, **160**, 291–298.
- 73 L. Yi and S. W. Ragsdale, *J. Biol. Chem.*, 2007, **282**, 21056–21067.
- 74 S. W. Ragsdale and L. Yi, *Antioxid. Redox Signaling*, 2011, **14**, 1039–1047.
- 75 H. Ikushiro, A. Nagami, T. Takai, T. Sawai, Y. Shimeno, H. Hori, I. Miyahara, N. Kamiya and T. Yano, *Sci. Rep.*, 2018, **8**, 14228.
- 76 M. Sono, S. Sun, A. Modi, M. S. Hargrove, B. Molitor, N. Frankenberg-Dinkel and J. H. Dawson, *J. Biol. Inorg. Chem.*, 2018, **23**, 1085–1092.
- 77 F. Zhong, G. P. Lisi, D. P. Collins, J. H. Dawson and E. V. Pletneva, *Proc. Natl. Acad. Sci. U. S. A.*, 2014, **111**, E306–E315.
- 78 K. Tang, M. Knipp, B.-B. Liu, N. Cox, R. Stabel, Q. He, M. Zhou, H. Scheer, K.-H. Zhao and W. Gärtner, *J. Biol. Chem.*, 2015, **290**, 19067–19080.
- 79 B. Molitor, M. Stassen, A. Modi, S. F. El-Mashtoly, C. Laurich, W. Lubitz, J. H. Dawson, M. Rother and N. Frankenberg-Dinkel, *J. Biol. Chem.*, 2013, **288**, 18458–18472.
- 80 M. del, C. Carrica, I. Fernandez, M. A. Martí, G. Paris and F. A. Goldbaum, *Mol. Microbiol.*, 2012, **85**, 39–50.
- 81 T. Motomura, M. Suga, R. Hienerwadel, A. Nakagawa, T.-L. Lai, W. Nitschke, T. Kuma, M. Sugiura, A. Boussac and J.-R. Shen, *J. Biol. Chem.*, 2017, **292**, 9599–9612.
- 82 H. C. Lee, T. Hon, C. Lan and L. Zhang, *Mol. Cell. Biol.*, 2003, **23**, 5857–5866.
- 83 E. M. Dioum, J. Rutter, J. R. Tuckerman, G. Gonzalez, M.-A. Gilles-Gonzalez and S. L. McKnight, *Science*, 2002, **298**, 2385–2387.
- 84 J. Bass and M. A. Lazar, *Science*, 2016, **354**, 994–999.
- 85 Y. Mukaiyama, T. Uchida, E. Sato, A. Sasaki, Y. Sato, J. Igarashi, H. Kurokawa, I. Sagami, T. Kitagawa and T. Shimizu, *FEBS J.*, 2006, **273**, 2528–2539.
- 86 M. Ishida, T. Ueha and I. Sagami, *Biochem. Biophys. Res. Commun.*, 2008, **368**, 292–297.
- 87 K. Yoshii, F. Tajima, S. Ishijima and I. Sagami, *Biochemistry*, 2015, **54**, 250–259.
- 88 M. Ebert, P. Schweyen, M. Bröring, S. Laass, E. Härtig and D. Jahn, *J. Biol. Chem.*, 2017, **292**, 15468–15480.
- 89 K. Ogawa, J. Sun, S. Taketani, O. Nakajima, C. Nishitani, S. Sassa, N. Hayashi, M. Yamamoto, S. Shibahara, H. Fujita and K. Igarashi, *EMBO J.*, 2001, **20**, 2835–2843.
- 90 Y. Zenke-Kawasaki, Y. Dohi, Y. Katoh, T. Ikura, M. Ikura, T. Asahara, F. Tokunaga, K. Iwai and K. Igarashi, *Mol. Cell. Biol.*, 2007, **27**, 6962–6971.
- 91 S. Hira, T. Tomita, T. Matsui, K. Igarashi and M. Ikeda-Saito, *IUBMB Life*, 2007, **59**, 542–551.
- 92 K. Igarashi and M. Watanabe-Matsui, *Tohoku J. Exp. Med.*, 2014, **232**, 229–253.
- 93 K. Igarashi, T. Kurosaki and R. Roychoudhuri, *Nat. Rev. Immunol.*, 2017, **17**, 437–450.
- 94 M. Watanabe-Matsui, A. Muto, T. Matsui, A. Itoh-Nakadai, O. Nakajima, K. Murayama, M. Yamamoto, M. Ikeda-Saito and K. Igarashi, *Blood*, 2011, **117**, 5438–5448.

- 95 H. Kato, A. Itoh-Nakadai, M. Matsumoto, Y. Ishii, M. Watanabe-Matsui, M. Ikeda, R. Ebina-Shibuya, Y. Sato, M. Kobayashi, H. Nishizawa, K. Suzuki, A. Muto, T. Fujiwara, Y. Nannya, L. Malcovati, M. Cazzola, S. Ogawa, H. Harigae and K. Igarashi, *Nat. Immunol.*, 2018, **19**, 1059–1070.
- 96 J. Shen, X. Sheng, Z. Chang, Q. Wu, S. Wang, Z. Xuan, D. Li, Y. Wu, Y. Shang, X. Kong, L. Yu, L. Li, K. Ruan, H. Hu, Y. Huang, L. Hui, D. Xie, F. Wang and R. Hu, *Cell Rep.*, 2014, **7**, 180–193.
- 97 T. Gotoh, J. K. Kim, J. Liu, M. Vila-Caballer, P. E. Stauffer, J. J. Tyson and C. V. Finkielstein, *Proc. Natl. Acad. Sci. U. S. A.*, 2016, **113**, 13516–13521.
- 98 L. Yin, V. Dagnea and C. E. Bauer, *J. Biol. Chem.*, 2012, **287**, 13850–13858.
- 99 L. Botello-Morte, M. T. Bes, B. Heras, Á. Fernández-Otal, M. L. Peleato and M. F. Fillat, *Antioxid. Redox Signaling*, 2014, **20**, 1396–1406.
- 100 S. Pellicer, A. González, M. L. Peleato, J. I. Martínez, M. F. Fillat and M. T. Bes, *FEBS J.*, 2012, **279**, 2231–2246.
- 101 H. A. Laakso, C. L. Marolda, T. B. Pinter, M. J. Stillman and D. E. Heinrichs, *J. Biol. Chem.*, 2016, **291**, 29–40.
- 102 M. M. Verstraete, L. D. Morales, M. J. Kobylarz, S. A. Loutet, H. A. Laakso, T. B. Pinter, M. J. Stillman, D. E. Heinrichs and M. E. P. Murphy, *J. Biol. Chem.*, 2019, **294**, 11622–11636.
- 103 J. Reinking, M. M. S. Lam, K. Pardee, H. M. Sampson, S. Liu, P. Yang, S. Williams, W. White, G. Lajoie, A. Edwards and H. M. Krause, *Cell*, 2005, **122**, 195–207.
- 104 E. de Rosny, A. de Groot, C. Jullian-Binard, J. Gaillard, F. Borel, E. Pebay-Peyroula, J. C. Fontecilla-Camps and H. M. Jouve, *Biochemistry*, 2006, **45**, 9727–9734.
- 105 C. Aicart-Ramos, M. Valhondo Falcón, P. R. Ortiz de Montellano and I. Rodríguez-Crespo, *Biochemistry*, 2012, **51**, 7403–7416.
- 106 E. de Rosny, A. de Groot, C. Jullian-Binard, F. Borel, C. Suarez, L. Le Pape, J. C. Fontecilla-Camps and H. M. Jouve, *Biochemistry*, 2008, **47**, 13252–13260.
- 107 K. Kaasik and C. C. Lee, *Nature*, 2004, **430**, 467–471.
- 108 J. Yang, K. D. Kim, A. Lucas, K. E. Drahos, C. S. Santos, S. P. Mury, D. G. S. Capelluto and C. V. Finkielstein, *Mol. Cell. Biol.*, 2008, **28**, 4697–4711.
- 109 K. Kitanishi, J. Igarashi, K. Hayasaka, N. Hikage, I. Saiful, S. Yamauchi, T. Uchida, K. Ishimori and T. Shimizu, *Biochemistry*, 2008, **47**, 6157–6168.
- 110 K. Hayasaka, K. Kitanishi, J. Igarashi and T. Shimizu, *Biochim. Biophys. Acta*, 2011, **1814**, 326–333.
- 111 G. S. Lukat-Rodgers, C. Correia, M. V. Botuyan, G. Mer and K. R. Rodgers, *Inorg. Chem.*, 2010, **49**, 6349–6365.
- 112 S. Okano, M. Akashi, K. Hayasaka and O. Nakajima, *Neurosci. Lett.*, 2009, **451**, 246–251.
- 113 F. Yang, X. Xia, H.-Y. Lei and E.-D. Wang, *J. Biol. Chem.*, 2010, **285**, 39437–39446.
- 114 V. Jain, M. Yogavel and A. Sharma, *Structure*, 2016, **24**, 1476–1487.
- 115 G. Levicán, A. Katz, M. de Armas, H. Núñez and O. Orellana, *Proc. Natl. Acad. Sci. U. S. A.*, 2007, **104**, 3135–3140.
- 116 M. Faller, M. Matsunaga, S. Yin, J. A. Loo and F. Guo, *Nat. Struct. Mol. Biol.*, 2007, **14**, 23–29.
- 117 A. C. Partin, T. D. Ngo, E. Herrell, B.-C. Jeong, G. Hon and Y. Nam, *Nat. Commun.*, 2017, **8**, 1737.
- 118 J. Quick-Cleveland, J. P. Jacob, S. H. Weitz, G. Shoffner, R. Senturia and F. Guo, *Cell Rep.*, 2014, **7**, 1994–2005.
- 119 I. Barr, A. T. Smith, Y. Chen, R. Senturia, J. N. Burstyn and F. Guo, *Proc. Natl. Acad. Sci. U. S. A.*, 2012, **109**, 1919–1924.
- 120 H. M. Girvan, J. M. Bradley, M. R. Cheesman, J. R. Kincaid, Y. Liu, K. Czarnecki, K. Fisher, D. Leys, S. E. J. Rigby and A. W. Munro, *Biochemistry*, 2016, **55**, 5073–5083.
- 121 J.-J. Chen, *Blood*, 2007, **109**, 2693–2699.
- 122 S. Taniuchi, M. Miyake, K. Tsugawa, M. Oyadomari and S. Oyadomari, *Sci. Rep.*, 2016, **6**, 32886.
- 123 H. P. Harding, I. Novoa, Y. Zhang, H. Zeng, R. Wek, M. Schapira and D. Ron, *Mol. Cell*, 2000, **6**, 1099–1108.
- 124 J. Igarashi, A. Sato, T. Kitagawa, T. Yoshimura, S. Yamauchi, I. Sagami and T. Shimizu, *J. Biol. Chem.*, 2004, **279**, 15752–15762.
- 125 M. Martinkova, J. Igarashi and T. Shimizu, *FEBS Lett.*, 2007, **581**, 4109–4114.
- 126 J. Igarashi, T. Sasaki, N. Kobayashi, S. Yoshioka, M. Matsushita and T. Shimizu, *FEBS J.*, 2011, **278**, 918–928.
- 127 K. Yoshii, S. Ishijima and I. Sagami, *Biochem. Biophys. Res. Commun.*, 2013, **437**, 386–391.
- 128 K. Yamanaka, H. Ishikawa, Y. Megumi, F. Tokunaga, M. Kanie, T. A. Rouault, I. Morishima, N. Minato, K. Ishimori and K. Iwai, *Nat. Cell Biol.*, 2003, **5**, 336–340.
- 129 Y. Kim, J. Park, S. Kim, M. Kim, M.-G. Kang, C. Kwak, M. Kang, B. Kim, H.-W. Rhee and V. N. Kim, *Mol. Cell*, 2018, **71**, 1051–1063.e6.
- 130 N. B. Johnson, K. M. Deck, C. P. Nizzi and R. S. Eisenstein, *J. Biol. Chem.*, 2017, **292**, 15976–15989.
- 131 H. Ishikawa, M. Kato, H. Hori, K. Ishimori, T. Kirisako, F. Tokunaga and K. Iwai, *Mol. Cell*, 2005, **19**, 171–181.
- 132 M. Ogura, R. Endo, H. Ishikawa, Y. Takeda, T. Uchida, K. Iwai, K. Kobayashi and K. Ishimori, *J. Inorg. Biochem.*, 2018, **182**, 238–248.
- 133 Y. Kubota, K. Nomura, Y. Katoh, R. Yamashita, K. Kaneko and K. Furuyama, *J. Biol. Chem.*, 2016, **291**, 20516–20529.
- 134 R.-G. Hu, H. Wang, Z. Xia and A. Varshavsky, *Proc. Natl. Acad. Sci. U. S. A.*, 2008, **105**, 76–81.
- 135 D. J. Gibbs, J. Bacardit, A. Bachmair and M. J. Holdsworth, *Trends Cell Biol.*, 2014, **24**, 603–611.
- 136 A. Varshavsky, *Protein Sci.*, 2011, **20**, 1298–1345.
- 137 S.-J. Chen, X. Wu, B. Wadas, J.-H. Oh and A. Varshavsky, *Science*, 2017, **355**, eaal3655.
- 138 H. Ishikawa, M. Nakagaki, A. Bamba, T. Uchida, H. Hori, M. R. O'Brian, K. Iwai and K. Ishimori, *Biochemistry*, 2011, **50**, 1016–1022.
- 139 C. Kitatsuji, K. Izumi, S. Nambu, M. Kurogochi, T. Uchida, S. Nishimura, K. Iwai, M. R. O'Brian, M. Ikeda-Saito and K. Ishimori, *Sci. Rep.*, 2016, **6**, 18703.
- 140 K. Kobayashi, M. Nakagaki, H. Ishikawa, K. Iwai, M. R. O'Brian and K. Ishimori, *Biochemistry*, 2016, **55**, 4047–4054.

- 141 S. M. Kapetanaki, M. J. Burton, J. Basran, C. Uragami, P. C. E. Moody, J. S. Mitcheson, R. Schmid, N. W. Davies, P. Dorlet, M. H. Vos, N. M. Storey and E. Raven, *Nat. Commun.*, 2018, **9**, 907.
- 142 D. L. Stauff, V. J. Torres and E. P. Skaar, *J. Biol. Chem.*, 2007, **282**, 26111–26121.
- 143 M. C. Surdel, B. F. Dutter, G. A. Sulikowski and E. P. Skaar, *ACS Infect. Dis.*, 2016, **2**, 572–578.
- 144 Y. Ito, S. Nakagawa, A. Komagata, M. Ikeda-Saito, Y. Shiro and H. Nakamura, *FEBS Lett.*, 2009, **583**, 2244–2248.
- 145 A. Doi, H. Nakamura, Y. Shiro and H. Sugimoto, *Acta Crystallogr., Sect. F: Struct. Biol. Commun.*, 2015, **71**, 966–971.
- 146 C. Juillan-Binard, A. Picciocchi, J.-P. Andrieu, J. Dupuy, I. Petit-Hartlein, C. Caux-Thang, C. Vivès, V. Nivière and F. Fieschi, *J. Biol. Chem.*, 2017, **292**, 2485–2494.
- 147 R. B. Piel, M. T. Shiferaw, A. A. Vashisht, J. R. Marcero, J. L. Praissman, J. D. Phillips, J. A. Wohlschlegel and A. E. Medlock, *Biochemistry*, 2016, **55**, 5204–5217.
- 148 L. Yi, P. M. Jenkins, L. I. Leichert, U. Jakob, J. R. Martens and S. W. Ragsdale, *J. Biol. Chem.*, 2009, **284**, 20556–20561.
- 149 A. S. Fleischhacker, A. Sharma, M. Choi, A. M. Spencer, I. Bagai, B. M. Hoffman and S. W. Ragsdale, *Biochemistry*, 2015, **54**, 2709–2718.
- 150 I. Bagai, R. Sarangi, A. S. Fleischhacker, A. Sharma, B. M. Hoffman, E. R. P. Zuiderweg and S. W. Ragsdale, *Biochemistry*, 2015, **54**, 2693–2708.
- 151 R. Davydov, A. S. Fleischhacker, I. Bagai, B. M. Hoffman and S. W. Ragsdale, *Biochemistry*, 2016, **55**, 62–68.
- 152 A. S. Fleischhacker, E. L. Carter and S. W. Ragsdale, *Antioxid. Redox Signaling*, 2018, **29**, 1841–1857.
- 153 B. A. Kochert, A. S. Fleischhacker, T. E. Wales, D. F. Becker, J. R. Engen and S. W. Ragsdale, *J. Biol. Chem.*, 2019, **294**, 8259–8272.
- 154 S. Hou, M. F. Reynolds, F. T. Horrigan, S. H. Heinemann and T. Hoshi, *Acc. Chem. Res.*, 2006, **39**, 918–924.
- 155 S. E. J. Williams, P. Wootton, H. S. Mason, J. Bould, D. E. Iles, D. Riccardi, C. Peers and P. J. Kemp, *Science*, 2004, **306**, 2093–2097.
- 156 L. A. Abriata, D. Albanesi, M. Dal Peraro and D. de Mendoza, *Acc. Chem. Res.*, 2017, **50**, 1359–1366.
- 157 C. P. Zschiedrich, V. Keidel and H. Szurmant, *J. Mol. Biol.*, 2016, **428**, 3752–3775.
- 158 I. Gushchin, I. Melnikov, V. Polovinkin, A. Ishchenko, A. Yuzhakova, P. Buslaev, G. Bourenkov, S. Grudin, E. Round, T. Balandin, V. Borshevskiy, D. Willbold, G. Leonard, G. Büldt, A. Popov and V. Gordeliy, *Science*, 2017, **356**, eaah6345.
- 159 F. Jacob-Dubuisson, A. Mechaly, J.-M. Betton and R. Antoine, *Nat. Rev. Microbiol.*, 2018, **16**, 585–593.
- 160 J. Boczkowski, J. J. Poderoso and R. Motterlini, *Trends Biochem. Sci.*, 2006, **31**, 614–621.
- 161 R. Motterlini and R. Foresti, *Am. J. Physiol.: Cell Physiol.*, 2017, **312**, C302–C313.
- 162 R. Motterlini and L. E. Otterbein, *Nat. Rev. Drug Discovery*, 2010, **9**, 728–743.
- 163 J. L. Burns, D. D. Deer and E. E. Weinert, *Mol. Biosyst.*, 2014, **10**, 2823–2826.
- 164 D. Garcia, E. Orillard, M. S. Johnson and K. J. Watts, *J. Bacteriol.*, 2017, **199**, e00003–e00017.
- 165 J. A. Walker, S. Rivera and E. E. Weinert, *Adv. Microb. Physiol.*, 2017, **71**, 133–169.
- 166 D. P. Arora, S. Hossain, Y. Xu and E. M. Boon, *Biochemistry*, 2015, **54**, 3717–3728.
- 167 B. Bacon, L.-M. Nisbett and E. Boon, *Adv. Microb. Physiol.*, 2017, **70**, 1–36.
- 168 E. R. Derbyshire and M. A. Marletta, *Annu. Rev. Biochem.*, 2012, **81**, 533–559.
- 169 M. Follmann, N. Griebenow, M. G. Hahn, I. Hartung, F.-J. Mais, J. Mittendorf, M. Schäfer, H. Schirok, J.-P. Stasch, F. Stoll and A. Straub, *Angew. Chem., Int. Ed.*, 2013, **52**, 9442–9462.
- 170 S. Hossain and E. M. Boon, *ACS Infect. Dis.*, 2017, **3**, 454–461.
- 171 S. Hossain, L.-M. Nisbett and E. M. Boon, *Acc. Chem. Res.*, 2017, **50**, 1633–1639.
- 172 A. P. Hunt and N. Lehnert, *Acc. Chem. Res.*, 2015, **48**, 2117–2125.
- 173 J. O. Lundberg, M. T. Gladwin and E. Weitzberg, *Nat. Rev. Drug Discovery*, 2015, **14**, 623–641.
- 174 W. R. Montfort, J. A. Wales and A. Weichsel, *Antioxid. Redox Signaling*, 2017, **26**, 107–121.
- 175 L.-M. Nisbett and E. M. Boon, *Biochemistry*, 2016, **55**, 4873–4884.
- 176 L. Plate and M. A. Marletta, *Trends Biochem. Sci.*, 2013, **38**, 566–575.
- 177 C. Szabo, *Nat. Rev. Drug Discovery*, 2016, **15**, 185–203.
- 178 D. E. Williams, L.-M. Nisbett, B. Bacon and E. Boon, *Antioxid. Redox Signaling*, 2017, **29**, 1872–1887.
- 179 E. A. Sher, M. Shaklai and N. Shaklai, *PLoS One*, 2012, **7**, e33039.
- 180 S. Minegishi, I. Sagami, S. Negi, K. Kano and H. Kitagishi, *Sci. Rep.*, 2018, **8**, 11996.
- 181 R. Klemz, S. Reischl, T. Wallach, N. Witte, K. Jürchott, S. Klemz, V. Lang, S. Lorenzen, M. Knauer, S. Heidenreich, M. Xu, J. A. Ripperger, M. Schupp, R. Stanewsky and A. Kramer, *Nat. Struct. Mol. Biol.*, 2017, **24**, 15–22.
- 182 L. Cáceres, A. S. Necakov, C. Schwartz, S. Kimber, I. J. H. Roberts and H. M. Krause, *Genes Dev.*, 2011, **25**, 1476–1485.
- 183 S. Hou, R. Xu, S. H. Heinemann and T. Hoshi, *Proc. Natl. Acad. Sci. U. S. A.*, 2008, **105**, 4039–4043.
- 184 M. M. A. Al-Owais, J. L. Scragg, M. L. Dallas, H. E. Boycott, P. Warburton, A. Chakrabarty, J. P. Boyle and C. Peers, *J. Biol. Chem.*, 2012, **287**, 24754–24764.
- 185 G. Wang, *Metallomics*, 2017, **9**, 634–645.
- 186 G. Yuan, C. Vasavda, Y.-J. Peng, V. V. Makarenko, G. Raghuraman, J. Nanduri, M. M. Gadalla, G. L. Semenza, G. K. Kumar, S. H. Snyder and N. R. Prabhakar, *Sci. Signaling*, 2015, **8**, ra37.
- 187 R. Makino, S. Park, E. Obayashi, T. Iizuka, H. Hori and Y. Shiro, *J. Biol. Chem.*, 2011, **286**, 15678–15687.

- 188 E. Martin, V. Berka, E. Bogatenkova, F. Murad and A.-L. Tsai, *J. Biol. Chem.*, 2006, **281**, 27836–27845.
- 189 J. R. Stone and M. A. Marletta, *Biochemistry*, 1994, **33**, 5636–5640.
- 190 S. Yazawa, H. Tsuchiya, H. Hori and R. Makino, *J. Biol. Chem.*, 2006, **281**, 21763–21770.
- 191 R. Makino, S. Yazawa, H. Hori and Y. Shiro, *Biochemistry*, 2012, **51**, 9277–9289.
- 192 F. Rao, Q. Ji, I. Soehano and Z.-X. Liang, *J. Bacteriol.*, 2011, **193**, 1543–1551.
- 193 R. Martins, J. Maier, A.-D. Gorki, K. V. M. Huber, O. Sharif, P. Starkl, S. Saluzzo, F. Quattrone, R. Gawish, K. Lakovits, M. C. Aichinger, B. Radic-Sarikas, C.-H. Lardeau, A. Hladik, A. Korosec, M. Brown, K. Vaahtomeri, M. Duggan, D. Kerjaschki, H. Esterbauer, J. Colinge, S. C. Eisenbarth, T. Decker, K. L. Bennett, S. Kubicek, M. Sixt, G. Superti-Furga and S. Knapp, *Nat. Immunol.*, 2016, **17**, 1361–1372.
- 194 T. Uchida, T. Funamizu, M. Chen, Y. Tanaka and K. Ishimori, *ACS Chem. Biol.*, 2018, **13**, 750–760.
- 195 L. R. C. Vasconcellos, F. F. Dutra, M. S. Siqueira, H. A. Paula-Neto, J. Dahan, E. Kiarely, L. A. M. Carneiro, M. T. Bozza and L. H. Travassos, *Proc. Natl. Acad. Sci. U. S. A.*, 2016, **113**, E7474–E7482.
- 196 L. F. Bennett, C. Liao, M. D. Quickel, B. S. Yeoh, M. Vijay-Kumar, P. Hankey-Giblin, K. S. Prabhu and R. F. Paulson, *Sci. Signaling*, 2019, **12**, eaap7336.
- 197 S. B. Sankar, R. K. Donegan, K. J. Shah, A. R. Reddi and L. B. Wood, *J. Biol. Chem.*, 2018, **293**, 11358–11373.
- 198 H. Ibrahim, P. Mulyk and D. Sen, *ACS Omega*, 2019, **4**, 15280–15288.
- 199 N. Nishimura, W. Tsuchiya, J. J. Moresco, Y. Hayashi, K. Satoh, N. Kaiwa, T. Irida, T. Kinoshita, J. I. Schroeder, J. R. Yates, T. Hirayama and T. Yamazaki, *Nat. Commun.*, 2018, **9**, 2132.
- 200 K. Konishi, K. Ishida, K.-I. Oinuma, T. Ohta, Y. Hashimoto, H. Higashibata, T. Kitagawa and M. Kobayashi, *J. Biol. Chem.*, 2004, **279**, 47619–47625.
- 201 K. Kobayashi, S. Yoshioka, Y. Kato, Y. Asano and S. Aono, *J. Biol. Chem.*, 2005, **280**, 5486–5490.
- 202 H. Sawai, H. Sugimoto, Y. Kato, Y. Asano, Y. Shiro and S. Aono, *J. Biol. Chem.*, 2009, **284**, 32089–32096.
- 203 J. M. Kurth, J. N. Butt, D. J. Kelly and C. Dahl, *Biosci. Rep.*, 2016, **36**, e00422.
- 204 J. M. Kurth, J. A. Brito, J. Reuter, A. Flegler, T. Koch, T. Franke, E.-M. Klein, S. F. Rowe, J. N. Butt, K. Denkmann, I. A. C. Pereira, M. Archer and C. Dahl, *J. Biol. Chem.*, 2016, **291**, 24804–24818.
- 205 J. A. Brito, K. Denkmann, I. A. C. Pereira, M. Archer and C. Dahl, *J. Biol. Chem.*, 2015, **290**, 9222–9238.
- 206 L. P. Jenner, J. M. Kurth, S. van Helmont, K. P. Sokol, E. Reisner, C. Dahl, J. M. Bradley, J. N. Butt and M. R. Cheesman, *J. Biol. Chem.*, DOI: 10.1074/jbc.RA119.010084.
- 207 B. Kartal, W. J. Maalcke, N. M. de Almeida, I. Cirpus, J. Gloerich, W. Geerts, H. J. M. Op den Camp, H. R. Harhangi, E. M. Janssen-Megens, K.-J. Francoijs, H. G. Stunnenberg, J. T. Keltjens, M. S. M. Jetten and M. Strous, *Nature*, 2011, **479**, 127–130.
- 208 A. Dietl, C. Ferousi, W. J. Maalcke, A. Menzel, S. de Vries, J. T. Keltjens, M. S. M. Jetten, B. Kartal and T. R. M. Barends, *Nature*, 2015, **527**, 394–397.
- 209 Y.-L. Du, H.-Y. He, M. A. Higgins and K. S. Ryan, *Nat. Chem. Biol.*, 2017, **13**, 836–838.
- 210 J. Beltrán, B. Kloss, J. P. Hosler, J. Geng, A. Liu, A. Modi, J. H. Dawson, M. Sono, M. Shumskaya, C. Ampomah-Dwamena, J. D. Love and E. T. Wurtzel, *Nat. Chem. Biol.*, 2015, **11**, 598–605.
- 211 M. D. Kleven, M. Dlakić and C. M. Lawrence, *J. Biol. Chem.*, 2015, **290**, 22558–22569.
- 212 K. Kim, S. Mitra, G. Wu, V. Berka, J. Song, Y. Yu, S. Poget, D.-N. Wang, A.-L. Tsai and M. Zhou, *Biochemistry*, 2016, **55**, 6673–6684.
- 213 M. Ganasen, H. Togashi, H. Takeda, H. Asakura, T. Tosha, K. Yamashita, K. Hirata, Y. Nariai, T. Urano, X. Yuan, I. Hamza, A. G. Mauk, Y. Shiro, H. Sugimoto and H. Sawai, *Commun. Biol.*, 2018, **1**, 120.
- 214 Y. Wei, A. Tinoco, V. Steck, R. Fasan and Y. Zhang, *J. Am. Chem. Soc.*, 2018, **140**, 1649–1662.
- 215 R. D. Lewis, M. Garcia-Borràs, M. J. Chalkley, A. R. Buller, K. N. Houk, S. B. J. Kan and F. H. Arnold, *Proc. Natl. Acad. Sci. U. S. A.*, 2018, **115**, 7308–7313.
- 216 S. B. J. Kan, X. Huang, Y. Gumulya, K. Chen and F. H. Arnold, *Nature*, 2017, **552**, 132–136.
- 217 S. C. Hammer, G. Kubik, E. Watkins, S. Huang, H. Minges and F. H. Arnold, *Science*, 2017, **358**, 215–218.
- 218 K. Chen, X. Huang, S. B. J. Kan, R. K. Zhang and F. H. Arnold, *Science*, 2018, **360**, 71–75.
- 219 R. K. Zhang, K. Chen, X. Huang, L. Wohlschlagel, H. Renata and F. H. Arnold, *Nature*, 2019, **565**, 67–72.
- 220 I. Cho, Z.-J. Jia and F. H. Arnold, *Science*, 2019, **364**, 575–578.
- 221 O. Shoji, Y. Aiba and Y. Watanabe, *Acc. Chem. Res.*, 2019, **52**, 925–934.
- 222 O. Shoji and Y. Watanabe, *Metallomics*, 2011, **3**, 379–388.
- 223 E. Sato, I. Sagami, T. Uchida, A. Sato, T. Kitagawa, J. Igarashi and T. Shimizu, *Biochemistry*, 2004, **43**, 14189–14198.
- 224 J. S. Dias, A. L. Macedo, G. C. Ferreira, F. C. Peterson, B. F. Volkman and B. J. Goodfellow, *J. Biol. Chem.*, 2006, **281**, 31553–31561.
- 225 A. E. Fortunato, P. Sordino and N. Andreakis, *J. Mol. Evol.*, 2016, **82**, 279–290.
- 226 J. Ma, X. Zhang, Y. Feng, H. Zhang, X. Wang, Y. Zheng, W. Qiao and X. Liu, *J. Biol. Chem.*, 2016, **291**, 26670–26685.